The University Of Sheffield.

Hybrid steel wire strands with carbon fibre reinforced plastics

Alon Ratner

A thesis submitted in partial fulfilment of the requirements for the degree of Doctor of Philosophy

The University of Sheffield
Faculty of Engineering
Department of Mechanical Engineering

11/02/2016

Abstract

It has been hypothesised that weight reduction in ropes can be realised by the hybridisation of steel strands with non-metallic carriers in order to improve the efficiency of hoisting processes, most notably in mining applications. While this has been attempted by replacing steel central wires with unreinforced polymers and parallel fibre cores, this investigation has considered the replacement of steel wires with carbon fibre reinforced plastic rods.

Fibre reinforced plastics are valued for their high strength-to-weight ratios and ubiquity. Since load sharing is maximal between materials of similar stiffness in a hybrid system, high strength carbon fibres were identified as the most feasible reinforcements for achieving compatible mechanical properties with those of high strength steel wires. A nylon polymer matrix was chosen to provide a reasonable balance between toughness, environmental stability and cost.

A pultruder was designed and constructed in order to produce carbon fibre/nylon 12 rods for the creation of novel steel/CFRP hybrid strands. Development of the pultruder highlighted challenges in manufacturing that have been solved for industrial processes but remain underrepresented in academic research. Cost effective and flexible laboratory-scale techniques included fibre spreading by rollers, powder impregnation and the use of heating strips. Superior consolidation of the polymer matrix was obtained in rods pultruded from commingled stretch-broken carbon fibre/nylon tows, which emerged as the most appropriate feedstock.

The Young's modulus and tenacity of hybrid carbon fibre/vinyl ester central rods were found to exceed that of standard steel strands, which in turn were higher than that of hybrid strands produced with in-house pultruded rods. Although this identified a need for the refinement of manufacturing conditions, it identified a lower bound of material properties required of the central rod in order to improve the tenacity of a hybrid strand. The finding of higher tenacity for the hybrid carbon fibre/vinyl ester strands demonstrated the feasibility of hybridising steel wire strands with non-metallic rods as a novel means of increasing the strength-to-weight ratio of strands. Finite element modelling of strands with a range of non-metallic core materials confirmed the material selection process by predicting the suitability of carbon fibre reinforced plastics over other core materials in improving the tenacity of hybrid strands.

Acknowledgements

I would like to recognise the kindness of friends who were there at times of need through purely altruistic motivations. Simon Hayes and Peter Bailey gave me crucial insights into the development of the pultrusion line and their interest in the minutiae of the construction proved to be of critical importance. I owe my competency in the manufacturing of composites to Austin Lafferty, whose efforts in training our group and the continuous support he has given to the laboratory have underpinned the abilities of an academic generation of students in composites materials. I would like to thank Constantinos Soutis, Christophe Pinna, Jose Curiel Sosa and Stephen King for their advice on finite element modelling. Mike Jackson's assistance has been decisive not only to our group but also to the many technical undertakings of this project. My thanks to AdAM for their generous supply of nylon powder and to Kurt Bonser for his support.

It has been a pleasure to work with Bridon, whose support for the project has been constant. All work related to the testing of strands was made possible by Pengzhu Wang, whose guidance in the application of rope technology has been invaluable.

I could not have developed the foundations for vital disciplines of engineering without the help of our community of researchers; classical laminate theory from Ioannis, science of strong materials from Yu, the finite element method from Galal and Akin and the applications of composites from Pete. Mulyadi, Steve, Zurina, Sofia, Saravanan, Carlos, Elliott, Diyar, Khaled, Nithian, Andrew, Miguel and Wilfried have also been a second family. I owe special thanks to Adam and Teddy for their commendable tolerance of my eccentricities.

I would like to thank my families, both natural and surrogate for their support. For the past quarter of a century Ben has provided both the inspiration and courage for me to reach each stage of my career and I have no doubt that I would not have made it this far without his friendship.

Lastly, I would like to pay tribute to those in whom I found strength when I was most alone, including Campbell, Cantrell, Claypool, Del Naja, Fallon, Hurt, Hütz, Lanegan, Marshall, McDowell, Patton, Van Zandt, Vedder, Waits and the many others who are too numerous to name.

Contents

List of Figures

List of Tables

Nomenclature

E – Stiffness (Pa)
σ – Stress (Pa)
P – Load (N)
A – Cross-sectional area (m^2)
d – diameter of a rod (m)
L – span between supports in three point bend tests (m)
$\Delta P/\Delta y$ – rate of change of flexion (N/m)
ε – strain
J – strain energy (J)
α – lay angle (°)
r_w – winding radius (m)
z_w – lay length (m)
F_i – tension in a wire (N)
P_i – axial load on a wire (N)
Q_i – shear load on a wire (N)
S_i – tension in the axial direction of a strand (N)
z – number of outer wires in a strand
r_c – core wire radius (m)
r_h – outer wire radius (m)

Glossary of Terms

Aaramid – 'aromatic polyamide', also refers to fibres made from these long chain polymers. Commercial examples include Kevlar, Twaron and heterocyclic polymers such as Zylon.
Back ionisation – the phenomenon by which a target surface acquires a charge equal to that of an incoming stream of ions, which prevents any further charging of the surface due to electrostatic repulsion.
Birdcage – the appearance of one or more outer wires to unwind and protrude from the regular helical shape of a strand or rope in a shape reminiscent of a birdcage.
Bobbin – a drum from which fibres or wires are unwound.
Catenary – a chain or a flexible curve made from links or sections or wire rope.
Characteristic length – the length at which the breaking load of a rope is equal to its weight under gravity.
Commingled fibres/tows – a bundle of filaments from two or more material types that have been spun together.
Core – the central carrying component in a rope or strand. In yarns and strands this may be a single wire, while in ropes it may be a central yarn or strand.
Corona spray – the generation of charges through dielectric breakdown of air, either by exposure to a potential difference or a plasma source, which are then pneumatically transported to a target.
Fibre volume fraction – the volume inside a composite material that is represented by fibres.
Forming/heating die – a matched mould through which impregnated fibres are consolidated or cured in a pultrusion process.

Hybrid rope – a rope composed of carriers from more than one material type.
Jacobian – shorthand from 'Jacobian matrix determinate' is a parameter typically between 1 and -1 of finite element mesh quality, with 1 representing a regular cuboid and smaller values indicating lower element regularity.
Kinematic constraint – a boundary condition placed on a group of nodes in a finite element simulation that prevents motion in specified directions.
King wire – the central wire in a yarn or strand.
Lay angle – the incident angle made by the path of a helical wire with the central axis of helical rotation.
Lay length – the periodicity of a helical path made by a wire; one lay length is the distance along the central axis of rotation required for a full helical rotation of the wire.
Parallel fibre rope – a rope composed of independent filaments that are not chemically bonded by a matrix material as in a fibre reinforced plastic. Parallel fibre cores are sheathed in a flexible plastic coating to constrain lateral motion of the filaments.
Pultrusion – continuous manufacture of a fibre reinforced plastic with a constant cross-section by pulling impregnated fibres through a heated die.
Rope – generally, any assembly of smaller uniaxial tendons that is used to carry a load in tension. In wire or multi-strand technology, 'rope' is used to refer to a carrier that is composed of 'strand' or 'yarn' repeating units which are themselves composed of wires'.
Rule of mixtures – an analytical model of a composite that relates the nominal macroscopic stiffness under a given loading condition to that of its material constituents.
Sheave – a grooved pulley for hoisting wire rope.
Size – a surface treatment applied to filaments to improve adhesion and handling of fibre tows.
Step – a segment of a simulation solved by ABAQUS 6.10.
Strand – a helical assembly of wires that either represents a constituent part a rope or a complete load carrying device in its own right. In ropes with many individual carriers, often referred to as larger than a 'yarn' but in smaller diameter ropes the terms are sometimes used synonymously.
Stretch broken fibres – yarns that have been stretched until some proportion of the filaments have broken. The remaining discontinuous filaments are then spun into tows.
Void content – The volume inside a composite material that is represented by an absence of material or by a non-solid phase unintentionally included during manufacturing, such as air.
Winding radius – distance between the centre of rotation of a path made by a helical wire and its lateral displacement from that point.
Wire – fundamental element in a metallic rope, consisting of the smallest diameter carrier.
Yarn – the smallest assembly of wires that is repeatedly used to create larger sections of a strand or rope. Sometimes used synonymously with 'strand'.

Glossary of Acronyms

C3D8 – Three dimensional brick elements with eight nodes, used in finite element modelling
CF – Carbon Fibre
CFRP – Carbon Fibre Reinforced Plastic
DSC – Differential Scanning Calorimetry
FRP – Fibre Reinforced Plastic
PA – PolyAmide
PEEK – Poly(EtherEtherKetone)

‘The Æsir now began to fear that they would not get the wolf bound. So Alfather sent the youth, who is called Skírnir, and is Freyr’s messenger, to some dwarfs in Svartalfaheim, and had them make the fetter which is called Gleipner. It was made of six things: of the footfall of cats, of the beard of woman, of the roots of the mountain, of the sinews of the bear, of the breath of the fish, and of the spittle of the birds. If you have not known this before, you can easily find out that it is true and that there is no lie about it, since you must have observed that a woman has no beard, that a cat’s footfall cannot be heard, and that mountains have no roots; and I know, forsooth, that what I have told you is perfectly true, although there are some things that you do not understand.’

- Gylfanning, Prose Edda

1 Introduction

Dynamic ropes for mining applications are required to be strong, durable and reliable. For more than a century these specifications have been met by steel wire ropes. However, the relatively high density of steel inhibits the productivity of deep mining operations because the self-weight of the ropes that are required to hoist material becomes limiting. The main aim of this investigation is to develop a hybrid strand composed of steel wires and fibre reinforced plastic rods that will possess a higher strength to weight ratio than existing steel strands.

This section outlines the scope of the project and its key challenges. It also briefly introduces the materials and technologies utilised in the manufacturing research that was undertaken. To avoid a cumbersome and unduly self-referential text, exhaustive reviews of prior research are included as relevant in succeeding chapters.

1.1 A history of ropes

Since antiquity ropes have been an important feature of technology and have played a vital role in enabling bulk traction beyond earthbound movement. The earliest material evidence for the use of cordage in yarns comes from prehistoric fishing nets found at Korpilathi swamp in Antrea, Finland that carbon dating suggests were produced in Mesolithic times [1]. Given the confidence with which these nets were used for their intended purpose it is presumable that human experimentation with binding fibres to produce yarns extends to earlier periods.

An awareness of ropes is found in many ancient cultures and thus became items not only of technological utility but also of cultural significance [2-4]. Early depictions of manufacture have also survived in Egyptian burial chambers [5]. The use of these ropes in large constructions has been confirmed by numerous finds of papyrus and flax ropes in Egypt and descriptions of their use by classical authors [6-8]. Evidence of the reliability and strength of these ropes is abundant. The Coliseum in Rome was once covered by an enormous awning with the aid of sturdy ropes [9].

The style of rope manufacture did not radically change until the Industrial Revolution, during which the efficacy of rope production was greatly improved by the innovation of the ropewalk. These rooms were hundreds of metres in length and were often located near harbours where they provided cordage for shipwrights [10]. At the time of writing, the ropery at Chatham dockyard still houses a working ropewalk.

Ropes and their manufacture changed dramatically with the introduction of wire rope which superseded chains in strength and durability [11]. The innovations that accompanied wire ropes were profound and heralded a new age in applications for tensile loading, including continuous manufacture of steel ropes with vastly improved durability and flexibility in design [12]. Advances in steel production further transformed the state of the industry [13].

Some of the processes developed more than a hundred years ago are still employed today. The importance of these modern techniques was noted by Boris Artzybasheff in his introduction to his illustrations of these novel processes, shown in Figure 1.1 [14]:

“I am thrilled by machinery’s force, precision and willingness to work at any task, no matter how arduous or monotonous it may be. I would rather watch a thousand ton dredge dig a canal than see it done by a thousand spent slaves lashed into submission.”

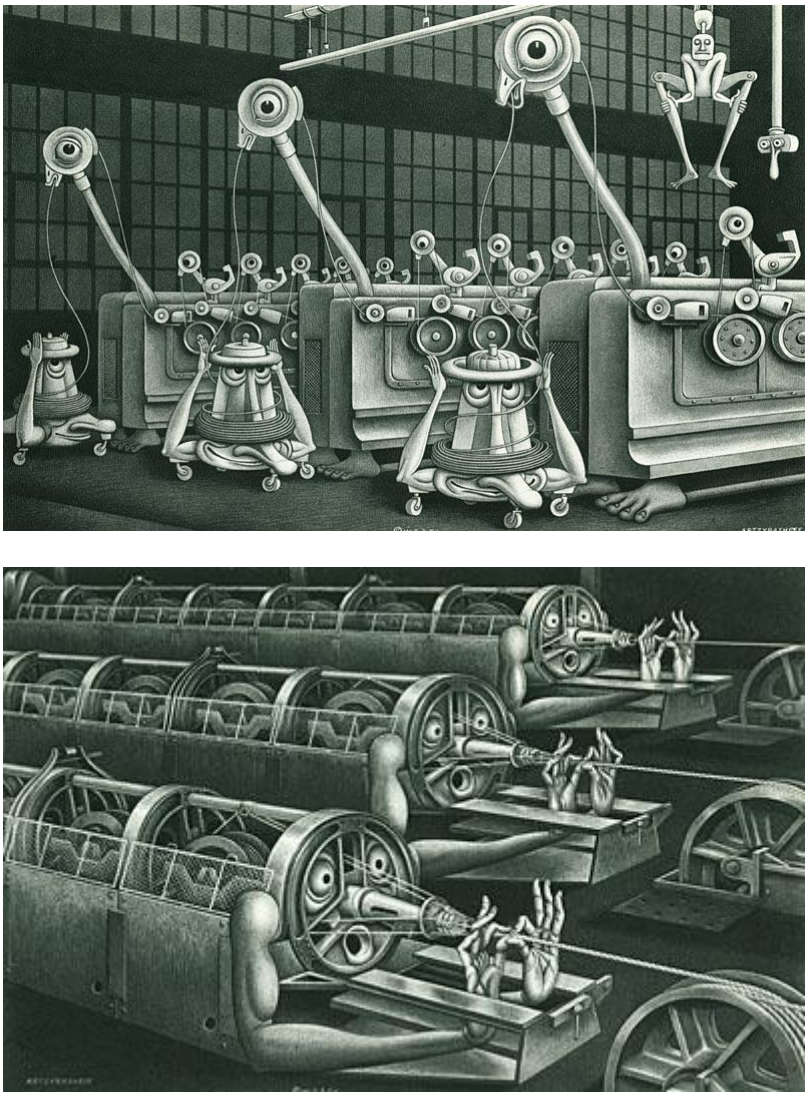

Figure 1.1 ‘Wire drawing machines’ and ‘Stranding of Wire Rope’ [14]. Images have been reproduced with special permission from Titan Books.

1.2 Wire ropes

Each carrier that makes up a rope is wound in a helical shape about a central axis, which may contain a continuous core. The pattern of winding determines many of the physical properties of the rope [15]. The terminology used to describe the order of scale from an individual wire to a rope is described in Figure 1.2 [16]:

wire → yarn → strand → rope

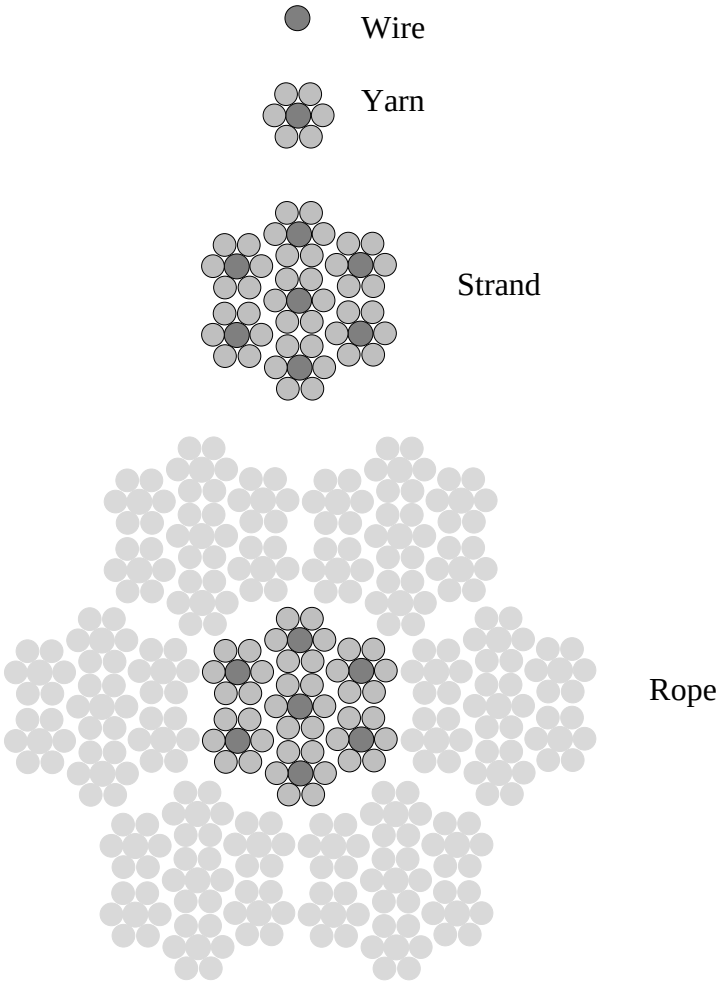

Figure 1.1 Nomenclature of elements in a wire rope construction.

This project considers a simple construction known as a wire strand core, shown in Figure 1.3. This consists of 6 helical wires wound around a straight ‘king’ wire. This is also collectively referred to as a ‘core’ since it may form the inner basis for larger multi-strand ropes, an example of which is shown in Figure 1.4.

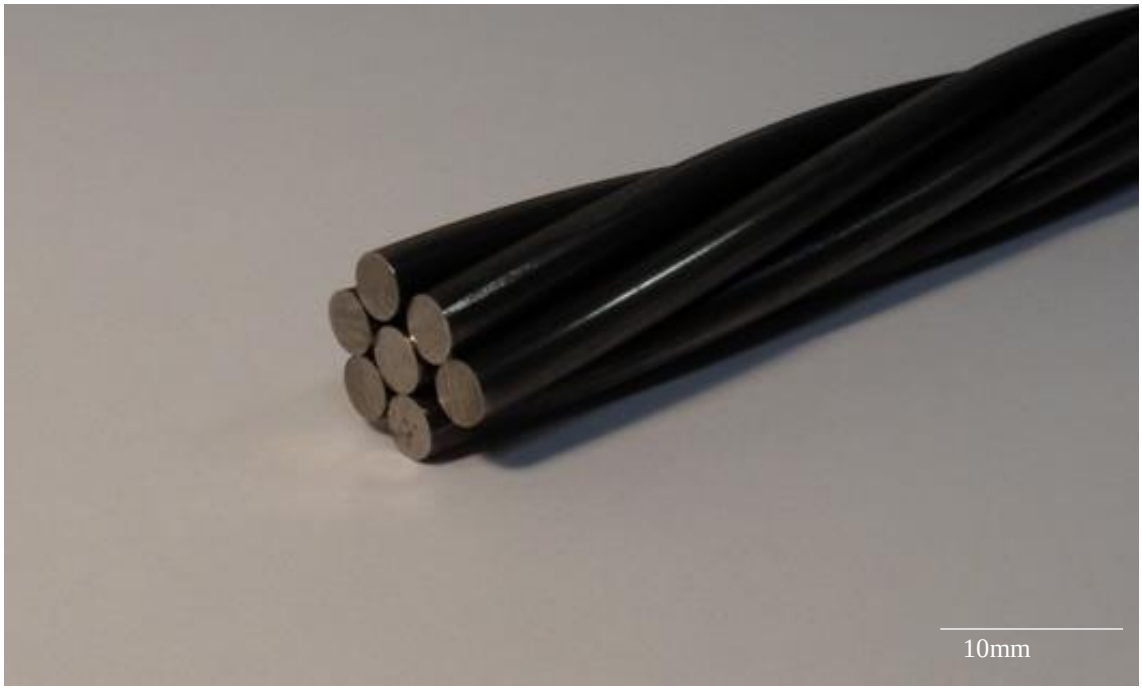

Figure 1.3 Wire strand core.

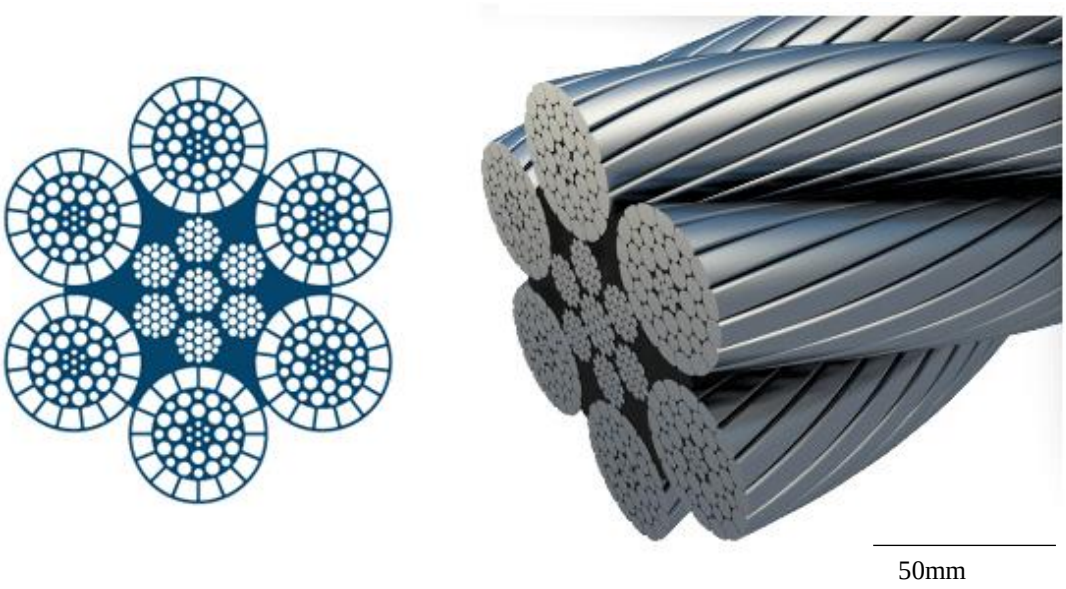

Figure 1.4 A multistranded rope, Dyform for offshore winch applications, Bridon International.

Although the majority of contemporary research is concerned with multistranded ropes, for reasons of feasibility this project is limited to wire strand cores.

1.2.1 Steel and fibre ropes

Steel is the material of choice for most wire ropes. The properties of high tensile strength and stiffness and ductility have made steel a high performing and economical material [17]. Steel is obtained in the form of large diameter rods that are drawn into filaments [18]:

- The rods are heated in order to achieve a phase transformation to austenite and are then rapidly cooled in order to produce a lamellar microstructure that is conducive to cold drawing.
- The steel rods are drawn into wires at low temperatures to reduce their diameters. Cold drawing increases strength while reducing the ductility of the wires.
- The surface of the wire may be coated to prevent corrosion and wires are often zinc coated by electro-dripping or galvanisation. Wires are then redrawn to recover strength and to smoothen the surface.

Stranding is the process by which many wires may be consolidated into a single construction. This process has been illustrated in a schematic diagram in Figure 1.5. Bobbins carrying each wire are fed into a forming die that determines the geometry of the strand. The rate at which the capstan rotates determines the helical angle and thus the lay length of the strand.

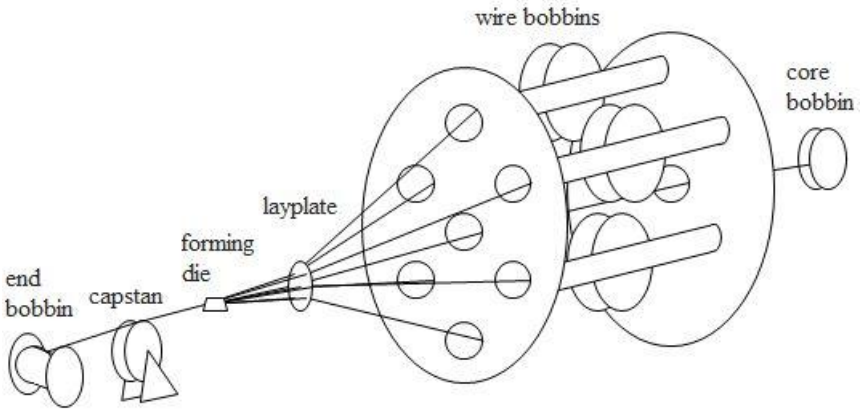

Figure 1.5 Stranding from wire and core bobbins.

Fibre ropes have higher strength-to-weight ratios, greater flexibility and better shock resistance than steel wire ropes but are less resistant to abrasion, cutting and creep [19]. For instance, for similarly laid 12mm strands, the strength-to-weight ratios of nylon, polyester, aramid and steel are 27.4tons/m, 22.4tons/m, 85.4tons/m and 15.1tons/m, respectively [20]. Some common uses of synthetic fibre ropes are provided below:

- Nylon is principally considered for its energy absorption, durability and abrasion resistance [21].
- Polyester is valued for reasonable stiffness at low cost [22].
- Aramid fibres are more expensive than those made from commodity plastics and are characterised by high tensile stiffness, low susceptibility to creep, thermal resilience and good abrasion resistance [23].

Liquid crystal polymers have provided the majority of high stiffness and strength fibres. Outstanding mechanical and thermal properties are found among aromatic aramids such as Kevlar, heretocyclic polymers such as Zylon and liquid crystalline and aromatic crystalline polyesters such as Vectran [24].

1.2.2 Lightweight ropes

Since the 19th Century steel wire ropes have become an indispensable part of hoisting in mines. Steel wires initially replaced natural fibres and eventually surpassed catenaries in

strength. In doing so, they have enabled deeper mineral extraction. Wire rope cables are also used in compliant oil and gas platforms such as tension leg platforms, which are stiff with respect to their displacement from the seabed.

Weight is an important design factor in mining applications. The ‘characteristic length’ of a tether is defined as the maximum breaking load of the material divided by its mass per unit length. It gives an indication of the longest conceivable length of a continuous material before its self-weight overcomes its maximum breaking load. In practice the maximum length of a rope will be much lower, owing to its role in hoisting additional weight, deterioration of its strength during its service life and the safety factor of the application. The characteristic lengths of some materials are given in Figure 1.6 [25].

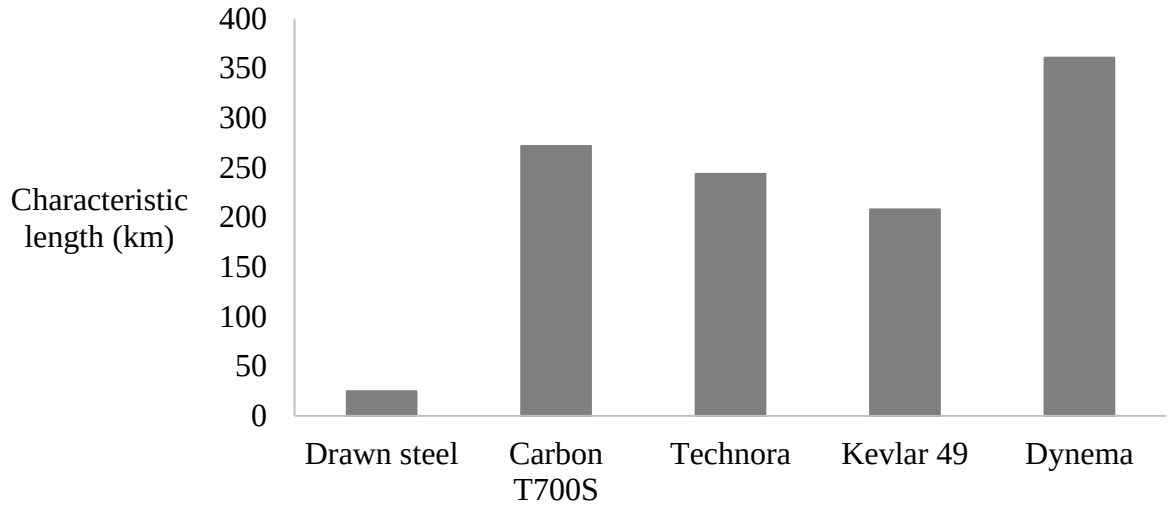

Figure 1.6 Characteristic lengths of drawn steel rod and high performance synthetic rope fibres.

It is clear that lightweight materials with higher tensile strength per unit mass will perform better with respect to self-weight than steel. This means that mining shafts can hoist more material from greater depths, which increases productivity as ore can be extracted at a higher rate. Lightweight ropes also contribute less to the weight of tension leg platforms, meaning that weight savings can be passed onto essential features of the working and habitable spaces within the platforms themselves [26].

Although weight reduction is expected to increase productivity, synthetic fibre ropes are unlikely to survive repeated maintenance and deterioration due to abrasion and crushing in motion when in contact with winding drums. This is a consequence of the relatively low compression strength of polymer fibres, which lack the out-of-plane strength and stiffness of drawn steel wires. This complication poses a design challenge, which is compounded by a lack of experimental data and product testing [27]. Parallel fibre ropes also encounter excessive heating due to internal friction and polymer ropes show lower tensile strength and stiffness at elevated temperatures. This has been partly responsible for observed damage in dynamic ropes moving over sheaves [28].

1.2.3 Hybrid ropes

Steel and fibre hybrid ropes were suggested as early as 1977 [29]. Klees et al. provided a commonly accepted description of a hybrid rope consisting of a jacketed synthetic fibre core surrounded by helically laid steel strands [30]. Hybrid ropes seek to take advantage of the durability of steel wires while benefiting from the weight reduction offered by synthetic fibres. The productivity of a mine shaft decreases with greater depth as the self-weight of the rope takes up an increasing proportion of the hoisted mass. For this reason the efficiency provided by a higher strength-to-weight ratio becomes increasingly competitive at greater depths [31]. Rebel, Verreet and Briem reviewed two ways in which hybrid ropes may influence rope selection; by reducing the weight of ropes with the same breaking strength or by increasing the strength of ropes with the same mass. They found that a weight reduction of 20% could increase skip capacity by 50% at depths of 3000m. Most importantly, they suggested that changes in rope design to accommodate a fibre core may not entail replacement of existing sheaves and drum sleeves [32].

Developments for hybrid ropes have largely been undertaken for steel outer strands and parallel laid cores. While fibre reinforced plastics (FRP) have been used for the construction of bridges [33], their high cost has largely deterred their use in lightweight ropes for deep water mooring [25].

Parallel fibres only interact by mutual friction, whereas chemical bonding in FRPs enables load sharing between reinforcing fibres. This permits FRPs to distribute a given load across the fibres with near-equal extension. In bending a FRP also possesses greater flexural stiffness since it elastically behaves as a single beam rather than as a bundle of individual parallel fibres. FRPs rarely have a fibre volume fraction above 60% so the axial tensile stiffness and strength of the FRP are lower in comparison with those of a parallel fibre rope. Nevertheless, the unified nature of FRPs is closer to that of the homogeneous steel wires already in use, which may allow them to more easily overcome issues of durability and technology transfer.

Above all, the single greatest advantage of a hybrid steel-FRP rope may lie in the vast potential for materials selection in both fibres and polymers. This is most apparent in their synergistic properties by which the advantages of a particular constituent can be complemented by its partner materials.

1.3 Project aims

Hybrid ropes are largely at an industrial, rather than academic stage of development. This is not uncommon for the wire rope industry, which has not produced a large collection of publically accessible information; one the most commonly cited experimental data sets for steel wire ropes was created by Utting and Jones [34, 35]. Acquired knowledge about the performance of steel ropes will not be directly applicable to hybrid ropes. Given the relatively narrow range of data for steel wire technologies [33], it is easy to anticipate that a body of information regarding the study of hybrid ropes will be needed in order to develop the technology beyond its academic origins. This project aims to contribute to reducing the gap in understanding between steel and hybrid structures by characterising appropriate polymeric materials and generating foundational data about the feasibility of hybrid strands. This is to be achieved through in-depth materials characterisation using novel testing methodologies and finite element analysis of new assemblies of wires and rods that are representative of the

strands. Since there is no prior experience in manufacturing and testing steel and FRP hybrid strands, there are also no datasets regarding the tensile strength and stiffness properties of these components. In addition to creating these points of reference for future research and development, this project also aims to simulate hybrid strands in order to extend the investigation to hybrid materials that are outside of the scope of experimentation. Project objectives can be summarised as follows:

- Identify rod materials that are suitable for increasing the strength-to-weight ratio of strands by hybridisation with steel wires
- Develop a manufacturing process to produce hybrid strands
- Develop a testing methodology in order to characterise the tensile properties of hybrid strands
- Simulate tension in strands hybridised with a range of FRPs in order to increase the scope of materials analysis and validate the materials selection process

1.3.1 Project overview

Realisation of steel-FRP hybrid ropes is a wide topic that requires consideration from a number of engineering techniques in order to fulfil the project aims. These are covered by the chapters of this thesis:

1 Introduction
   - An overview was provided of project goals, the context of research in the area of study, current manufacturing techniques.
   - This chapter also reviews screening of appropriate materials for FRP rods and provides an introduction to FRP manufacturing techniques.

2 Design and construction of the pultruder
   - After a period of review and development of appropriate technologies, a lab-scale pultruder was designed and constructed in order to manufacture carbon fibre/thermoplastic rods.
   - The pultruder made use of a number of modular processes, including mechanical spreading of fibres, powder impregnation of fibres, pre-heating of impregnated tows, consolidation of tows within a heated die and traction pulling of rods.

3 Pultrusion optimisation and productivity
   - Rods were pultruded from sized and unsized carbon fibres and nylon 12 powder, as well as from commingled tows of carbon and nylon 12 filaments.
   - Trials were undertaken to determine optimal manufacturing parameters and rods were pultruded in order to provide specimens for tensile and flexural tests. Rods were also pultruded to make hybrid steel-FRP strands.

4 Experimental methodology
   - Flexural and tensile specimens were prepared from pultruded rods for the determination of flexural and tensile stiffness and strength. Cross-sections of rods were also prepared for use in optical microscopy in order to evaluate microstructural features and estimate fibre volume fraction and void content.
   - Hybrid strand consisting of steel wires and FRP rods were produced in order to provide specimens for the determination of tensile stiffness and strength.

5 Experimental results
   - Presentation of optical micrographs of cross-sections and estimations of fibre volume fraction and void content for rods pultruded from different fibre and matrix feedstocks.

- The flexural and tensile stiffness and strength of rods compared against those of a control group. The tensile stiffness and strength of hybrid strands was analysed in order to determine the tenacity, or breaking load divided by mass, of the strands.

6 Discussion
- An appraisal of manufacturing techniques was made following evaluation of optical micrographs, which showed morphological features arising from processing conditions. These were used to explain differences in the fibre volume fraction and void content between rods with different materials.
- Trends in the flexural and tensile stiffness and strength of the rods were also correlated with material types and processing conditions. Ultimately, characterisation of the rods informed trends in the measured tensile stiffness and strength of hybrid strands, which were evaluated in comparison with steel strands.

7 Finite element modelling
- Simulation of the hybrid ropes allowed out-of-laboratory estimations for the tensile strength and stiffness of a number of hybrid material combinations.
- These were validated with the measured outcomes from Chapter 5 and analysed with respect to the discussion offered in Chapter 6.

8 Conclusion and evaluation
- Major findings were summarised and the outcomes of the project were evaluated with respect to its stated aims.
- Suggestions were also made for continuing the study of the role played by FRPs in steel hybrid strands.

1.4 Materials selection

Research and development of steel wire ropes includes continuous improvements in manufacture, particularly in the cold drawing of galvanised wires [36]. While ropes with different steel compositions have been proposed [37, 38], the focus of research in hybrid ropes has been to maximise the strength-to-weight ratio by the inclusion of a non-metallic core material. To this end, the materials selection made in this project is concerned with FRP materials complementary to steel.

1.4.1 Statement of problem; design challenges

The central difficulty in implementing hybrid ropes is the mismatch in properties between the core and surrounding strands, which in particular includes tensile strength and stiffness. The former touches on the high strength-to-weight ratio of FRPs, which has prompted research into their use for weight reduction in ropes. The latter is the most difficult to address and will represent the bulk of research and development.

Material homogeneity is an acceptable assumption for highly drawn steel in multistrand ropes and it implies uniformity of tensile stiffness. In the case of this not being true, load sharing is unevenly carried between components. Load sharing between carriers is essential as it directly affects the highest possible strength of the rope. This implies a design criterion:

Load sharing is maximal between components of equivalent stiffness.

Hybrid materials are therefore a special case, where material properties must be tailored to approach equivalence. It therefore falls to the designer to ensure that the Young's modulus of

the FRP core matches the Young's modulus of the outer strands as closely as possible. This may be achieved with a suitable choice of materials and composition for the FRP core.

The problem is complicated by the different stress-strain properties of both materials, which have been schematically represented in Figure 1.7. FRPs do not typically exhibit ductile plasticity and are less extensible than steel. Hybrid ropes of such different materials are therefore only likely to be serviceable within a limited elastic range. Barring creep effects, there is a narrow window of strain within which the hybrid materials will perform in harmony. A caveat is that plasticity is inevitable in large multi-stranded ropes due to crushing between wires, especially for dynamic ropes stored on drums. Strain hardening and long-term changes in material properties arising from creep are therefore likely to influence the behaviour of hybrid ropes in commercial applications [39].

An overly stiff FRP core will result in catastrophic failure at an early stage as the stress is overwhelmingly concentrated in the core. Conversely, a more compliant core will not share an appreciable load and will therefore inadequately contribute to the strength of the rope. The need to reconcile the stiffness of both materials is therefore a practical necessity in the design of hybrid ropes.

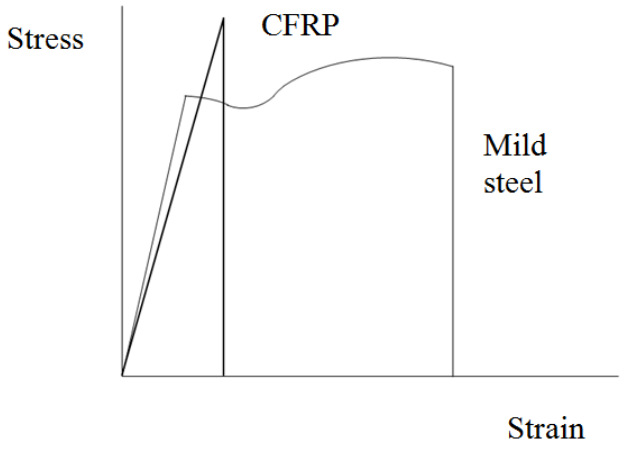

Figure 1.7 Schematic stress-strain curves for a typical carbon fibre reinforced plastic and mild steel.

1.5 Elasticity of FRPs

FRPs are characterised by their orthotropic or anisotropic properties. These are described by classical laminate theory, which describes the mechanical behaviour of bonded plies. Anisotropy is particularly noticeable in affecting strength and stiffness away from the fibre direction. The tensile stiffness of a lamina with unidirectional fibres is at a maximum parallel to their orientation but it greatly decreases with any angular deviation from the fibre direction [40].

1.5.1 Rule of mixtures

Following Hooke's law, separate equations for the tensile stiffness of the fibre, E_f and matrix, E_m components of a composite may be represented by the following expressions. These relate the stress in the fibres, σ_f and matrix, σ_m to the strain experienced by the composite, ε:

$$\sigma_f = E_f \varepsilon \quad \text{(eq. 1.1)}$$

$$\sigma_m = E_m \varepsilon \quad \text{(eq. 1.2)}$$

With the assumption that perfect bonding between the fibre and matrix would produce uniform load transfer between constituents, a load placed upon the composite is shared by both components. Therefore, a load, P acting on the composite is related to the loads acting on the fibres, P_f and matrix, P_m with respective surface areas A_f and A_m:

$$P = P_f + P_m = \sigma_f A_f + \sigma_m A_m \quad \text{(eq. 1.3)}$$

The rule of mixtures is an analytical tool for estimating the tensile stiffness of a composite from its constituents, though its accuracy is limited to properties in the fibre direction. It is derived from eq. 1.3 and relates the observed macroscopic stiffness of the composite, E, to that of the fibres, E_f and matrix, E_m in proportion to the volume that is occupied by the respective constituents, known as the fibre and matrix volume fractions, V_f and V_m [41]:

$$E_1 = E_f V_f + E_m V_m = E_f V_f + E_m (1 - V_f) \quad \text{(eq. 1.4)}$$

An assumption implicit in this derivation is that stresses only arise from external loads and therefore the rule of mixtures does not consider the residual stresses from Poisson contraction and shrinkage during curing. Nor does it consider the effects of manufacturing, such as the void content, which can noticeably reduce shear strength, even at low concentrations [42]. In addition to properties such as tensile stiffness and strength, fibre volume fraction and void content are therefore important parameters for the characterisation of a composite material.

1.6 Materials selection criteria

In order to successfully complement steel in a dynamic hybrid rope, a FRP must contribute to the following properties:

- Mechanical
  - In order to share load and contribute to the strength of the hybrid, the FRP should have a high stiffness, close to steel if possible.
  - For the FRP to remain competitive it should have high tensile strength.
  - Since the rope is likely to suffer from wear and tear and sudden loading, it is desirable for the FRP to be tough and relatively tolerant of damage accumulation.
- Thermal
  - Internal friction is reduced by lubrication but in moving ropes can still generate considerable heat. A FRP must still be serviceable at elevated temperatures.
- Long term
  - The FRP core should be resistant to creep and fatigue under the environmental conditions that it is subjected to during use.

1.7 Fibre selection

Glass, aramid and carbon fibres dominate the market for plastic reinforcement, with glass outweighing any other reinforcement by volume and global value, at approximately $29.4bn in 2013 [43]. By value carbon fibres share a large minority of the market, at an estimated $10.25bn in 2012 [44] while Aramid FRPs constitute a much smaller proportion of demand.

The share of high performance synthetic fibres commonly used for lightweight ropes such as Dyneema and Spectra, which are rarely used as reinforcing fibres for FRPs, is negligible on a global scale [45].

Fibres of each material type are anything but 'standard' – for instance the strength and stiffness of carbon fibres can vary by several factors between different products. Some typical properties of leading products are given in Table 1.1.

Table 1.1 Physical properties of a range of typical reinforcements.

Fibre type	Product	Strength (MPa)	Stiffness (GPa)	Density (gcm^{-3})
Glass [46]	E-glass	3445	72.8	2.58
	S-glass	4890	86.9	2.46
Aramid [47-49]	Kevlar 29	2800	80.0	1.44
	Kevlar 49	3600	115.0	1.44
	Zylon HM	5800	280.0	1.56
Carbon [50]	Torayca T700S	4900	230.0	1.80
	Torayca T300	3530	230.0	1.76
	Torayca MJ60	3920	588.0	1.93

As can be seen from Table 1.1, it is the density of carbon and aramid fibres that most distances them from glass fibres, giving stiffness- and strength-to-weight ratios. On the basis of a tensile stiffness that is much lower than that of steel, it is possible to exclude glass fibres from any further consideration.

Of the aramids, only heterocyclic aromatic liquid crystalline polymers such as polybenzobisoxazole (PBO, trade name Zylon), or polybenzimidazole (PBI) are comparable to carbon fibre with respect to strength and stiffness. These are lyotropic polymers with rod-like repeating units and the thermal and chemical resistances of these fibres are among the highest of any known polymers [51, 52]. These exceptional properties largely arise from the absence of flexible molecular units, which results in a totally planar aromatic system and conjugation across adjoining single bonds imitates the strength of double bonds.

At the time of writing, Zylon is sold at a price around an order of magnitude higher than the cheapest intermediate stiffness carbon fibres. This makes them even less competitive than carbon fibres with respect to cheaper reinforcements or steel as a wire material. Although the price of these fibres might fall, their currently prohibitive cost excludes them from further serious materials selection.

1.7.1 Carbon fibre as a suitable reinforcement

Carbon fibres are produced from two main precursors; polyacrylonitrile (PAN) and pitch [53]. Pitch-derived fibres consist of highly oriented graphitic sheets that are characterised by large crystallites and small spacing between layers. This gives rise to high tensile stiffness and electrical conductivity parallel to the alignment of graphitic planes. This contrasts with high strength carbon fibres that are less stiff and conductive but possess greater extensibility [54]. Consequently, carbon fibre products have a wide range of mechanical properties, as demonstrated in Figure 1.8.

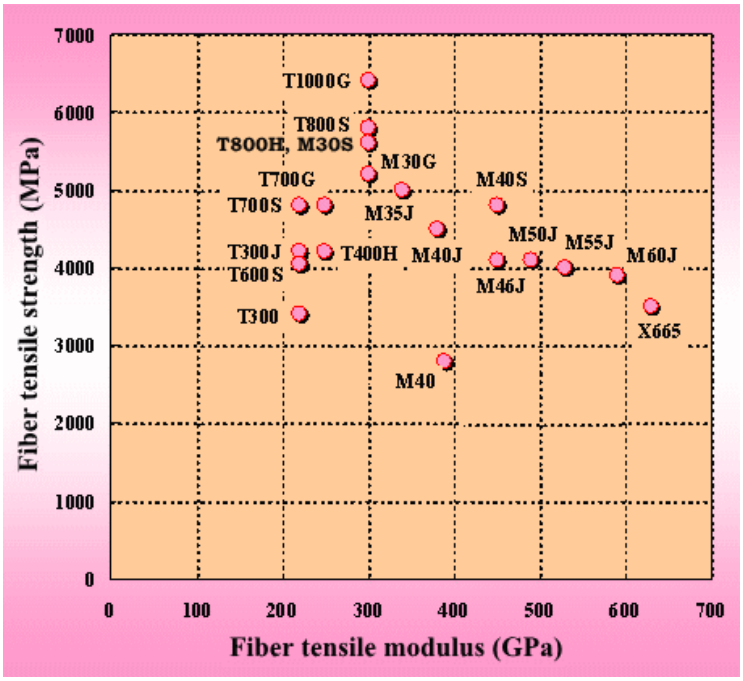

Figure 1.8 Strength and stiffness properties of carbon fibres manufactured by Torayca [50].

1.7.2 Stretch broken carbon fibres

Improvement in the flexibility of yarns has long been achieved in the textile industry by the practice of reducing the length of continuous filaments and spinning them into staple fibres [55]. When applied to FRP woven fabrics, this technique allows for better handling and draping in order to overcome the difficulty of forming FRPs into sharp curves and corners. An initial obstacle to the widespread application of this technology was an established distrust of fabrics that have been spun from intentionally shortened filaments, concerning higher cost of materials and variance in fibre length. However, products using stretch-broken fibres have since penetrated the composites market [56].

The introduction of discontinuities into long carbon fibres can be achieved by stretching the fibres until breaking [57]. By spinning the resulting discontinuous fibres, a tow can be achieved in which fibres are longer than the critical length above which the fibre may still fully contribute to axial and shear loading. ‘Stretch broken’ carbon fibre tows are commonly used for the creation of pre-forms, whereby the carbon fibres are spun together with thermoplastic filaments to create commingled tows. Fabrics that are woven from them benefit from an increased flexibility of the tows, while suffering from a moderate reduction in strength and stiffness [58].

1.7.3 Extensibility of carbon fibre as an additional criterion

Dynamic ropes can be expected to deform through bending and torsion, so it is not sufficient to design for axial displacement alone. The highest stiffness fibres are also the most brittle, with extension-to-break as little as 0.7%. Fibre misalignment during manufacture, movement of rods during stranding and helical winding of rods to create multi-stranded wire ropes further reduces the practical upper limit to axial extensibility offered by the components in a hybrid rope. Extensibility is therefore an important factor in choosing FRPs, with high strength carbon fibres offering greater flexibility than their high stiffness counterparts.

1.8 Matrix selection

While fibre reinforcement is mostly responsible for the strength and stiffness of FRPs, the polymer matrix plays an equally important role in determining most other properties. It is in this sense that the material is a reinforced plastic, even if by volume the matrix is a minority component. Matrix polymers can be drawn from a wide field, such as that shown in Figure 1.9. For the purposes of this project they should fulfil the following requirements:

- Mechanical
    - The polymer should not be unduly brittle since dynamic ropes undergo flexion during service. The polymer should also possess a high enough tensile strength and stiffness to permit load sharing between filaments.
    - High toughness is also a necessary quality for impact and cut resistance.
- Thermal
    - To be serviceable at the high temperatures encountered due to internal friction the mechanical properties of the polymer must not degrade. This requires a high heat deflection temperature and insensitivity to thermally promoted creep since working ropes have long periods of service.
- Microstructure
    - The polymer must be chemically compatible with the reinforcing fibre to ensure adequate bonding.

1.8.1 High performance thermoplastics

These criteria largely limit the selection to high performance thermoplastics:

- Mechanical
    - While thermosetting resins can be toughened in order to reduce the effect of crack propagation, the cross-linked networks of high performance epoxies are still brittle in comparison with many thermoplastic matrices.
    - Although vulcanised elastomeric matrices may surpass thermoplastics in toughness and flexibility, their inferior stiffness is undesirable as it may limit maximal load sharing between fibres.
- Thermal
    - Viscoelastic properties set an upper bound to the retention of strength and stiffness at high temperatures. Among thermoplastics, semi-crystalline polymers are known for their high service temperatures and long-term creep resistance.
- Chemical
    - Thermoplastics such as polypropylene and ultra-high molecular weight polyethylene are known for relatively low surface energies and inertness. While this is favourable for resistance to chemical degradation, it limits the degree to which these polymers can adhere to reinforcing fibres.

These criteria narrow the field to high performance thermoplastics. These polymers are known for high strength, stiffness, impact resistance and thermal stability, which is represented by high melting points and glass transition temperatures. Each polymer exhibits different traits and no single plastic is exemplary in every desired category. Some polymers have been adapted to take advantage of a combination of chemical properties, such as copolymierised polyamide-imides which have exceptional abrasion resistance. The disadvantages of these polymers are high material cost and difficulty in processing due to

their high viscosities. Thermoplastics tend to have viscosities ranging between 100Pas to 5000Pas, whereas thermosetting resins are typically in the region of 1Pas [59].

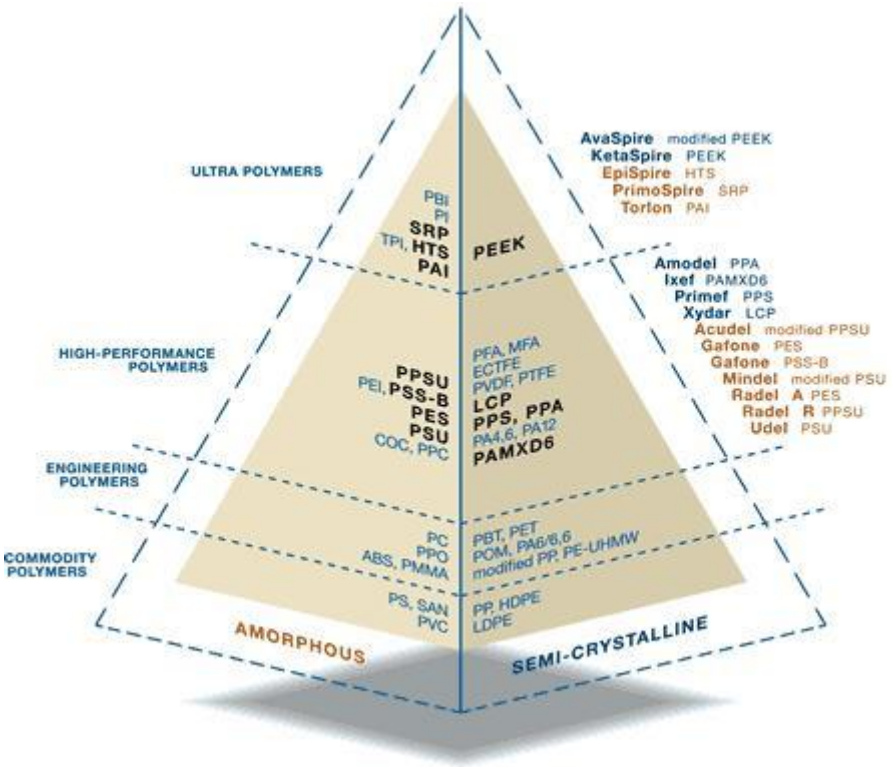

Figure 1.9 Hierarchy of plastics supplied by Solvay by applicability [60].

1.8.2 Polyamides

Polyamides are overwhelmingly used in synthetic fabrics and ropes. They can be aromatic or aliphatic, with aramids being those polyamides that have at least 85% of amide groups directly bonded to aromatic rings [23]. These materials are widely known by their trade names, such as Kevlar and Nomex, as developed by DuPont [61].

The properties of aliphatic polyamides are largely determined by the regular spacing of amide linkages along the backbone, which contribute to strong intermolecular forces between individual chains. Alternation between methylene and amide groups results in a combination of amorphous and crystalline regions, which yields properties that are intermediate between purely aliphatic and aromatic polymers. Closer spacing of amide groups correlates with higher stiffness, melting temperature and chemical stability, while even numbers of methylene intermediate groups are associated with higher melting temperatures [62].

Chemical structure therefore plays an important role in determining the applicability of the commercial nylons. Nylon 66, 6, 11 and 12 are the majority aliphatic polyamides by market consumption and are predominantly used in mechanical engineering applications, which take advantage of their stiffness, wear resistance, chemical stability and toughness [62].

1.9 Overview of FRP manufacture

Techniques for the manufacture of FRPs are manifold, though those involving the use of an autoclave have become predominant for the aerospace industry. Commercially significant methods include [63]:

- Autoclave curing of prepreg
    - The ability to achieve a high fibre volume fraction and controlled fibre structure with various reinforcing fibres makes pregreg a regular choice for high performance composites. Pre-impregnated plies can be laid flat or bent into ribs on the laminate surface. Cutting may be automated although lay-up is often done by hand.
    - This manufacturing route is characterised by a long production cycle when autoclave and hand lay-up time is considered. High costs may also be encountered due to the reliance on expensive equipment, labour intensive processes and low rates of production.
- Automated fibre placement
    - Automated processes seek to reduce waste and increase productivity, typically through the placement of individual strips of prepreg onto a desired mandrel. A part can be built up through repeated placement by a robotic head, which may heat the strips at the point of contact with a mandrel or mould.
    - Although this process may eliminate manual errors and in some cases obviate the need for autoclave curing, the cost of machinery and implementation still remains higher than conventional techniques for most applications.
- Hand lay-up of wet resin
    - Hand lay-up remains a popular manufacturing route for liquid resins that can be safely handled in workshop conditions. It is particularly well suited to prototyping and teams of skilled operators are competitive with automated processes in both the cost and rate of production.
    - Production lines involving wet lay-up often cure with a vacuum-assisted oven. In high performance applications the lower void contents offered by autoclaves are favourable, though the rate of production is considerably lower.
- Resin transfer moulding
    - In addition to infusion this is route represents an automated alternative to wet lay-up or pre-impregnation. A dry reinforcing component is placed into a mould and resin is injected into the moulding under pressure.
    - This method is typically only competitive for large and complex artefacts where the cost of the mould is justifiable and where the viscosity of the resin is not prohibitive and the dry fibre pre-form is sufficiently permeable.
- Pultrusion
    - Dry fibres are pulled through an impregnation stage and a heated die in a single automated process.
    - Pultrusion is one of the few truly continuous composite manufacturing routes with one of the lowest capital costs. It is limited by the die shape and continuity of the cross-section, making it only practical for repeated manufacture of similar pieces.

1.9.1 Autoclave

This is the predominant route by which the highest quality FRP components are made, from small test panels to the fuselages of aircraft. Autoclaves are typically used to cure panels made from prepregs, which offer consistently high fibre volume fractions. After manual or

automated lay-up a part is placed into a vacuum bag and heated under pressure, as shown in Figure 1.10. The consolidation of a thermoplastic composite is shorter than the cure cycle of a thermosetting resin but may require a higher pressure and temperature during consolidation due to the relatively high resin viscosity [64].

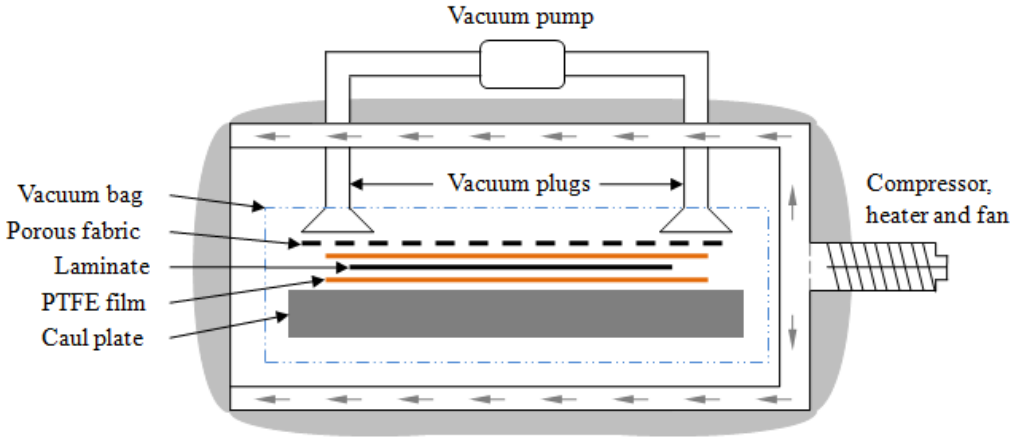

Figure 1.10 Vacuum consolidation and cure of a laminate inside of an autoclave.

Processing of thermoplastic composites follows distinct phases of melting, consolidation and solidification:

- Plies may be autoclaved and the entire composite heated through its thickness. By contrast prepreg tape for filament winding is intensely heated at the location at which the unconsolidated segment is applied to the existing structure [65].
- The temperature is held following melting and pressure is applied during a consolidation stage to minimise the concentration of voids. This encourages permeation of the fibre architecture and ensures that the resin adequately flows around the fibres [66].
- Pressure is maintained while the composite cools below the glass transition temperature to maintain dimensional stability. The rate of cooling determines the crystallinity of semi-crystalline thermoplastics such as PEEK [67].

1.9.2 Wet lay-up

Wet lay-up is most commonly used with thermosetting resins. The resin is mixed with a hardener and is dappled or pressed into dry fabrics at ambient temperatures below the gel point. The part is then either vacuum bagged or placed directly into an oven. Resin bleed-out has a crucial role to play in controlling the fibre volume fraction so panels made this way are rarely cured under pressure [68]. Lay-up in thermoplastics is complicated by the stiffness of the plies and lack of adhesion to a mould below the melting temperature. Adhesion techniques usually involve welding or thermoforming plies to a mould surface [69].

1.9.3 Pultrusion

Fibres are drawn through a die after impregnation by a resin, which may be thermosetting or thermoplastic. All pultrusion lines have some or all of the following features, as shown in Figure 1.11 [70]:

- Creels
    - Fibres are unloaded from bobbins subjected to constant tension.
- Guides/spreaders

  - Fibres are separated to expose the greatest possible surface area for impregnation.
- Heating before and after impregnation
  - Pre-heating may improve adhesion between the resin and fibres.
  - Post-heating allows partial consolidation if interruption of pultrusion is desired.
- Impregnation chamber
  - Adhesion of the polymer to the fibres.
- Heating die
  - Consolidation or curing of the resin to the fibres.
- Cooling unit
  - In-line cooling of the consolidated article.
- Pullers/downstream processing
  - Pulling force and speed are critical parameters for finished article properties.
  - Downstream processes may include cutting, coating and storage.

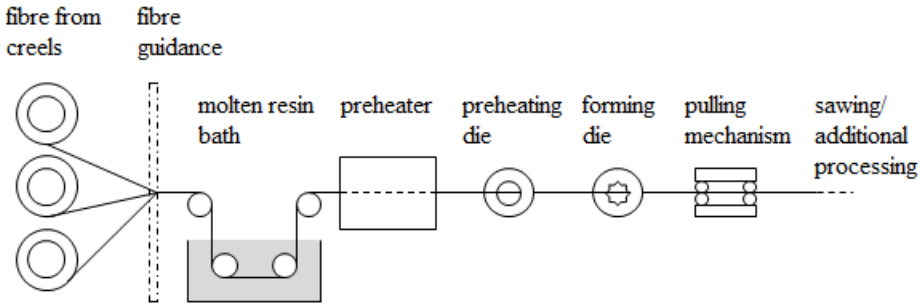

Figure 1.11 In-line thermoplastic pultrusion [71].

1.10 Finite element modelling of ropes

Application of the finite element method to rope applications evolved from attempts to numerically solve analytical models, such as those developed by Feyrer [18] for wire ropes or van Luijk [72] for fibre yarns. Early development in the finite element modelling of ropes focussed on simulating the interrelationships between mechanical processes, such as the simultaneous torsional, bending and axial deformation of a rope [73]. This enabled a holistic approach to characterising wire rope systems, which came to supplement a growing body of understanding about steel wire ropes at a time when demand for offshore mooring was being met by longer and heavier ropes [74]. While previous experimental datasets, such as those produced by Costello et al. [75], focussed on bending and torsional effects, the study of contact between wires became increasingly pertinent to researchers. The complexity of contact between wires, including deformation, friction and plasticity necessitated the use of finite element modelling to accurately predict the behaviour of ropes [76]. This was applied to the simulation of multi-layered ropes with many points of crossover between individual wires [77].

Parallel developments in the simulation of ancillary processes, such as rope termination, have highlighted the importance of finite element modelling in aiding the design process for meeting strength and endurance specifications [78]. As finite element modelling became more widely utilised in the design of ropes and hoisting systems, techniques were developed to cope with the high computational cost of modelling nonlinear behaviour [79]. These strategies have included the use of connector elements [80] and the simulation of a representative cross-section of the rope that is either analysed in isolation or is mirrored with

symmetry conditions [81]. However, a disadvantage of simplifying the rope system is to reduce the range of properties that can be accurately represented by the model. This may introduce errors in prediction when phenomena that rely on the complex interrelationship between parameters are indirectly inferred from such models [82].

The need for increasingly representative models and the steady decrease in the cost of computational resources have promoted the increasingly widespread use of 3D elements to simulate whole segments of ropes. In doing so, researchers encountered a design challenge in generating helical geometries, which has stimulated the adaptation of commercial software packages to create accurate representations [83-86]. State-of-the-art in finite element modelling increasingly simulates whole lay-lengths of ropes and seeks to estimate properties such as contact stresses between wires that are not directly observable [87-89].

Simulation of steel ropes still encounters problems of insufficient experimental data to validate models [90]. While knowledge is increasingly abundant for steel wire ropes, at the time of writing there are no experimental datasets or publications relating to the simulation of hybrid steel and FRP strands. This suggests a need for both the experimental and numerical analysis of hybrid strands.

1.11 Concluding summary

Steel wire ropes represent an important innovation in hoisting technology and through steady advances in metallurgy and stranding will continue to improve in strength and durability. Although in many ways a proven and reliable material, the high density of steel sets a practical upper limit to the strength-to-weight ratio achievable for wire ropes. This is an important factor in hoisting applications where the self-weight of a steel wire rope significantly reduces the productivity of deep mine shafts. Lightweight synthetic fibre materials have been proposed as an alternative means of obtaining higher strength-to-weight ratios but lack the long-term durability for use in dynamic ropes. Hybrid ropes, in which the inner core of a steel wire rope is replaced with a lower density polymeric material, may take advantage of the established strength and durability of the outer steel wires while benefiting from reduced overall weight afforded by the lighter core.

An ideal core material will complement the outer steel wires by adequately sharing load, which is maximal for materials of similar stiffness. Unlike parallel fibre bundles, the fibres within FRPs are chemically bound together and internally act in unison under an external load. This gives advantages in lower internal friction and higher bending stiffness as well as a solid cross-section. These features suggest that a FRP core may be more compatible with outer steel wires than a parallel fibre core. Owing to their superior strength and stiffness, carbon fibre has been identified as a suitable reinforcement, while a balance of high stiffness, toughness and temperature stability make high performance thermoplastics appropriate matrix polymers.

Pultrusion is a cost effective and well established technique for the production of unidirectional FRPs with constant cross-section. Chapter 2 covers the design and construction of an in-house pultruder for the purpose of manufacturing carbon fibre/thermoplastic pultruded rods from a range of feedstocks for use in making hybrid strands. This features a discussion of the design process and selection of processing technologies, which included mechanical fibre spreading, electrostatic powder impregnation, pre-heating and consolidation of impregnated tows, water cooling and traction pulling of consolidated rods.

The characterisation of the tensile strength and stiffness of hybrid strands requires novel testing techniques. The development of the methodology has been outlined in Chapter 4 and results have been presented in Chapter 5. Additionally, finite element modelling has thus far been limited to the simulation of ropes and strands with steel wires. Chapter 6 presents the results of the novel use of simulation techniques to predict the tensile strength and stiffness of hybrid strands.

1.12 References

1. Mökkönen, T., New AMS dates of the neolithic and bronze age ceramics. Estonian Journal of Archaeology, 2008. 15(1)
2. James, T.G.H., A Wooden Figure of Wadjet with Two Painted Representations of Amasis. The Journal of Egyptian Archaeology, 1982. 68, p. 156-165
3. Grim, J. and M.E. Grim, Viewing the Hana Matsuri at Shimoawashiro, Aichi Prefecture. Asian Folklore Studies, 1982. 41(2), p. 163-185
4. Judges 16:12, in Old Testament.
5. Bohr, J. and K. Olsen, The ancient art of laying rope. EPL (Europhysics Letters), 2011. 93(6), p. 60004
6. Lucas, A., Harris, J. R., Ancient Egyptian Materials and Industries. 4th ed. 2000, Dover Publications
7. Herodotus, The Histories. Vol. Book VII (The Persian War).
8. Hammond, N.G.L. and L.J. Roseman, The Construction of Xerxes' Bridge over the Hellespont. The Journal of Hellenic Studies, 1996. 116, p. 88-107
9. Sear, F., Roman Architecture. New ed. 1998, Routledge
10. Spate, O.H.K., Geographical Aspects of the Industrial Evolution of London Till 1850. The Geographical Journal, 1938. 92(5), p. 422-432
11. McCord, I., Improvement in the mode of manufacturing round flexible wire ropes for steering. 1839: United States
12. Roebling, J.A., Improvement in tops for wire ropes. 1849: United States
13. Barraclough, K.C., Steel Making Before Bessemer: Blister Steel - The Birth of an Industry. 1st ed. Vol. 1. 1984, IOM Communications Ltd
14. Artzybasheff, B., Machinalia, in As I See. 2008, Titan
15. Jürgen, K.H., et al., Wire ropes, in Encyclopedia of Materials: Science and Technology, K.H.J. Buschow, et al., Editor. 2001, Pergamon
16. Beltran, J.F. and E.B. Williamson, Degradation of rope properties under increasing monotonic load. Ocean Engineering, 2005. 32(7), p. 826-844
17. Miller, B.A., Wire Ropes, in Encyclopedia of Materials: Science and Technology, K.H.J. Buschow, W.C. Robert, C.F. Merton, I. Bernard, J.K. Edward, M. Subhash, and V. Patrick, Editors. 2004, Elsevier Oxford. p. 1-10
18. Feyrer, K., Wire Ropes: Tension, Endurance, Reliability. Illustrated ed. 2007, Berlin, Springer
19. Foster, G.P., Advantages of Fiber Rope Over Wire Rope. Journal of Industrial Textiles, 2002. 32(1), p. 67-75
20. McKenna, H.A., Hearle, J. W. S., O'Hear, N., Handbook of Fibre Rope Technology. 2004, Cambridge, Woodhead Publishing
21. Richardson, G.M., H.E. Stanley, and W.W. Heckert, RECENT PROGRESS IN POLYAMIDE AND POLYESTER FIBERS. Annals of the New York Academy of Sciences, 1957. 67(11), p. 910-931

22. Petruska, D., J. Geyer, R. Macon, M. Craig, A. Ran, and N. Schulz, Polyester mooring for the Mad Dog spar--design issues and other considerations. Ocean Engineering, 2005. 32(7), p. 767-782
23. García, J.M., F.C. García, F. Serna, and J.L. de la Peña, High-performance aromatic polyamides. Progress in Polymer Science, 2010. 35(5), p. 623-686
24. Chae, H.G. and S. Kumar, Rigid-rod polymeric fibers. Journal of Applied Polymer Science, 2006. 100(1), p. 791-802
25. Del Vecchio, C.J.M., Light weight materials for deep water moorings, in Department of Engineering. 1992, University of Reading
26. Edwards, F.A., Hoisting Systems, in SME Mining Engineering Handbook, H.L. Hartman, Editor. 1996, Society for Mining, Metallurgy, and Exploration, Inc.
27. Dietz, P., Lohrengel, A., Schwarzer, T., Wächter, M., Problems related to the design of multi layer drums for synthetic applications, in OIPEEC. 2009: Stuttgart, Germany
28. Gilmore, J., D. Stenvers, R. Chou, Mts, and Ieee, Some Recent Developments of Rope Technologies - Further Enhancements of High Performance Ropes, in Oceans 2008, Vols 1-4. 2008, Ieee New York. p. 82-88
29. Neslow, K., Wire rope with load-carrying fiber elements. 1979, Google Patents
30. Data, H.L., R.B. Hoganson, and D.A. Klees, Rope with fiber core and method of forming same. 1989, Google Patents
31. Ridge, I.M.L., O'Hear, N., Verreet, R., Grabandt, O., Das, C.A., High strength fibre cored steel wire rope for deep hoisting applications, in OIPEEC Conference. 2007: Johannesburg, South Africa
32. Rebel, G., R. Verreet, U. Briem, and AusImm, Composite steel wire ropes for mine hoisting applications. Hoist and Haul 2005. Vol. 2005. 2005. 381-390
33. Bakis, C.E., L.C. Bank, V.L. Brown, E. Cosenza, J.F. Davalos, J.J. Lesko, A. Machida, S.H. Rizkalla, and T.C. Triantafillou, Fiber-reinforced polymer composites for construction-state-of-the-art review. Journal of Composites for Construction, 2002. 6(2), p. 73-87
34. Rasmussen, W.W., P.P. Riggs, and N.H. Simpson, Fiber reinforced plastic impregnated wire rope. 1983, Google Patents
35. Kenji Honda, d. and T. Sawafuji, Composite rope and manufacture thereof. 1987, Google Patents
36. Wells, H.C., R.L. Edmonds, N. Kirby, A. Hawley, S.T. Mudie, and R.G. Haverkamp, Collagen Fibril Diameter and Leather Strength. Journal of Agricultural and Food Chemistry, 2013. 61(47), p. 11524-11531
37. Ikeda, T., Fiber-reinforced composite cable. 1992, Google Patents
38. O'Leary, D.N. and G.E. Attenburrow, Differences in strength between the grain and corium layers of leather. Journal of Materials Science, 1996. 31(21), p. 5677-5682
39. Lohrengel, A., Stahr, K., Wachter, M. Simulation of fibre ropes and their effects on the strain scenario of multi-layer wound rope drums. in Simulating Rope Applications. 2013. Oxford, OIPEEC
40. Bhatnagar, A. and S.C. Lakkad, Temperature and orientation dependence of the strength and moduli of glass reinforced plastics. Fibre Science and Technology, 1981. 14(3), p. 213-219
41. Hull, D., Clyne, T. W., Elastic Properties, in An Introduction to Composite Materials. 1996, Cambridge University Press Cambridge. p. 81-101
42. Huang, H. and R. Talreja, Effects of void geometry on elastic properties of unidirectional fiber reinforced composites. Composites Science and Technology, 2005. 65(13), p. 1964-1981

43. Visiongain, The Composites Market 2013-2023: Glass Fibre (GFRP), Carbon Fibre (CFRP) & Aramid Fibre (AFRP). 2013
44. Experts, I., Carbon Fibers & Carbon Fiber Reinforced Plastics (CFRP) - A Global Market Overview. 2013
45. Marsh, E., Introduction, in Market developments in composites in infrastructure - Building new markets, E. Marsh, Editor. 2000, Elsevier Amsterdam. p. 1-31
46. Hartman, D., Greenwood, M. E., Miller, D. M., High strength glass fibres. 2006, AGY, Owens Corning: South Carolina
47. Giannelis, E.P., Polymer-layered silicate nanocomposites: Synthesis, properties and applications. Applied Organometallic Chemistry, 1998. 12(10-11), p. 675-680
48. Shim, V.P.W., C.T. Lim, and K.J. Foo, Dynamic mechanical properties of fabric armour. International Journal of Impact Engineering, 2001. 25(1), p. 1-15
49. Ellis, T.S. and J.S. D'Angelo, Thermal and mechanical properties of a polypropylene nanocomposite. Journal of Applied Polymer Science, 2003. 90(6), p. 1639-1647
50. Ali, M.A.-h. and R.H. Elleithy, Viscoelastic properties of polypropylene/organo-clay nano-composites prepared using miniature lab mixing extruder from masterbatch. Journal of Applied Polymer Science, 2011. 121(1), p. 27-36
51. So, Y.-H., Rigid-rod polymers with enhanced lateral interactions. Progress in Polymer Science, 2000. 25(1), p. 137-157
52. So, Y.-H., S.J. Martin, K. Owen, P.B. Smith, and C.L. Karas, A study of benzobisoxazole and benzobisthiazole compounds and polymers under hydrolytic conditions. Journal of Polymer Science Part A: Polymer Chemistry, 1999. 37(14), p. 2637-2643
53. Chung, D.D.L., Processing of carbon fibers, in Carbon Fiber Composites. 1994, Butterworth-Heinemann
54. Mochida, I., S.H. Yoon, N. Takano, F. Fortin, Y. Korai, and K. Yokogawa, Microstructure of mesophase pitch-based carbon fiber and its control. Carbon, 1996. 34(8), p. 941-956
55. Dae Hoon Lee, U. Chowdhary, Moon Hwo Seo, and Boong Soo Jeon, Effect of the Stretch Breaking Process on Fiber Length Distribution. Textile Research Journal, 2009. 79(7), p. 626-631
56. Black, S., Aligned discontinuous fibres come of age, in Composites World. 2008, Gardner Publications
57. Ross, R., Will stretch-broken carbon fiber become the new material of choice?, in Composites World. 2006, Gardner Publications
58. Gibson, A.G. and J.A. Månson, Impregnation technology for thermoplastic matrix composites. Composites Manufacturing, 1992. 3(4), p. 223-233
59. Drozdov, A.D. and J. deC. Christiansen, Cyclic viscoelastoplasticity of polypropylene/nanoclay composites. Mechanics of Time-Dependent Materials, 2012. 16(4), p. 397-425
60. Grande, J.A. New 'Ultra' Thermoplastics Contend for Top of Performance Pyramid. 2007 04/09/2011; January 2007: http://www.ptonline.com/articles/new-'ultra'-thermoplastics-contend-for-top-of-performance-pyramid
61. McGrail, P.T., Polyaromatics. Polymer International, 1996. 41(2), p. 103-121
62. Kohan, M.I., Polyamides and Polyimides, in Plastics Materials, J.A. Brydson, Editor. 1999, Butterworth-Heinemann Oxford. p. 478-530
63. Strong, A.B., Fundamentals of Composites Manufacturing. 1st ed, ed. C.A. Ploskonka. 1989, Dearborn, Society of Manufacturing Engineers

64. Bader, M.G., Selection of composite materials and manufacturing routes for cost-effective performance. Composites Part A: Applied Science and Manufacturing, 2002. 33(7), p. 913-934
65. Funck, R. and M. Neitzel, Improved thermoplastic tape winding using laser or direct-flame heating. Composites Manufacturing, 1995. 6(3-4), p. 189-192
66. Ye, L., K. Friedrich, J. Kästel, and Y.-W. Mai, Consolidation of unidirectional CF/PEEK composites from commingled yarn prepreg. Composites Science and Technology, 1995. 54(4), p. 349-358
67. Gao, S.-L., Kim, J-K. Crystallinity and interphase properties of carbon fiber/PEEK matrix composites. in ICCM 12. 2000. Paris
68. Stringer, L.G., Optimization of the wet lay-up/vacuum bag process for the fabrication of carbon fibre epoxy composites with high fibre fraction and low void content. Composites, 1989. 20(5), p. 441-452
69. Andersen, B.J. and J.S. Colton, Automation of Thermoplastic Composite Processing. Journal of Composite Materials, 1990. 24(2), p. 150-174
70. Starr, T.F., Pultrusion for engineers. 2000, Cambridge, Woodhead Publishing
71. Van de Velde, K. and P. Kiekens, Thermoplastic pultrusion of natural fibre reinforced composites. Composite Structures. 54(2-3), p. 355-360
72. Djaja, R.G., P.J. Moss, A.J. Carr, G.A. Carnaby, and D.H. Lee, Finite Element Modeling of an Oriented Assembly of Continuous Fibers. Textile Research Journal, 1992. 62(8), p. 445-457
73. Chiang, Y.J., Characterizing simple-stranded wire cables under axial loading. Finite Elements in Analysis and Design, 1996. 24(2), p. 49-66
74. Hobbs, R.E. and M. Raoof, Behaviour of cables under dynamic or repeated loading. Journal of Constructional Steel Research, 1996. 39(1), p. 31-50
75. Conway, T.A. and G.A. Costello, Response of a strand with elliptical outer wires. International Journal of Solids and Structures, 1991. 28(1), p. 33-42
76. Jiang, W.G., M.S. Yao, and J.M. Walton, A concise finite element model for simple straight wire rope strand. International Journal of Mechanical Sciences, 1999. 41(2), p. 143-161
77. Jiang, W.G., J.L. Henshall, and J.M. Walton, A concise finite element model for three-layered straight wire rope strand. International Journal of Mechanical Sciences, 2000. 42(1), p. 63-86
78. Bradon, J.E., C.R. Chaplin, and I.M.L. Ridge, Analysis of a resin socket termination for a wire rope. Journal of Strain Analysis for Engineering Design, 2001. 36(1), p. 71-88
79. Smith, R.G., Reiter, W. F., Vitupier, G., Lovejoy, S. C., Nonlinear Modeling of Flexible Cable Loads on Large Sheaves. Journal of Bridge Engineering, 2005. 10(1), p. 5-11
80. Lugrís, U., J.L. Escalona, D. Dopico, and J. Cuadrado, Efficient and accurate simulation of the rope–sheave interaction in weight-lifting machines. Proceedings of the Institution of Mechanical Engineers, Part K: Journal of Multi-body Dynamics, 2011. 225(4), p. 331-343
81. Jiang, W.-G. and J.L. Henshall, Torsion-extension coupling in initially twisted beams by finite elements. European Journal of Mechanics - A/Solids, 2001. 20(3), p. 501-508
82. Jiang, W.-G., M.K. Warby, and J.L. Henshall, Statically indeterminate contacts in axially loaded wire strand. European Journal of Mechanics - A/Solids, 2008. 27(1), p. 69-78

83. Stanova, E., G. Fedorko, M. Fabian, and S. Kmet, Computer modelling of wire strands and ropes Part I: Theory and computer implementation. Advances in Engineering Software, 2011. 42(6), p. 305-315
84. Erdönmez, C. and C.E. İmrak, New Approaches for Model Generation and Analysis for Wire Rope, in Computational Science and Its Applications - Iccsa 2011, Pt Iv, B. Murgante, O. Gervasi, A. Iglesias, D. Taniar, and B.O. Apduhan, Editors. 2011, Springer-Verlag Berlin Berlin. p. 103-111
85. Erdönmez, C. and C.E. İmrak, Modeling Techniques of Nested Helical Structure Based Geometry for Numerical Analysis. Strojniski Vestnik-Journal of Mechanical Engineering, 2011. 57(4), p. 283-292
86. İmrak, C.E. and C. Erdönmez, ON THE PROBLEM OF WIRE ROPE MODEL GENERATION WITH AXIAL LOADING. Mathematical & Computational Applications, 2010. 15(2), p. 259-268
87. Judge, R., Z. Yang, S.W. Jones, and G. Beattie, Full 3D finite element modelling of spiral strand cables. Construction and Building Materials, 2012. 35, p. 452-459
88. Fontanari, V., M. Benedetti, and B.D. Monelli, Elasto-plastic behavior of a Warrington-Seale rope: Experimental analysis and finite element modeling. Engineering Structures, 2015. 82, p. 113-120
89. Stanova, E., G. Fedorko, S. Kmet, V. Molnar, and M. Fabian, Finite element analysis of spiral strands with different shapes subjected to axial loads. Advances in Engineering Software, 2015. 83, p. 45-58
90. Ghoreishi, S.R., T. Messager, P. Cartraud, and P. Davies, Validity and limitations of linear analytical models for steel wire strands under axial loading, using a 3D FE model. International Journal of Mechanical Sciences, 2007. 49(11), p. 1251-1261

2 Design and construction of the pultruder

A pultrusion line was built in the Composite Systems Innovation Centre for the production of carbon fibre reinforced thermoplastic rods. As described in §1.9.3, pultrusion represents a cost effective and highly productive means of manufacturing unidirectional FRPs with continuous cross-sections. While there are numerous European commercial and academic organisations with the ability to produce composite pultruded sections from thermosetting resins, at the time of writing there are far fewer bodies involved with the pultrusion of engineering thermoplastics. A bespoke machine within the department offered the best opportunity to obtain rods from these materials.

2.1 Design process

Above all, the pultrusion line would have to be flexible in the range of materials it could process. As had already been established through the materials selection in §1.6, a successful FRP for this application would most likely be a carbon fibre reinforced engineering thermoplastic. With this in mind, each individual operation within the pultrusion line was separately designed according to restrictions of budget, time and floor space. The following principles were adhered to in designing the pultrusion line:

- Flexibility
    - The pultrusion line would have to accommodate a number of different operating parameters, including the range of materials, speed of production, temperature of consolidation and sample length.
- Balance between processes
    - A large number of processes needed to be balanced, requiring each component to be adaptable and to work smoothly in concert with others.
- Lab-scale
    - The pultrusion line would have a limited space in which to work, which would set a close limit to the size of the machine and its consumption of materials.
- Modular
    - The machine would have to be made from modular components that could easily be removed or replaced as extensive optimisation was anticipated. It was also forecast that the department would move buildings at some time during the project and that the machine would need to move with it.
- Project limitations
    - The pultrusion line would be constrained by the funds and duration available to the project.

2.1.1 Initial design plan

Design and construction of the pultruder began with a proposal to academic and industrial partners. It featured a design plan that sought to provide cost-effective solutions for each of the individual processes found in a pultrusion line, as previously summarised in 1.9.3. The following technologies were planned for the pultrusion line, as is shown in Figure 2.1, which contrast with the completed pultrusion line that is shown in Figure 2.2:

- Creels
    - Carbon fibre bobbins with springs to provide resistance to unwinding, in order to maintain tension in the tows for fibre alignment. Later in the construction phase this was found superseded by the discovery of spreading by pinch rollers.

- Guides/spreaders
  - After collimation with brass eyelets, the tows were intended to be spread solely by passing them over and under wooden rollers. In actuality, spreading would be entirely replaced by a single pinch roller.
- Heating before and after impregnation
  - A heater before powder impregnation was intended to lower surface tension in the fibres for better adhesion. However, this was quickly abandoned because the credibility of the idea was not supported by the work of other researchers.
  - A tube furnace was planned in order to soften of the powder in impregnated tows. This was found to be too expensive and a tube pre-heater was later improvised.
- Impregnation chamber
  - Electrostatic powder impregnation was identified as being most appropriate for this project and was the technology that was later employed. However, a planned facility for the mixing and blending of powders was outside of the scope of the project.
- Heating die
  - Cartridge heaters sunk into the body of the die were expected to provide heating. These were eventually replaced with a more economical heating strip.
- Cooling unit
  - A series of cooling basins in which the rods would be showered with cold water and dried between stages was abandoned due to lack of space and the impracticality of this cooling technique.
- Pullers/downstream processing
  - Motorised caterpillar threads were expected to be bought wholesale from a single supplier without need for assembly from a number of components. Manual cutting with a knife was planned until it became clear that it would not be possible to cut the rods by hand while the pultruder was still running.

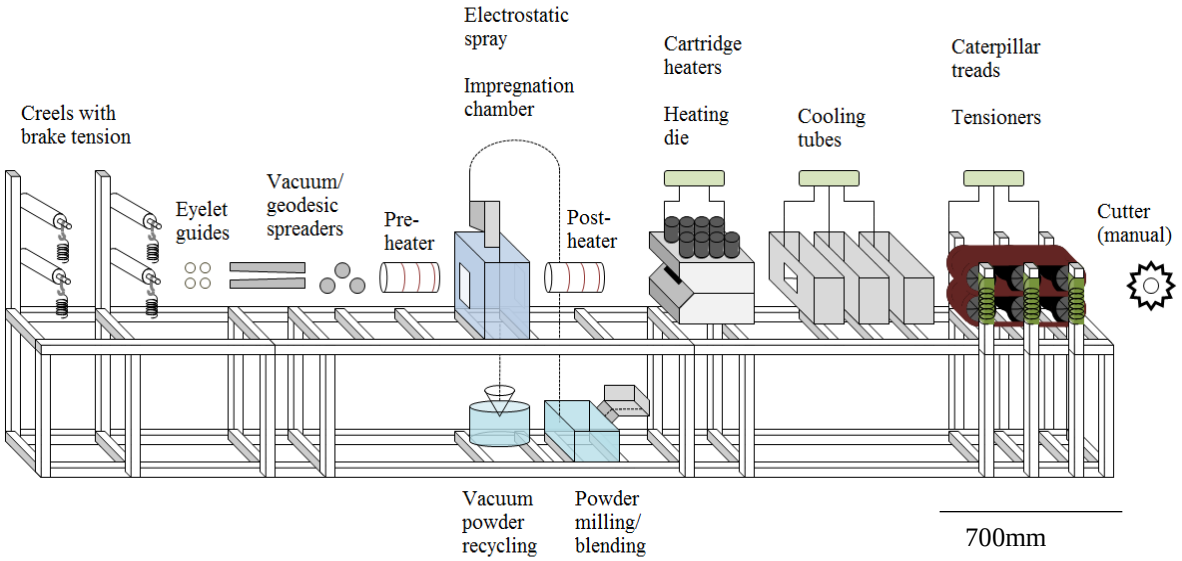

Figure 2.1 Schematic diagram of the prototype designed at the project's conception.

The design process for each stage of the pultrusion line and the actual solutions that were employed are covered in greater detail in the following sections of this chapter. A complete list of components, suppliers and prices at the time of purchase can be found in Appendix D.

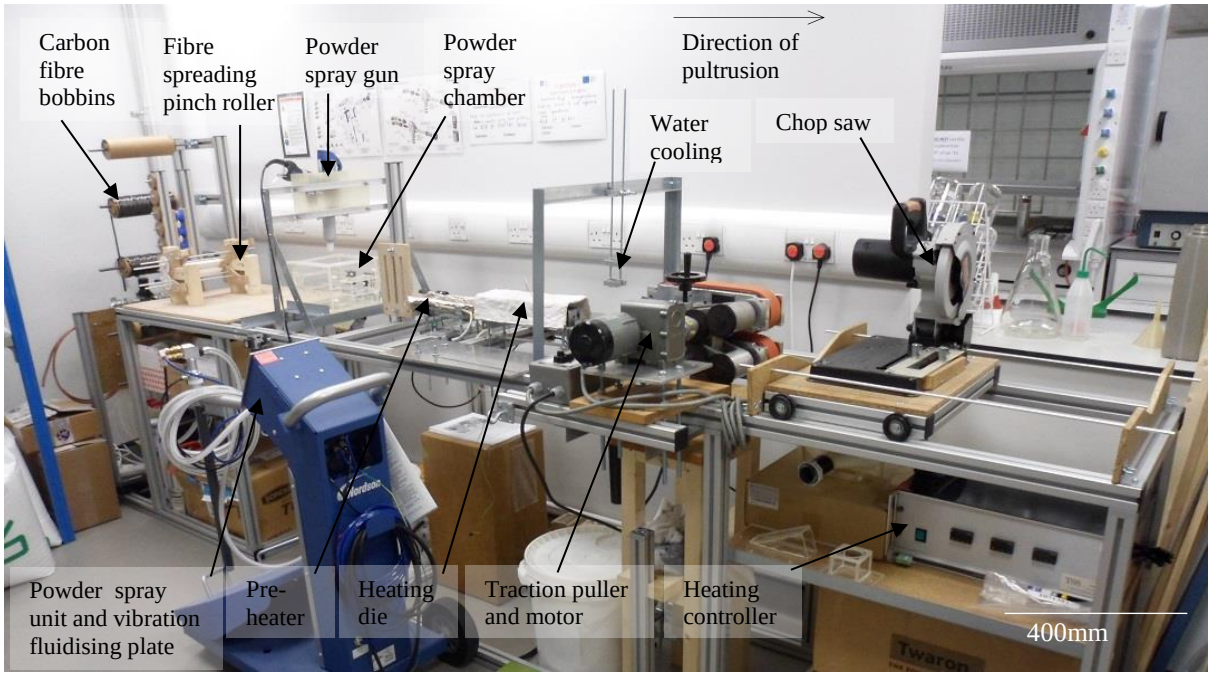

Figure 2.2 The pultrusion line designed and built at the Composite Systems Innovation Centre, University of Sheffield.

2.2 Fibre delivery

Carbon fibre tows were unloaded from bobbins placed on racks at the beginning of the line. The tension in the bobbins was initially controlled by the tension in polypropylene strands looped around pulleys that were attached to the bobbins. These were fed over smooth acetal plastic pulleys and delivered into the fibre spreading section, which can be seen in Figure 2.3. However, this system became redundant as the control of fibre tension was later governed solely by a set of rollers. Brass eyelets were previously used to collimate the delivery of fibres but were found to unnecessarily pinch the tows.

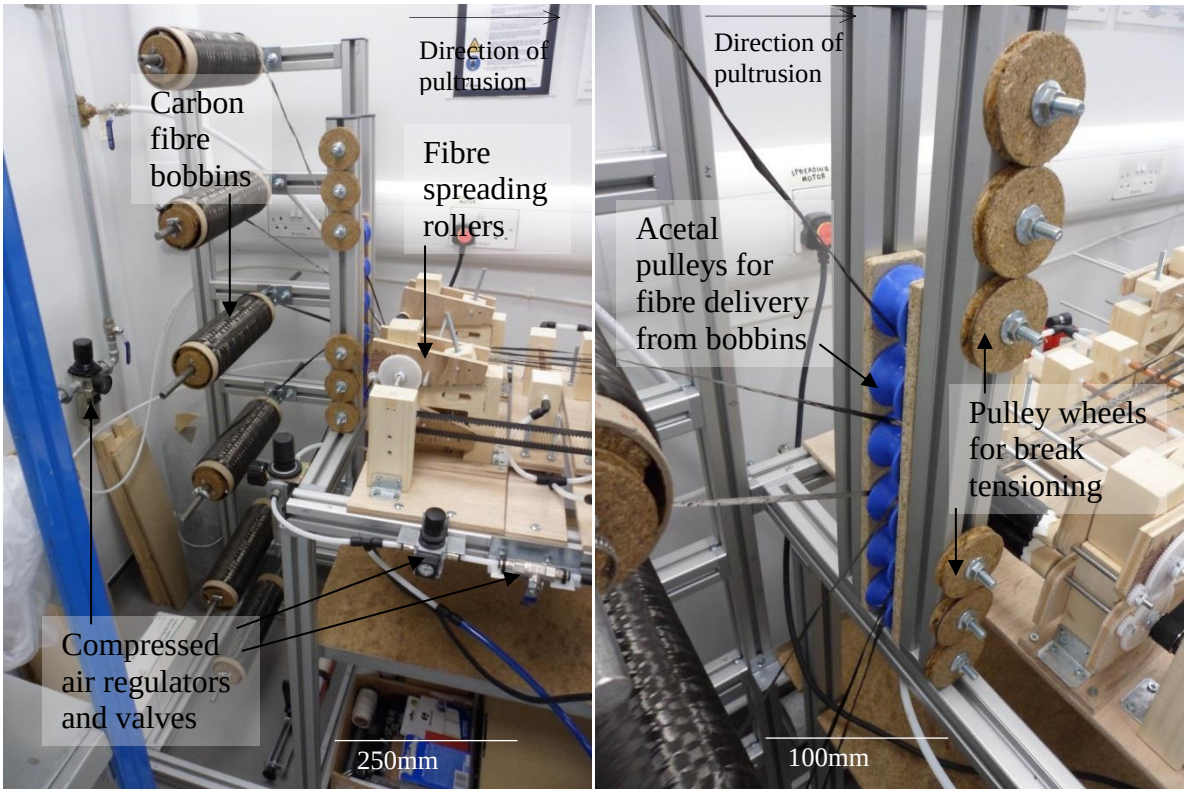

Figure 2.3 Fibres delivered from bobbins and carried over pulleys to the first pinch roller.

2.3 Fibre tension and spreading

Consistency in the tension of tows improves article reproducibility [1] by promoting fibre alignment [2]. This can be achieved by a number of methods including resistance from magnets or electric servo motors. The simplest case, which is well suited to providing relatively low tension, is spring braking in which tension can be controlled linearly with extension of the spring.

The degree to which tows are impregnated is dependent on the available surface area of the fibres and the probability with which polymer particles reach vacant fibre sites. Fibre spreading is essential for improving coverage and may be achieved by mechanical or pneumatic separation. Mechanical spreading often involves passing the fibres over and under pins or convex rollers [3]. Pneumatic spreading encourages fibre separation by pulling the fibres towards a region of low air pressure, such as that encountered in a Venturi slot [4]. Examples are provided in Figure 2.4.

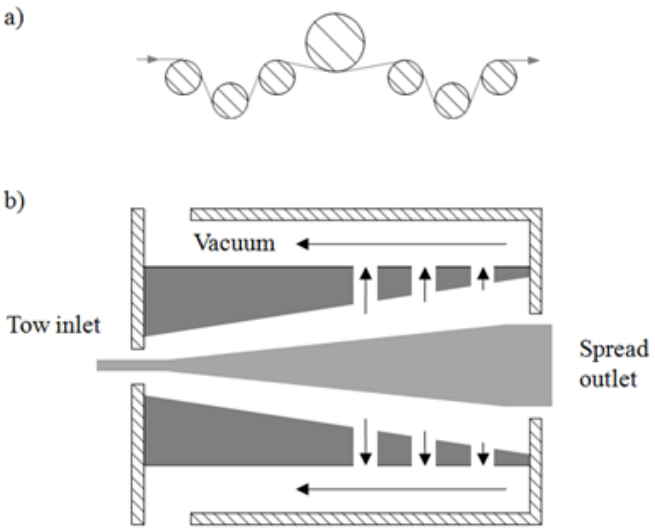

Figure 2.4 A schematic diagram showing a) mechanical spreading over and under rollers and b) spreading using a Venturi slot.

2.3.1 Mechanical spreading

Spreading using only the assistance of rollers was attempted first. For this purpose, wooden tool handles were smoothed with lacquer, so that unsized carbon fibres would not split or tear when moving across blemishes on the surface. Over time, the lacquer became worn and stained but otherwise proved sufficiently tough to withstand abrasive damage from the highly tensioned fibres as they moved across the rollers.

The first attempt involved a shadow board into which the rollers were bolted, with the intention that the tows would be forced to snake over and under the rollers, as seen in Figure 2.5. The tows were expected to spread out as they conformed to the rounded profile of the rollers. However, it quickly became apparent that the carbon fibres could not easily traverse the 180° turns between one roller and the next without some degree of fibre breakage.

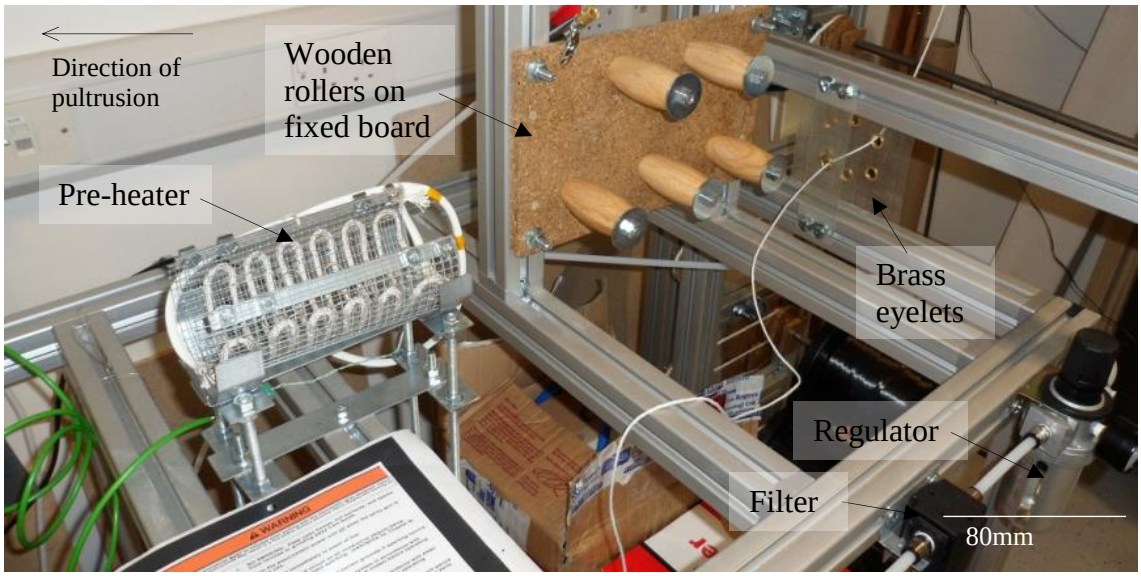

Figure 2.5 Large and fixed separation between wooden rollers.

The fixed-hole shadow board was replaced with long slots for adjusting the height of the rollers, shown in Figure 2.6. An improved arrangement was found in which the tows were staggered as they entered the spreading section. This permitted a shallower angle, which was more forgiving on the wooden rollers and less likely to harm the fibres.

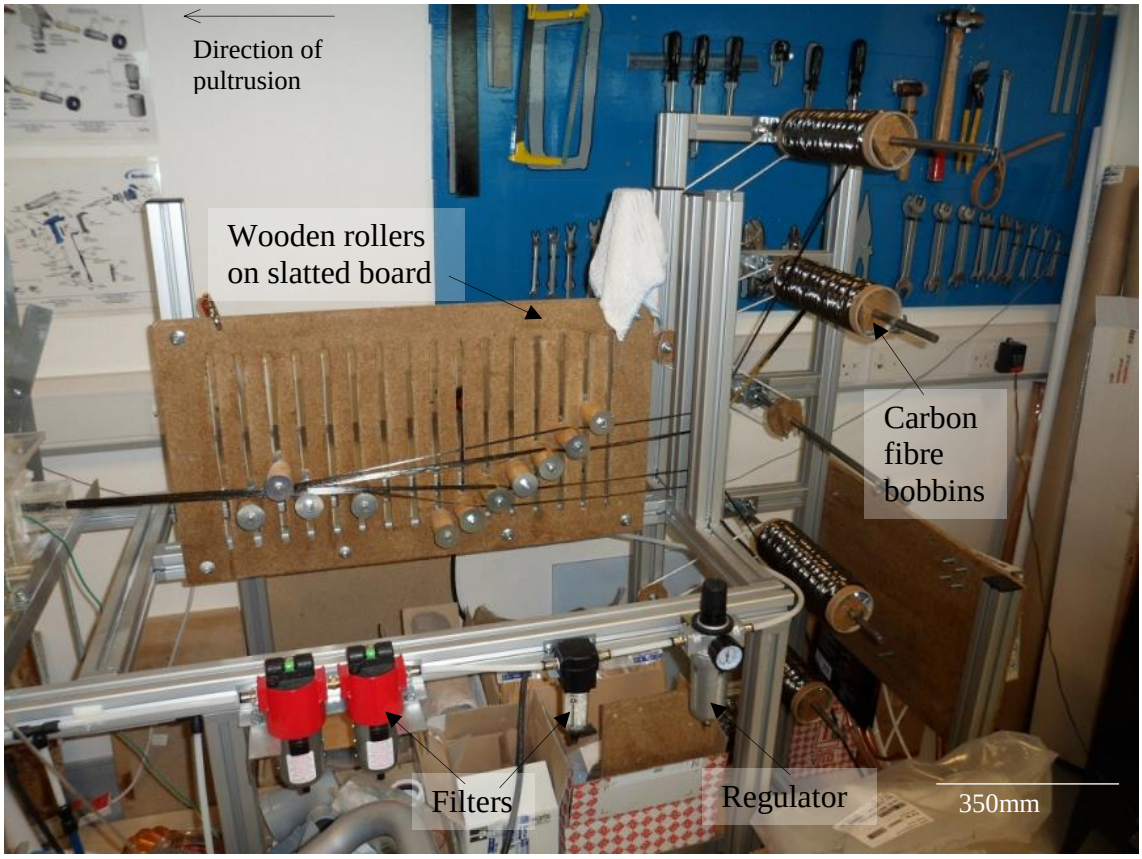

Figure 2.6 Slotted shadow board with shallow angles between rollers.

However, a trade-off between tension in the fibres and the degree of spreading was soon encountered, although this was not alluded to in journal articles studied prior to the design process. Increased tension improves fibre alignment but reduces spreading in the tow. Since the rollers achieve spreading by the pressure exerted by the fibres against the curved surface, there exists a minimal tension for any spreading to occur. The maximum tow width achieved by varying the tension in the fibres was neither low enough to allow good through-thickness powder impregnation, nor high enough for fibre alignment at the die entrance. For this reason, alternative methods for fibre spreading were attempted.

2.3.2 Pneumatic spreading

Several pneumatic spreading arrangements were also tried, which are shown in Figure 2.7. The first was an attempt to build a Venturi slot tunnel, using the low pressure generated by an Edwards Speedivac 2 vacuum pump. The drop in pressure across the whole width of the tow was so weak that it was unable to result in any noticeable movement of the fibres towards the sides of the slot and this technique was abandoned.

A more direct approach was attempted in which compressed air was forced into a closed box as tows were pulled through it. A number of chambers of different volumes were built and the number and width of the slots were reduced by degrees in order to maximise the pressure within the chambers. Even for the chamber of the smallest practical size the compressed air line exerted an insufficient pressure to achieve any noticeable spreading.

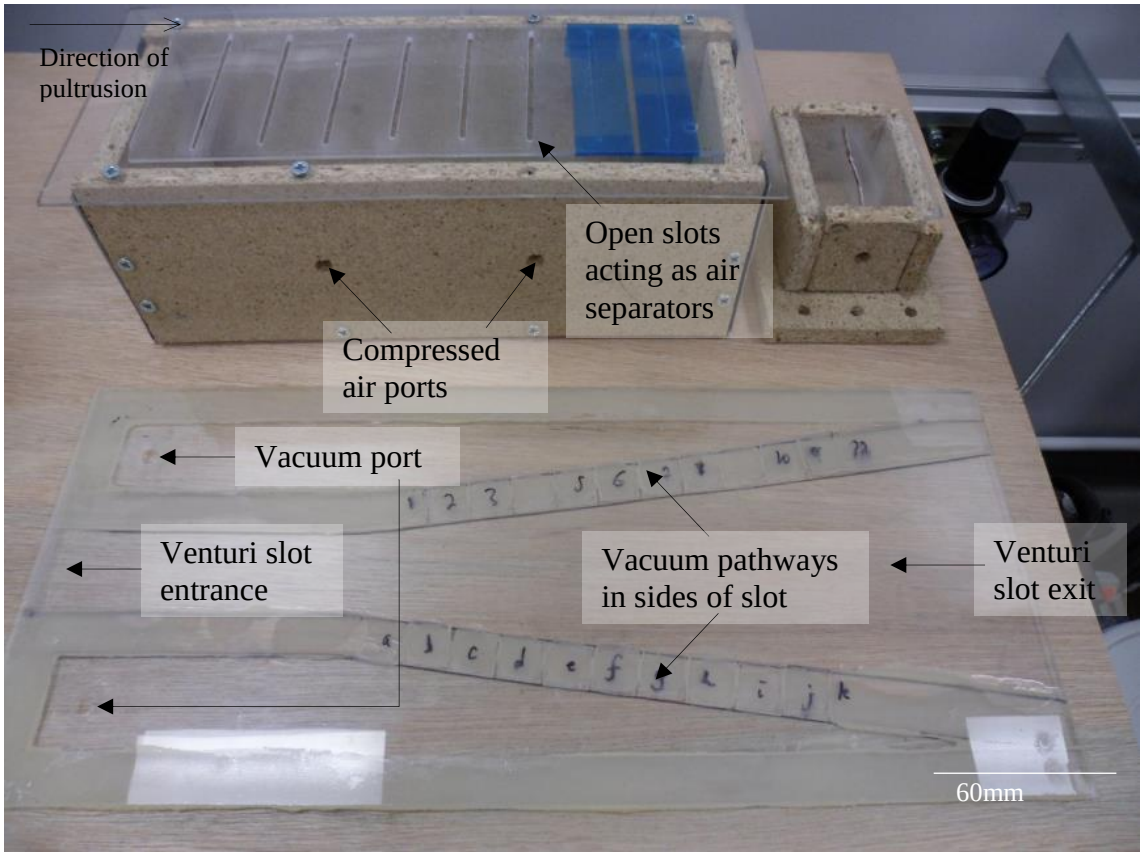

Figure 2.7 Pressurised air boxes (above) and Venturi slot tunnel (below).

With these options exhausted, it was concluded that neither the pressure of the compressed air supply nor the suction of the vacuum pump could be adequately enhanced by confining the space of operation. Spreading was attempted purely by passing the tows over an air current, as shown in Figure 2.8. For this purpose, two air knives were made by cutting 1mm slots in copper piping. A single unsized carbon fibre tow was spread to approximately twice its width, which was the best that could be achieved with any technique. However, this was only possible with the full output of the air compressor and without any tension in the fibres; the only downward force upon the tow being its own weight.

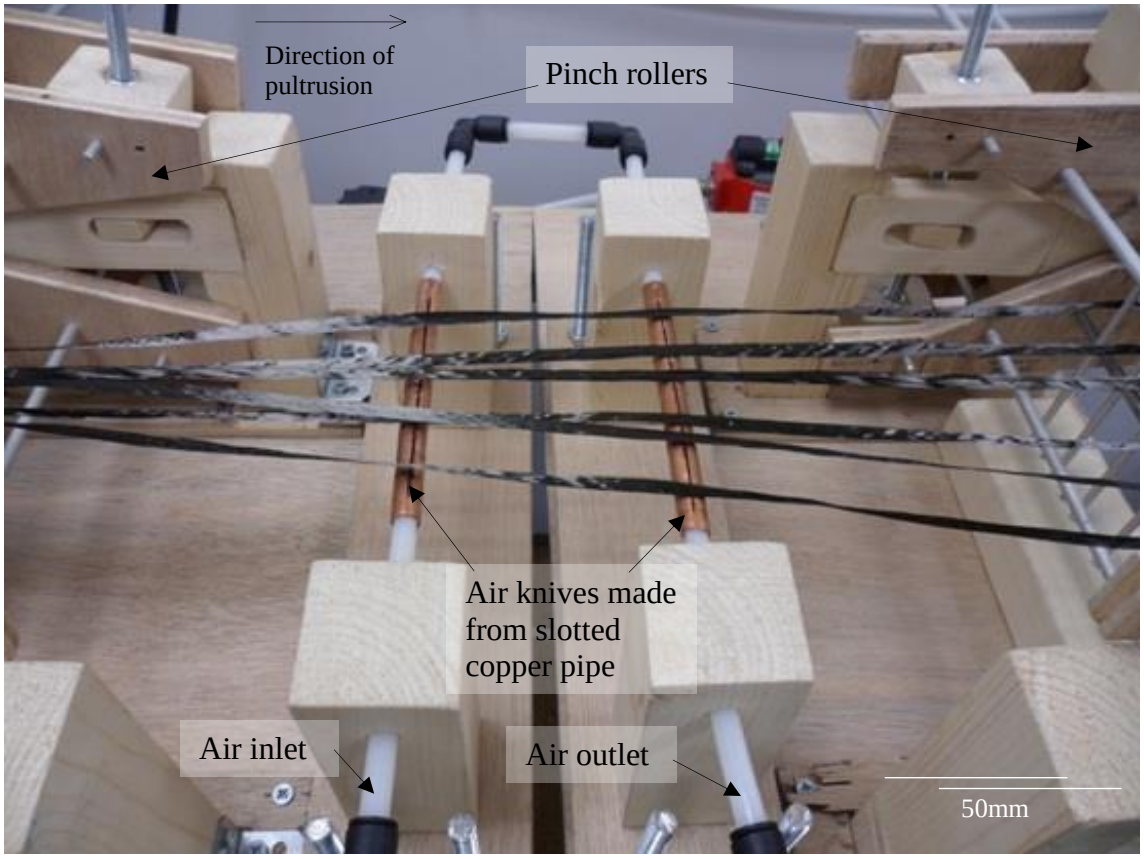

Figure 2.8 Air knives fed from a source of compressed air.

2.3.3 Mechanical-pneumatic spreading

It was therefore deduced that some combination of mechanical and pneumatic spreading might be optimal. As shown by El-Dessouky [5], it is possible to introduce separate regions of high and low tension in order to achieve both fibre alignment and spreading in a single production line. These regions behave as separate processes; low tension spreading of the fibres for the powder impregnation of the tows and high tension for heating and final consolidation of the aligned powder impregnated tows.

Two pinch rollers were constructed with a fixed space between them in order to maintain a region of lower tension. The compression between the rollers was controlled by means of vertical axis screws. The rotational speed of both sets of rollers was coupled by the motorisation of one set of rollers and transmission of power to the other set. The tows were slack between the two sets of rollers, so that the tension acting upon them was only the result of the compressed air, which was provided by the air knives. In this way the slack tows between the pinch rollers experienced the lowest practical tension. An overview of these processes is shown in Figure 2.9.

The rollers were made from 25mm diameter wooden dowels. A thin layer of polyurethane foam, taken from the grip material of a tennis racket, was adhered to the dowels. The carbon fibre tows were not observed to smoothly pass over this surface, so the foam was further covered in a polyethylene wrapping film. Application of the wrapping film turned out to be an important discovery and it provided an ideal surface. When the rollers were tightened, the foam beneath the film conformed to the shape of the carbon fibre tows. However, even at

maximum tightening the friction between the fibres and the wrapping film was low enough to allow the fibres to slip through the rollers when tension was applied by the traction puller. There was still sufficient back force upon the fibres to keep them aligned. The polyethylene and foam layers covering the wooden dowel rollers were thus highly effective in holding the fibres in place without causing fibre damage. The innovation of using soft pinch rollers to constrain the position of the moving fibres was essential for spreading the fibres for powder impregnation as well as maintaining tension in the line.

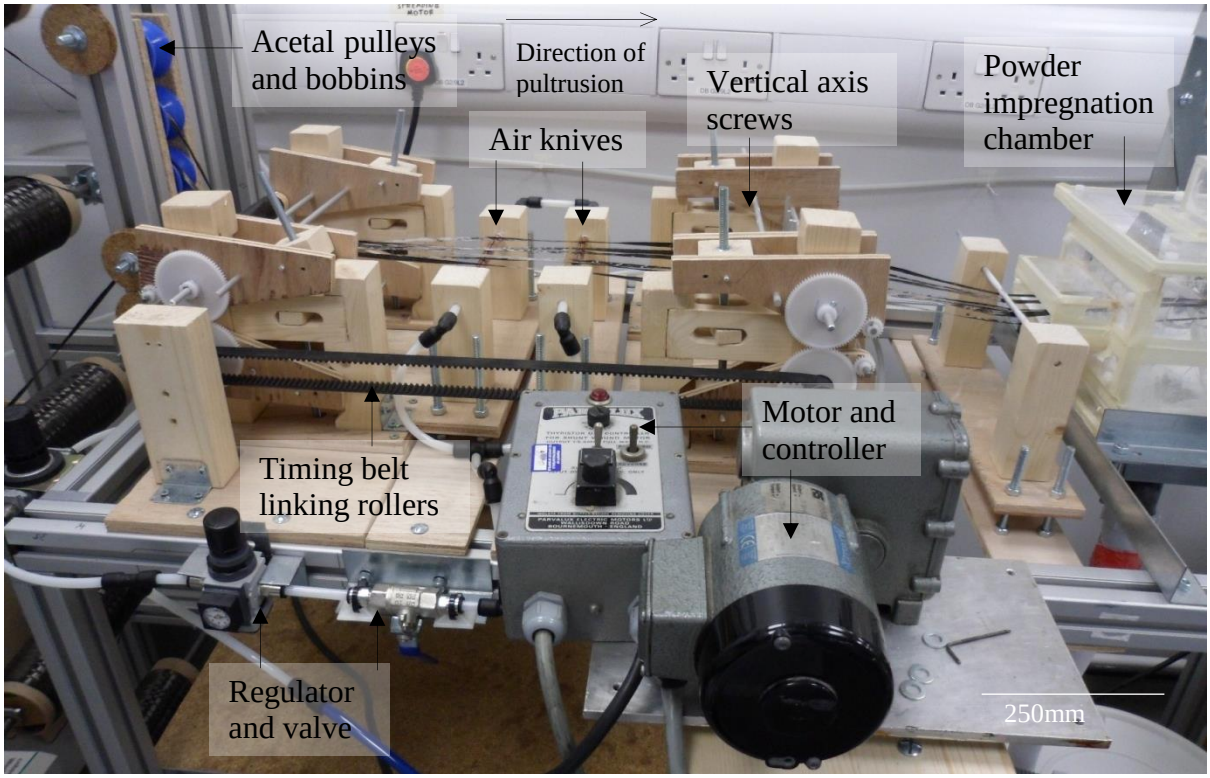

Figure 2.9 Overview of mechanical-pneumatic fibre spreader, with power transmission.

Gears of different diameters were necessary in order to guarantee clearance between the wooden pullers and the roller shaft, as shown in Figure 2.10. This resulted in a gear ratio of 4:1 between the motor and the roller shafts.

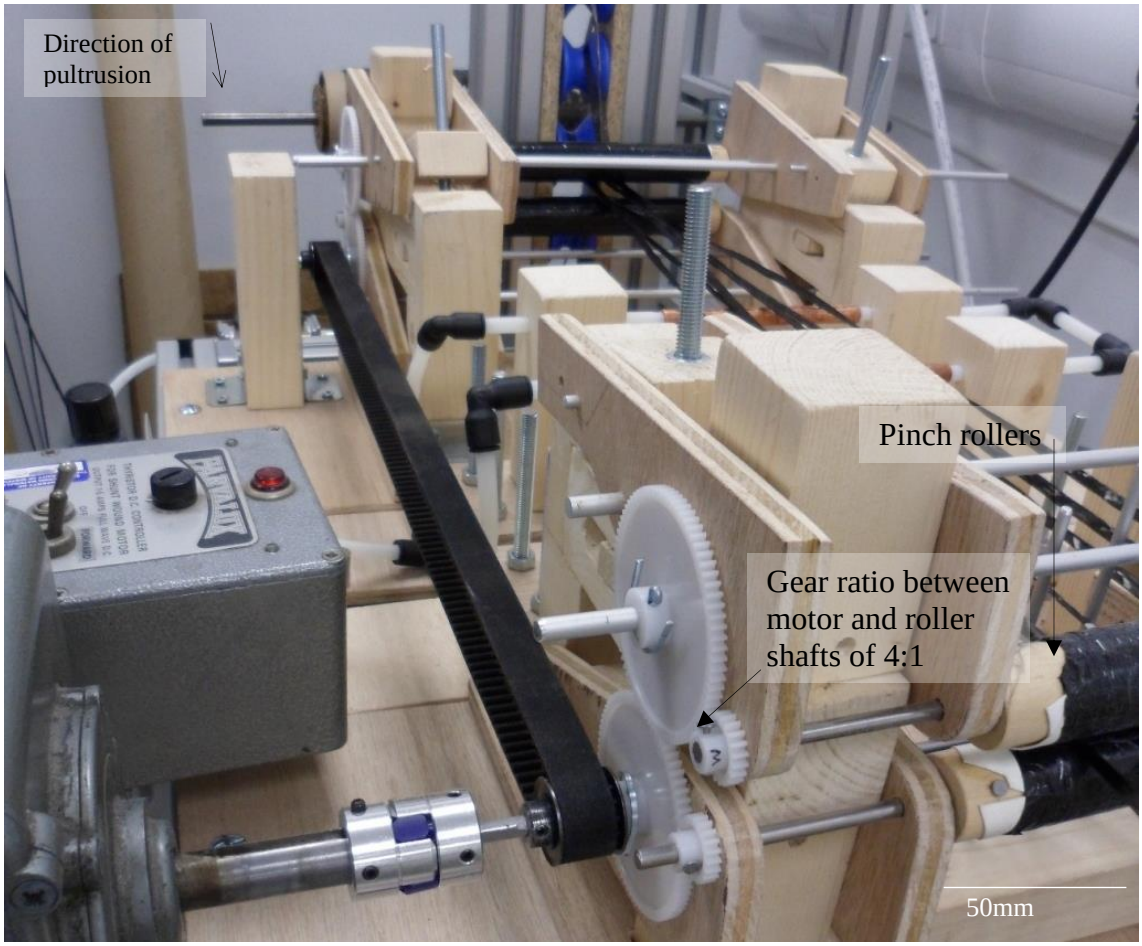

Figure 2.10 Power transmission between driven shaft and rear pinch rollers.

2.3.4 Rollers as a sole means of spreading

It became clear throughout trials that the pinch rollers were providing more than just a slack region of low tension. The pinch roller closest to the powder impregnation chamber were also flattening the tows and holding them apart before they passed beneath the powder spray gun. While the air knives were able to produce modest spreading of unsized fibres, they did not offer any appreciable spreading of tows of sized fibres at any air pressure. Therefore, the use of air knives was discontinued but the pinch roller alone continued to flatten and spread the tows, with the aid of an exaggerated comb to guide the fibres towards the rollers, as shown in Figure 2.11. In this manner the pinch roller itself acted both as a tensioner and as a mechanical spreader.

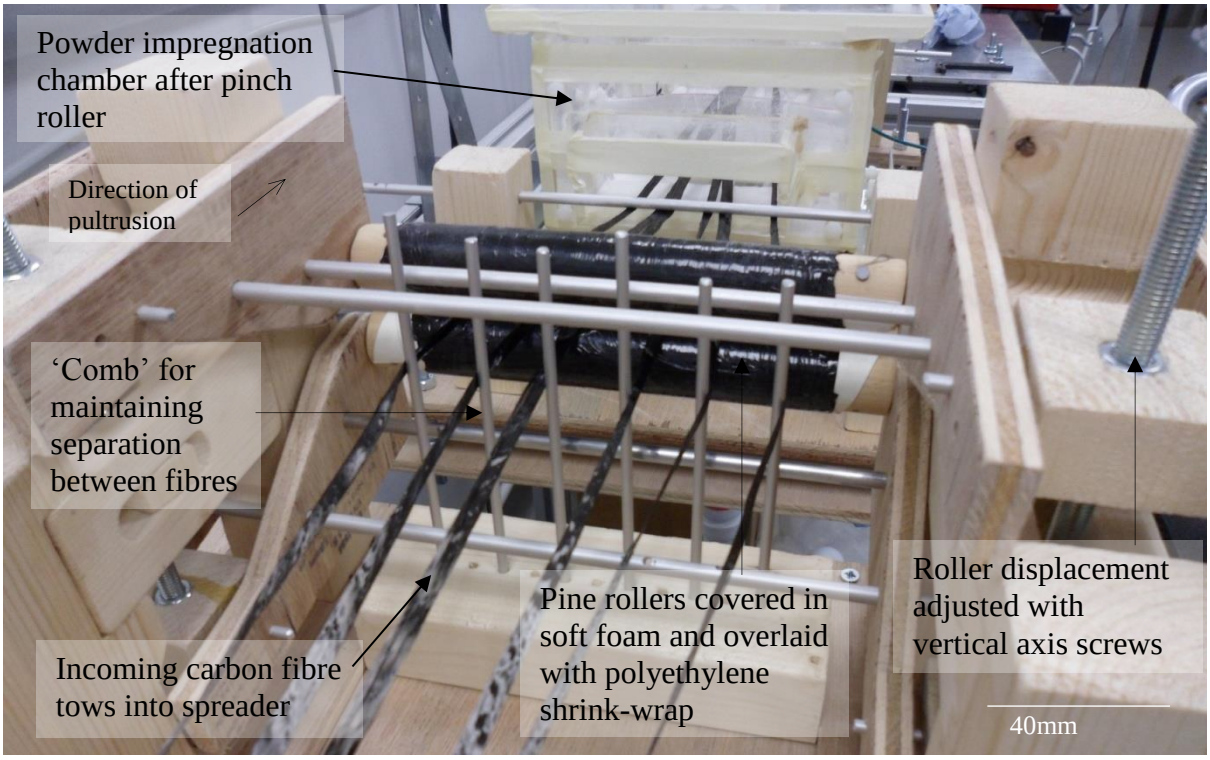

Figure 2.11 View of fibres leaving pinch rollers and entering powder spray chamber.

2.4 Fibre impregnation

Fibre impregnation is perhaps the single most complex process in pultrusion manufacturing since it involves the greatest number of variables and the range of available techniques is multitudinous. Fibre impregnation may be achieved by a number of methods:

- Powder impregnation is typically performed by showering neutrally earthed fibres with a cloud of charged polymer particles, some of which adhere to the upper and undersides of the passing tow. Electrostatic attraction between is sufficient to keep the powder attached to the fibres before consolidation or uptake onto bobbins as a pre-impregnated tow [6]. This process is shown in Figure 2.12.
- Impregnation is possible by molten polymer, whereby the fibres enter a heated bath or pass beneath the outlet of an extruder. In the former case, the fibres become impregnated by squeezing the polymer onto the fibres as they are forced onto hard pins. In the latter case, the fibres pass through a die where the molten polymer leaves the extruder, as is shown in Figure 2.13. In either case the fibres are spread before impregnation and the temperature is controlled in order to overcome the viscosity of the molten polymer [7].
- An alternative form of liquid impregnation of thermoplastics is with a bath of polymer in solution. This technique benefits from lower friction between the powder and fibres in the slurry [8]. Although this reduces the time necessary to consolidate relatively high viscosity plastics, the solvent must be removed before consolidation [9]. Gibson and Månson reported melt viscosities of 280Pas for carbon fibre/PEEK and 100Pas for carbon fibre/nylon 12 composites [6]. Typical processing temperatures of these thermoplastic composites are 400°C and 270°C, respectively [10, 11].
- Comingled feedstocks consist of mixed thermoplastic and reinforcement fibres. These are spun together and loaded onto bobbins that are directly pulled through the heating die without an impregnation process, shown in Figure 2.14. The fibre volume fraction and

dispersion of reinforcing fibres within the FRP are controlled by the density and distribution of filaments [12].

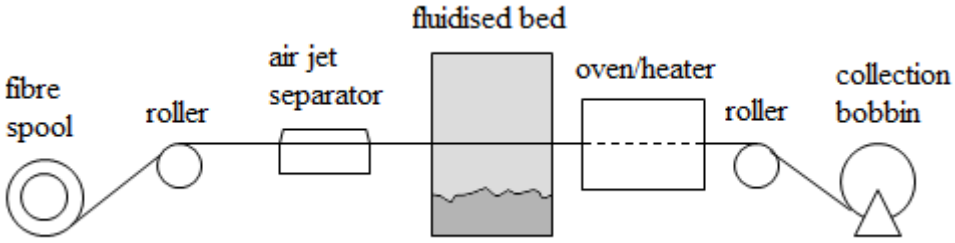

Figure 2.12 Powder impregnation of a tow.

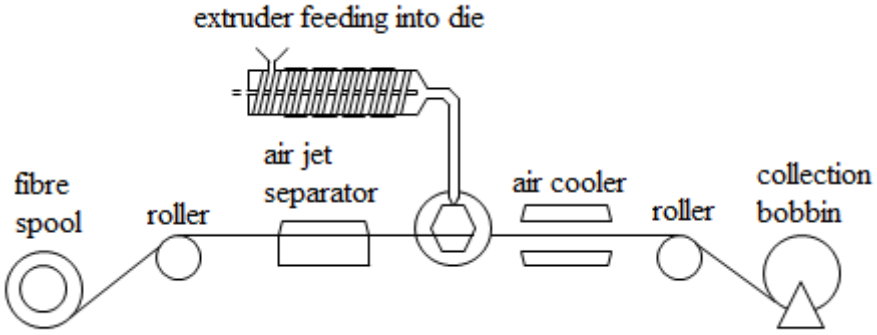

Figure 2.13 Fibre impregnation by thermoplastic extrusion.

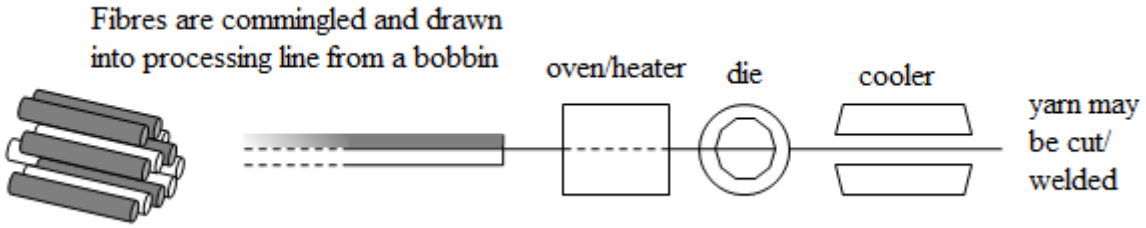

Figure 2.14 Feedstock from commingled tows.

2.4.1 Powder impregnation

Powder impregnation is made attractive by its independence from the viscosity of the resin, high rate of processing and fine control of polymer deposition. Potential damage incurred by pressing the fibres under high tension against submerged rollers and the hazards of a hot or caustic open bath are avoided, as is the cost of production for spinning of a comingled feedstock. Drawbacks include limiting the fibre selection to electrically conductive fibres and the influence of the particle size distribution of the powder.

Delivery of the powder to the fibres relies on adequate dispersion. Fluidisation creates a stable particulate/fluid mixture to ensure that the powder does not aggregate due to attractive intermolecular forces between polymer chains. The process is optimised so that air bubbles remain small and of a similar size to the powder particles, giving the bed a ‘boiling’

appearance. Optimal fluidisation is shown in image b) in Figure 2.15, in which the powder and air bubbles are well mixed while images a) and c) show inadequate fluidisation that gives rise to discrete regions of agglomerated powder and air bubbles [7].

- Conventional fluidisation passes the tows over and under pins that mechanically force an air-fluidised powder into the fibres. Forcible impregnation at the pins is similar to that used in molten polymer beds [13].
- Electrostatic fluidisation involves the passage of reinforcement through a cloud of charged particulates [14]. In acoustic fluidisation the action is the same, except that charge is produced by frictional vibration rather than an electric field.
- The powder may be circulated so that the fibres are continually showered by particulates [15]. Gravitational layering involves dusting the tow in a cascade of falling powder. The powdered tow is typically reversed in direction and the process repeated on the underside of the fibres so that both sides are exposed to the powder curtain [16]. This is different to the fluidised bed approach in that the tow is not immersed in a powder bath.

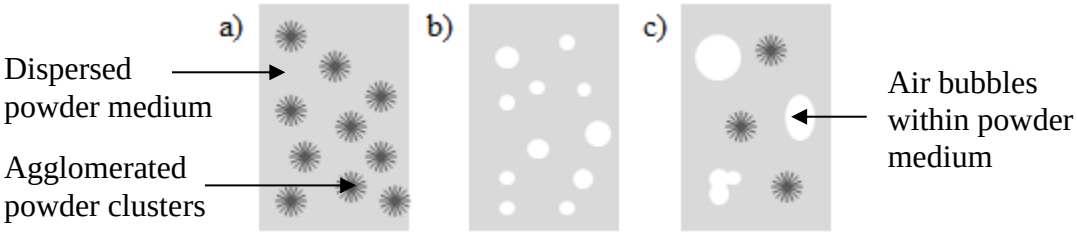

Figure 2.15 Fluidisation of powder phase showing a) agglomeration without fluidisation, b) fluidisation with air bubbles with similar diameters to that of the powder particles and c) aggregation of gas bubbles without adequate dispersion of powder clusters.

2.4.2 Electrostatic spray impregnation

Electrostatic spray deposition aerodynamically forces an ionised powder towards a target, rather than passively coating as is done in a fluidised bed. This is typically achieved by spraying a fluidised powder through a corona powder gun. The gun passes the powder through an ionised air stream that acquires its charge from an electric field that is strong enough to break down the air. The efficiency of charge transfer between powder and air is relatively low and only a fraction of a percent of the ions transfer charge to the powder. The surface of the fibre is therefore bombarded with free ions, which quickly shield the target from additional deposition. This limits the thickness of the polymer coating and a combination of electrostatic and pneumatic forces are required to impregnate crevices between fibres [17].

Electrostatic spraying was chosen for its versatility in the large range of thermoplastics it is capable of delivering and for its accurate control the rate of powder deposition, which directly affects the fibre volume fraction of the finished FRP. Spent powder can also be recycled, making it economical, which is an important factor considering the high cost of the engineering thermoplastics used in this project. Furthermore, installation of a corona spray into the pultrusion line is both safer and more straightforward than liquid solvent or molten alternatives. The high electrical conductivity of carbon fibres also makes them amenable to use with this technology.

A Nordson Encore LT Manual Powder System was acquired for this project, which is a vibration-fluidised powder system with a manually operated corona spray gun. As shown in Figure 2.16, powder spraying was implemented as follows:

- The tows passed through a transparent spray booth specially constructed entirely from plastic insulating materials.
- The gun was attached to a frame above the line, allowing the powder to be sprayed downwards through the top of the spray chamber onto the passing tows.
- The fibres were grounded with an earthed copper pipe beneath the path of the spray.
- Ventilation was provided beneath the chamber by means of a Dyson DC22 vacuum cleaner. A deep bucket was connected beneath the powder chamber so that the powder was drawn into the bucket rather than being sucked into the vacuum cleaner for ease of collection and reuse.

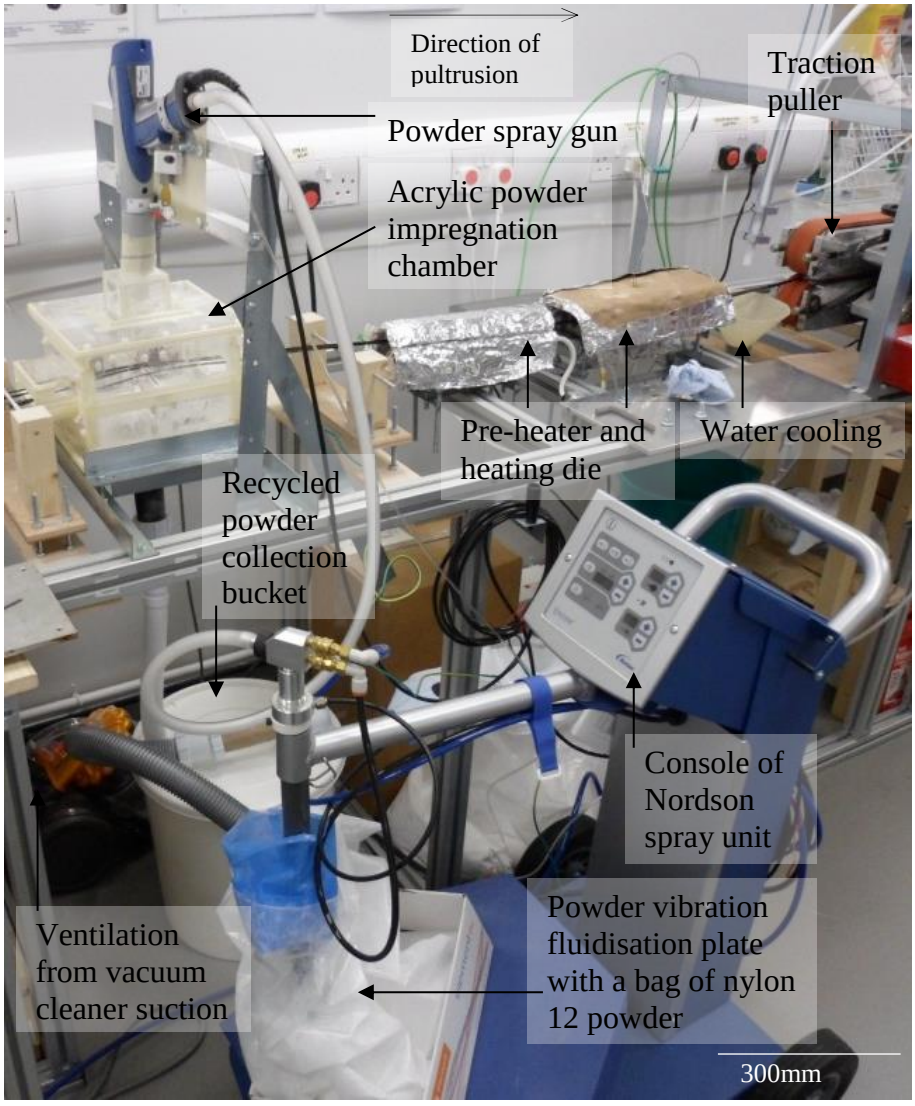

Figure 2.16 Corona spray gun attached to the vibration-fluidised bed with powder feed and control unit. The spray gun was mounted above the powder chamber.

Following advice given by Nordson, a number of different operating conditions were experimented with in order to find an optimal solution. This is covered in greater detail in §3.2.3, which describes the process by which optimal electrostatic spraying conditions were

obtained. Each production run had slightly different variables, although some general principles were noted during trials:

- Spraying was most successful with the gun mounted vertically above the path of the tows.
- As small an air flow as possible was used that still produced the optimal coverage. Strong air pressure could overwhelm the electrostatic attraction with the grounded fibres by blowing away accumulated powder.
- The small distance between the gun and the target meant that the resistance of the air gap was low. The current could therefore be lowered in order to reduce the number of free ions that contribute to back ionisation – the process by which a target that has gradually become charged by exposure to the corona stream repels further free ions arriving at the surface. The potential difference was also lowered for better penetration of Faraday cages within recesses between fibres, which may have been otherwise deterred by a high field strength pushing charges away from those areas. The 'smart' current control on the Encore LT automatically adjusts the potential difference to match a desired current and this device was used to actively control the potential difference in the vicinity of the tows.

2.5 Heating

After impregnation, the polymer-coated fibres were pulled into a heated die. The geometry and temperature of the die, the pulling speed and the tension in the tows were critical factors in controlling the properties of the FRP article [18].

Of great importance is the residence time spent by a given point along the tow inside the die. The task of balancing rates of production and heating may be complicated for thermosetting resins, which must emerge from the die fully cured but not overheated. For this reason dies for thermosetting resins tend to be in the region of 1m in length and line speeds must be chosen to allow for adequate curing inside the die [19]. Lower pulling rates may be found to increase article properties by improved wetting of the fibres by the resin and a higher degree of crosslinking but excessive heating may degrade the polymer. Thermoplastics consolidate rather than cure, during which the matrix melts and wets the fibres through interpenetration of the tows. Shorter dies than those used for thermosetting resins are therefore more appropriate and rates of production may be higher [20].

However, since line speed is also crucial for determining fibre spreading and impregnation, a compromise must be sought between these processes. For instance, the production of towpregs seeks to create pre-impregnated tows with minimal consolidation for use as a precursor in separate manufacturing processes. Typical line speeds for manufacture of tow-pregs are between 2.0m/min and 6.0m/min. By contrast, line speeds for pultrusion may be found to be optimal between 0.7m/min and 1.2m/min [4, 21]. The line speeds used for the pultrusion of rods in this project are discussed in greater detail in §3.2.5.

Pre-heating of impregnated tows can improve adhesion between the fibre and matrix by lowering the viscosity of the polymer to ease the passage of the tows into the die [22]. Pre-heaters may be placed before the entrance of the forming die or the die itself may have more than one heating zone, with temperatures gradually changing throughout its length [20, 23].

2.5.1 Process of consolidation

Once the impregnated tows enter the die, the only forces acting upon them arise from the pressure exerted by the die walls and by thermal expansion. Unlike an autoclave, there is no

source of external pressure on the FRP, meaning that the quality of consolidation is largely determined by the line speed, pulling force and rates of heating [24]. Because of the high viscosity of engineering thermoplastics, the void content in pultrusions can be high relative to components made with the assistance of vacuum and external pressure in an autoclave [25].

Thermoplastic particles that are deposited onto fibres appear to form bridges between individual filaments. During consolidation, the extent to which molten polymer droplets spread along the fibres by capillary action is determined by their wettability [22]. The number of fibres in contact with a polymer bridge may vary but it has been shown that consolidation by capillary spreading can be effectively modelled with the polymer in contact with three fibres [26]. Close packing gives rise to a hexagonal arrangement of fibres and polymer particles in the fibre direction, as shown in Figure 2.17.

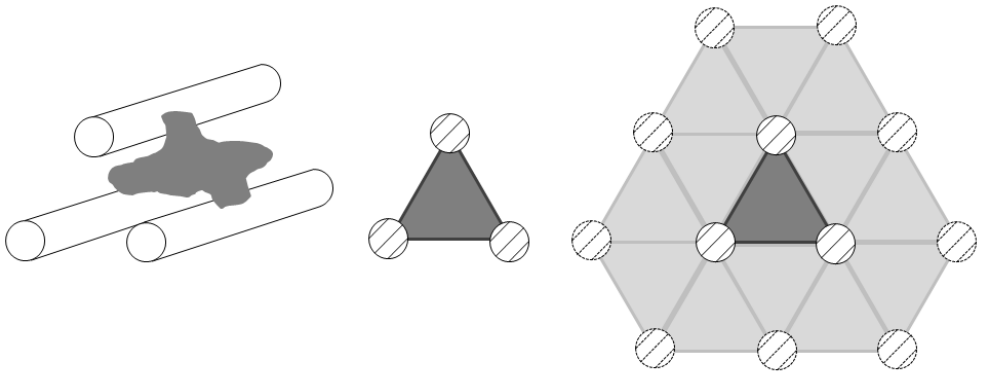

Figure 2.17 Adhesion of a polymer bridge to three fibres within a hexagonal packing arrangement.

2.5.2 Split die and heating

A 300mm constant cross-section split die was designed and ordered from Robert van Doren Pultrusion, shown in Figure 2.18. The two halves of the die were machined from hardened stainless steel and the matching surfaces were chrome plated. A circular channel with a diameter of 3.25mm was cut through the middle. Although a modest parabolic lip was machined onto both ends of the die, during trials this was not found to be sufficient to guide the fibres into the channel. A ¾" trumpet was wire eroded into the entry of the die by Cheshire Wire Erosion to improve smooth entry of the impregnated tows into the channel.

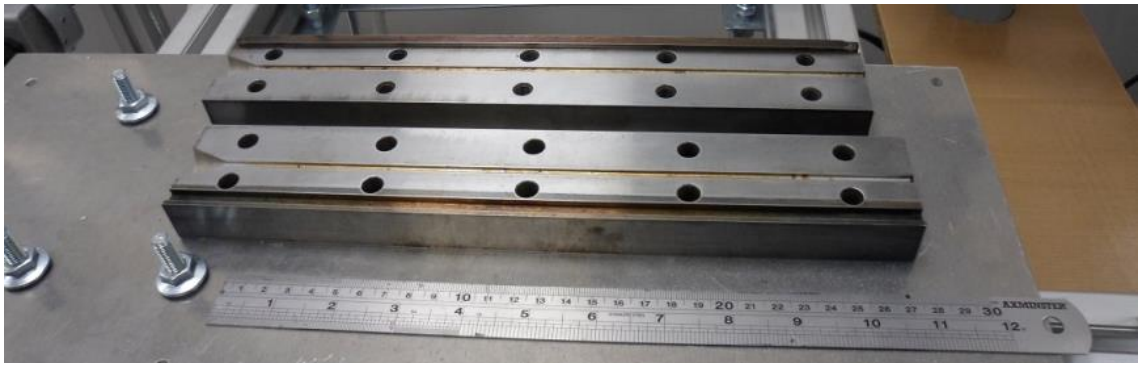

Figure 2.18 Split die halves.

The die was judged too small to safely mount cartridge heaters through its thickness without creating uneven heating zones. Heating was therefore provided by a high temperature Omega STH102-060 heating tape which was wrapped around the width of the closed split die, shown in Figure 2.19. Temperature control was achieved by means of a thermocouple probe inserted into a deep hole made in the top of the die, which terminated a few millimetres above the inside wall of the die. This provided an approximate *in situ* measurement of the temperature close to the channel, which was used to control the die temperature.

The heating tape was found to be insufficiently powerful to heat the die to the required temperature without the aid of insulation. A steel wire frame coated with fire cement and internally covered with reflective foil provided a thermal barrier and helped to regulate the temperature.

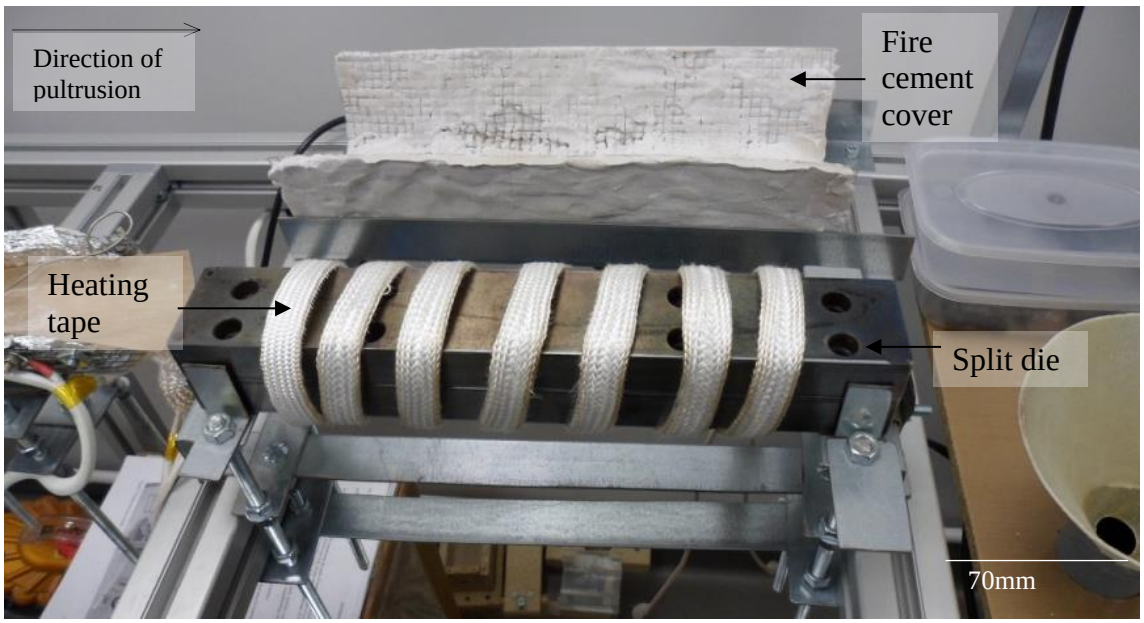

Figure 2.19 Split die with heating tape.

Pre-heating of tows before entry to the heating die softens the powder by heating the impregnated polymer above its melting temperature [12]. Noncontact heating was achieved by wrapping an Omega FGR-060 heating strip within a steel wire shell that was protected from powder debris by reflective foil, shown in Figure 2.20. The shell was enclosed within a fire cement covered tube to provide insulation. Temperature control was afforded by a thermocouple probe that ran along the top of the tube, just above the tow as it passed through the pre-heater.

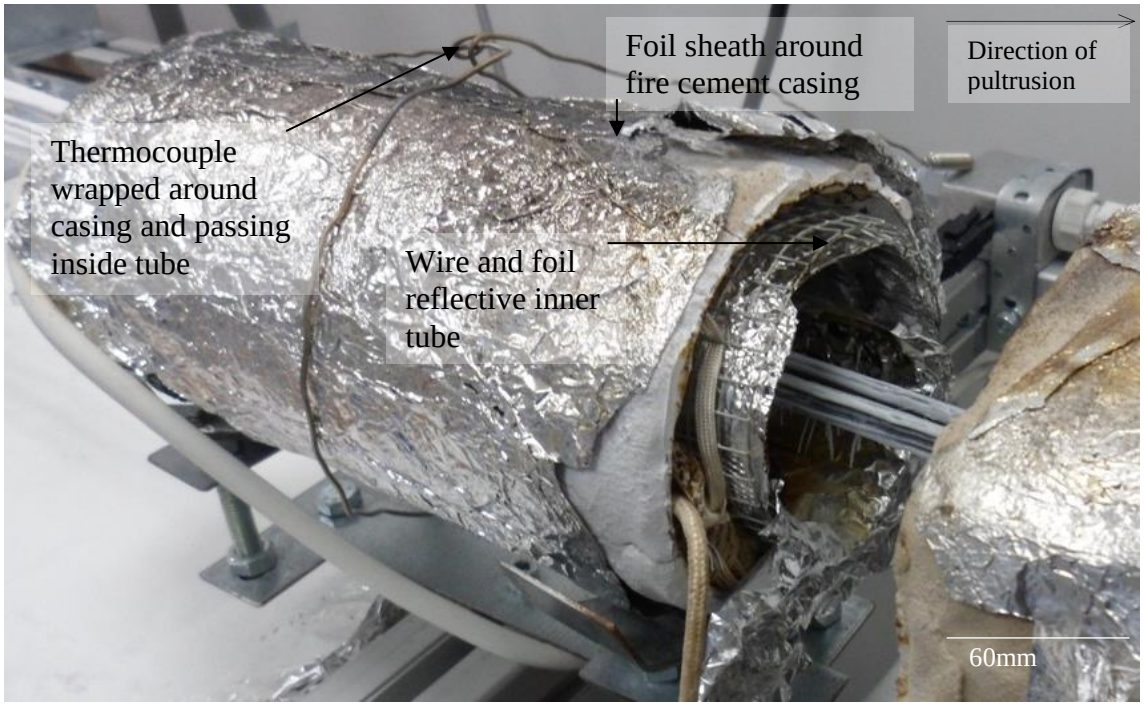

Figure 2.20 Pre-heater before heating die with foil-wrapped fire cement cover.

Temperature control was provided by a central control box, which was assembled by Frank Fletcher at the Department of Electronic and Electrical Engineering. The power cables and thermocouples led to Omega SSRDIN Solid State Relays and 1/32 DIN Programmable i-Series Temperature Controllers.

2.6 Cooling

A water stream cooled the rods as they emerged from the heated die. Due to the lack of available space, it was not possible to include a series of post-heating and cooling stages that would have afforded precise control of the cooling regime, shown in Figure 2.21. This is important because of the dependence of crystallisation on the cooling profile of semi-crystalline thermoplastics [27]. The rate of cooling by the jet of water and the distance between it and the exit of the die were fixed so the only variable affecting the rate of cooling was the pulling speed. Percentage crystallinity of the polymer was expected to be higher at lower pulling speeds, which would have allowed longer periods for the rods to cool under the water stream [28].

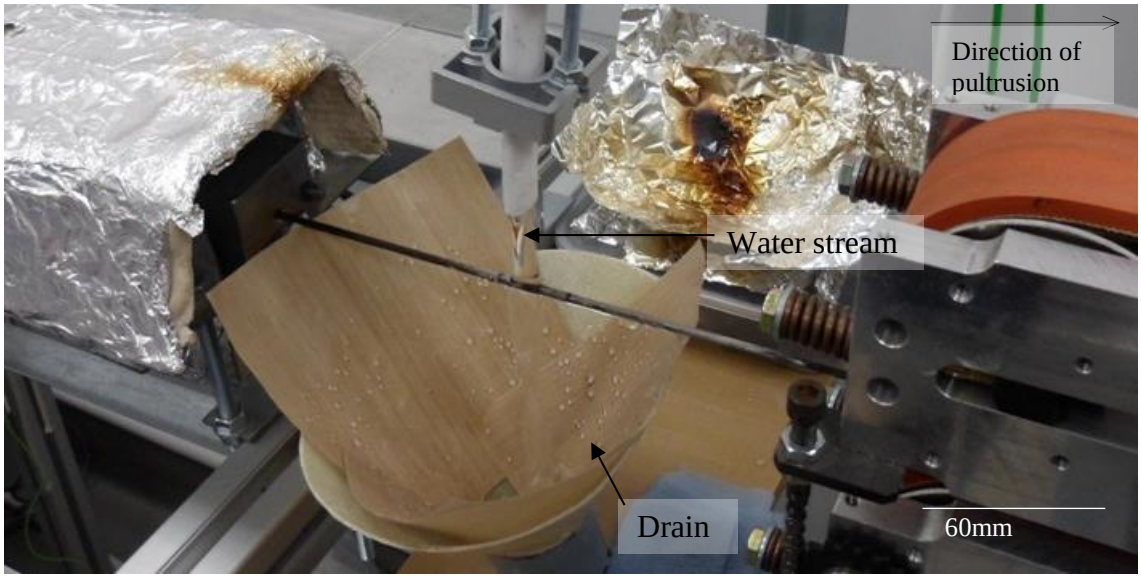

Figure 2.21 Water cooling of the pultruded rods.

2.7 Pulling and cutting

Traction was provided by a Versa Machinery C-22 Caterpillar Puller. The displacement between the tracks was controlled manually above the gears, as can be seen in Figure 2.22. A DC shunt motor was coupled to the puller. Finally, a chop saw with a diamond wheel was placed on sliding tracks and to cut of the consolidated rods into required lengths.

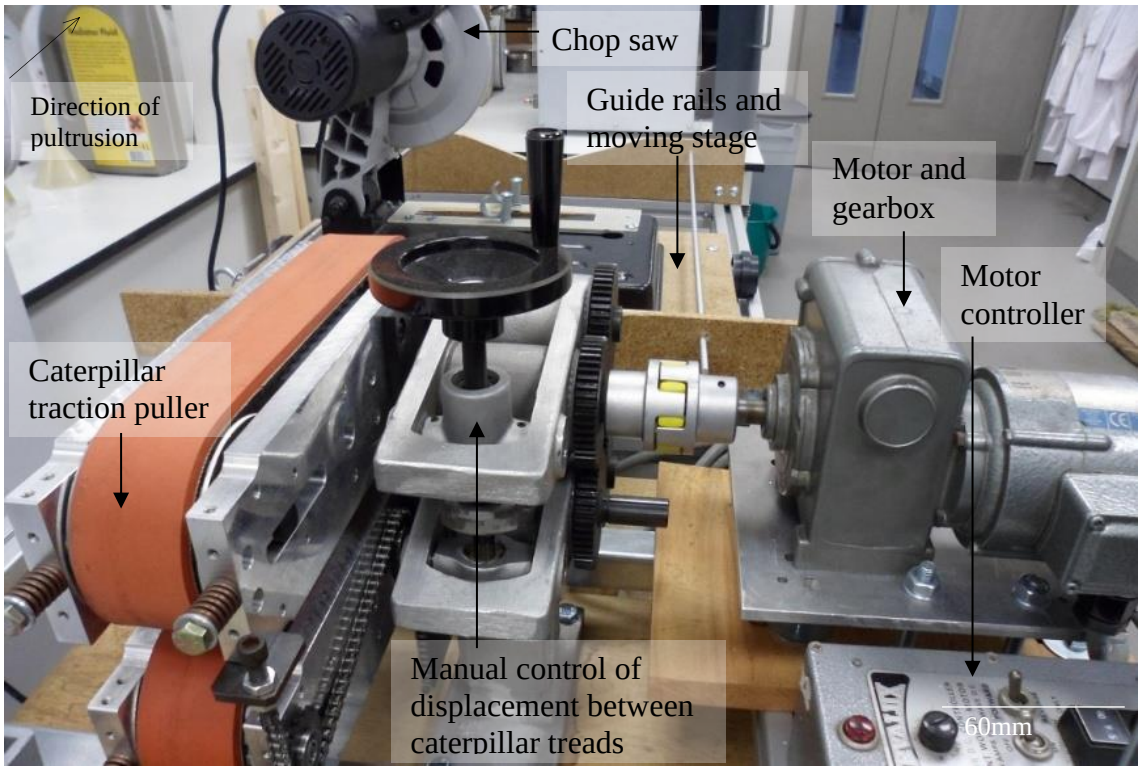

Figure 2.22 Traction provided by the motorised puller.

2.8 Concluding summary

A pultruder was designed and built for the continuous manufacture of carbon fibre reinforced thermoplastic rods to be used in the manufacturing of hybrid strands. The design process was guided by the need to prioritise flexibility of purpose and resulted in a modular assembly. Fibre delivery, spreading, polymer impregnation of the fibres, consolidation and cooling were thus created as separate but interdependent processes within the overall pultrusion line.

Fibre spreading was found to be a deciding factor in ensuring good consolidation of the tows. Various pneumatic-mechanical spreading techniques were trialled and a single set of pinch rollers was found to be most successful for separating the tows and spreading the fibres. To the knowledge of the author, the importance of fibre spreading in ensuring consolidation for pultrusion of thermoplastics has been underrepresented in publications, making this a significant finding. Powder impregnation was achieved by an electrostatic spray gun, which offered the best versatility and economy with the lowest safety risk to the operator. A pre-heater was installed prior to the split die that was heated with an electrical strip and both heaters were monitored from the same control point. Cooling was provided by a stream of water and a chop saw allowed emerging rods to be cut to length.

The processes developed in this chapter were used to manufacture rods for the production of novel steel and FRP hybrid strands. Chapter 3 describes in detail the optimisation trials were conducted to determine optimal processing conditions for the pultrusion of rods from different fibre and polymer feedstocks. This includes a summary of standard manufacturing conditions for each material type and an inventory of the pultruded rods that were produced for this project.

2.9 References

1. Ericksen, L.D., Prepreg Winding Delivery Systems. 2007
2. Jaklitsch, D.J.B., M. T.; Pattie, E. R., An Examination of Processing Variables in the pultrusion of Glass Reinforcements with an Epoxy-Anhydride Resin System. Army Lab Command, Watertown MA Material Technology Lab, 1991
3. Vodermayer, A.M., J.C. Kaerger, and G. Hinrichsen, Manufacture of high performance fibre-reinforced thermoplastics by aqueous powder impregnation. Composites Manufacturing, 1993. 4(3), p. 123-132
4. Nunes, J.P., J.F. Silva, A.T. Marques, N. Crainic, and S. Cabral-Fonseca, Production of Powder-Coated Towpregs and Composites. Journal of Thermoplastic Composite Materials, 2003. 16(3), p. 231-248
5. Rodríguez-Llamazares, S., B.L. Rivas, M. Pérez, F. Perrin-Sarazin, A. Maldonado, and C. Venegas, The effect of clay type and of clay–masterbatch product in the preparation of polypropylene/clay nanocomposites. Journal of Applied Polymer Science, 2011. 122(3), p. 2013-2025
6. Gibson, A.G. and J.A. Månson, Impregnation technology for thermoplastic matrix composites. Composites Manufacturing, 1992. 3(4), p. 223-233
7. Vaidya, U.K. and K.K. Chawla, Processing of fibre reinforced thermoplastic composites. International Materials Reviews, 2008. 53(4), p. 185-218
8. Ho, K.K.C., S.R. Shamsuddin, S. Riaz, S. Lamorinere, M.Q. Tran, A. Javaid, and A. Bismarck, Wet impregnation as route to unidirectional carbon fibre reinforced thermoplastic composites manufacturing. Plastics, Rubber and Composites, 2011. 40(2), p. 100-107

9. Tang, L., L. Li, X. Yi, and Z. Pan, Aqueous powder slurry manufacture of continuous fiber reinforced polyethylene composite. Polymer Composites, 1997. 18(2), p. 223-231
10. TenCate. CETEX TC1200 PEEK Resin System. 22/11/2012: http://smartsite.tencate.com/TenCate/Aerospace_composites/documents/TCAC%20USA%20docs/TCAC%20USA%20Datasheets/DataSheet/TC1200_DS_Web.pdf
11. TenCate. CETEX TC910 nylon 6 resin system. 23/09/2015: http://www.tencate.com/emea/Images/CETEX-TC910_DS_081213_Web28-25292.pdf
12. Carlsson, A. and B. Tomas Åström, Experimental investigation of pultrusion of glass fibre reinforced polypropylene composites. Composites Part A: Applied Science and Manufacturing, 1998. 29(5–6), p. 585-593
13. Lutz, A., Funck, R., Harmia, T., Friedrich, K. A new impregnation tool for on-linem manufacturing of thermoplastic composites. in Eleventh International Conference on Composite Materials. 1997. Gold Coast, Queensland, Australia, Woodhead
14. Duvall M., R.K. In-situ manufacture using an electrostatic spray process and filament winding. in Tenth International Conference on Composite Materials. 1995. Whistler, Canada, Woodhead
15. Nunes, J.P., C.A. Bernardo, A.S. Pouzada, and D.D. Edie, Formation and Characterization of Carbon/Polycarbonate Towpregs and Composites. Journal of Composite Materials, 1997. 31(17), p. 1758-1777
16. Johnston N. J., T.T.W., Marchello J. M., Grenoble R. W. Automated fabrication of high performance composites: An overview of research at the Langley Research Centre. in Eleventh International Conference on Composite Materials. 1997. Gold Coast, Queensland, Australia, Woodhead
17. Hughes, J.F., Electrostatic Powder Coating. 1984, Letchworth, Research Studies Press
18. Chen, C.-H. and C.-C.M. Ma, Pultruded fibre reinforced polyurethane composites II. Effect of processing parameters on mechanical and thermal properties. Composites Science and Technology, 1992. 45(4), p. 345-352
19. Starr, T.F., Pultrusion for engineers. 2000, Cambridge, Woodhead Publishing
20. Outwater, J.O. The use of a small pultruder for specimen preparation. in Eleventh International Conference on Composite Materials. 1997. Gold Coast, Queensland, Australia, Woodhead
21. Guo, Z. and B. Hagström, Preparation of polypropylene/nanoclay composite fibers. Polymer Engineering & Science, 2013. 53(10), p. 2035-2044
22. Connor, M.T., Consolidation mechanisms and interfacial phenomena in thermoplastic powder impregnated composites in Departement des matériaux. 1995, École polytechnique fédérale de Lausanne: Lausanne
23. Wang, Z. and T.J. Pinnavaia, Hybrid Organic−Inorganic Nanocomposites: Exfoliation of Magadiite Nanolayers in an Elastomeric Epoxy Polymer. Chemistry of Materials, 1998. 10(7), p. 1820-1826
24. Chafidz, A., M. Kaavessina, S. Al-Zahrani, and M. Al-Otaibi, Polypropylene/organoclay nanocomposites prepared using a Laboratory Mixing Extruder (LME): crystallization, thermal stability and dynamic mechanical properties. Journal of Polymer Research, 2014. 21(6), p. 1-18
25. Hegde, R., G. Bhat, J. Spruiell, and R. Benson, Structure and properties of polypropylene-nanoclay composites. Journal of Polymer Research, 2013. 20(12), p. 1-13

26. Connor, M., S. Toll, J.-A.E. Månson, and A.G. Gibson, A Model for the Consolidation of Aligned Thermoplastic Powder Impregnated Composites. Journal of Thermoplastic Composite Materials, 1995. 8(2), p. 138-162
27. Saiello, S., J. Kenny, and L. Nicolais, Interface morphology of carbon fibre/PEEK composites. Journal of Materials Science, 1990. 25(8), p. 3493-3496
28. Ahmed, F., S.C. Joshi, and Y.C. Lam, Three-Dimensional FE–NCV Modeling of Thermoplastic Composites Pultrusion. Journal of Thermoplastic Composite Materials, 2004. 17(5), p. 447-462

3 Pultrusion optimisation and productivity

From the conception of its design through to its use at the Composite Systems Innovation Centre, the pultruder underwent a process of continual improvement and optimisation, including relocation to a larger facility. During this time the manufacturing protocol for FRP rods was vigorously refined.

This chapter includes a description of the experimental procedures employed during pultrusion and an assessment of optimised manufacturing conditions. For an exhaustive review of operational procedures for the pultrusion line, please refer to Appendix A.

3.1 Materials

3.1.1 Carbon fibre tows

During manufacture, sized carbon fibres are coated with a small quantity of epoxy to improve adhesion between filaments to improve handling and chemical compatibility between the reinforcement and matrix [1]. However, the enhanced adhesion between filaments was also expected to inhibit spreading of tows before the powder impregnation stage. With this in mind, rods were pultruded using dry tows containing sized and unsized fibres in order to investigate the effect of filament distribution on mechanical properties. Rods were also produced from commingled carbon fibre/nylon tows obtained from Schappe. Using their proprietary intermingling technology, these tows represent an ideal case of fibre distribution in which the reinforcement and matrix are already well mixed before entering the pultruder.

Unfortunately it was not possible to obtain tows of different types with the same number of filaments, leading to different filament counts between feedstock types, shown in Table 3.1. Rods were thus produced from three different carbon fibre tows: sized tows (Grafil TR30S 12k), unsized tows (Toray T700SC-60E 24k) and commingled tows (Schappe TPFL 6k).

Table 3.1 Tensile modulus, tensile strength and density of reinforcement types [2-4].

Reinforcement type	Sized carbon fibre Grafil TR30S 12k	Unsized carbon fibre Toray T700SC-60E 24k	Schappe TPFL 6k
Tow tensile modulus (GPa)	235	230	245
Tow tensile strength (MPa)	4410	4900	3800
Density (g/cm^3)	1.79	1.80	1.78

3.1.2 Nylon 12 powder

Nylon 12 powder was chosen for its relative availability. Unlike most high performance aromatic semi-crystalline thermoplastics, nylon can be processed below 300°C, which permitted safe handling of the heating die within the tolerances given by health and safety protocols in place at the laboratory. Nylon 12 is also the matrix material for Schappe's commingled tows, making a direct comparison between rods produced from dry fibre reinforcement and commingled tows more relevant.

Nylon 12 powder was obtained in the form of Duraform PA, which was sourced from 3DSystems and kindly donated to this project by the Centre for Advanced Additive Manufacturing (AdAM) at the University of Sheffield.

Polyamides are well known for absorbing large quantities of water in comparison with other synthetic polymers, with nylon-6 absorbing as much as 9% by mass of water. Water enters the amorphous phase of the polymer structure and mobilises chains by weakening the hydrogen bonds between coincident amide groups. This serves to lower the glass transition temperature and reduce the stiffness of the polymer [5, 6]. Polymer feedstock can be dried in advance of processing, although a complete absence of water may not be optimal. In promoting chain mobility, water may act as a plasticising agent and nylons have been observed to become excessively brittle when fully dried [7]. Sudduth reported manufacturers' guidelines for the injection moulding of nylon-6,6 and recommended a water content between 0.15% and 0.35% by weight of the polymer and that the water content be permitted to stabilise before use to prevent variation in processing conditions and dimensional warping [8]. Nylon 12 absorbs considerably less moisture than other nylons and as such has a lower equilibrium moisture content [9]. Duraform PA, the nylon 12 powder used in this study, has been reported as having a moisture content at equilibrium at 23°C and 50% relative humidity of 0.41% [10, 11]. Due to the relatively low moisture content inherent to the powder at laboratory conditions, the polymer was not dried prior to use.

3.1.3 Commercial carbon fibre/epoxy rods

Tests were also carried out on commercially available 3mm diameter carbon fibre/epoxy rods sourced from Easy Composites, which were included as a control group. A summary of their use in this project can be found in §3.3.4.

3.2 Control of major processing variables

Through familiarisation with the working parameters of the pultruder and their optimisation, the following processing variables were observed to have the greatest influence on the properties of the produced articles:

- Powder spray delivery
    - As powder coating occurred by electrostatic attraction, control of air speed was important in preventing powder from being pneumatically blown away from the surface of the tow.
    - The magnitude of voltage and current affected the rate of back-ionisation and charge penetration of the fibre surface area.
    - Loading of the polymer on the carbon fibre tows was controlled by the rate of deposition of powder into the spray stream.
- Line speed
    - The time spent by dry tows beneath the path of the electrostatic spray gun affected the rate at which powder accumulated at the surface.
    - Line speed also determined the residence time of a given volume of a rod inside the heating die and pre-heater. This directly affected the local degree of polymer flow and the extent of consolidation.
- Pre-heater temperature
    - Before entering the heating die, the powder-coated tow was softened by the pre-heater. This reduced the viscosity of the polymer before it reached the die entrance.

- Heating die temperature
    - Reduced viscosity of thermoplastic resins at higher temperatures contributed to better consolidation.
    - The temperature of the die was controlled to avoid polymer degradation.

Of these parameters, only the line speed was varied between manufacturing operations. The pre-heater and heating die temperatures and the cooling rate were kept constant and these factors became part of the standard operating conditions:

- Control of the cooling regime was beyond the abilities of the equipment due to limitations of space and consistency in the temperature of the water, which was supplied from a commonly used water line.
- The temperature of the pre-heater was kept at 220°C, which was found to be sufficient to melt the powder without allowing the molten polymer to drip off the tow.
- Degradation of the polymer was visible at temperatures exceeding 300°C. Due to the inherent limitation in the responsiveness of the temperature controller, temperature fluctuations of ±10ºC were observed. The maximum temperature judged safe to avoid harmful spikes in the heating die temperature was therefore 280°C, as determined by thermogravimetric analysis in §3.2.1. This maximal temperature was used in anticipation of the polymer viscosity being lower at higher temperatures.

3.2.1 Heating and cooling

Thermogravimetric analysis of nylon 12 powder was performed with a Perkin Elmer Pyris 1 TGA. The test was undertaken at a heating rate of 10°C/min within an atmosphere composed of two parts of pure nitrogen and one part of air. The analysis shows that mass change of the powder was noticeable above 300°C, which can be taken as the temperature for significant degradation of the polymer. It was expected that the FRP would consolidate more easily at lower polymer viscosities [12], which are attainable at higher temperatures. The temperature of the heating die was therefore held at the highest safe temperature, at which the polymer would be least viscous without experiencing degradation. From the thermogravimetric analysis graph shown in Figure 3.1 this was judged to occur at 290°C. The die was thus heated to 280°C for all pultrusion trials to account for fluctuations in the temperature control.

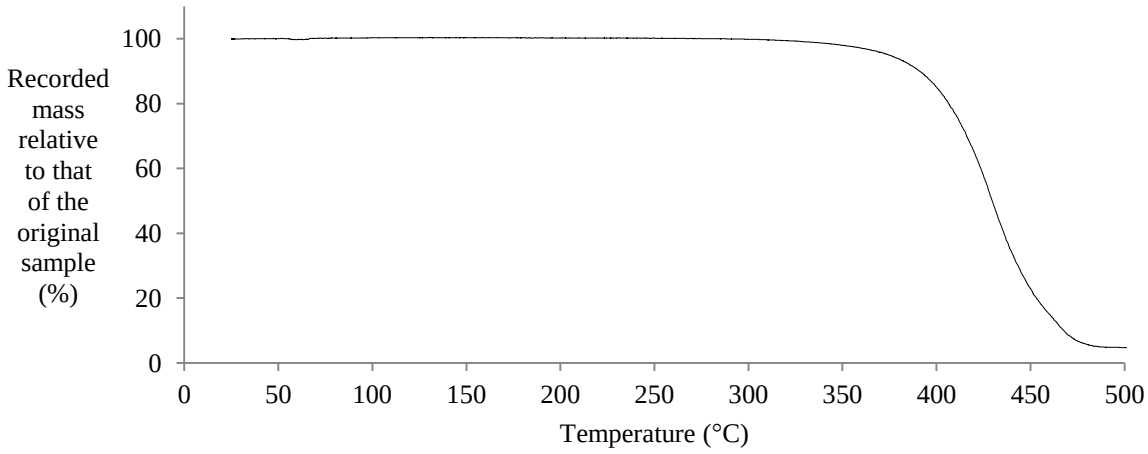

Figure 3.1 Thermogravimetric analysis of Duraform PA nylon 12 powder.

As nylon 12 typically melts between 175-180°C [13], the pre-heater was held above this temperature. A trade-off was found between uniformity of melting across the width and depth of the impregnated tow and the lowering of viscosity at elevated temperatures. If the temperature was too low, the powder would not fully melt and if it was too high the polymer would flow towards the underside of the tow. At 220°C the nylon powder was observed to fully melt evenly around the carbon fibre tow without pooling at the bottom. The pre-heater was operated at this temperature for all pultrusions.

3.2.2 Measurement of polymer crystallinity

Differential scanning calorimetry (DSC) was performed on a Perkin Elmer DSC 8500 to ascertain the crystallinity of unprocessed nylon powder and polymer that had been heated and cooled in the pultrusion process. Samples were taken from Duraform PA12 powder feedstock and flakes of unreinforced resin stripped from a pultruded rod of 2 tows of unsized carbon fibres and nylon 12, which had been processed at a standard line speed of 3.3mm/min. The heating rate was recorded as the change in energy with increasing temperature relative to an empty reference pan. Percentage crystallinity was calculated using the area under the melting and crystallisation peaks during the DSC cycle. These regions are highlighted with dashed lines in the DSC plots for both experiments in Figure 3.2 and Figure 3.3.

The percentage crystallinity of the polymer was determined from the DSC plots using the area within the peaks, which was bound within the 'virtual baseline' as described in ISO 11357. The area under the peaks was determined by integrating the change in the heating rate that was recorded at each discrete temperature increment. As outlined by Shah [14], the difference in melting and crystallisation enthalpies can be compared with the heat of melting of a sample that is 100% crystalline. Gogolewski, et al determined a theoretical heat of melting of 209.3 J/g for 100% crystalline nylon 12 [15]. The product of the heating rate and temperature therefore gave the following relations:

$$\text{Area under peak } (\text{JKs}^{-1}) = \frac{\text{heat} \times \text{temperature}}{\text{time}} \qquad \text{(eq. 3.1)}$$

$$\text{Energy of phase change } (\text{J}) = \frac{\text{peak area}}{\text{heating rate}} \qquad \text{(eq. 3.2)}$$

$$\text{Enthalpy of phase change } (\text{Jg}^{-1}) = \frac{\text{Energy of phase change}}{\text{sample mass}} \qquad \text{(eq. 3.3)}$$

$$\text{Polymer crystallinity } (\%) = \left(\frac{\text{Melting}-\text{Crystallisation enthalpies}}{\text{Heat of melting of 100\% crystalline polymer}}\right) \times 100 \qquad \text{(eq. 3.4)}$$

Following this methodology gave percentage crystallinity of 43.4% for the unprocessed Duraform PA12 powder and 23.9% for the unreinforced polymer taken from the pultruded rod. This indicates that under standard processing conditions the polymer cooled sufficiently quickly to inhibit extensive crystallisation of the matrix. The decrease in crystallinity following processing indicates that the polymer sample had cooled relatively quickly, or else the crystallinity would not have appeared to have changed. This finding demonstrates that the method of water cooling by immersion in a stream of water was valid for cooling the rod to a temperature below its melting point.

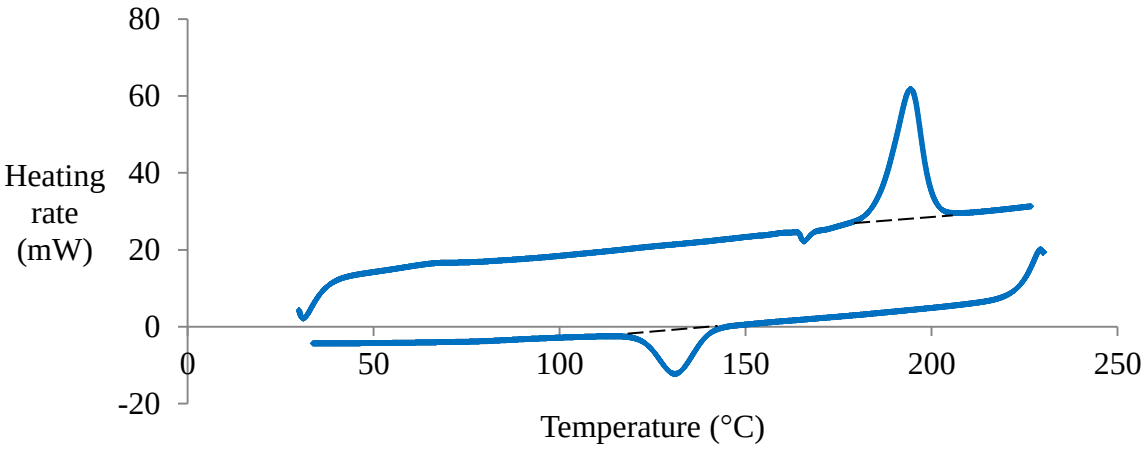

Figure 3.2 DSC of untreated Duraform PA12, performed at a heating rate of 50°C/min, with 'virtual baselines' shown as a dotted lines.

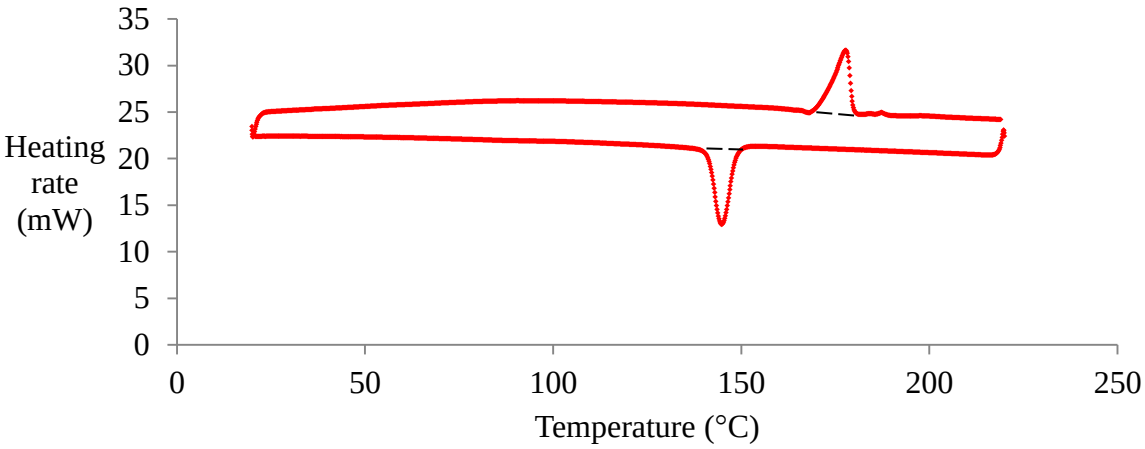

Figure 3.3 DSC of pure nylon 12 taken from an unreinforced section of a pultruded rod of 2 tows of unsized carbon fibre, performed at a heating rate of 20°C/min, with 'virtual baselines' shown as a dotted lines.

As shown by Starkweather et al. and Bessell et al., there is an approximately linear relationship between the bulk tensile stiffness of polyamides and percentage of crystallinity within a range of 10% to 50% [16, 17]. Taking percentage crystallinities of the processed and unprocessed polymer as 23.9% and 43.4% as measured by DSC, the processed polymer has approximately 55% of the crystallinity of the unprocessed polymer. As stated in the Duraform PA datasheet [18], the Young's modulus of the unprocessed nylon 12 is 1.59GPa. Assuming a linear relationship between polymer stiffness and crystallinity, the Young's modulus of the processed polymer from the cooled rod may therefore be estimated as 0.88GPa, or 55% that of the unprocessed polymer.

The work of Bessell, et al. suggested a non-linear correlation between crystallinity and other mechanical properties such as toughness and yield stress. They concluded that a variety of microstructural factors, including spherulite size and molecular weight distribution, contribute to these trends [16]. While a linear relationship between polymer stiffness and degree of crystallinity has been broadly shown to hold for polyamides, crystallisation

mechanisms and the resulting morphology of crystallites is dissimilar between nylons of differing chemical structure and thermal history [19]. For instance, even-even nylons such as PA-66 and PA-610 are known to form a triclinic α-structure [20] and uneven nylons and even nylons with more than seven carbon atoms, have been shown to predominantly form a monoclinic γ-structure [21]. Furthermore, depending on the conditions of crystallisation, a variety of crystal phases may be stable in PA-12 [22]. The complex dependence of tensile strength and impact resistance on the crystallinity, molecular composition and thermal history of a nylon polymer prevents a straightforward estimation of these properties as has been undertaken above for Young's modulus.

3.2.3 Parameters for electrostatic spraying

As noted in §2.4.2, at greater air flow rates, pneumatic forces overcome the electrostatic attraction between the oncoming powder and the fibres. For this reason air velocity is inversely proportional to the efficiency of deposition [23]. Given the small distance between the spray gun and the fibres, optimisation involved delivering a minimal total volumetric flow to prevent blowing away powder that had adhered to the fibre surface. The 'smart flow' function was enabled on the Nordson spray gun, which automatically adjusted the atomising air pressure with respect to the total volumetric flow, ensuring that the powder velocity remained constant throughout operation. The minimal powder flow rate that resulted in any appreciable constant flow was found to occur at a setting of 30% of total flow. As the input pressure was 5.0bar, this gave a powder flow pressure of approximately 1.5bar. At a flow pressure of 1.5bar, the minimal atomising air flow pressure was found to occur at 19% of the total powder flow pressure, or approximately 0.29bar. Fine control of air flow was unstable below these minimal limits of powder flow and atomising air pressures, which were taken to be the lowest possible deposition rates for this model of spray gun. Nevertheless, this minimal output was found to give a slightly excessive powder coating so all manufacturing was therefore done at these rates.

To reduce back-ionisation and encourage penetration of Faraday cages appearing at recesses between fibres, it was imperative to keep current and voltage at relatively low levels [24]. This was especially important to this application, where the distance between the tows and spray gun was small and the resistance of the air gap was therefore low. Using the 'recoat' low power option on the control console, the current and voltage were set at 15μA and 40kV.

3.2.4 Coping with the accumulation of excessive resin

Pultrusion does not apply external pressure to the FRP, which is common practice with an autoclave or hot press curing. The only forces acting on the tows are therefore friction with the internal walls of the die and the pressure exerted onto the fibres by the squeezing of excess polymer at the die entrance, as noted in §2.5.1. A surplus of polymer at the die entrance was therefore taken as a sign that the fibres were carrying as much resin into the die as possible. The opposite – a deficit in the quantity of resin entering the die – would imply that there would not be enough resin to be fully wet out the fibres during the consolidation phase.

A surplus was observed for all manufacturing conditions. If the excess of resin forming at the die entrance was not removed, it would slowly degrade over a period of hours and seize at the die entrance, preventing the ingress of any further tows, as shown in Figure 3.4. To prevent

this from happening, the molten resin was regularly picked out of the die entrance with a machinist's scribe, shown in Figure 3.5 and Figure 3.6.

Figure 3.4 If not removed, excess polymer at the die entrance would degrade and block the die, causing the tows to seize at the entrance.

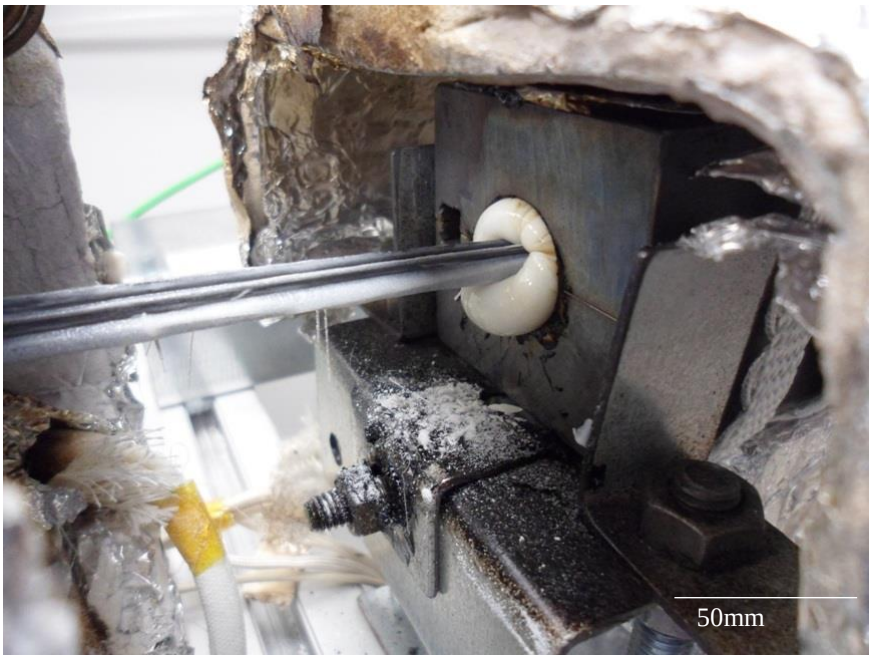

Figure 3.5 Excess polymer building up at the die entrance.

Figure 3.6 Extraction of molten polymer using a machinist's scribe.

3.2.5 Line speed

The motors controlling the traction and pinch rollers were both geared with a maximum rotational speed of 3.3rpm. In order for the fibres to be delivered at the same rate as they were pulled through the die, the feed rate of the pinch rollers and the pulling rate had to be the same. Tension in the fibres was maintained by actually setting the speed of the pinch roller slightly slower than this, whereby the tows were stretched until the tension in the fibres overcame the frictional resistance of the rollers. Tows were thus fed into the powder chamber by a combination of slipping and sliding over the pinch rollers.

Due to manual setting of the motor speed using an analogue dial, line speed was varied in half 'units' of the motor controller. A speed of 2.0 units was found to be the minimum at which the controller could accurately hold a constant rate of rotation, owing to backlash from the high gear ratio. Adjustments of the dial between manufacturing on different days resulted in some minor inconsistencies across the line speeds. For instance, the rods for tensile tests were produced at line speeds ranging between 3.1cm/min to 3.6cm/min.

3.2.6 Summary of standard manufacturing conditions

Unless otherwise stated, the following conditions were used in the manufacturing of all pultruded rods:

- Sized and unsized fibres were spread by the action of a pinch wheel, through which the fibres were held separated before entering the powder chamber. Commingled tows did not require spreading since the reinforcing and polymer fibres were already intermingled prior to use, which is described in §3.2.7.
- The electrostatic spray gun was operated with the following conditions:
    - The powder flow pressure was 30% of overall input pressure, or 1.5bar.
    - The atomising air pressure was 19% of the powder flow, or 0.29bar.
    - The current and voltage were 15µA and 40kV, respectively.
- The temperatures of the pre-heater and heating die were 220°C and 280°C, respectively.

- The line speed was set at 3.3cm/min.
    - Some productions were undertaken at varying line speeds to test the effect of this parameter. A summary of rods produced for these tests is provided in §3.3.2.

3.2.7 Pultrusion with commingled tows

At most, 11 tows could be squeezed into the die without catching on its edges. However, this still left a significant air gap between tows, which became apparent during the manufacturing stage. There was no accumulation of excessive polymer at the die entrance and the rods that emerged were not uniform in cross-section, as seen in Figure 3.7 and Figure 3.8.

Figure 3.7 Pultrusion of bare commingled tows did not result in a build-up of polymer at the die entrance, which indicated an inadequate quantity of polymer.

Figure 3.8 A non-circular rod of fused commingled tows emerging from the heating die.

To overcome this deficit of polymer entering the die, the commingled tows were sprayed with nylon 12 powder as they passed through the powder chamber. The resin of the commingled tows was the same polyamide as the powder, which ensured compatibility between the two matrices. Despite containing a high proportion of insulating polymer and having a relatively small surface area of contact with the grounding strip inside the powder chamber, the tows were nonetheless sufficiently conductive to permit electrostatic spraying. However, as the tows were not spread out, they were only coated by the nylon powder on the outside of the tows.

Pultrusion was unsuccessful with 10 , 11 or 12 commingled tows; in both these cases manufacturing terminated with fibres being caught at the die entrance. By process of reducing the number of tows in separate trials, continuous pultrusion was achieved with 9 commingled tows, albeit with a higher volume of powder spray. The standard electrostatic spraying conditions of 1.5bar of powder flow pressure and 0.29bar for atomising air pressure were not high enough to result in excess resin forming at the die entrance. This was corrected by increasing the atomising air pressure to 20% of the powder flow, or 0.3bar. This gave a sufficient coating on the commingled tows to result in the accretion of polymer at the die entrance. In all other respects, the standard manufacturing conditions used in the putlrusion of dry carbon fibre reinforcement were maintained, including manual removal of excessive resin at the die entrance.

A consistently lower quality of surface finish was encountered for rods manufactured with commingled tows, which manifested as loops of torn fibres that adhered loosely to the surface of the rods. Given the discontinuous nature of the stretch-broken carbon fibres, it is postulated that this resulted from filaments snagging on the seam of the split die. This was only observed for rods produced from the commingled tows, as shown in Figure 3.9.

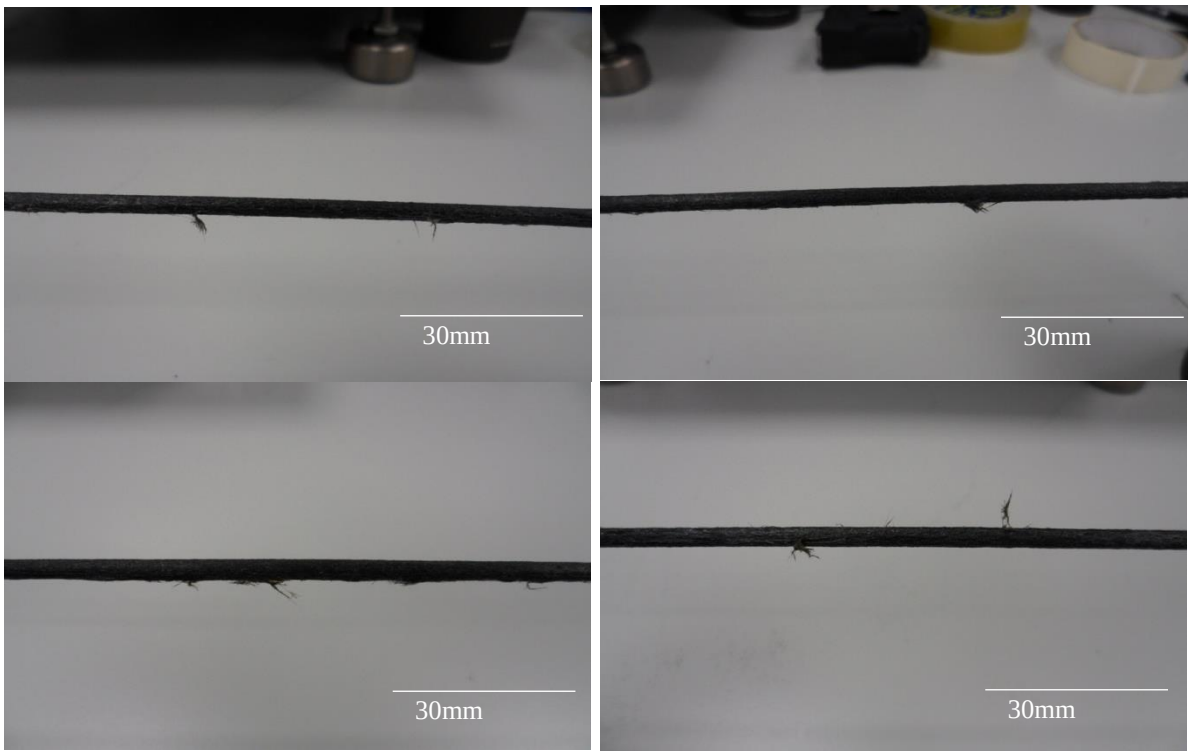

Figure 3.9 Images of deformities occurring along the length of a rod pultruded from 9 tows of commingled tows coated with nylon 12 powder.

3.3 Pultruded article productivity

With a storage capacity of six racks, the pultrusion line was capable of delivering a maximum of 6 tows of dry reinforcement, or 12 commingled tows that had been spooled onto narrower bobbins. As the unsized carbon fibre tows had 24000 filaments, in comparison with 12000 for the sized fibres, twice the fibre loading was attainable with the same number of bobbins for the unsized carbon tows. As noted in §3.1.1, this was an unfortunate consequence of not being able to source tows of the same filament count from different feedstocks. Rods were produced with different loadings of reinforcement for the purpose of evaluating the effect of fibre volume fraction on the mechanical properties of the pultruded rods.

Although the racks were capable of delivering 6 tows of unsized fibres, a practical maximum of 4 tows was possible before the die entrance seized from overloading with loosely bonded filaments. Pultrusion of 5 tows of unsized fibres was only possible for short distances, beyond which manufacturing had to be terminated. An example of the difficulties encountered is given in Figure 3.10. For this reason, rods from unsized fibres were created with 2, 3 and 4 tows.

Figure 3.10 Die seizure during attempt to pultrude 5 tows of unsized fibres.

The severity of fibre discontinuities in tows from unsized fibres reflected the lack of a binding agent to provide cohesion between filaments. Fibre alignment was maintained by the tension in the tows from the traction puller, which acted on whole tows rather than individual longitudinal fibres. The tension in fibres that were not directly pulled was therefore maintained by friction or entanglement with neighbouring filaments. As fibres reached the entrance to the heating die, contact with the hard surface of the walls of the die caused misdirection of fibres not tightly bound within the tow, such as discontinuous fibres that were

the product of fibre breakage. Lacking a guiding tension to pull them through the die, these loose fibres collected in tangles at the die entrance, as demonstrated in Figure 3.11. This was exacerbated by the powder impregnation process. Although a minimal air velocity was used for powder spraying, as described in §3.2.3, the pneumatic pressure was enough to separate discontinuous fibres from the main body of the tows before reaching the die entrance, as shown in Figure 3.12.

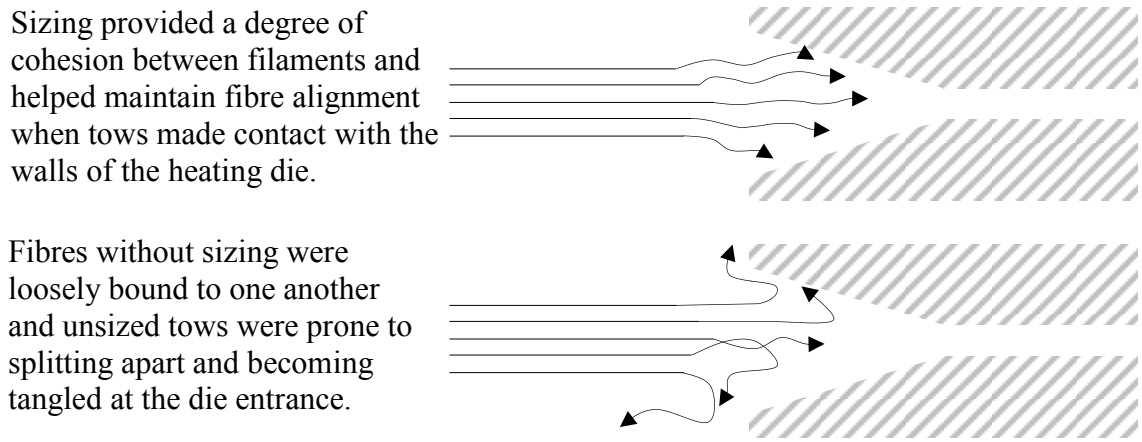

Figure 3.1 Schematic diagram of tangling of discontinuous fibres in unsized tows.

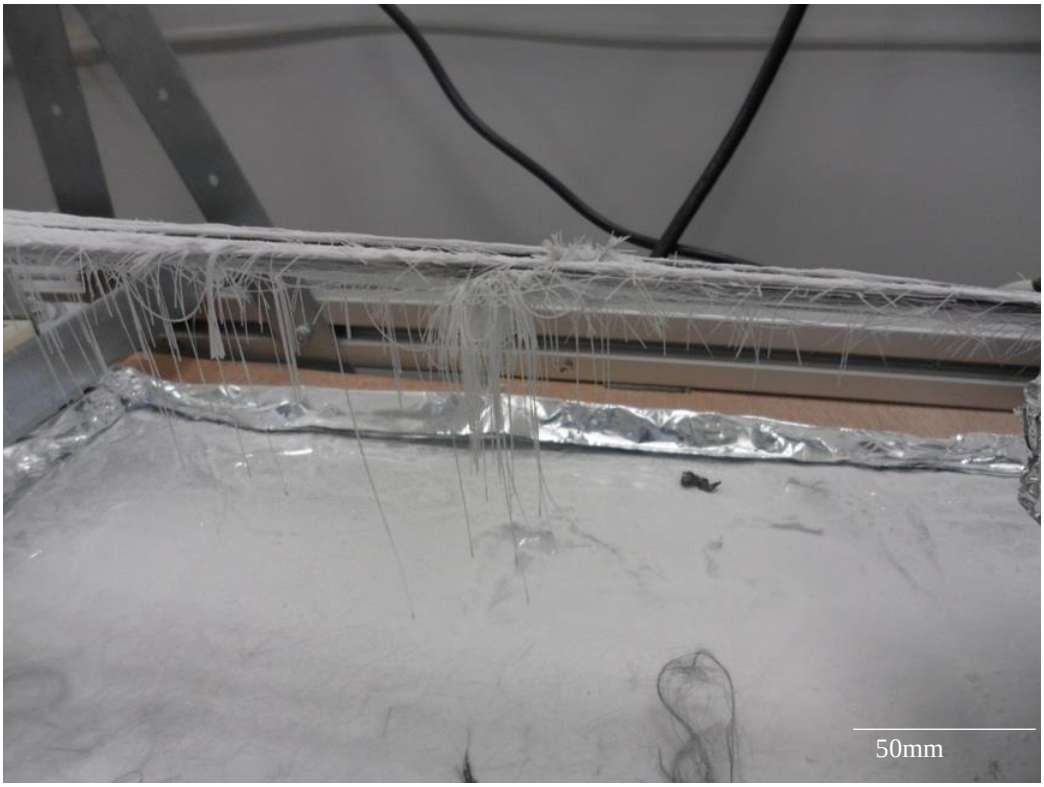

Figure 3.12 Severe discontinuities encountered in unsized tows following powder spraying.

While 2.5m rods were successfully pultruded from tows of sized fibres and commingled tows for the creation of hybrid FRP and steel strands, unavoidable die seizure due to discontinuous fibres prevented the pultusion of rods of this length from unsized fibres, as shown in Figure 3.13 and Figure 3.14. For this reason, hybrid strands could not be made from rods of unsized fibres.

Figure 3.13 Die seizure due to the discontinuities in unsized fibres.

Figure 3.14 Matted fibres emerged from the die after loose fibres were caught at the entrance.

3.3.1 Pultruded rods for tensile tests

As described in depth in §4.4, ASTM D3039 was taken as a guide for conducting tensile tests on pultruded rods. For this purpose, rods for each fibre type were cut into ten 390mm samples. Pultruded rods were produced from three different loadings of carbon fibre for sized and unsized carbon fibre bobbins, whereas one loading was used for pultrusion of the commingled tows. An inventory of the rods produced for tensile tests is provided in Table 3.2.

Table 3.2 Summary of the pultruded rods produced for tensile tests.

Reinforcement type	Fibre loading	Line speed (cm/min)
Sized carbon fibre Grafil TR30S 12K	4 tows (48k)	3.3
	5 tows (60k)	3.6
	6 tows (72k)	3.3
Unsized carbon fibre Toray T700SC-60E 24k	2 tows (48k)	3.3
	3 tows (72k)	3.2
	4 tows (96k)	3.1
Schappe TPFL	9 tows (54k)	3.3

3.3.2 Pultruded rods for flexural tests

100mm pultruded rods were cut for flexural test samples that performed according to ISO 14125, as described in §4.3. Aside from those rods manufactured with non-standard line speeds, standard manufacturing conditions were used for all other rods. A summary of the rods produced for flexural tests is given in Table 3.3. Short sections for optical microscopy were also taken from the rods pultruded for flexural tests at intervals of 100mm.

Table 3.3 Summary of rods produced for flexural tests.

Reinforcement type	Fibre loading	Line speed (cm/min)
Sized carbon fibre Grafil TR30S 12K	4 tows (48k)	3.3 4.7 6.4 7.4 9.0
	5 tows (60k)	3.6 5.0 6.5 6.9 8.3
	6 tows (72k)	3.3 4.4 6.9 7.9 8.5
Unsized carbon fibre Toray T700SC-60E 24k	2 tows (48k)	3.3
	3 tows (72k)	3.2
	4 tows (96k)	3.1
Schappe TPFL	9 tows (54k)	3.3

3.3.3 Pultruded rods for hybrid strands

2.5m pultruded rods were produced for the creation of hybrid strands at the Bridon Technology Centre in Doncaster. Rods were produced from 6 tows of sized fibres and 9 tows of commingled tows, as summarised in Table 3.4.

Table 3.4 Summary of pultruded rods produced for the creation of hybrid strands.

Reinforcement type	Fibre loading	Line speed (cm/min)
Sized carbon fibre Grafil TR30S 12K	6 tows (72k)	3.3
Schappe TPFL	9 tows (54k)	3.3

3.3.4 Pultruded rod control groups

Commercially obtained pultruded FRP rods were also tested alongside the aforementioned rods pultruded from sized and unsized fibres and commingled tows. 3mm diameter rods made from carbon fibre and thermosetting epoxy resin were bought from Easy Composites in order to provide a control group. These were used to compare the performance of in-house pultruded rods with a commercially available product. Rods from Easy Composites were included in tension and flexion tests. However, the creation hybrid strands required 2.5m rods, which was longer than the 3rd party supplier of the carbon fibre/epoxy rods was willing to provide. For this reason, rods from carbon fibre and thermosetting vinyl ester rods were kindly provided by Bridon. A control group of hybrid steel and carbon fibre/vinyl ester was therefore produced for tension tests of hybrid strands. A summary of control rods used is provided in Table 3.5.

Table 3.5 Summary of carbon fibre/epoxy and carbon fibre/vinyl ester control groups.

Control group	Source	Tests
Carbon fibre/epoxy	Easy Composites	Tension of rods Flexion of rods
Carbon fibre/vinyl ester	Bridon	Tension of hybrid strands

3.4 Concluding summary

Rods were pultruded from nylon 12 powder and tows of sized and unsized dry fibres and commingled carbon fibre and nylon 12 filaments. Parameters affecting electrostatic powder spray, line speed and the temperature of the pre-heater and heating die were found to exert the greatest influence on article quality. Optimisation trials were undertaken to ascertain standard manufacturing conditions, which were used to pultrude rods for flexural and tensile tests as well as sections for optical microscopy and longer 2.5m rods for producing hybrid strands. The techniques used to prepare samples from these rods and the methodologies undertaken for testing them are presented in Chapter 4, which also describes the development of novel methodologies for the characterisation of the tensile strength and stiffness of hybrid strands.

3.5 References

1. Dennis, H.R., D.L. Hunter, D. Chang, S. Kim, J.L. White, J.W. Cho, and D.R. Paul, Effect of melt processing conditions on the extent of exfoliation in organoclay-based nanocomposites. Polymer, 2001. 42(23), p. 9513-9522
2. Yuan, Q. and R.D.K. Misra, Impact fracture behavior of clay–reinforced polypropylene nanocomposites. Polymer, 2006. 47(12), p. 4421-4433
3. Paul, D.R. and L.M. Robeson, Polymer nanotechnology: Nanocomposites. Polymer, 2008. 49(15), p. 3187-3204
4. Tanniru, M., Q. Yuan, and R.D.K. Misra, On significant retention of impact strength in clay–reinforced high-density polyethylene (HDPE) nanocomposites. Polymer, 2006. 47(6), p. 2133-2146
5. Reuvers, N.J.W., H.P. Huinink, H.R. Fischer, and O.C.G. Adan, Quantitative Water Uptake Study in Thin Nylon-6 Films with NMR Imaging. Macromolecules, 2012. 45(4), p. 1937-1945
6. Preda, F.-M., A. Alegría, A. Bocahut, L.-A. Fillot, D.R. Long, and P. Sotta, Investigation of Water Diffusion Mechanisms in Relation to Polymer Relaxations in Polyamides. Macromolecules, 2015. 48(16), p. 5730-5741
7. Paterson, M.W.A. and J.R. White, Effect of water absorption on residual stresses in injection-moulded nylon 6,6. Journal of Materials Science, 1992. 27(22), p. 6229-6240
8. Sudduth, R.D., Hydrolysis effects on the molecular weight degradation of condensation polymers as estimated from their prior drying condition. Polymer Engineering & Science, 1996. 36(16), p. 2135-2141
9. Giles Jr, H.F., J.R. Wagner Jr, and E.M. Mount Iii, 22 - Processing Recommendations for Various Resin Systems, in Extrusion, H.F.G.R.W.M. Mount, Editor. 2005, William Andrew Publishing Norwich, NY. p. 207-219
10. Zarringhalam, H., N. Hopkinson, N.F. Kamperman, and J.J. de Vlieger, Effects of processing on microstructure and properties of SLS Nylon 12. Materials Science and Engineering: A, 2006. 435–436, p. 172-180

11. Systems, D. Duraform PA for SLS. 2001 23/09/2015: http://www.3dsystems.com/products/datafiles/lasersintering/datasheets/DuraForm_uk.pdf
12. Hegde, R., G. Bhat, J. Spruiell, and R. Benson, Structure and properties of polypropylene-nanoclay composites. Journal of Polymer Research, 2013. 20(12), p. 1-13
13. Fina, A., F. Cuttica, and G. Camino, Ignition of polypropylene/montmorillonite nanocomposites. Polymer Degradation and Stability, 2012. 97(12), p. 2619-2626
14. Shah, B., V.K. Kakumanu, and A.K. Bansal, Analytical techniques for quantification of amorphous/crystalline phases in pharmaceutical solids. Journal of Pharmaceutical Sciences, 2006. 95(8), p. 1641-1665
15. Gogolewski, S., K. Czerntawska, and M. Gastorek, Effect of annealing on thermal properties and crystalline structure of polyamides. Nylon 12 (polylaurolactam). Colloid and Polymer Science, 1980. 258(10), p. 1130-1136
16. Bessell, T.J., D. Hull, and J.B. Shortall, The effect of polymerization conditions and crystallinity on the mechanical properties and fracture of spherulitic nylon 6. Journal of Materials Science, 1975. 10(7), p. 1127-1136
17. Starkweather, H.W., G.E. Moore, J.E. Hansen, T.M. Roder, and R.E. Brooks, Effect of crystallinity on the properties of nylons. Journal of Polymer Science, 1956. 21(98), p. 189-204
18. 3DSystems. Duraform PA Plastic. 21/09/2014: http://www.3dsystems.com/sites/www.3dsystems.com/files/DS_DuraForm_PA_US.pdf
19. Xenopoulos, A., Clark, E. S., Physical Structure, in Nylon Plastics Handbook, M.I. Kohan, Editor. 1995, Hanser/Gardner Publications, Inc. Cincinnati, Ohio. p. 107-138
20. Bunn, C.W. and E.V. Garner, The Crystal Structures of Two Polyamides ('Nylons'). Proceedings of the Royal Society of London A: Mathematical, Physical and Engineering Sciences, 1947. 189(1016), p. 39-68
21. Dencheva, N., T.G. Nunes, M.J. Oliveira, and Z. Denchev, Crystalline structure of polyamide 12 as revealed by solid-state 13C NMR and synchrotron WAXS and SAXS. Journal of Polymer Science Part B: Polymer Physics, 2005. 43(24), p. 3720-3733
22. Dencheva, N., Z. Denchev, M.J. Oliveira, T.G. Nunes, and S.S. Funari, Relationship between the crystalline structure and mechanical behavior in isotropic and oriented polyamide 12. Journal of Applied Polymer Science, 2008. 109(1), p. 288-302
23. Százdi, L., B. Pukánszky Jr, G.J. Vancso, and B. Pukánszky, Quantitative estimation of the reinforcing effect of layered silicates in PP nanocomposites. Polymer, 2006. 47(13), p. 4638-4648
24. Schmidt, D., D. Shah, and E.P. Giannelis, New advances in polymer/layered silicate nanocomposites. Current Opinion in Solid State and Materials Science, 2002. 6(3), p. 205-212

4 Experimental methodology

The mechanical properties of the pultruded rods were elucidated with tensile and flexural tests, and the morphology of cross-sections was analysed with photomicrographs. The methodologies for these tests are presented in this chapter.

4.1 Specimen geometry

The geometries of all specimens were recorded prior to testing. These were used in the determination of all materials properties, including cross-sectional areas used for the calculation of Young's modulus. Rod lengths were measured using a millimetre-scale steel ruler and rod diameters were measured using digital callipers with an accuracy of ±0.01mm.

4.1.1 Rod diameters

All diameters were measured three times along the length of each tensile or flexural sample. In the case of ten tensile or flexural samples, this produced a data set of 30 recorded diameters for each rod type. The diameters of rods that were produced for the testing of hybrid strands were measured 10 times at regular intervals along the full 2.5metre length. The mean diameter of each dataset was taken as the definitive value for each rod type.

4.2 Optical microscopy

Optical micrographs were recorded for all the rods produced for flexural tests. A total of 19 operating conditions were analysed, which are summarised in Table 4.1.

Table 4.1 Summary of test conditions analysed by optical microscopy.

Reinforcement type	Fibre loading	Line speeds analysed (cm/min)
Sized carbon fibre Grafil TR30S 12K	4 tows (48k)	3.3, 4.7, 6.4, 7.4, 9.0
	5 tows (60k)	3.6, 5.0, 6.5, 6.9, 8.3
	6 tows (72k)	3.3, 4.4, 6.9, 7.9, 8.5
Unsized carbon fibre Toray T700SC-60E 24k	2 tows (48k)	3.3
	3 tows (72k)	3.2
	4 tows (96k)	3.1
Schappe TPFL	11 tows (54k)	3.5

4.2.1 Preparation of microscopy samples

Individual 10mm long cross-sections was taken for optical microscopy at intervals of 100mm from the length of the main rod pultruded for flexural samples, as noted in §3.3.2. Of the 10 samples acquired from each rod, six were chosen at random for cold casting in epoxy, which was the most that would fit into each casting cup. These were carefully aligned on a piece of masking tape to ensure that the ends of the samples were flush with one another, as shown in Figure 4.1. They were also weighed to prevent them from floating in the casting epoxy.

Samples were cast with red EpoColor epoxy resin, which was mixed and then poured under vacuum into polypropylene cups containing the samples using a Buehler Cast n' Vac assembly.

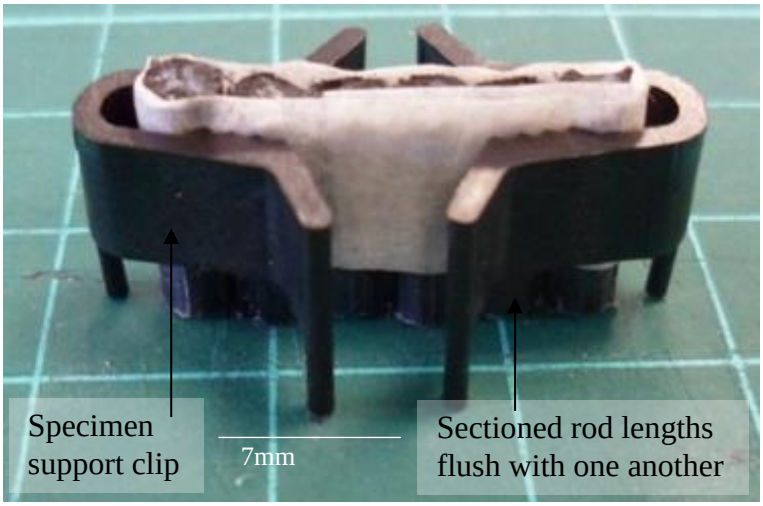

Figure 4.1 Specimen Support Clips from Buehler provided additional stability.

4.2.2 Grinding and polishing

The methodology for grinding and polishing was derived from Buehler's worked example for carbon fibre reinforced composites [1], which is summarised in Table 4.2. Samples were ground and polished on a Buehler AutoMet 250, allowing samples to be ground and polished in sets of five, with a much greater efficiency and precision than if they had been done by hand.

The grinding stage was implemented to cut away the rough top layer of the cast epoxy, which left an even surface for polishing. Grinding papers were discarded after one minute of use, ensuring that the samples were always exposed to a well-oriented SiC abrasion face. In this manner the samples were initially ground in three separate one minute stages with P600 paper and then for one minute with P1200 paper. Grinding was performed with the head and platen rotating concurrently at rotational frequencies of 60rpm and 179rpm, respectively. The rotational frequency of the platen was set as a prime number to avoid harmonic resonance.

The polishing stage was undertaken with increasingly fine diamond suspensions using counter-current rotation. Samples were first polished for 4 minutes with a 9µm suspension and then for 4 minutes with a 6µm suspension. These steps were followed by polishing with a fine 0.05µm suspension for one and a half minutes.

Table 4.2 Methodology for grinding and polishing microscopy samples.

Step	Surface	Abrasive	Fluid	Force	Time (min:sec)	Platen speed (rpm)	Head speed (rpm)	Relative rotation
1	BuehlerMet SiC	P600	Water	20N	3:00	179	60	Concurrent
2	BuehlerMet SiC	P1200	Water	20N	1:00	179	60	Concurrent
3	TexMet	9µm polycrystalline diamond suspension	Water	20N	4:00	179	60	Counter-current
4	TexMet	6µm polycrystalline diamond suspension	Water	20N	4:00	199	60	Counter-current
5	MasterTex	0.05µm polycrystalline diamond suspension	Water	20N	1:30	73	60	Counter-current

4.2.3 Determination of fibre and void volume fractions

Measurement of fibre volume fraction is ordinarily performed by analysing multiple photomicrographs of small areas of the material that are assumed to be representative of the whole cross-sections [2]. However, the morphology of the pultruded cross-sections showed so much variation in fibre and void volume fractions that a random selection of independent regions could not have been representative of the whole. It was therefore necessary to analyse whole cross-sections of the rods.

Optical microscopy was undertaken using a Nikon Eclipse LV150 optical microscope with Buehler OmniMet software. Bright field and dark field images were taken at a magnification of x5 for each cross-section and stitched together into montages. A higher magnification would have been preferable but the computer lacked the computational power required to stitch together images generated at higher magnifications.

While dark field images were effective in capturing colouration, the contrast was not well suited to differentiating between carbon fibres and the polymer matrix. Under the reversed contrast of the bright field, carbon fibres shone as bright spots against the matrix, which also contrasted effectively with the dark recesses of voids. Dark field montages were therefore captured for discussion of morphology while analyses of volume fractions were performed on bright field montages.

The casting resin appeared as the same contrast as the polymer matrix in bright field images so prior to analysis these areas were cut out using Inkscape image editing software and mounted on a black background. The ‘Object’ tool in the Buehler OmniMet software was first used to calculate the number of pixels of the whole area of the cross-section relative to the casting resin in the background, shown in Figure 4.2. Then it was used to calculate the proportion of the whole cross-sectional area that was taken up by fibres at the brightest contrast and by voids at the darkest contrast above the black background, as demonstrated in Figure 4.3.

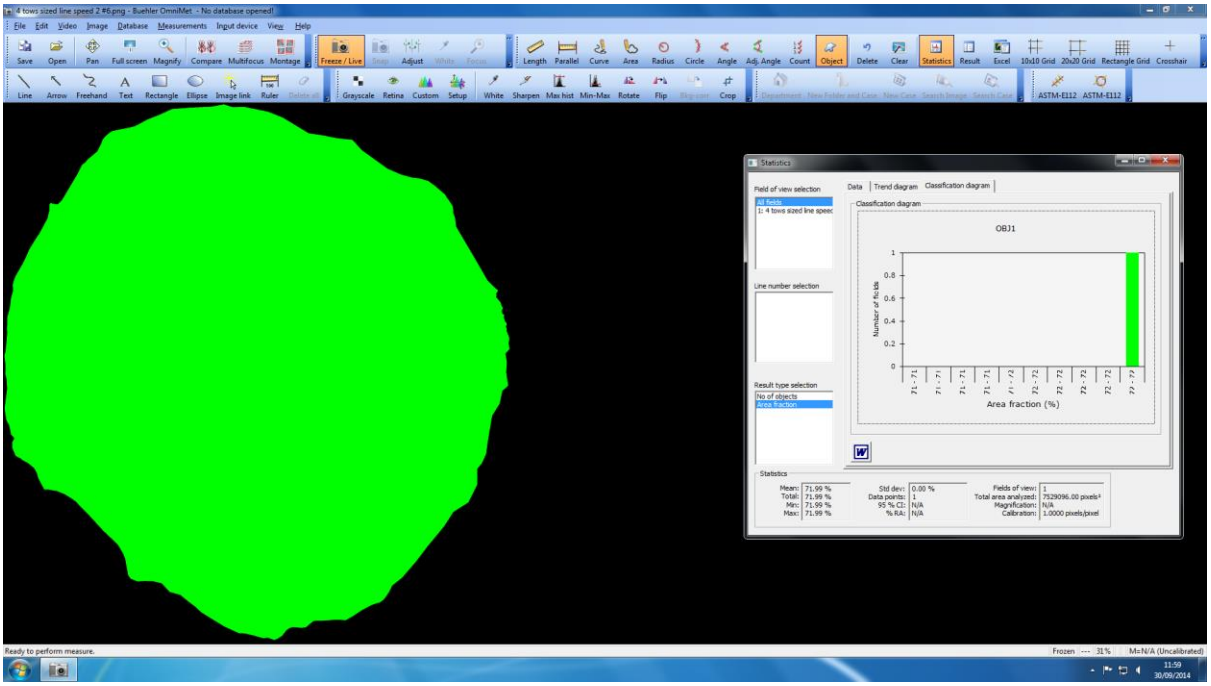

Figure 4.2 Calculation of the total area of cross-section by contrast analysis

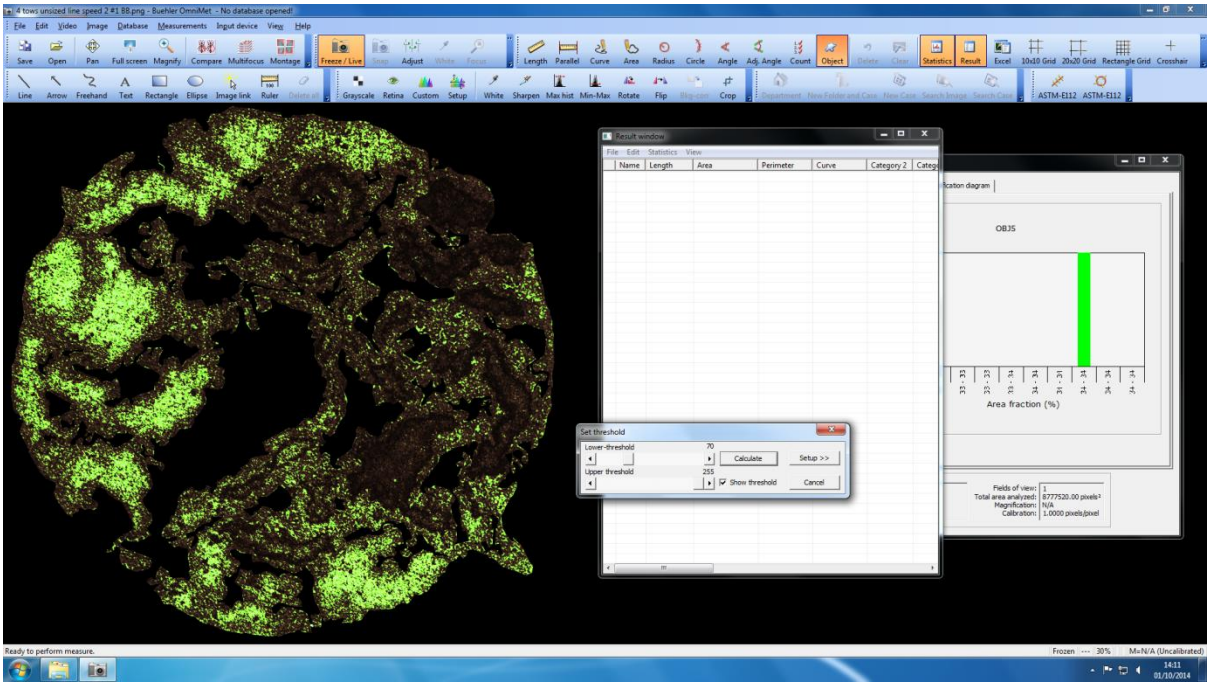

Figure 4.3 Calculation of fibre volume fraction by analysis of the area with the brightest contrast.

Fibre and void volume fractions were therefore determined by the area of the features as a proportion of the cross-sectional area:

$$\text{Fibre volume fraction } (\%) = \frac{\text{Area of brightest contrast}}{\text{Cross} - \text{sectional area}} \qquad \text{(eq. 4.1)}$$

$$\text{Void content (\%)} = \frac{\text{Area of darkest contrast}}{\text{Cross} - \text{sectional area}} \quad \text{(eq. 4.2)}$$

The definitive fibre volume fractions and void contents have been presented for each material type in Figure 5.17 and Figure 5.18 in §5.2. These refer to the mean values taken from analysis of montages for each of the six rod cross-sections that were prepared for each of the manufacturing conditions that are listed in Table 4.1, as is shown in Figure 4.1.

While measurement of void content in this way gave mean values of the cross-sectional area of the voids, it did not give any indication of their three dimension morphology or volume. This might have given valuable information for assessing how defects arose in consolidation of the rods. For instance, the appearance of ovular or cylindrical voids might have suggested inadequate filling of the die cavity caused by insufficient polymer. By contrast, large spherical voids might have been formed by trapped air that was not forced out under a high enough internal pressure made by contact between the polymer and walls of the die. Unfortunately microscopic tomography techniques were beyond the budget and scope of this project. It consequently remains unknown whether or not the relatively large imprecision in measurement of void content, as shown in Figure 5.18 in §5.2, was the result of wide ranging differences in the size or shape of voids between samples, or some combination of both.

4.3 Flexural tests

Flexural tests were performed according to the methodology for three-point bend tests as dictated in ISO 14125. This recommends specimen lengths of 100mm and outer spans of 80mm for unidirectional reinforced plastics. The standard is designed for flat coupons and specifies a sample width of 15mm and height of 2mm, whereas the rods have a circular 3mm cross-section. For all purposes other than cross-sectional geometry, the standard was followed to the same specifications as those given for flat laminate coupon samples.

Three-point bend tests were performed on a Lloyd Instruments TA500 tensile test frame with a 500N load cell, suitable for the measurement of polymer samples. The following test conditions were followed, pertaining to ISO 14125:

- Rate of extension of 1mm/min.
- Samples were 100mm long and the span of outer supports 80mm.
- Extension was measured from the position of the cross-head.

Flexural stiffness and stress were calculated using equations for circular beams loaded at the centre point of the span between two simple supports [3]:

$$\text{Flexural stiffness } (\text{Nm}^{-2}) = \frac{4\text{L}^3}{3\pi\text{d}^4}\left(\frac{\Delta\text{P}}{\Delta\text{y}}\right) \quad \text{(eq. 4.3)}$$

Where L is the span between the supports, d is the diameter of the rod and $\Delta P/\Delta y$ is the rate of change in flexion; or the gradient in the measured load, P against a measured deflection, y in the elastic region of the flexural stress-strain curve.

Flexural strength was taken as the maximum stress measured from the stress/strain curve, following this equation:

$$\text{Flexural stress } (\text{Nm}^{-2}) = \frac{8PL}{\pi d^3} \qquad \text{(eq. 4.4)}$$

4.4 Tensile tests

Following the guidance of ASTM D3039, the even application of compression on samples in the test grips is best facilitated by the use of end tabs. Typically these are applied to flat coupons with broad surface areas of contact. However, the rods were limited to a minimal curved surface area. Specialised glass fibre and epoxy end tabs were manufactured by the means of wet lay-up. 16-plies of plain woven glass fibre were laid up with EL2 laminating resin, backed with peel ply to give a rough surface on both sides. All materials were sourced from Easy Composites. This technique produced 3mm thick laminates. Channels 2mm wide and 1.8mm deep were then milled into the surface of the laminates, as shown in Figure 4.4.

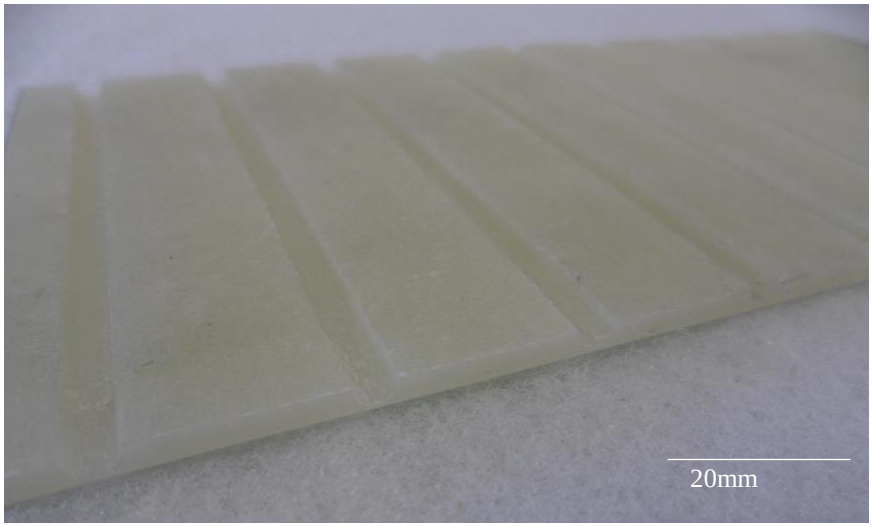

Figure 4.4 Specialised end tabs with channels milled into the surface of laminate.

The surface of the end tabs were then coated with Araldite 2015 epoxy adhesive and the 390mm rod samples were placed into the milled channels. The laminates were then pressed together, with both sides of the specimens loaded with 20kg steel plates to promote even contact at the bond line, the result of which is shown in Figure 4.5.

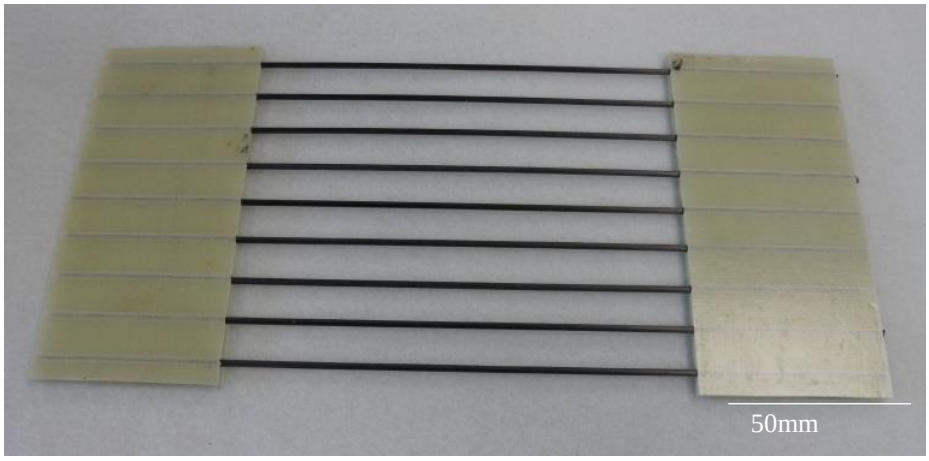

Figure 4.5. Rod samples with attached end tabs.

The end tabs were then cut with a diamond cutting blade to yield individual samples that conformed as closely as possible to the ASTM D3039 standard, shown in Figure 4.6. To this end, the gauge length of the samples was 190mm and the end tabs extended 100mm on either side of the gauge length, with a width of 20mm.

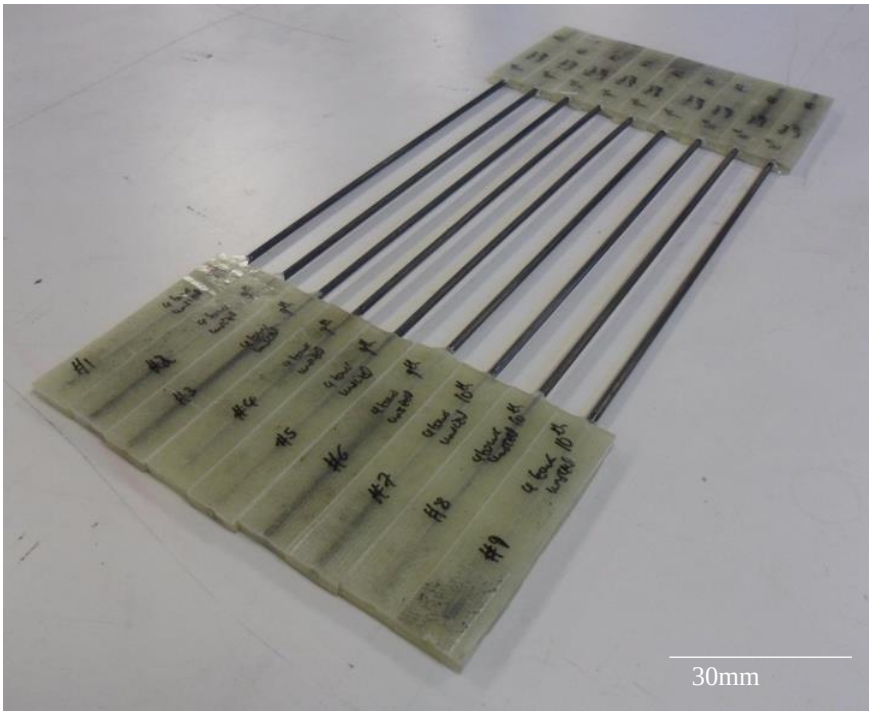

Figure 4.6 Completed tensile test specimens with end tabs.

4.4.1 Rod tensile test methodology

Tensile tests were undertaken at the test facility at the Bridon Technology Centre and were performed on a Zwick/Roell Z250 universal test frame using testXpert software. Samples were aligned with a mounting specially made to hold them parallel to the direction of loading. Samples were held in place by hydraulic grips with controlled pressure.

Using the methodology outlined in ASTM D3039, the following conditions were used for all the tests that were carried out in this part of the study:

- Rate of extension of 1mm/min.
- The gauge length of all samples was 190mm.
- Externally applied strain measuring devices such strain gauges or video extensometers avoid errors associated with deformation or movement of the test equipment or slipping of the coupon or end tabs within the jaws of the grips. For this reason, ASTM D3039 recommends the use of extensometers in order to provide more accurate values of strain. Unfortunately, it was not possible to use an extensometer with the available test equipment and it proved exceptionally difficult to find an alternative testing suite within the budget and time scale of the project. For this reason, extension was measured from movement of the cross-head.
    - This may have introduced inaccuracy into measurement of strain-dependent parameters such as Young's modulus or strain energy. The measured tensile stiffness for the rods was in the range of 42.6GPa to 76.2GPa, as shown in Figure

5.25 in §5.5.1, which should be considerably lower than the stiffness of the steel test frame. However, the stiffness of the test frame is unknown and therefore it is not possible to definitively quantify the compliance inherent in the measurement system during tests. This would be necessary for determining the extent to which compliance of the frame biased strain measurement during tests. Inaccuracies in strain measurement may also have arisen from gripping, which were minimised by the use of hydraulic jaws and specially designed end tabs.

  - The tensile stiffness of all tested rods was found to occur within a range of approximately 35GPa, as seen in Figure 5.25. Inaccuracies in the measurement of strain between individual would therefore have likely been of a similar magnitude so results between datasets should remain comparable.

- Tests were stopped when the measured load dropped to below 90% of its peak value. In practice, this occurred momentarily after the ultimate strength had been reached.
- The hydraulic pressure of the grips was set at 100bar.
  - No clear guidelines for the compression exerted by the grips were given by the standard. 100bar was found to be sufficient to prevent slipping of the end tabs without crushing them.

4.4.2 Determination of tensile properties

In addition to stress-strain curves, Young's modulus, ultimate tensile strength, strain-to-break and strain energy were used as quantitative parameters for assessing tensile properties. For all the properties that were calculated using cross-sectional area, these values were calculated using the mean rod diameter of the relevant dataset, as described in §4.1.1. For this reason all mechanical properties refer to the engineering rather than Cauchy (true) stress.

Young's modulus

Young's modulus was calculated by taking the stress-strain gradient between 0.2% and 0.4% of strain, or at the next available elastic region in the event of noise from pre-loading of the specimen. The gradient was found using equation (1) from ASTM E111:

$$\mathrm{E} = \frac{(\sigma_2 - \sigma_1)}{(\varepsilon_2 - \varepsilon_1)} \qquad \text{(eq. 4.5)}$$

E is the tensile modulus, σ_1 and σ_2 are the first and second values of stress found at the points of strain and ε_1 and ε_2 are values of strain at 0.2% and 0.4%, or at the nearest suitable region of elasticity.

Ultimate tensile strength and strain to break

As is shown in the stress-strain curves in Appendix B, there was considerable scatter in the first damage event, with some samples displaying ambiguity in the extent of the elastic region before plasticity. Ultimate tensile strength was therefore selected as the definitive measure of strength and its value was taken as the highest point in the stress-strain curve. Similarly, strain-to-break was taken as the value of strain corresponding to the ultimate tensile strength.

Strain energy

Strain energy, or the energy retained by a body under deformation [4], was calculated by integrating the region underneath a stress-strain curve. The magnitude of the distance between one datum of strain and the next was multiplied by the corresponding stress recorded at that point. These products of stress and strain increments were summed, giving the total energy per unit volume of the material:

$$\text{Specific strain energy } \left(\frac{\text{J}}{\text{m}^3}\right) = \sum_{i=0}^{n} \frac{\sigma_{ij}}{\varepsilon_i - \varepsilon_j} \quad \text{(eq. 4.6)}$$

σ_{ij} is the stress datum corresponding to the increment of strain between the points ε_i and ε_j.

The specific strain energy was then multiplied by the volume of the sample. Rods were assumed to be cylindrical. Thus volume was calculated by multiplying the cross-sectional area of the sample by the gauge length, giving the total energy of strain for the sample, the integration method for which is illustrated in Figure 4.7. The stress-strain graph shown in this figure is for the sixth tensile test sample from the set of rods manufactured from 9 tows of commingled tows, which is shown in Figure B. 27 in Appendix B.

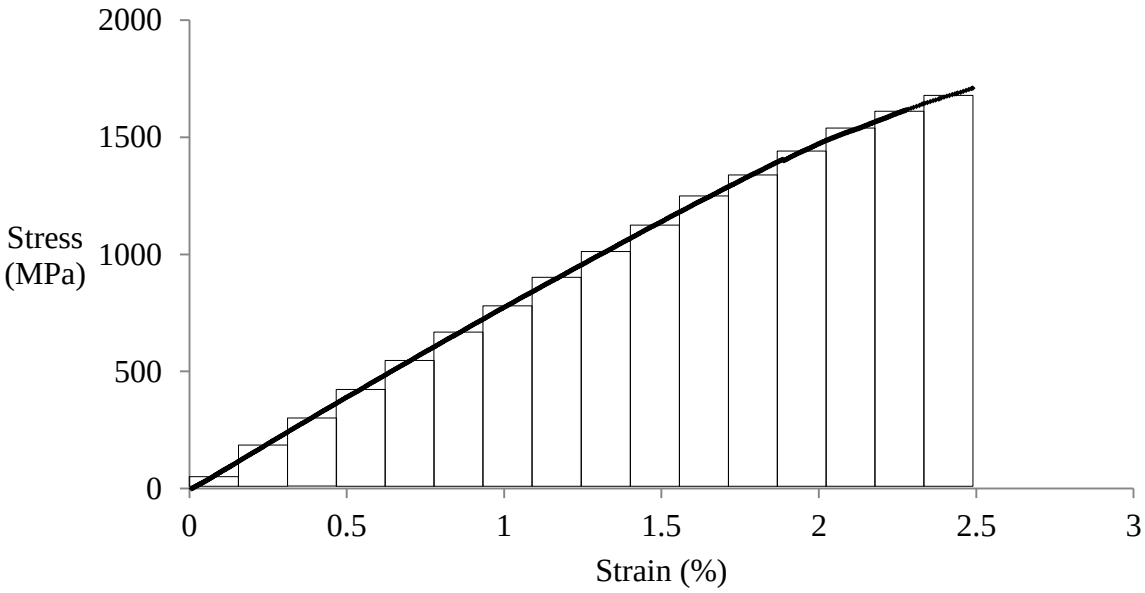

Figure 4.7 Example of integration scheme for determination of strain energy.

4.5 Tensile tests of hybrid strands

Since at the time of writing there were no industrially recognised standards for the fabrication of hybrid strands, test samples were prepared with due consideration of the bonding interaction between the outer steel wires and the FRP rods. 2200mm sections of steel strands were cut and disassembled in order to remove the central steel wire, shown in Figure 4.8. Five hybrid strands were produced with rods manufactured from 6 tows of sized fibres, five with carbon fibre/vinyl ester rods and four with rods manufactured from 9 tows of commingled tows.

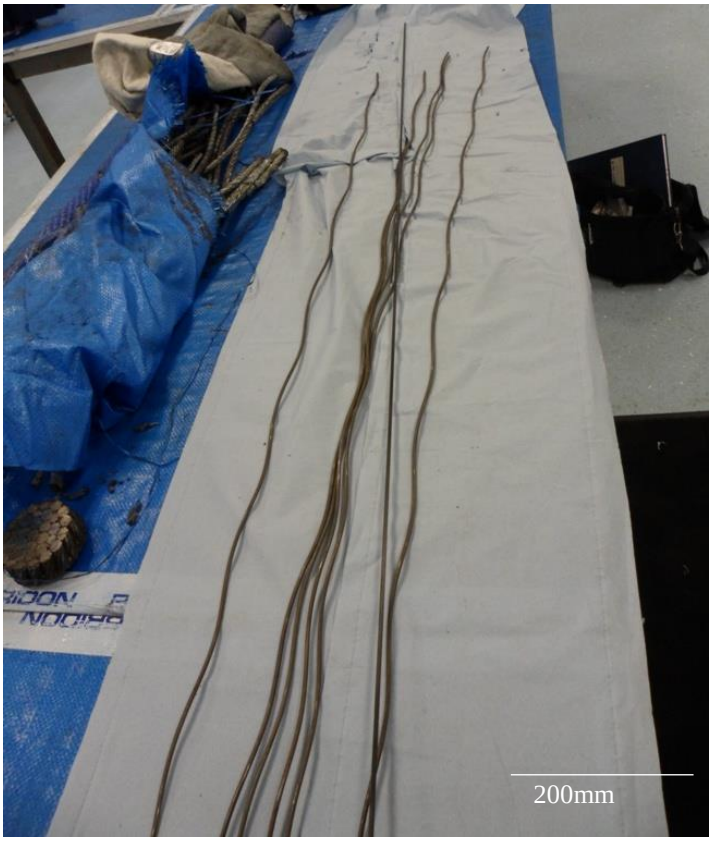

Figure 4.8 Disassembled steel strand.

Steel central wires that were removed from the strands were 3.25mm in diameter. The FRP rods were smaller in diameter; as shown in Figure 5.19 in §5.3 the mean diameters of rods from 6 sized tows and 9 commingled tows were 2.86mm and 2.91mm, respectively. To fill the cavity left between the rods and the outer wires, RT-375 fluoropolymer heat shrink tubing with a 0.25mm wall thickness sourced from Hilltop Insulation Sleeving Products was applied to the surface of the rods. This was closed by means of a heat gun.

The steel wires were then twisted by hand around the FRP rod that replaced the central steel wire that had earlier been removed from the strand. Since the rods would be encased within the strands, end tabs such as those used for the preparation of tensile tests of rods in §4.4 could not be directly applied to the samples. In order to ensure that the rod would not slide within the centre of the strand during testing, Araldite 2011 epoxy adhesive was applied to the surface of the rod at as the outer wires were replaced. Adhesive was only placed on the rod up to 400mm from the far ends of the strand, which would lie within the length of the grips, so it would not interfere with the tensile test within the gauge length. The process of re-stranding with the adhered central FRP rod is shown in Figure 4.9 and Figure 4.10.

Figure 4.9 Application of Araldite 2011 epoxy adhesive to the far ends of the strand, which were clamped within the testing grips.

To ensure that the outer wires were accurately re-stranded around the new central rods, the outer wires were rewound such that the ends of the wires were flush with one another. The wires were also grooved on the outside with numbers from 1 to 6 to denote their positions within the strand. This ensured that after re-stranding their positions relative to one another would be the same as before they were taken apart.

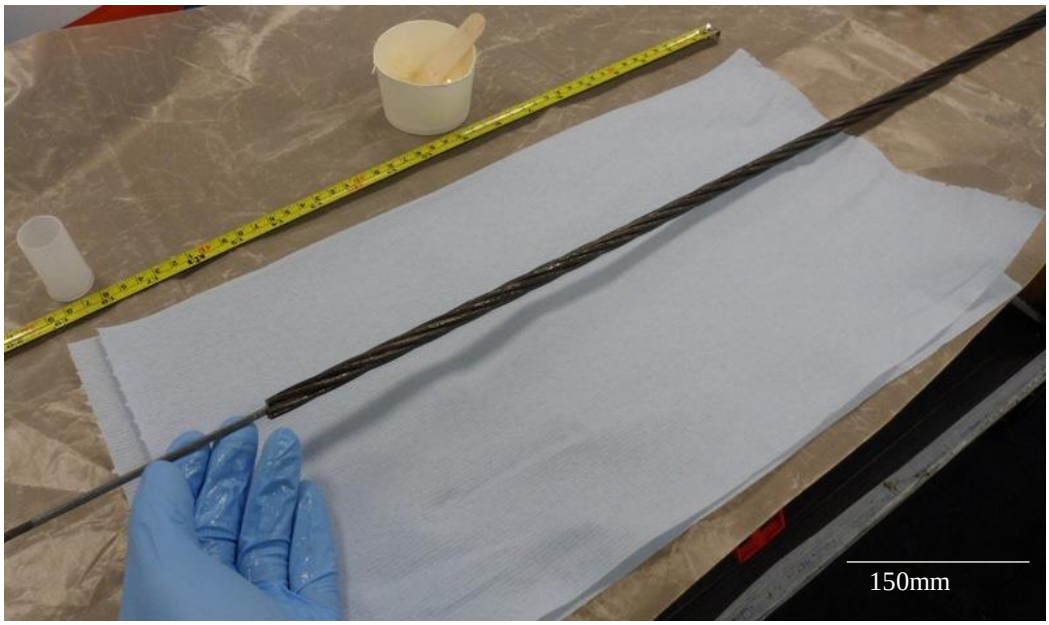

Figure 4.10 A closed strand with adhesive applied to the rod within the gripped length.

4.5.1 Strand tensile test methodology

Tests on 6 x 1 strands were performed at Bridon Technology Centre in Doncaster. Tests were undertaken on a horizontally mounted tensile test frame, which was capable of delivering forces up to 100kN. Strands were held in place by wedge grips supported by rollers, which allowed the grips to tighten around strands under the application of tension, as shown in Figure 4.11 and Figure 4.12.

Covers were rolled over the test area for safety in case wires splayed outside of the test frame upon breaking. An aperture was left in the central cover for a video extensometer, which included a lighting strip next to the camera, as seen in Figure 4.13.

Tests were carried out according to Bridon's internal standard and were performed with the following conditions:

- Rate of extension of 20mm/min.
- Samples were 2200mm long with a gauge length of 1000mm.
- Extension was measured by a video extensometer, which captured the relative motion of two coloured cable ties placed 600mm apart at the centre of the gauge length.

Figure 4.11 Horizontal tensile tester.

Figure 4.12 Specialised wedge grips with rollers.

Figure 4.13 Safety covers rolled into place during testing, with an aperture above the test area for the video extensometer and overhead lighting.

4.6 Inventory of tests

Table 4.3 shows a complete list of all the tests performed for each material type of the pultruded rods. Please note that for the purpose of performing tests on hybrid strands, carbon fibre/vinyl ester rods were substituted for the carbon fibre/epoxy rods as Easy Composites were unable to supply the required lengths, as previously noted in §3.3.3.

Table 4.3 Summary of all tests by material type. *Tests performed by Bridon.

Reinforcement type	Tows and fibre volume fraction (V_f)	Pultrusion line speed (cm/min)	Rod diameter	Rod flexion tests	Rod tension tests	Optical microscopy	Strand tension tests
Grafil TR30S sized carbon fibres, 12k filaments per tow	4 tows (48k) V_f = 28.7%	3.3	✓	✓	✓	✓	
		4.7	✓	✓			
		6.4	✓	✓			
		7.4	✓	✓			
		9.0	✓	✓			
	5 tows (60k) V_f = 28.2%	3.6	✓	✓	✓	✓	
		5.0	✓	✓			
		6.5	✓	✓			
		6.9	✓	✓			
		8.3	✓	✓			
	6 tows (72k) V_f = 33.9%	3.3	✓	✓	✓	✓	✓
		4.4	✓	✓			
		6.9	✓	✓			
		7.9	✓	✓			
		8.5	✓	✓			
Toray T700SC-60E, 24k filaments per tow	2 tows (48k) V_f = 31.3%	3.3	✓	✓	✓	✓	
	3 tows (72k) V_f = 37.7%	3.1	✓	✓	✓	✓	
	4 tows (96k) V_f = 42.4%	3.1	✓	✓	✓	✓	
Schappe TPFL commingled tows, 12k filaments per tow	9 tows (54k) V_f = 30.6%	3.5	✓	✓	✓	✓	✓
Easy Composites carbon fibre/epoxy	(unknown) V_f = 59.5%	(unknown)	✓	✓	✓	✓	
Carbon fibre/vinyl ester	(unknown)	(unknown)			*		✓

4.7 Hypotheses

Predictions were made for the outcome of the tests according to the material under investigation. In forming these hypotheses, assumptions underlying the test protocol could later be judged against its outcomes.

4.7.1 Flexural and tensile tests

From the rule of mixtures introduced in §1.5.1 [5] it can be presumed that tensile modulus will be higher in rods with a greater fibre volume fraction. The rule of mixtures predicts a linearly increasing trend for stiffness in the fibre direction, so this should be reflected in the Young's modulus of tensile tests and in the flexural stiffness.

The strength of FRPs is dependent on a number of failure modes that are particular to material properties and manufacturing procedures. Numerous criteria therefore exist for the prediction of composite failure [6]. Rule of mixtures equations that have been adapted to prediction of strength are semi-empirical and tailored to specific methodologies [7]. However, these methods suggest a fundamental trend of greater tensile strength with higher fibre volume fraction, which should also apply to the tensile strength of FRP rods [8]. It is therefore predicted that the tensile and flexural strength and stiffness of rods will be higher for increased fibre volume fraction. Flexural strength is also expected to be higher than the tensile strength because in bending a smaller region is exposed to maximum stress. This reduces the probability of a given rod section encountering potentially critical flaws [9].

Extensibility is expected to be higher for rods from the commingled tows due to their inclusion of stretch-broken fibres. However, this also implies that their tensile strength and stiffness is likely to be lower than FRP rods of an equivalent fibre volume fraction of fibres that have not been stretch-broken. The relative ease of shear between stretch broken fibres may improve extensibility [10], so this mechanism might also promote the storage of strain energy.

4.7.2 Optical microscopy

Fibre volume fraction should be observed to increase with a greater nominal fibre loading, while the morphology of the cross-section is expected to be dominated by the fibre treatment. As sized fibres are less well dispersed than unsized fibres, they should experience less interpenetration with the resin. Commingled carbon fibres are already well dispersed within the matrix, so these should show a better cross-sectional consolidation.

4.7.3 Hybrid strand tensile tests

There are scant data available for the mechanical properties of hybrid strands and none known to the author concerning strands with FRPs. In their publication of a study on steel multistrand ropes with UHMWPE cores, Amils, et al. found that the ratio of breaking load to linear weight of hybrid ropes was greater than that of steel ropes [11]. The tensile stiffness- and strength-to-weight ratios of the FRP rod and steel wire hybrid strands are therefore expected to be higher than steel strands of comparable cross-sectional geometry.

4.8 Concluding summary

Methodologies for the optical microscopy and tensile and flexural testing of rods have been presented in this section. Cross-sections of rods have thus been prepared for the examination of surface morphologies and determination of the fibre volume fraction and void content of pultruded rods. Methodology for the determination of flexural and tensile strength and stiffness have also been outlined, including a novel means of attaching end tabs to circular tensile test specimen. An innovative testing methodology has been developed for the testing of hybrid strands, which involved internal termination of the gripped ends of the strands to prevent slipping. Chapter 5 presents the results of experiments undertaken following the techniques described in this chapter.

4.9 References

1. Deshmane, C., Q. Yuan, and R.D.K. Misra, High strength–toughness combination of melt intercalated nanoclay-reinforced thermoplastic olefins. Materials Science and Engineering: A, 2007. 460–461(0), p. 277-287
2. Carlsson, L.A., Adams, D. F., Pipes, R. B., Processing of Composite Laminates, in Experimental Characterization of Advanced Composite Materials. 2014, CRC Press. p. 52-54
3. Yuan, Q., S. Awate, and R.D.K. Misra, Nonisothermal crystallization behavior of polypropylene–clay nanocomposites. European Polymer Journal, 2006. 42(9), p. 1994-2003

4. Ferreira, J.A.M., P.N.B. Reis, J.D.M. Costa, B.C.H. Richardson, and M.O.W. Richardson, A study of the mechanical properties on polypropylene enhanced by surface treated nanoclays. Composites Part B: Engineering, 2011. 42(6), p. 1366-1372
5. Hull, D., Clyne, T. W., Elastic Properties, in An Introduction to Composite Materials. 1996, Cambridge University Press Cambridge. p. 81-101
6. Hinton, M.J., A.S. Kaddour, and P.D. Soden, A comparison of the predictive capabilities of current failure theories for composite laminates, judged against experimental evidence. Composites Science and Technology. 62(12-13), p. 1725-1797
7. Lee, C., Hwang, W., Modified Rule of Mixtures for Prediction of Tensile Strength of Unidirectional Fiber-reinforced Composites. Journal of Materials Science Letters, 1998. 17(19), p. 1601-1603
8. Hull, D., Clyne, T. W., Strength of composites, in An Introduction to Composite Materials. 1996, Cambridge University Press Cambridge. p. 178-184
9. Lv, Y., Y. Huang, M. Kong, J. Yang, Q. Yang, and G. Li, Creep lifetime prediction of polypropylene/clay nanocomposites based on a critical failure strain criterion. Composites Science and Technology, 2014. 96(0), p. 71-79
10. Lee, K., S.W. Lee, and S.J. Ng, Micromechanical modeling of stretch broken carbon fiber materials. Journal of Composite Materials, 2008. 42(11), p. 1063-1073
11. Amils, X., Durmus, B., Smeets, P., Boesten, J., Weis, J. Characteristics of steel hybrid ropes with UHMWPE fibre core and their applications. in Simulating rope applications. 2013. Oxford, OIPEEC

5 Experimental results

Results from optical microscopy and flexural and tensile tests of pultruded rods and tensile tests of hybrid strands are presented in this chapter. All error bars placed on graphs in this chapter represent the standard deviation from the mean of the data set associated with the result.

Abbreviations have been introduced in this section to simplify the repetition of long phrases associated with types of pultruded rods. These are presented in Table 5.1.

Table 5.1 Abbreviations for types of pultrusions.

Reinforcement type	Fibre loading	Abbreviation	Intended meaning
Grafil TR30S sized carbon fibres, 12k filaments per tow	4 tows (48k)	4S	"Rods pultruded from 4 tows of sized fibres"
	5 tows (60k)	5S	"Rods pultruded from 5 tows of sized fibres"
	6 tows (72k)	6S	"Rods pultruded from 6 tows of sized fibres"
Toray T700SC-60E, 24k filaments per tow	2 tows (48k)	2U	"Rods pultruded from 2 tows of unsized fibres"
	3 tows (72k)	3U	"Rods pultruded from 3 tows of unsized fibres"
	4 tows (96k)	4U	"Rods pultruded from 4 tows of unsized fibres"
Schappe TPFL commingled tows, 12k filaments per tow	9 tows (54k)	9C	"Rods pultruded from 9 tows of commingled tows"
Easy Composites carbon fibre/epoxy	N/A	EC	"Rods from commercially available carbon fibre/epoxy pultrusions obtained from Easy Composites"
Carbon fibre/vinyl ester	N/A	VE	"Carbon fibre/vinyl ester rods from Bridon"

5.1 Optical microscopy morphology

Dark field montages were created for mounted rod cross-sections, using the methodology for sample preparation described in §4.2.1. The internal morphology of the cross-sections becomes apparent from these images, which generally show fibre reinforced areas surrounded by unreinforced polymer matrix. Bright field montages have also been presented in this section, which show the same images in reversed contrast and more clearly highlight features such as fibre-rich regions. For the sake of brevity, a selection of representative dark and bright field images have been presented together in separate sections for each material type.

Carbon fibre tows are clearly visible as grey bands, giving the appearance of slender islands within a white polymer sea. The cross-sections thus appear to resemble strips of FRP filled with an unreinforced polymer. Fibre-reinforced regions appear to be evenly consolidated, with the exception of macroscopic voids that appear as black spots and lines inside those grey areas. The outer edges of the cross-sections show considerable variation and it appears that the rods are in fact only approximately circular in diameter, with occasional tufts and corners.

5.1.1 Cross-section montages of rods from sized fibres

Carbon fibre tows of sized fibres appeared as narrow grey strips, interspersed with dark regions of voids. This is observed in dark field images of 4S, 5S and 6S, which are respectively shown in Figure 5.1, Figure 5.2 and Figure 5.3. It is possible to pick out where some of the individual tows begin and end. Higher loadings of carbon fibre appeared to result in more circular rods.

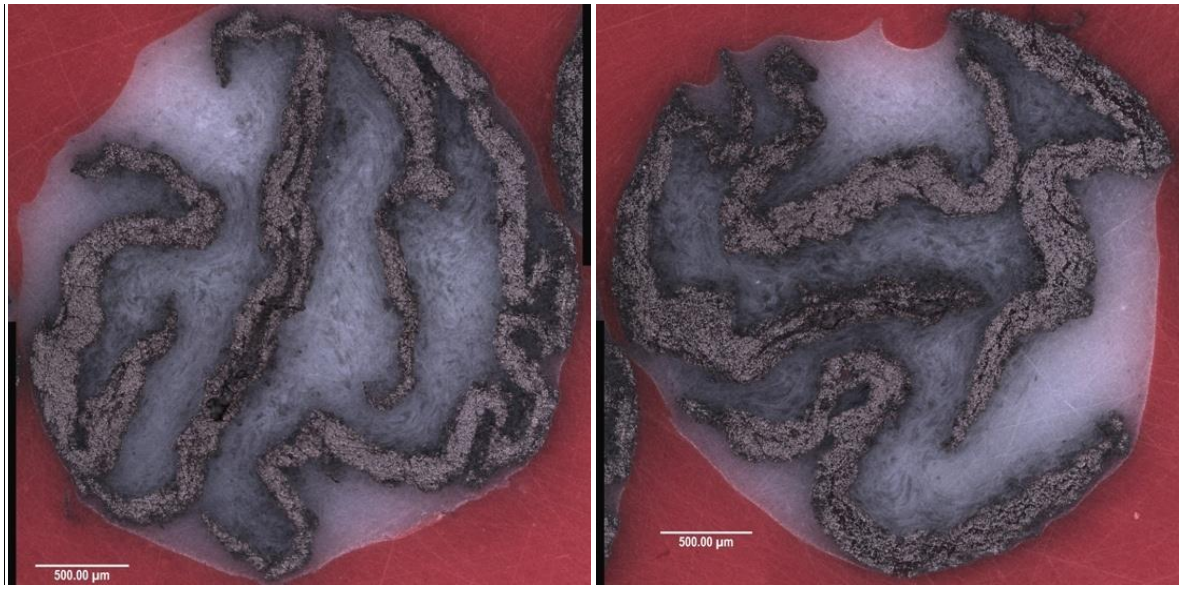

Figure 5.1 Dark field montages of rods from 4 tows of sized carbon fibres.

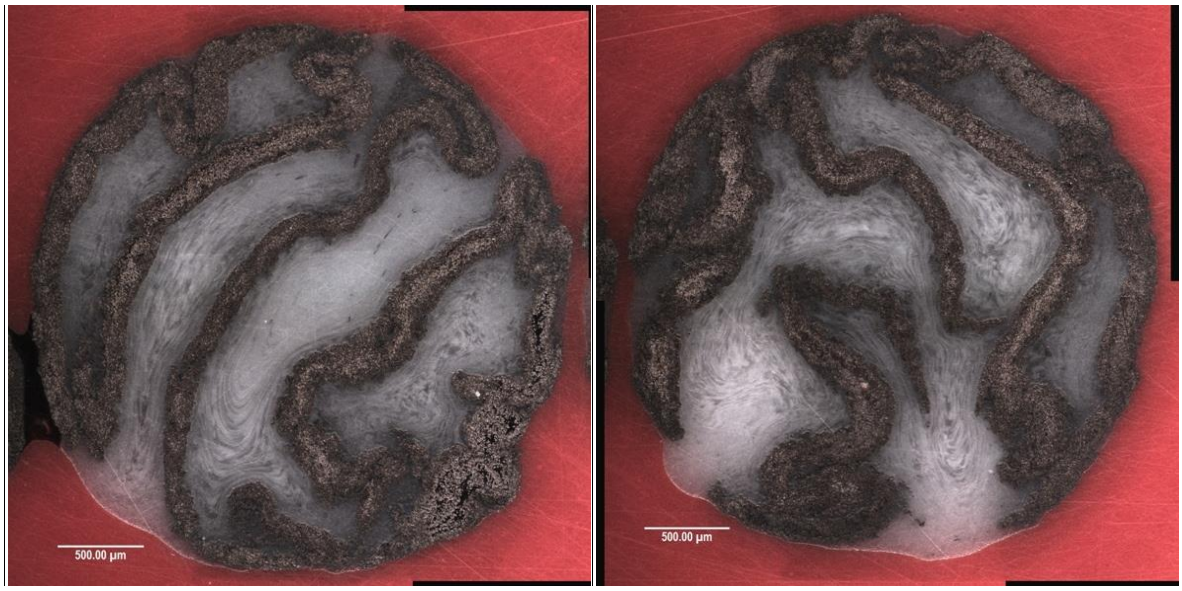

Figure 5.2 Dark field montages of rods from 5 tows of sized carbon fibres.

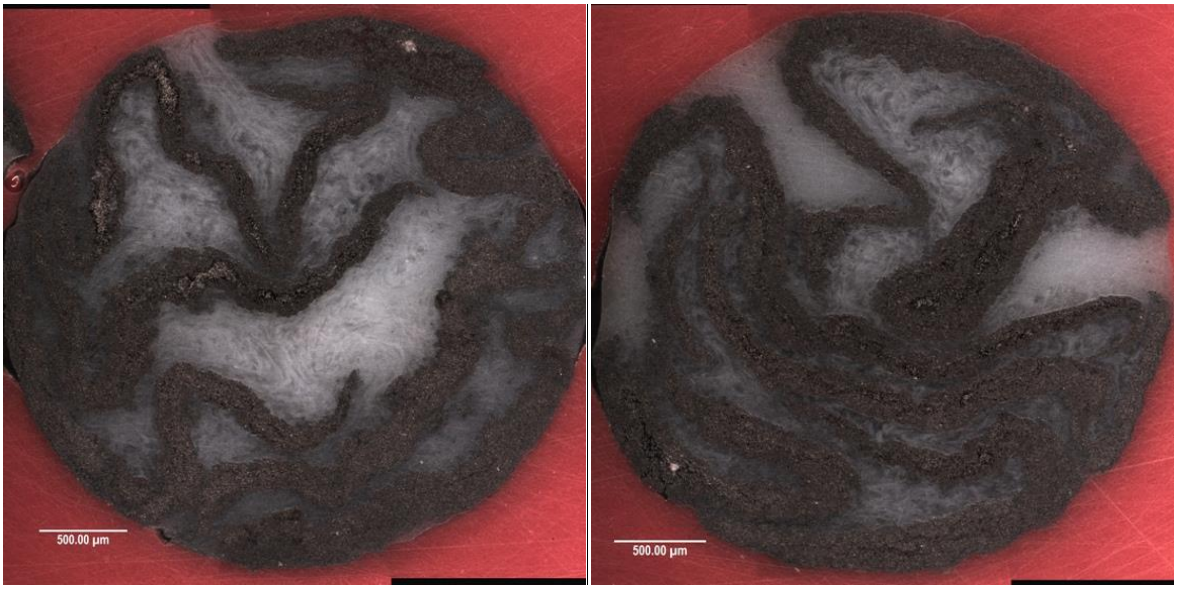

Figure 5.3 Dark field montages of rods from 6 tows of sized carbon fibres.

The serpentine nature of the FRP areas is more clearly visible from the bright field images, respectively shown for 4S, 5S and 6S in Figure 5.4, Figure 5.5 and Figure 5.6. So too are the voids, which appeared as almost completely black strips and holes in the grey fibre-reinforced regions.

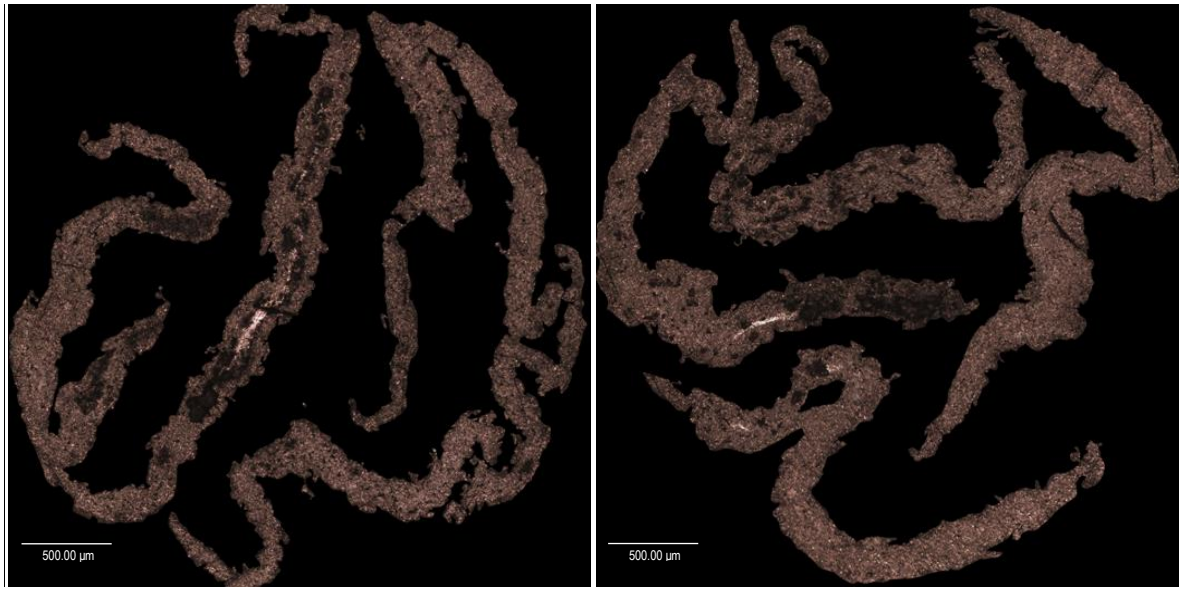

Figure 5.4 Bright field montages of rods from 4 tows of sized carbon fibres.

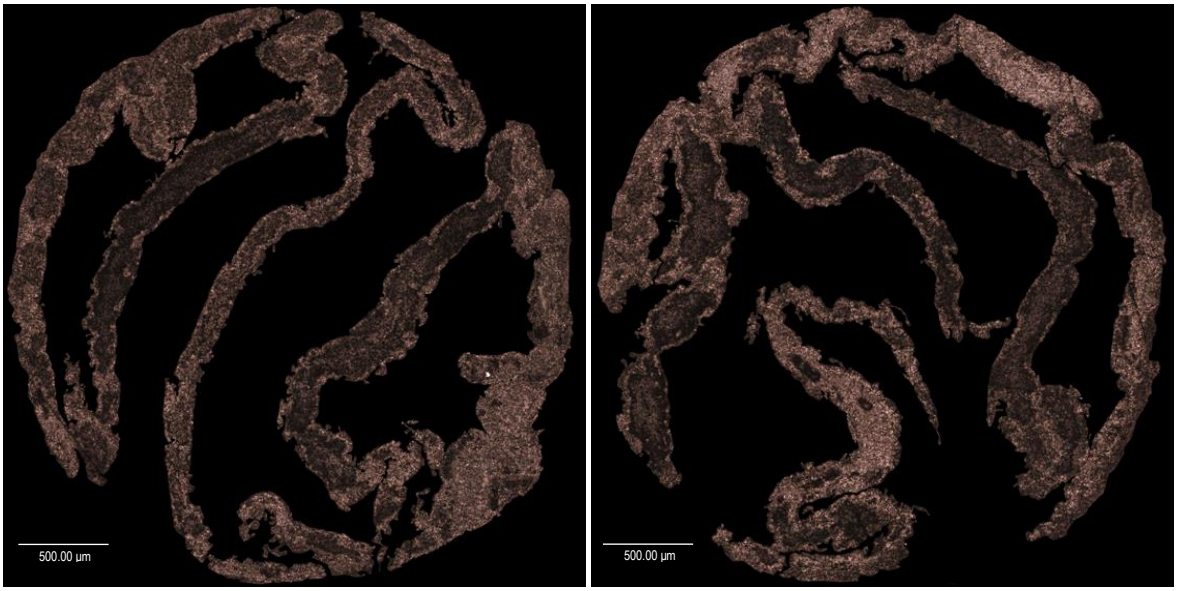

Figure 5.5 Bright field montages of rods from 5 tows of sized carbon fibres.

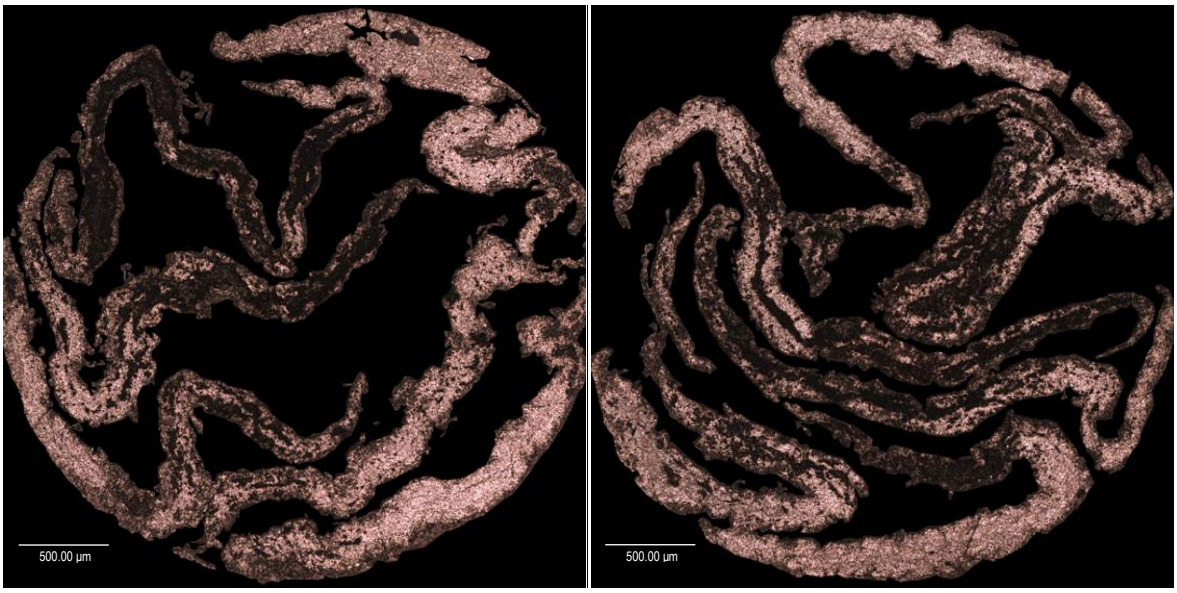

Figure 5.6 Bright field montages of rods from 6 tows of sized carbon fibres.

5.1.2 Cross-section montages of rods from unsized fibres

Unsized tows appeared to be thicker than sized tows, with less clearly visible boundaries between independent tows. As was observed for the rods from sized tows in §5.1.1, fibre-reinforced areas contrasted strongly with unreinforced matrix regions. Unsized tows showed conspicuous dry fibre regions, which had the appearance of dark voids filled with the reflective tips of carbon fibres. This can be seen in the dark field montages for 2U, 3U and 4U, which are respectively shown in Figure 5.7, Figure 5.8 and Figure 5.9. These were far larger and more prevalent than for the rods from sized fibres. Cross-sections of rods from 4U showed the greatest degree of filling of any cross-sections from sized or unsized tows. Only a minimal area in these cross-sections was taken up by unreinforced matrix and individual tows were largely unrecognisable.

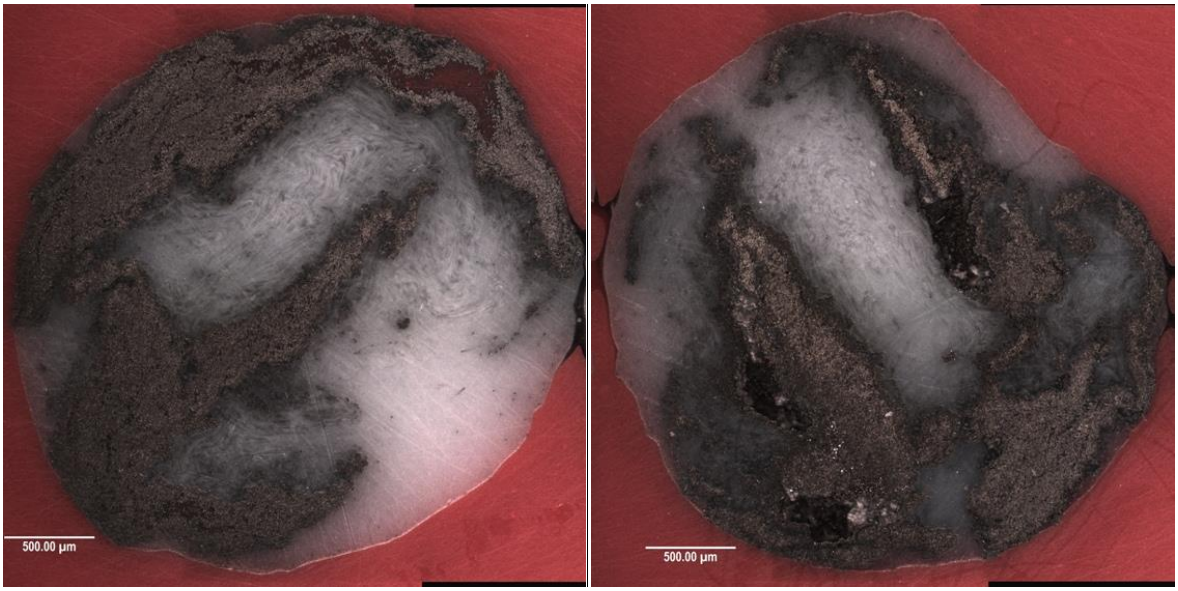

Figure 5.7 Dark field montages of rods from 2 tows of unsized carbon fibres.

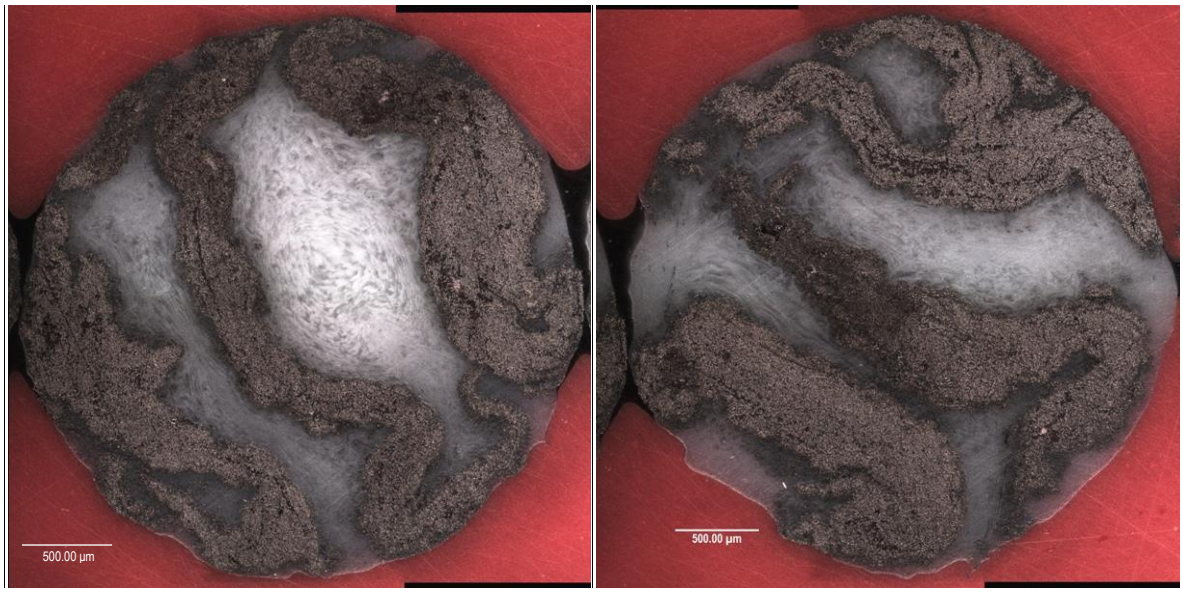

Figure 5.8 Dark field montages of rods from 3 tows of unsized carbon fibres.

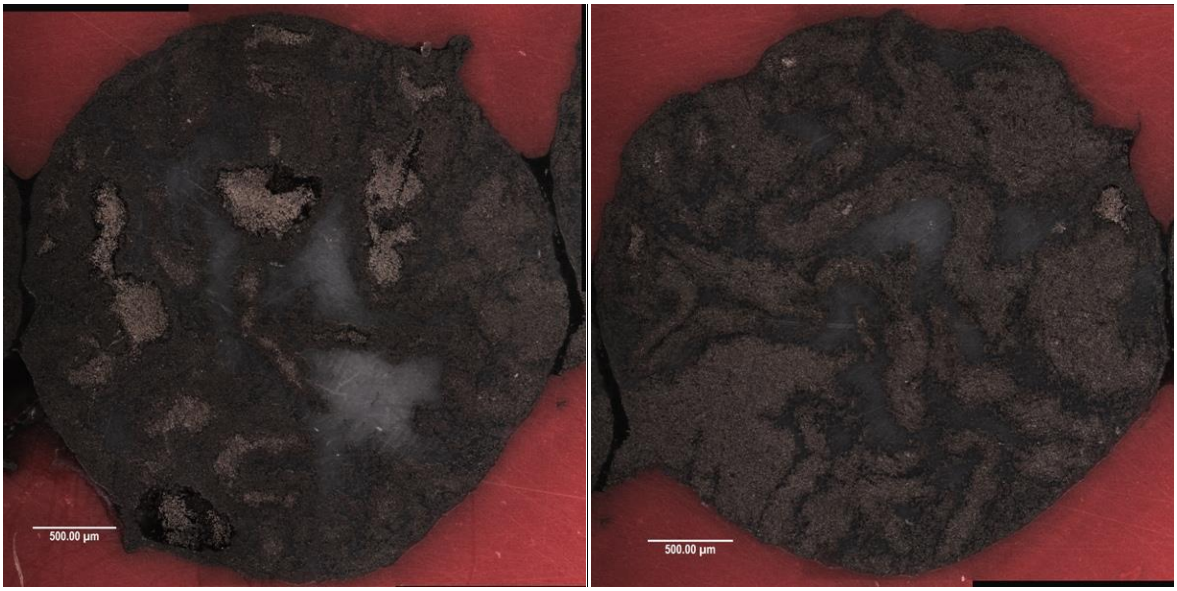

Figure 5.9 Dark field montages of rods from 4 tows of unsized carbon fibres.

Bright field images of 2U, 3U, 4U are shown respectively in Figure 5.10, Figure 5.11 and Figure 5.12. Fibre-rich but polymer-poor areas were apparent in these images and appeared as very dark grey areas punctuated with the brighter spots of carbon fibres. There was great variation in the distribution and frequency of these polymer-poor areas. This was seen most clearly in Figure 5.10, which showed the isolated fibre-reinforced regions of two cross-sections from 2U. The left image showed an almost complete freedom from polymer-poor regions, whereas several large patches appeared in the right image.

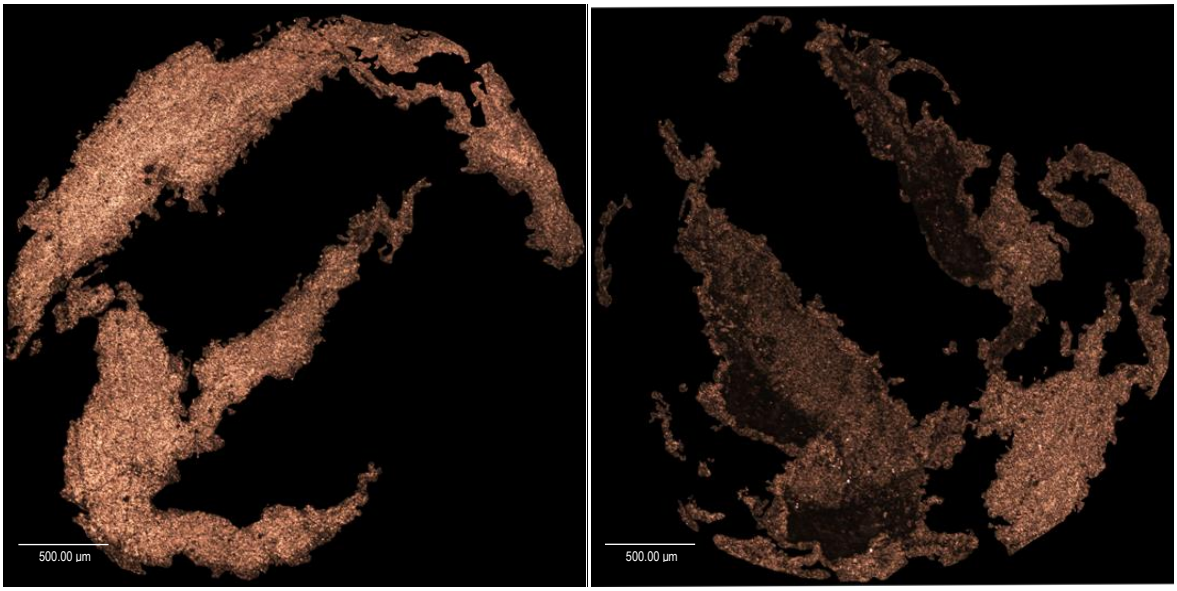

Figure 5.10 Bright field montages of rods from 2 tows of unsized carbon fibres.

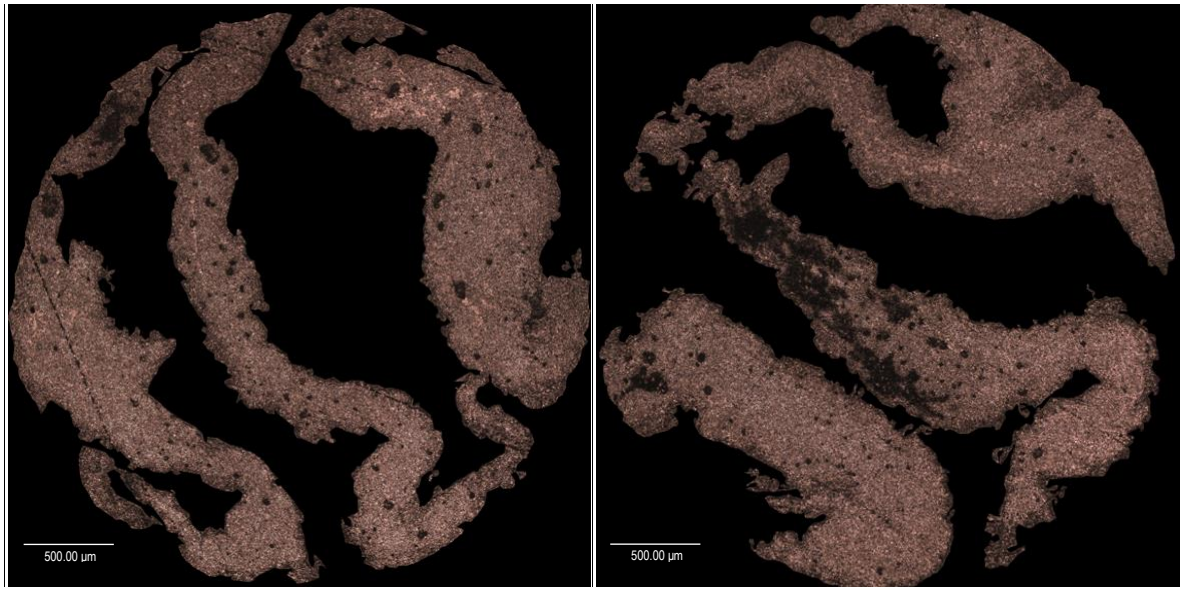

Figure 5.11 Bright field montages of rods from 3 tows of unsized carbon fibres.

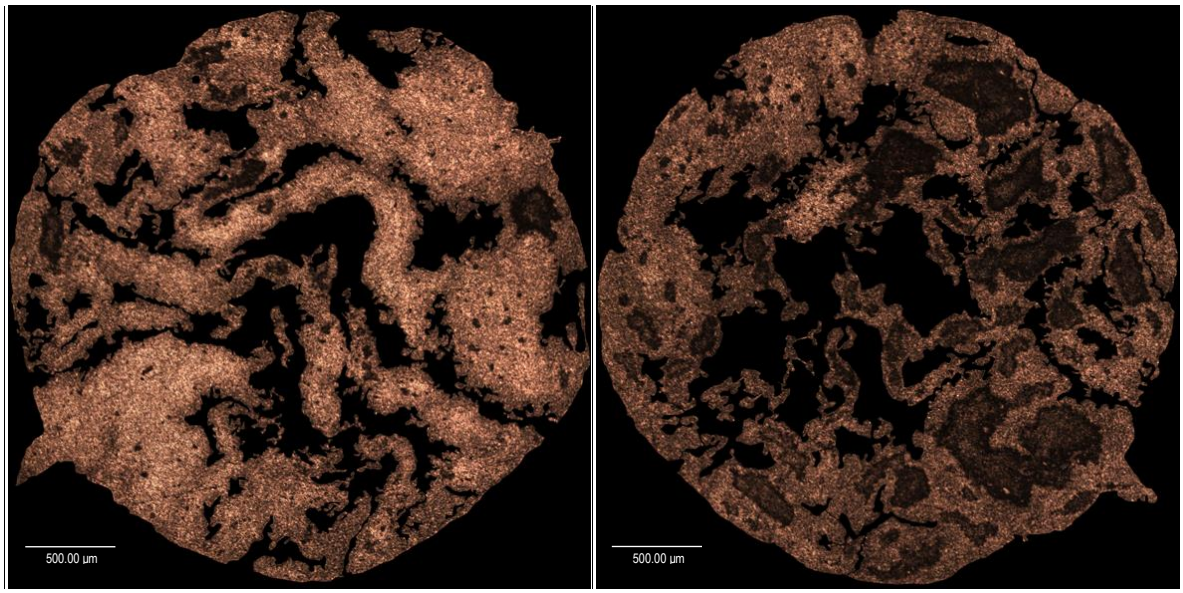

Figure 5.12 Bright field montages of rods from 4 tows of unsized carbon fibres.

5.1.3 Cross-section montages of rods from commingled tows

In the dark field images shown in Figure 5.13, commingled tows appeared to be separate from one another and individually surrounded by unreinforced polymer matrix. These showed differing levels of distortion, the greatest example being image c) in Figure 5.13, which is strewn at the edges with solid lumps of unreinforced white polymer and a halo of voids. The greatest macroscopic defect was seen in image d) in Figure 5.13, which took the form of a large void almost as large as the tows themselves. Otherwise, the interior of these tows did not appear to have a void content as high as that found in the cross-sections of pultrusions from sized and unsized tows, which were presented in §5.1.1 and §5.1.2.

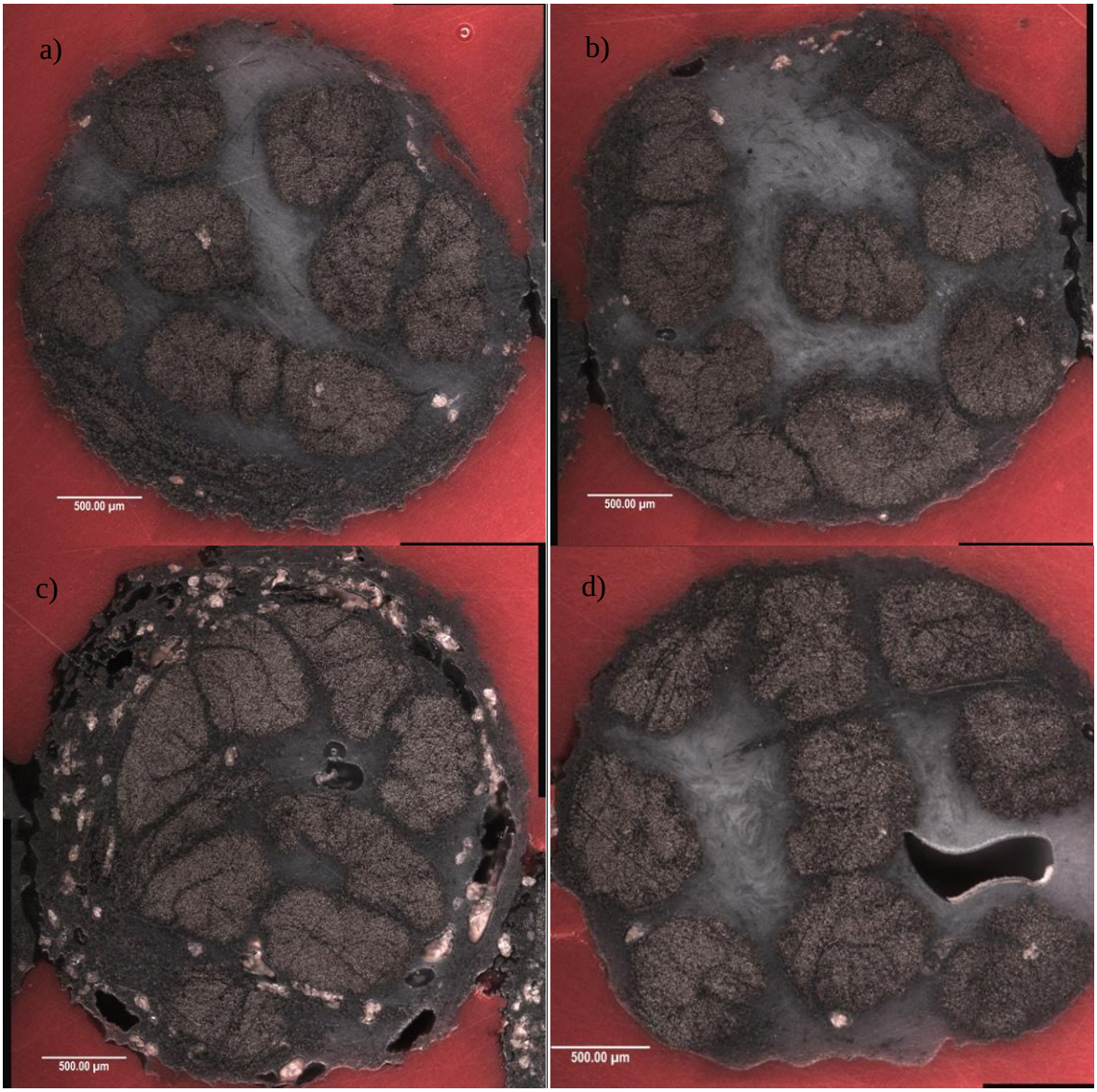

Figure 5.13 Dark field montages of rods from 9 tows of commingled tows.

The relative independence of separate tows became clearer in the bright field images shown in Figure 5.14. The fibre-reinforced regions within the tows appeared to be relatively well consolidated and were relatively free of voids. Polymer-poor regions were also entirely absent.

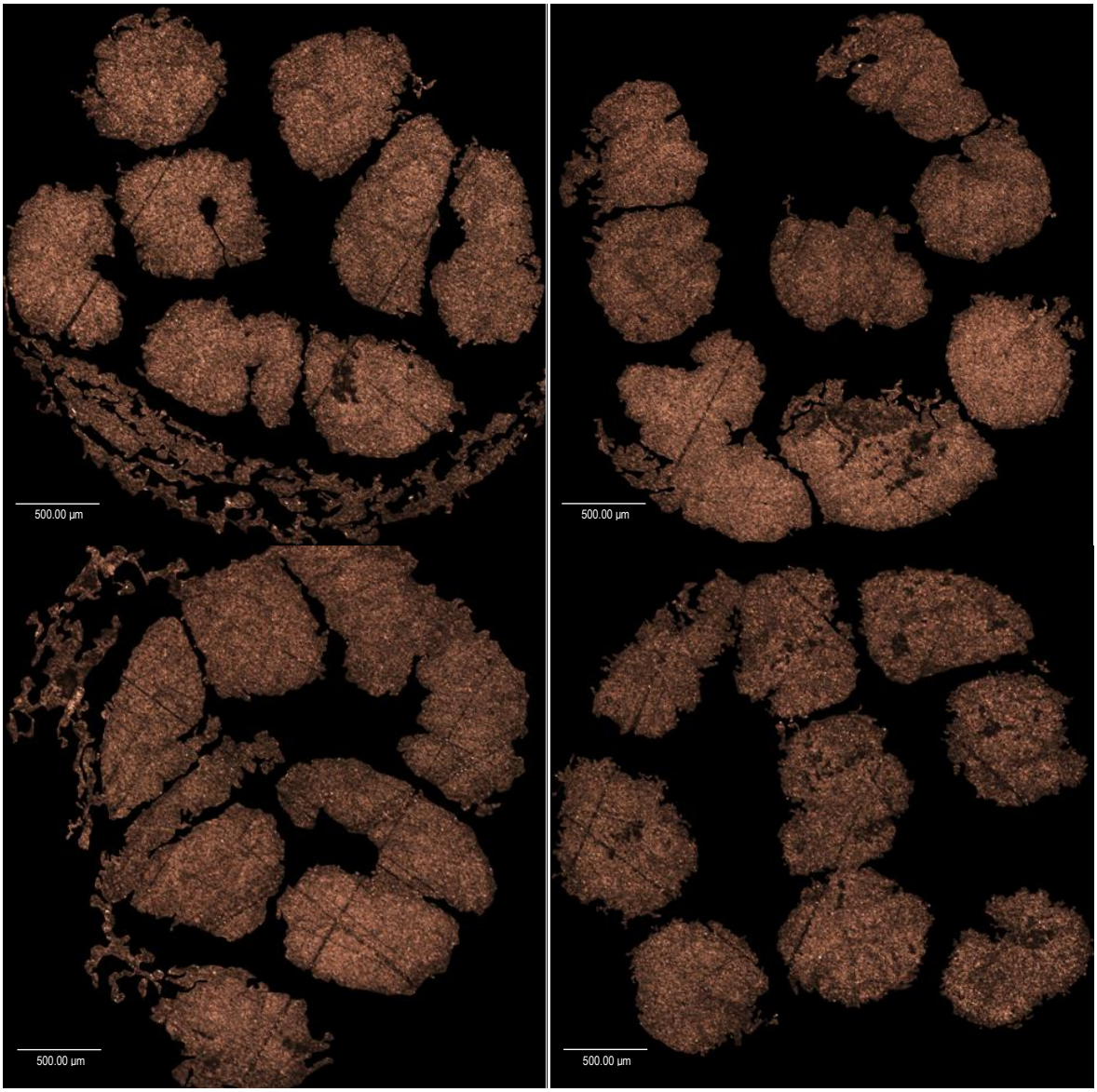

Figure 5.14 Bright field montages of rods from 9 tows of commingled tows.

5.1.4 Cross-sections of carbon fibre rods from Easy Composites

EC were entirely different to the thermoplastic pultruded rods in their morphologies, as shown in the dark field montages in Figure 5.15. The cross-sections appeared circular and without the crenulated edges seen in previous sections. The cross-sections also appeared to be evenly consolidated and without resin-rich or fibre-rich regions. There were far fewer visible macroscopic defects in these cross-sections than in those of the carbon fibre/thermoplastic pultruded rods.

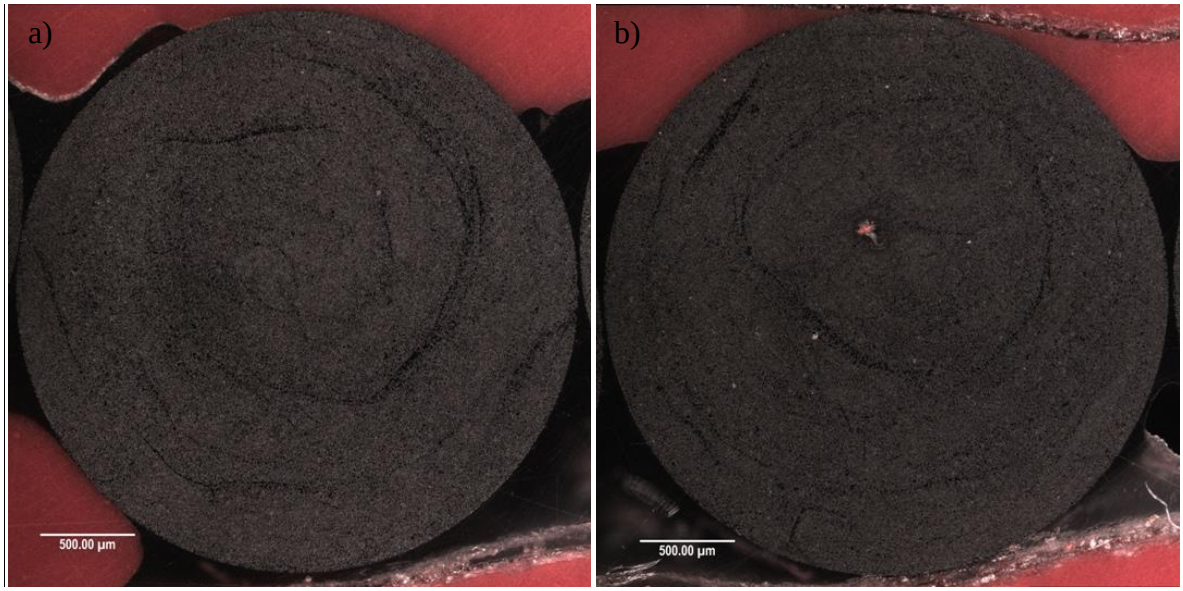

Figure 5.15 Dark field montages of Easy Composite carbon fibre rods.

Voids became clearer in the bright field images and appeared haphazardly distributed across whole cross-sections. The micrographs did not show any significant variation in consolidation or fibre distribution across the diameter of the cross-sections. Neither did the cross-sections appear to have any particular distortions at the edges, as could be seen with the carbon fibre/thermoplastic rods. A solitary large void could be seen in image b) in Figure 5.16.

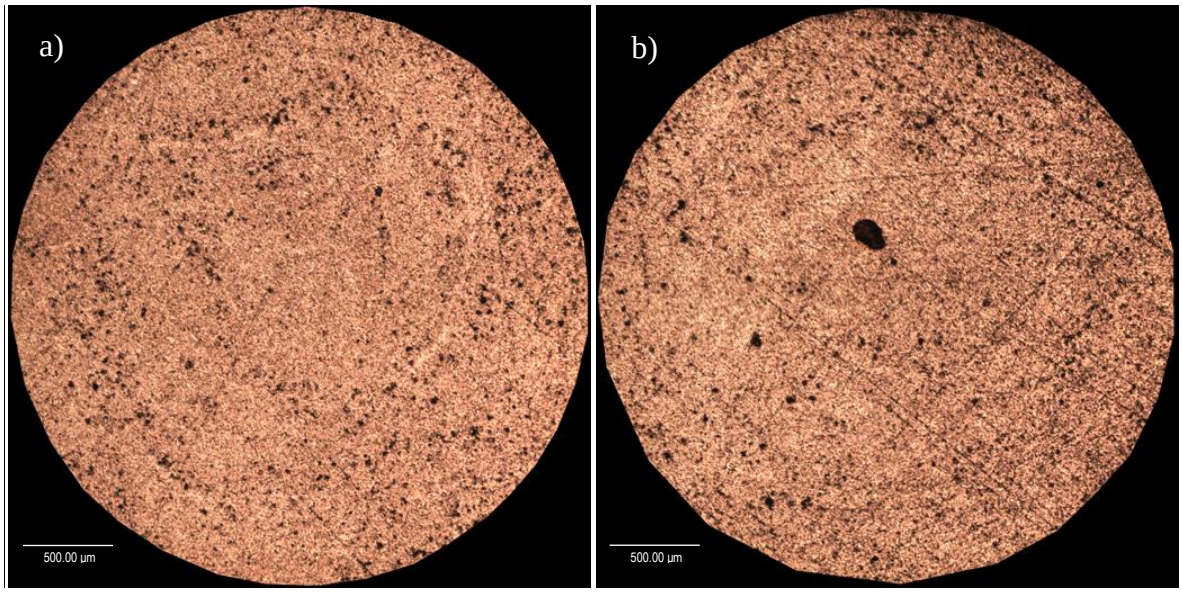

Figure 5.16 Bright field montages of Easy Composite carbon fibre rods.

5.2 Fibre volume fraction and void content

Fibre volume fraction and void content were calculated with the methodology described in §4.2.3. Although fibre volume fraction was seen to increase linearly with fibre loading, the correlation was not as strong as might be expected from a rule of mixtures treatment. This is because the quantity of polymer in the rods also rose with fibre loading, as is reflected in the

rod diameters presented in Figure 5.19 in §5.3. Overall, this resulted in fibre volume fractions that were not directly proportional to the fibre loading alone. For instance, Figure 5.17 shows that the fibre volume fraction of 4U is approximately 26% higher than 2U, despite having twice the the numbr of tows.

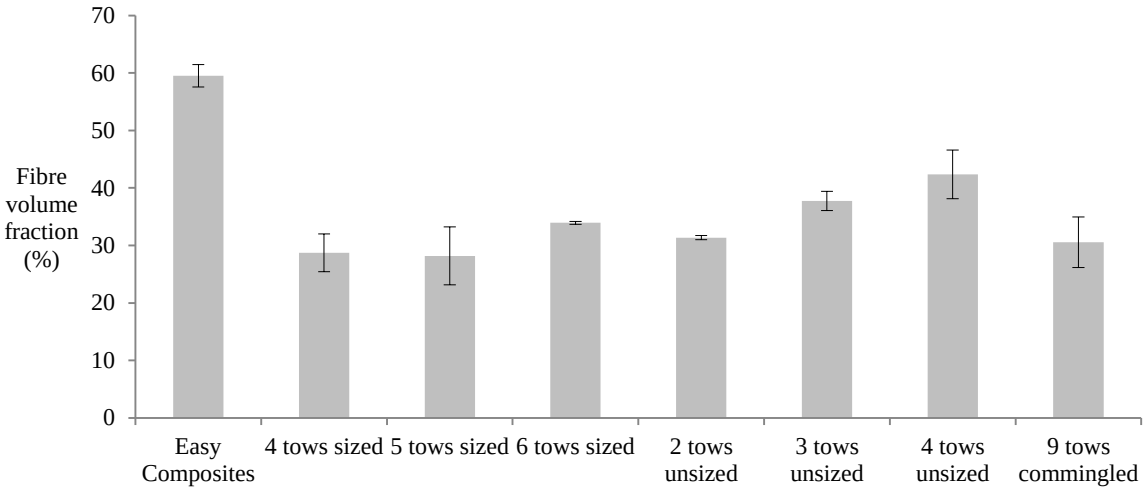

Figure 5.17 Fibre volume fraction of rod cross-sections.

There are no underlying trends in the void content of rods from sized and unsized fibres, which is shown in Figure 5.18. The statistical significance of this data is also questionable, owing the large variation in the void content calculated for individual material types, which was an average value taken from six montages as described in §4.2.3. This large variation is at least in part caused by the widely different morphologies occurring between individual cross-sections, a phenomenon identified in the description accompanying Figure 5.10 in §5.1.2. However, the fibre volume fraction of 9C is significantly lower than other carbon fibre/thermoplastic rods. The lowest void content was recorded for EC, at approximately 1.5%.

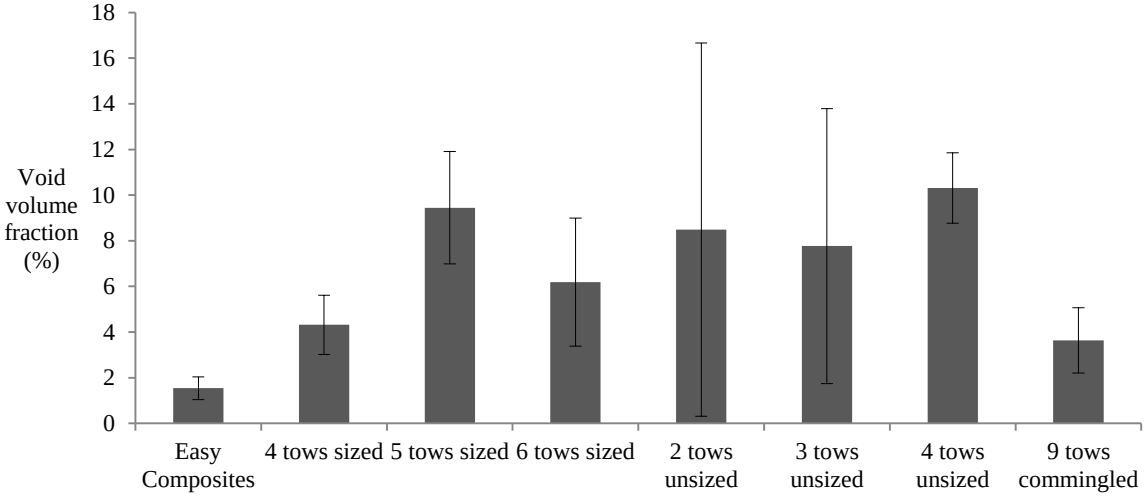

Figure 5.18 Void content as a volume fraction of rod cross-sections.

Taking the fibre volume fraction measurements in Figure 5.17 as definitive, graphs of mean rod diameter, flexural strength and stiffness and tensile strength and stiffness will be expressed in terms of the fibre volume fraction of each type of tow reinforcement. A summary of these values is given in Table 5.2.

Table 5.2 Fibre volume fractions

Reinforcement type	Fibre loading	Abbreviation	Fibre volume fraction (%)	Standard deviation (%)
Easy Composites commercially sourced rod	(unknown)	(unknown)	59.5	2.0
Grafil TR30S sized carbon fibres, 12k filaments per tow	4 tows (48k)	4S	28.7	3.3
	5 tows (60k)	5S	28.2	5.0
	6 tows (72k)	6S	33.9	0.3
Toray T700SC-60E, 24k filaments per tow	2 tows (48k)	2U	31.3	0.4
	3 tows (72k)	3U	37.7	1.7
	4 tows (96k)	4U	42.4	4.2
Schappe TPFL commingled tows, 6k filaments per tow	9 tows (54k)	9C	30.6	4.4

5.3 Measurement of rod diameters

Figure 5.19 compares the mean diameters for rods produced from different reinforcements at standard manufacturing conditions, which were described in §3.2.6. Except for 3U and 4U, rod diameters consistently fell below the diameter of the heating die channel. A general trend of increasing diameter with a greater fibre volume fraction can be discerned, with the lowest rod diameters being recorded for 4S, 2U and 9C, which also experienced the highest variance in diameter. The lowest variance was recorded for EC.

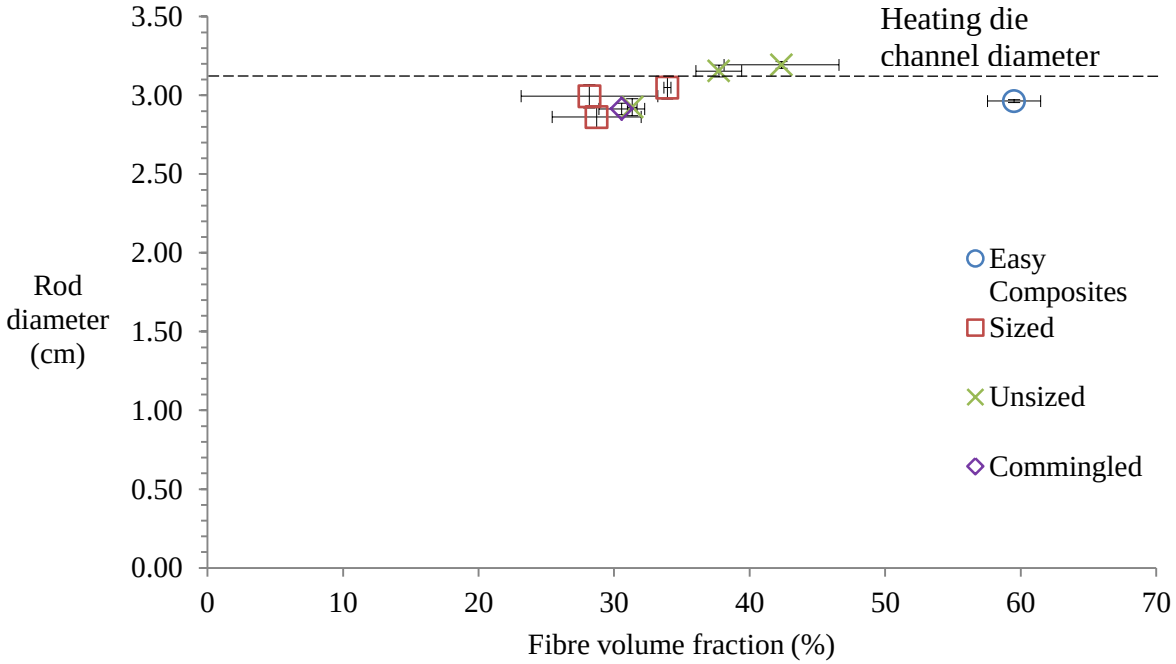

Figure 5.19 Mean diameters of flexural test samples produced from different reinforcements.

No correlation was found between rod diameter and the line speed. Values for the Pearson correlation coefficient are so close to zero that it can be said that there is no discernible trend over the range of line speeds that were tested. Deviation from the mean is also comparatively small and also without dependence on line speed for each result in these distributions. These

findings were observed for the rods produced from sized carbon fibres, which are shown in Figure 5.20.

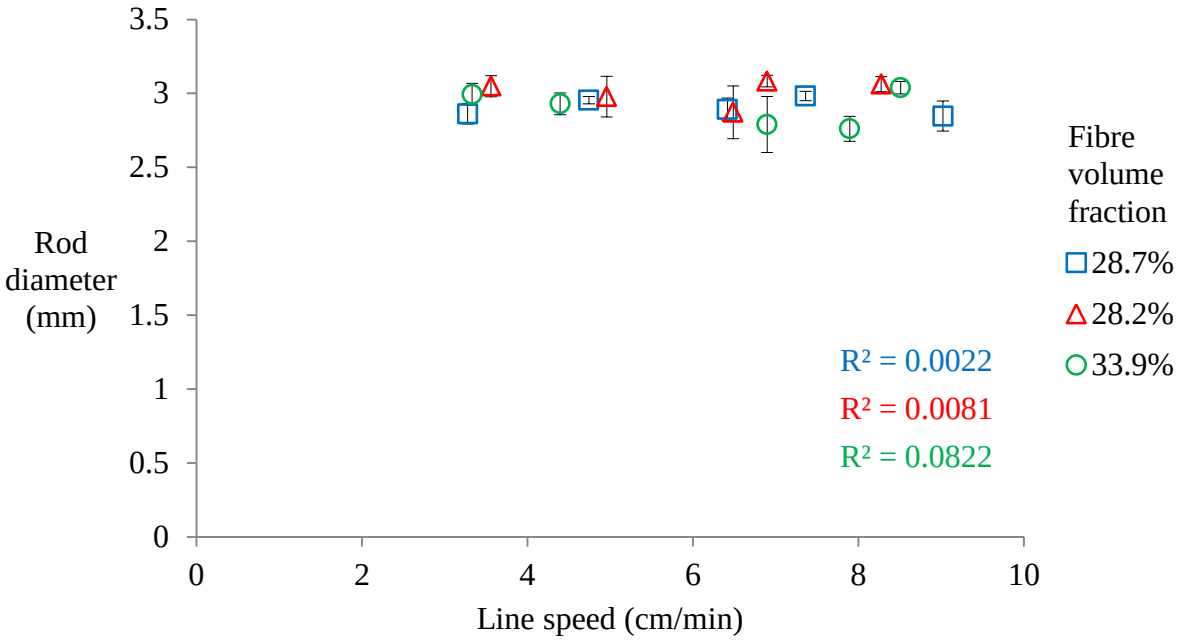

Figure 5.20 Variation in rod diameter with line speed for rods pultruded from sized carbon fibres, by fibre volume fraction.

5.4 Flexural tests

A positive correlation between flexural stiffness and fibre volume fraction was observed in Figure 5.21 for rods from sized and unsized fibres, with 6S and 4U contributing the highest flexural stiffness among carbon fibre/thermoplastic rods. The flexural stiffness of EC was greater by approximately 10GPa than that of the second highest value, belonging to 4U, although the variance in the mean was somewhat higher.

A correlation between flexural strength and fibre volume fraction was observed for rods from unszied fibres but not for rods from sized fibres, as seen in Figure 5.22. In addition, rods with sized fibres possessed consistently higher flexural modulus and strength than those rods from unsized fibres with a comparable number of filaments.

The flexural strength was recorded for 9C exceeded that of rods produced from sized and unsized fibres. However, the flexural strength of these rods was significantly lower than that of EC, which was more than twice as high as 9C.

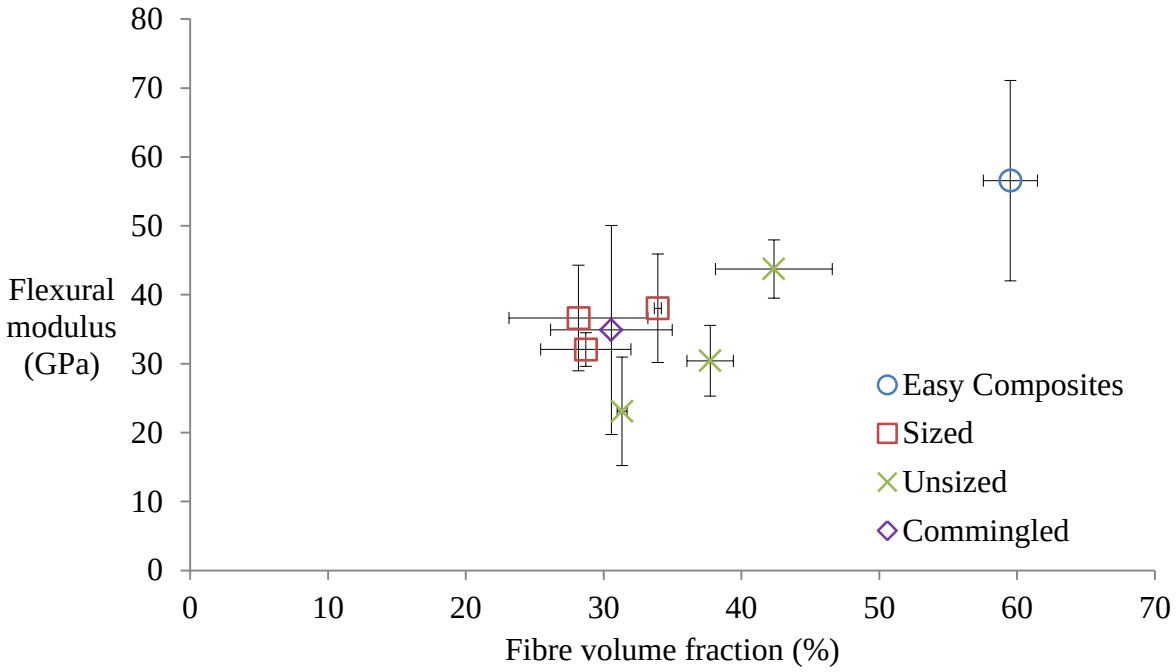

Figure 5.21 Flexural modulus of rods produced at standard manufacturing conditions, by fibre volume fraction.

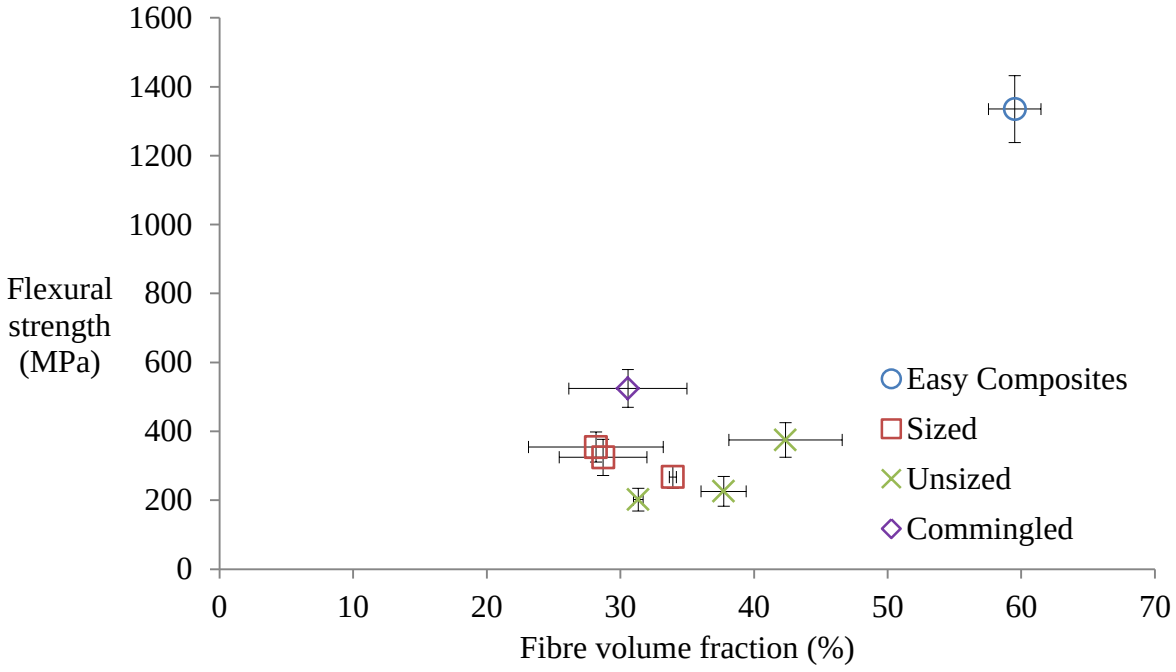

Figure 5.22 Flexural strength of rods produced at standard manufacturing conditions, by fibre volume fraction.

5.4.1 Effect of line speed on flexural properties

No clear correlation was observed between flexural modulus and line speed, with variance from the mean being greater than the weak linear trend suggested by the Pearson correlation coefficients. This is represented in Figure 5.23, which displays flexural modulus as a function of line speed for rods from sized carbon fibres. An even weaker correlation exists between

flexural strength and line speed, which is displayed in Figure 5.24, for rods from sized carbon fibres. These tests indicate that flexural strength and stiffness were effectively independent with respect to line speed over the range of line speeds tested.

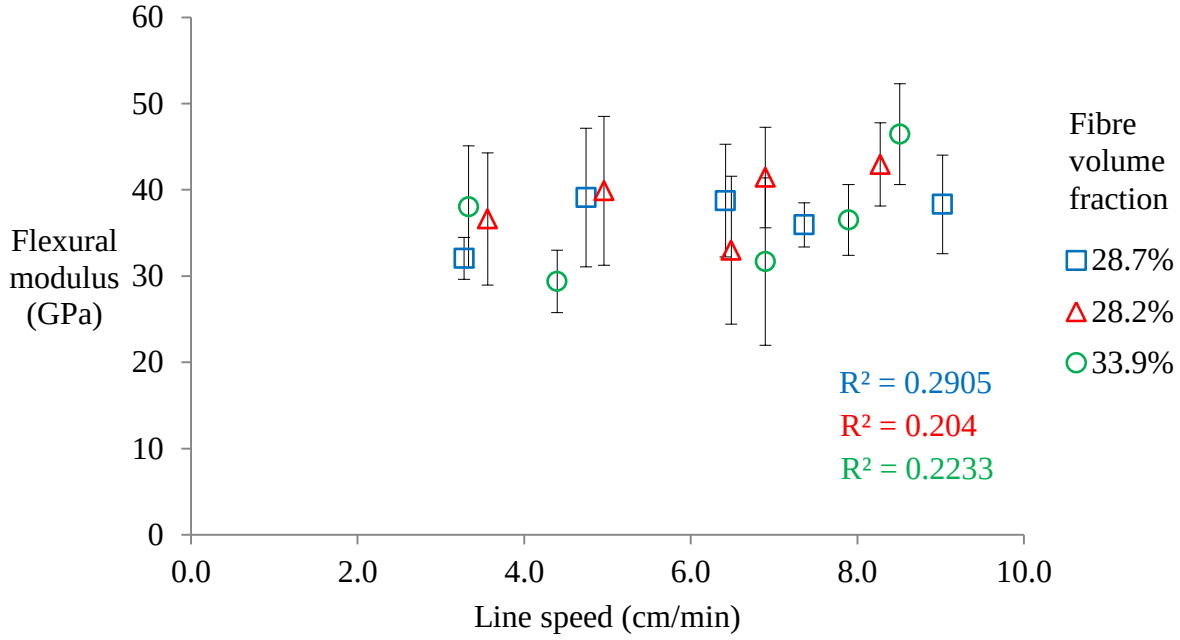

Figure 5.23 Variation in flexural modulus with line speed for rods from tows of sized carbon fibres, by fibre volume fraction.

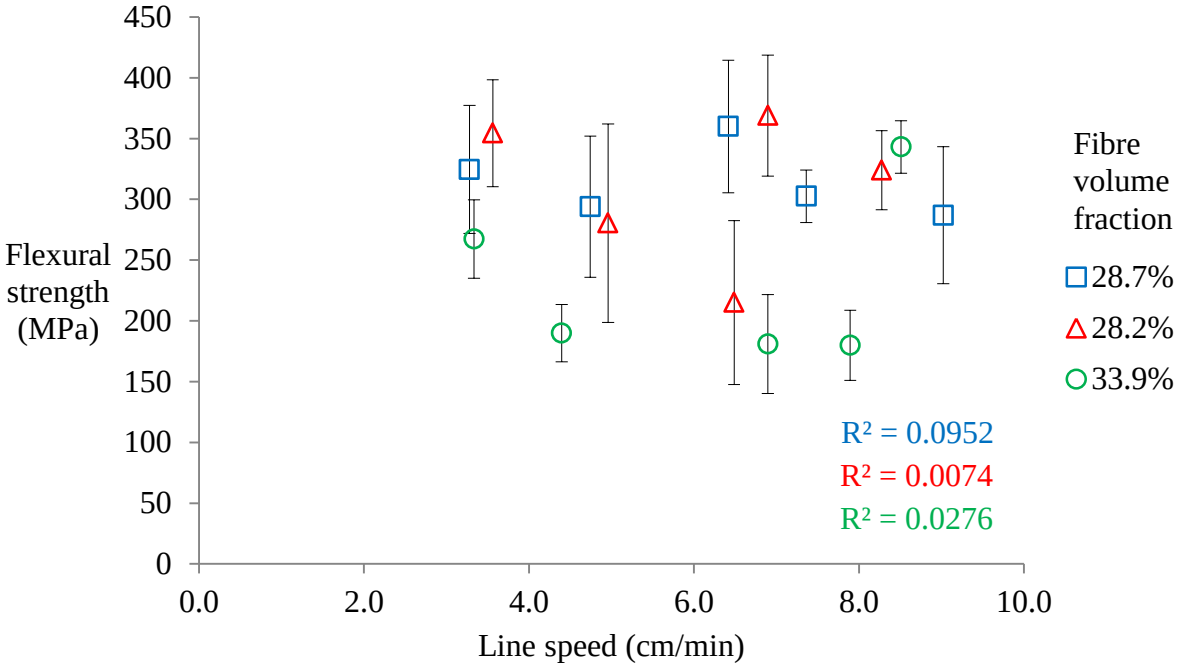

Figure 5.24 Variation in flexural strength with line speed for rods from tows of sized carbon fibres, by fibre volume fraction.

5.5 Tensile tests

Young's modulus and ultimate tensile strength of pultruded rods are presented in this section. A summary of all the stress-strain curves pertaining to the trends in this section can be found in Appendix A.

5.5.1 Young's modulus

As can be seen in Figure 5.25, the tensile modulus for rods was roughly in proportion to the fibre volume fraction. EC had a higher Young's modulus than any of the carbon fibre/thermoplastic pultruded rods.

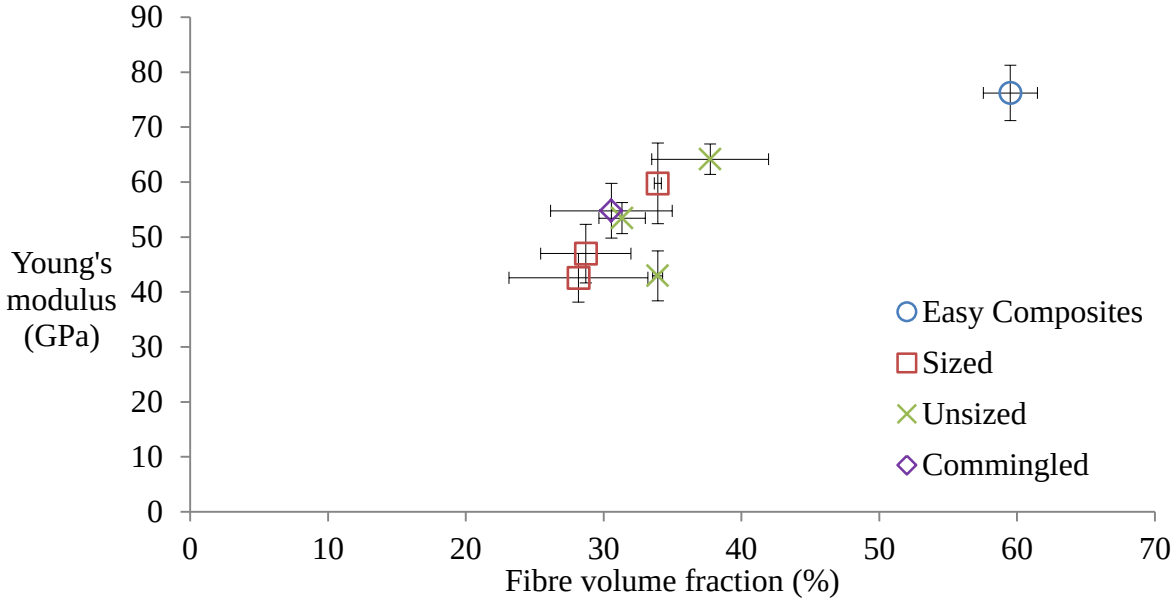

Figure 5.25 Young's modulus of rods produced at standard manufacturing conditions, by fibre volume fraction.

5.5.2 Ultimate tensile strength

Ultimate tensile strength for all specimens, presented in Figure 5.26, suggested a general trend of increasing mechanical properties with greater fibre volume fraction, although the trend was nonlinear. There is a similarity in the ultimate tensile strength of rods from sized and unsized carbon fibres of equivalent fibre volume fraction. 9C appears as an outlier, with ultimate tensile strength of 1069MPa. This seemingly disproportionate value contrasts with the comparative underperformance of these rods with respect to Young's modulus in Figure 5.25. Most strikingly, EC had a far higher mean strength than the carbon fibre/thermoplastic pultruded rods, at 1548MPa.

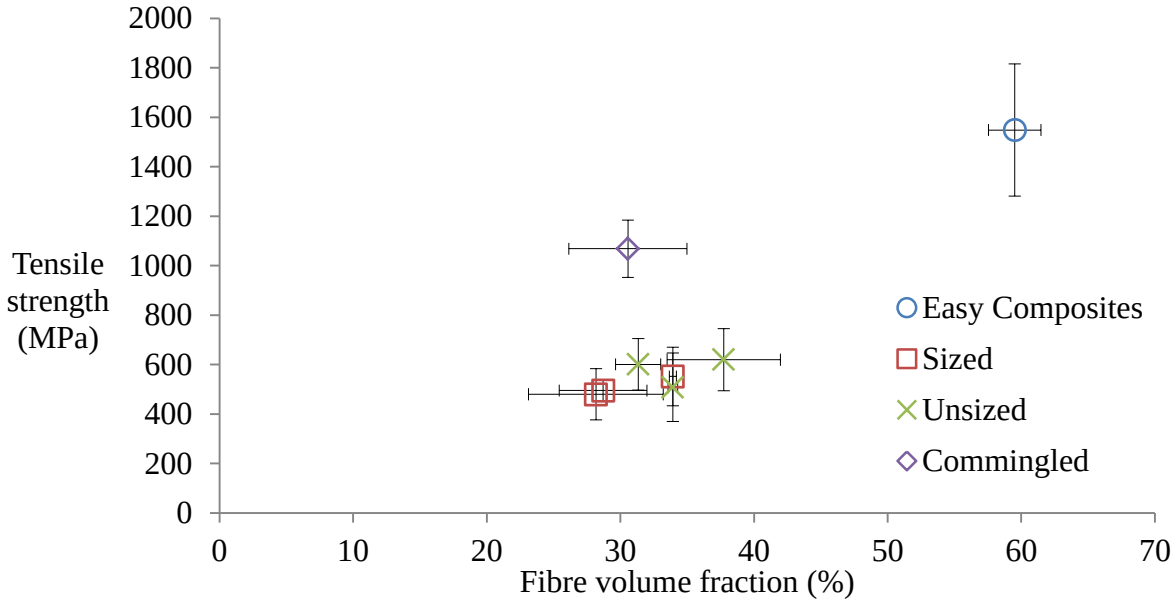

Figure 5.26 Ultimate tensile strength of rods produced at standard manufacturing conditions, by fibre volume fraction.

5.5.3 Strain-to-break

A trend of inverse proportionality between strain-to-break and fibre volume fraction can be observed in Figure 5.27 for rods produced from sized and unsized fibres. 9C, with a recorded a value of 2.28%, showed a strain-to-break that was almost 1% higher than the carbon fibre/thermoplastic rod with the next highest strain-to-break. At 2.38%, EC recorded the greatest strain-to-break.

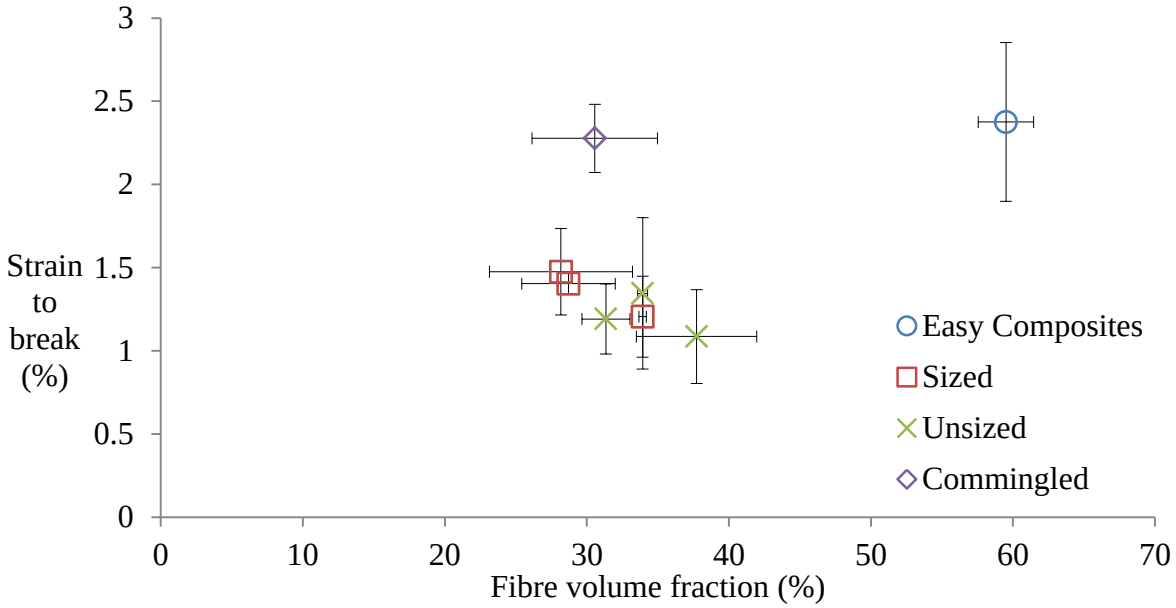

Figure 5.27 Strain-to-break of rods produced at standard manufacturing conditions, by fibre volume fraction.

5.5.4 Strain energy

Similarly to strain-to-break, 9C had a much greater mean value for strain energy, at more than two and a half times the magnitude of 4U, which was the next highest carbon fibre/thermoplastic rod. In turn, 9C was greatly outperformed by EC, as shown in Figure 5.28. There was no statistically significant relationship between strain energy and fibre volume fraction among rods produced from sized and unsized carbon fibres.

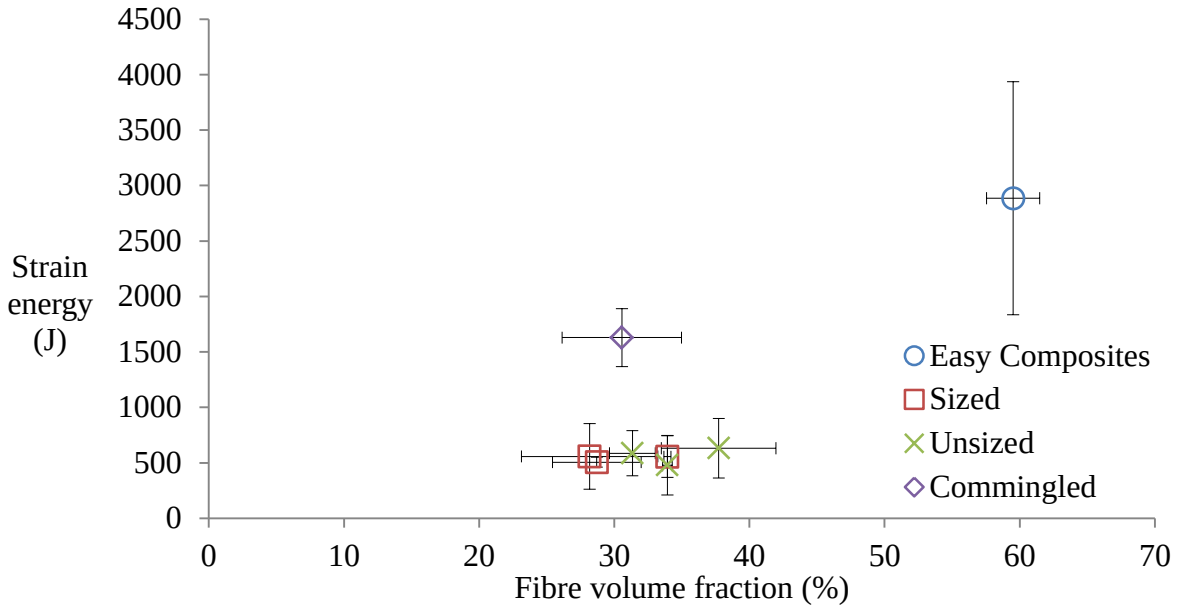

Figure 5.28 Strain energy of rods produced at standard manufacturing conditions, by fibre volume fraction.

5.6 Hybrid strand tensile tests

Due to software issues it was not possible to export data from the tensile machine used at Bridon for the testing of strands. Scans of hard copy print-outs of the test report delivered by the machine's software have therefore been included in Appendix C.

Since the rope industry typically specifies tensile strength in terms of weight or force per square millimetre, this has been converted to units of megapascal and gigapascal that are consistent with those used in FRP engineering. Strands with FRP central rods have been compared throughout this section with a strand composed entirely of steel wires. Due to restrictions in the availability of carbon fibre/epoxy rods of the required length, as outlined in §3.3.3, tests were instead performed on hybrid strands with carbon fibre/vinyl ester rods provided by Bridon.

The Young's modulus of strands with 6S and 9C , shown in Figure 5.29, was found to be lower than the fully steel strand by approximately 18GPa. By comparison, hybrid strands with VE rods had a Young's modulus 12GPa higher than the steel strands.

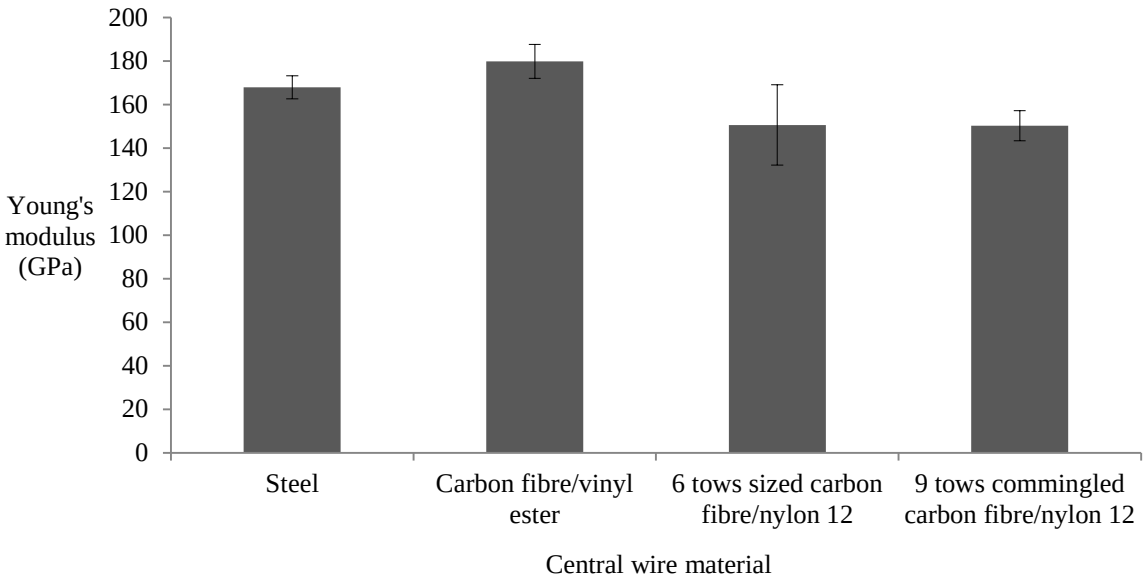

Figure 5.29 Young's modulus of strands by the material of the central wire or rod.

Ultimate tensile strength was lowest for hybrid strands with 6S and 9C. Steel strands were 100MPa stronger than hybrid strands with VE. This is described in Figure 5.30.

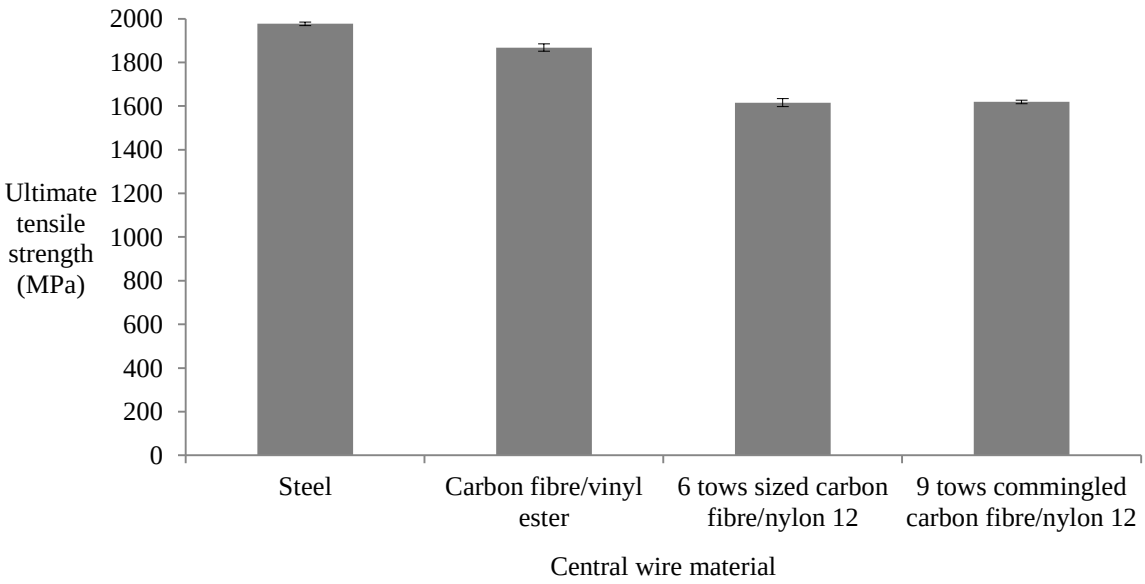

Figure 5.30 Ultimate tensile strength of strands by the material of the central wire or rod.

Strain-to-break was higher for steel strands than for those containing FRP cores, as shown in Figure 5.31.

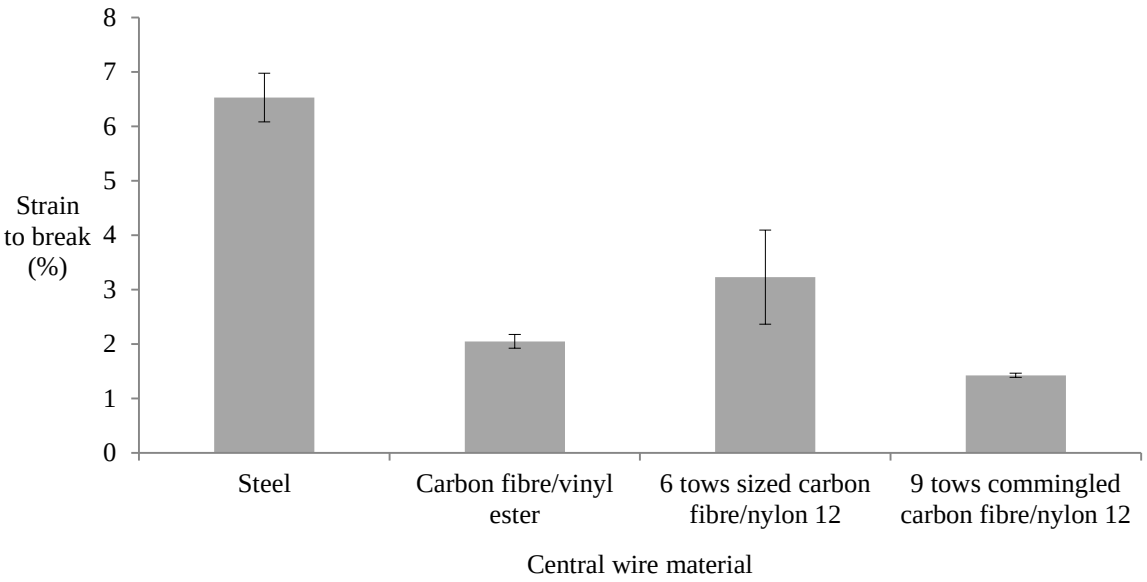

Figure 5.31 Strain-to-break of strands by the material of the central wire or rod.

As can be seen from stress-strain graphs in Appendix C, hybrid strands with 6S recorded comparatively higher strain-to-break than hybrid strands with 9C or VE. This can be attributed to multiple damage events that preceded ultimate failure, which appear as discontinuities in the stress-strain graphs, such as those shown in Figure 5.32 and Figure 5.33.

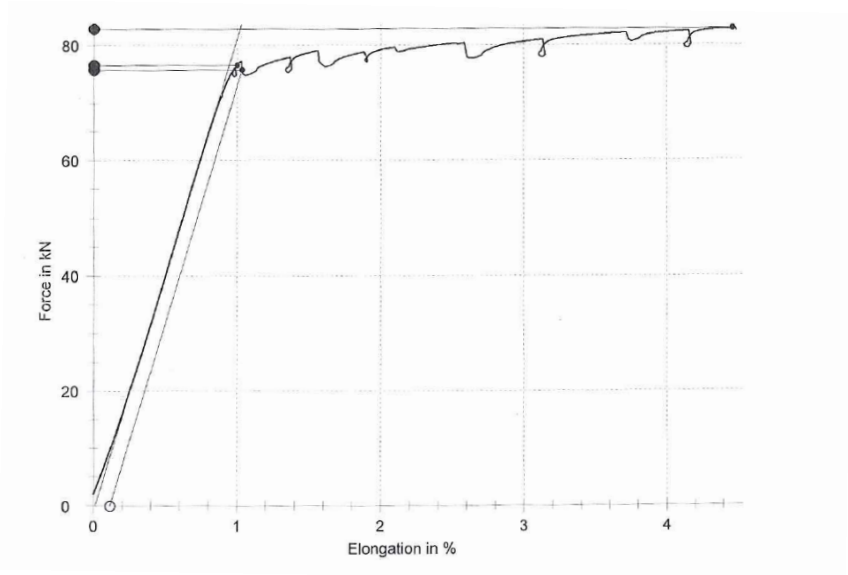

Figure 5.32 Tensile test 1 of a hybrid strand containing 6S. This graph can also be found in Appendix C, Figure C. 7.

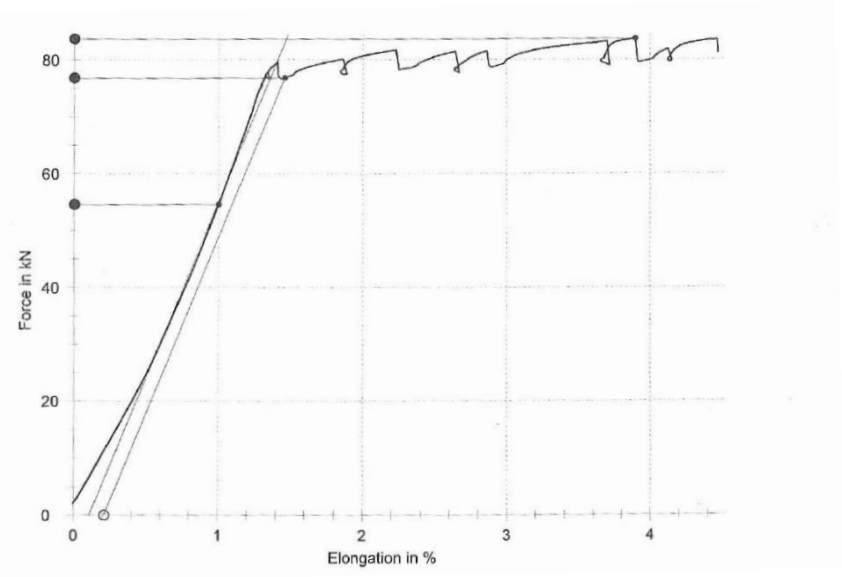

Figure 5.33 Tensile test 2 of a hybrid strand containing 6S. This graph can also be found in Appendix C, Figure C. 8.

Tenacity represents the tensile strength of the strand divided by its mass. The significant difference in ultimate tensile strength between steel strands and hybrid strands with 6S and 9C, shown in Figure 5.30, therefore resulted in them recording the lowest tenacity in spite of the lower mass of these hybrid strands, as seen in Figure 5.34. Given the similar tensile strength of steel strands and hybrid strands with VE, the latter showed the highest tenacity, owing to the lower density of their FRP central rods.

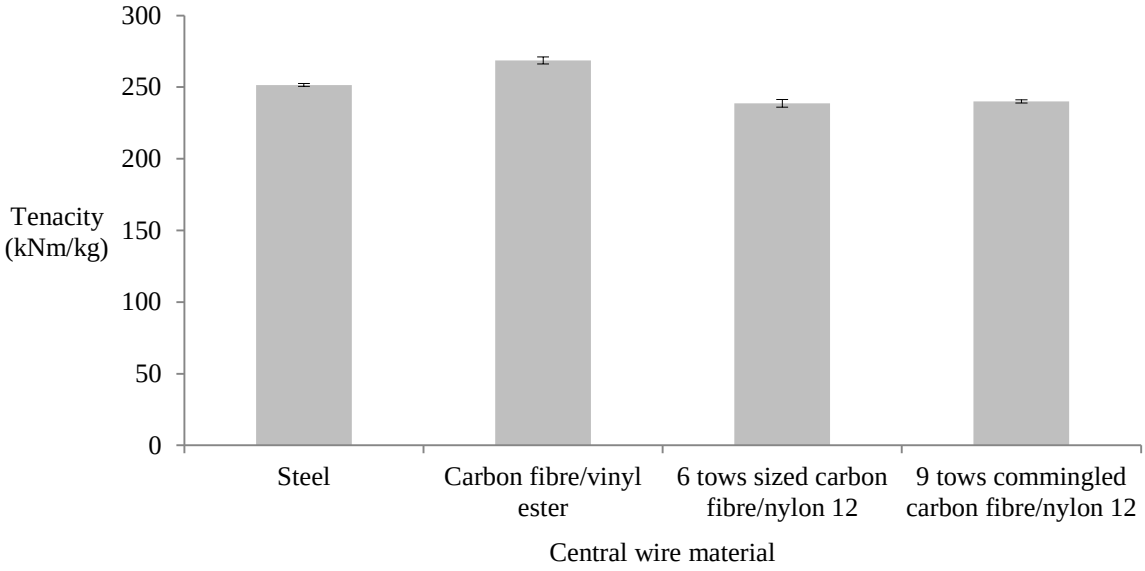

Figure 5.34 Tenacity of strands by the material of the central wire or rod.

5.6.1 Evaluation of testing methods

The failure of steel strands proceeded with splaying of the wires within the gauge length. This produced characteristic ‘birdcages’ in which the outer wires uncoiled around an intact section of a central wire, an example of which is given in Figure 5.35. Birdcages are known to occur due to local buckling when a rope twists about its axis of rotation and the winding radius of the outer wires increases with respect to the core wire [1]. The deformation seen in Figure 5.35 is related to the sudden release of tension in the outer wires upon breaking. This took the appearance of the outer wires recoiling into the characteristic shape of a birdcage.

Figure 5.35 Birdcage failure of a steel strand.

Hybrid strands failed without any indication of exterior damage. This was commensurate with the observation of lower strain-to-break of the hybrid strands, which indicated that the central FRP rod had failed before outer wires. Exceptions to this were the appearance of birdcages in two tests and the splintering of outer strands in another of hybrid strands with 6S. These failure modes belonged to those tests that recorded the highest strain-to-break. Images of hybrid strands containing 6S and VE after testing are shown in Figure 5.36 and Figure 5.37, respectively.

Figure 5.36 Hybrid strands with 6S after testing.

Figure 5.37 Hybrid strands with VE after testing.

Since the absence of external damage in all other cases raised the possibility that the samples had instead slipped in the grips, strands were disassembled to examine their interior, shown in Figure 5.38. Upon stripping the outer wires from the FRP core, the epoxy adhesive fell away in flakes and shards, suggesting that it had disintegrated by crushing in the wedge grips. The adhesive is therefore likely to have mechanically filled the strand rather than acted as a durable bonding agent. The shrink wrap tubing surrounding FRP core rods was heavily indented by the outer wires and appeared to have conformed to the helical shape of the strand, as shown in Figure 5.39.

Figure 5.38 Dismantled hybrid strand after testing.

Figure 5.39 Helical pattern indented into shrink wrap tubing surrounding FRP rod.

FRP rods were found to have broken within the gauge length, thereby demonstrating that they had not slipped within the grips. In some cases the fracture did not pierce the heat shrink tubing, an example of which is shown in image b) in Figure 5.40.

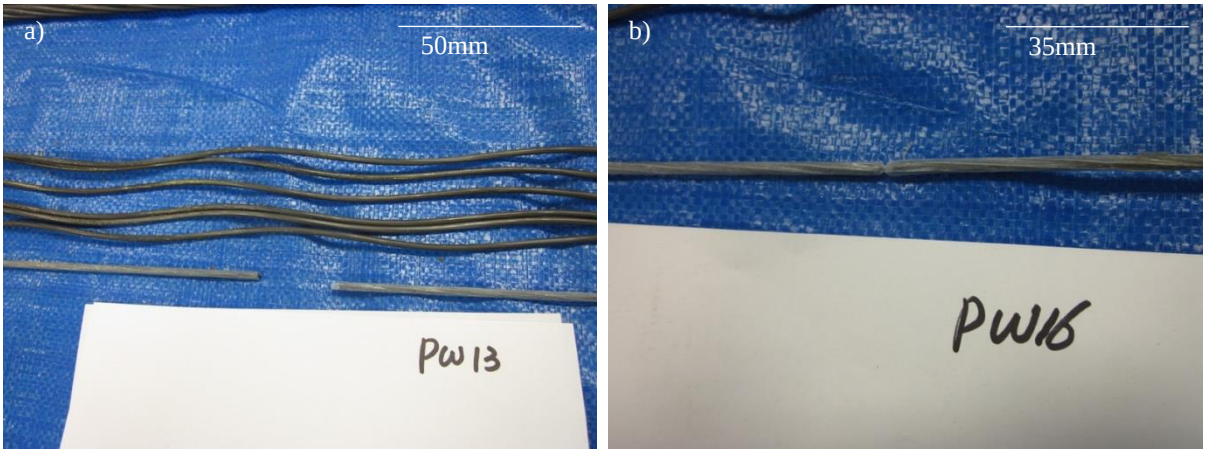

Figure 5.40 Broken FRP core rods in two hybrid strands.

In conclusion, these observations demonstrate that the methodology used for the tensile testing of hybrid strands was adequate for the determination of the maximum breaking force. Failure of hybrid strands was shown to occur in the FRP central rods rather than in the outer steel wires.

5.7 Concluding summary

Pultruded rods manufactured from different feedstocks have shown considerable variation in cross-sectional morphology, as well as flexural and tensile strength and stiffness. These differences have been reflected in the unprecedented characterisation of the tensile strength and stiffness of hybrid steel and FRP strands, which represents a novel dataset relating to the study of wire strands. Key findings from test results are summarised in this section:

- Optical microscopy of rods
    - For rods with sized and unsized fibres, cross-sections revealed serpentine tows of reinforcement within a body of largely unreinforced polymer. The perimeters of the rods were uneven and only approximately circular in shape.
    - Tows of unsized fibres were thicker, less sinuous and individually less distinguishable than those from sized tows. They also featured a greater prevalence of areas containing dry fibres. The cross-sections with the greatest loading of unsized fibres showed fewer areas of unreinforced polymer.
    - The cross-sections of rods with commingled fibres showed clearly divisible tows that appeared separated from one another by regions of unreinforced polymer matrix. The fibre reinforced areas showed regularity in consolidation, although macroscopic defects appeared close to the perimeters of the rods, which were irregular in shape.
    - Carbon fibre/epoxy rods showed the least variation in consolidation and were reinforced throughout the cross-section, without the frequent appearance of voids. These rods appeared to be free from fibre-rich areas and did not contain large sections of unreinforced matrix. The perimeters of the rods appeared to be circular.
- Fibre volume fraction and void content of rods
    - Although fibre volume fraction rose with the loading of carbon fibres, the quantity of polymer in the rod also increased with fibre loading.
    - Statistical uncertainty obscured any clear relationship between void content and fibre volume fraction. However, carbon fibre/epoxy rods appeared to have the lowest void content, while rods with commingled fibres appeared to have a lower void content than rods from sized and unsized fibres.
- Rod diameters
    - A trend of increasing rod diameter with greater fibre volume fraction was observed.
    - No correlation was observed between the diameter of rods from sized fibres and the line speed of pultrusion, over a range of speeds from 3cm/min to 9cm/min.
- Flexural tests of rods
    - Flexural stiffness increased with fibre volume fraction in rods from sized and unsized fibres, while the correlation between flexural strength and fibre volume fraction was only strongly observed for rods from unsized fibres. Rods from commingled fibres higher flexural strength than rods from sized and unsized fibres. Carbon fibre/epoxy rods displayed higher flexural strength and stiffness than any other rods.
    - Flexural strength and stiffness were not observed to correlate with line speed of manufacture over the range of tested speeds.

- Tensile tests of rods
    - There was a positive correlation between tensile strength and stiffness and fibre volume fraction for rods produced from sized and unsized fibres. Strain-to-break was inversely proportional to the fibre volume fraction of rods produced from sized and unsized fibres, while there was no statistically significant correlation for strain energy.
    - Among carbon fibre/thermoplastic rods, those from commingled fibres showed the highest tensile strength and strain-to-break.
    - Carbon fibre/epoxy rods demonstrated higher tensile strength, tensile modulus and strain energy than any other rods, while recording a comparable strain-to-break to rods from commingled fibres.
- Tensile tests of hybrid strands
    - The tensile strength and stiffness of hybrid strands with carbon fibre/thermoplastic rods were lower than those of steel strands or hybrids with carbon fibre/vinyl ester rods. Steel strands also recorded the highest strain-to-break.
    - The highest tenacity was found for hybrid strands with carbon fibre/vinyl ester rods. The tenacity of hybrid strands with carbon fibre/thermoplastic rods was lower than those of steel strands.
    - The methodology for tension testing of hybrid strands was found to give successful results, with samples breaking in the gauge length. Failure of hybrid strands was shown to occur internally through failure of the FRP rods.

5.8 References

1. Chaplin, C.R., Torsional failure of a wire rope mooring line during installation in deep water. Engineering Failure Analysis, 1999. 6(2), p. 67-82

6 Finite Element Modelling of a hybrid FRP and steel strand

Representative models that approximate the behaviour of working ropes have been pursued by numerous authors. Research has emphasised computational efficiency models, for instance the use of beam elements by Bechtold [1] to model a full lay length of a multistranded rope and the apportioning of a small symmetrical section of a stranded rope by Jiang [2] to investigate contact phenomena. The year-on-year fall in the cost and exclusivity of computational power has permitted a number of works on the finite element modelling of multistrand ropes to be performed using solid elements. An example is a study of sliding between strands that was undertaken by Stanova [3].

6.1 Analysis and geometry

Following from the work of Benndorf [4], Feyrer [5] derived analytical relations for the tension in wires and strands, which inform the equations quoted in this section. Figure 6.1 shows the notation used in this section to describe the forces and geometry associated with a helical wire.

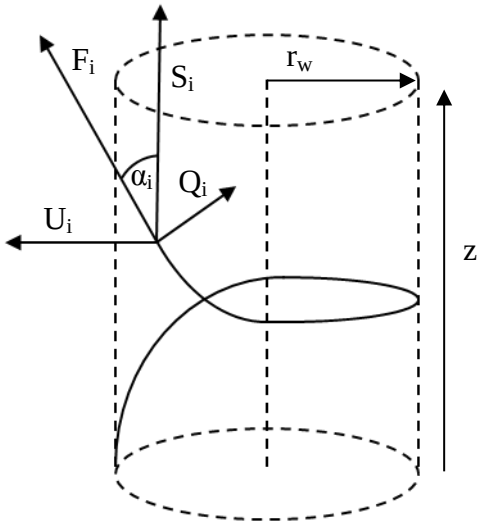

Figure 6.1 Geometry of an outer wire and its helical path.

At a given point on the helical path made by an outer wire, the tangential angle between the helix and the central wire is the lay angle, α. The winding radius, r_w, is taken as the distance between the centre of rotation of a wire and the vertical height of a point on the path, z from the base. The lay angle is therefore defined in terms of the lay length, z_w, which is the vertical distance required for a full rotation of the wire about its central axis:

$$\tan\alpha = \frac{2 \cdot \pi \cdot r_w}{z_w} \qquad \text{(eq. 6.1)}$$

The tension upon the wire, F_i, can be separated into its axial load, P_i, and the shear, Q_i acting on the wire. Assuming the shear to be small, the tension in the strand in the axial direction, S_i, is given by summation of the number of outer wires, z in addition to the core strand:

$$S_i = \sum_{i=0}^{n} z \cdot P_i = \sum_{i=0}^{n} z \cdot F_i \cdot \cos\alpha \qquad \text{(eq. 6.2)}$$

The force in a strand is also dependent on the degree of contraction that the surrounding wires exert upon the core, which may be significant if the core material is less compliant than that of the outer wires. This contraction ratio behaves like a structural Poisson's ratio. Analytical calculations are unlikely to suffice for the accurate determination of these properties and semi-empirical models only currently exist for homogeneous steel wire ropes. Numerical methods therefore offer a means of estimating tensile strength and stiffness without the need to derive an exhaustive analytical framework. While an analytical model would greatly benefit the discipline of hybrid ropes, it would be disproportionate to the aims of this project.

This section presents a three-dimensional model of one whole lay length of a hybrid strand. The core wire radius, r_c, was defined as 1.65mm and the radius of the outer wire, r_h, as 1.5mm, such that the ratio of the core wire to outer wire was 1.1. This gave diameters for the outer wires and the central wire of 3mm and 3.3mm, respectively. The single lay length was arbitrarily defined as 150mm for convenience, which in consideration of a winding radius of 3.15mm gave a lay length, α, of approximately 7.5°. The relationship between these values is shown in Figure 6.2.

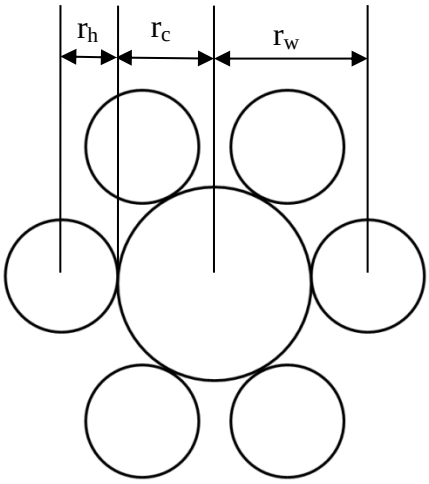

Figure 6.2 Helical, core and winding radii.

6.1.1 Hybrid strand stiffness

Individual wires in a strand interact only by contact; unlike a fibre reinforced plastic there is no direct load sharing by means of chemical bonding. For this reason the strand behaves as a hybrid structure rather than as a composite. The total reaction forces experienced by all the strands in response to a controlled displacement was therefore homogenised in order to record the Young's modulus of the strand, or the resistance to deformation given by the hybrid structure.

A relatively straightforward calculation was made from Hooke's law using the reaction forces acting on the strand, as shown in eq. 6.3. Stresses were computed using the cross-sectional area of the elements.

$$\text{Stiffness} = \frac{\left(\frac{\text{Reaction force}}{\text{Cross section}}\right)}{\text{Strain}} \quad \text{(eq. 6.3)}$$

Extension in each model was controlled by displacement, from which the strain was implicitly obtained.

6.1.2 Winding

Winding as a stage of manufacturing is not considered by this project due to the complexity of modelling cold drawing. This results in the permanent helical shape of the wires, as shown in Figure 6.3. From the point the macroscopic phenomena of the core, it is sufficient to use the materials properties of drawn steel wires after this stage of processing, which have been provided by Bridon [6]. However, the friction between wires has a strong influence on the mechanical properties of ropes [7]. In the modelling of strands in this section, an additional 'twist' step was applied before displacement. This represented the tightening of the strand prior to bearing load, during which wires the experienced greater contact forces with one another.

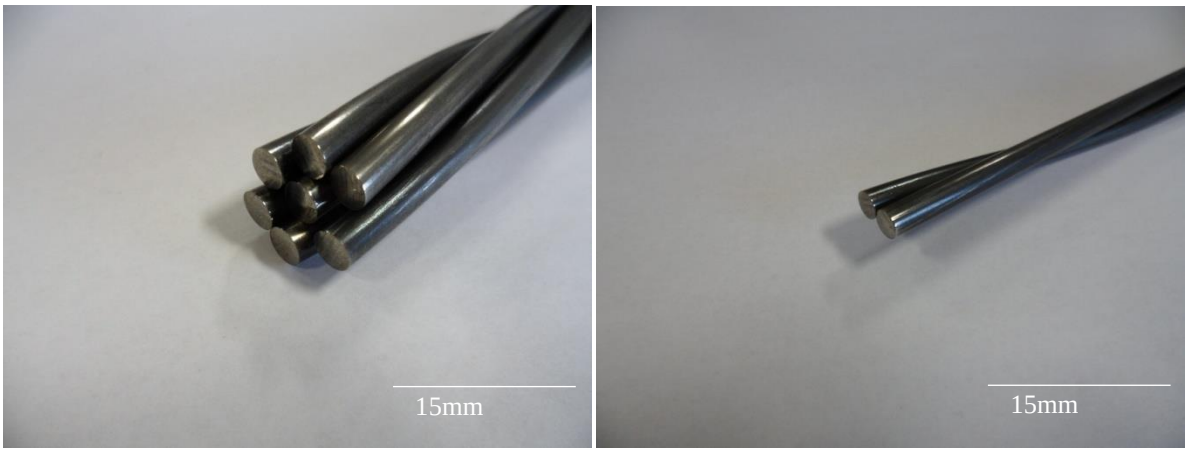

Figure 6.3 Outer wires retain their helical shape after winding.

6.2 Finite element model

A hybrid strand with a FRP central rod and steel outer wires was modelled using the finite element method. The geometry was sketched in ABAQUS 6.10 and exported to Hypermesh 9.0, where eight-node brick elements (C3D8) were individually defined along the imported lines using the 'solid mesh' 3D feature. This element type was chosen for its recommended adequacy in handling contact and for a suitable balance between computational cost and ease of convergence [8]. Orphan meshes were thus exported back to ABAQUS 6.10. The technique of using separate meshing software was developed by Erdönmez and İmrak for the creation of long helical models, such as those that encompass an entire lay length [9]. The element density was increased at the contacting surfaces between the core and the outer wires. In contact interactions the central rod was taken as the master surface and a finer mesh was found to be necessary on the outer wire slave surface in order to prevent interpenetration. Through persistent readjustment of the mesh, distorted elements were replaced so that no element had a Jacobian value below +0.32.

The geometries created in ABAQUS 6.10 consisted of shell instances upon which partition lines were drawn. Shell parts for the core and outer wire were added to the assembly in contact with one another. These were then copied and translated above the first two instances. The separation between the upper and lower instances informed the depth of the elements in the meshing stage, as shown in Figure 6.4, Figure 6.5 and Figure 6.6.

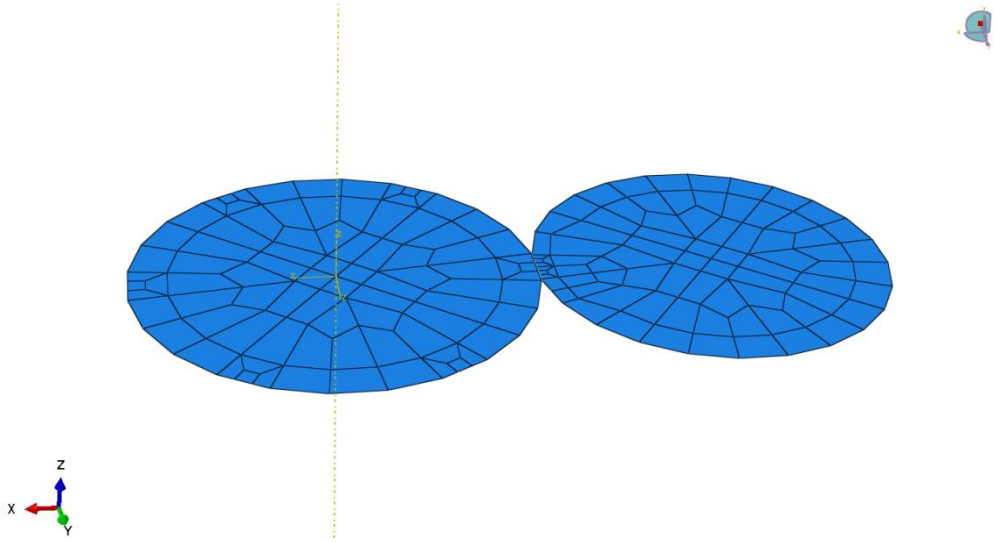

Figure 6.4 Shell parts with partition lines for the core and outer wires, with outer elements in contact with one another.

The central and outer wire instances were then rotated together about an axis through the centre of the central wire. This rotation of 0.9° gave rise to the helical twist of the outer wires, as every 'slice' of elements created between the two layers of partition lines retained the translation and rotation of those parts instanced in the assembly. It also meant that the surfaces of the elements on the core and outer wires always faced one another so that there would not be any clearance between the elements in contact, as shown in Figure 6.12. This strategy was found to be necessary in overcoming the problems of meshing a helical geometry discovered by Erdönmez and İmrak [9].

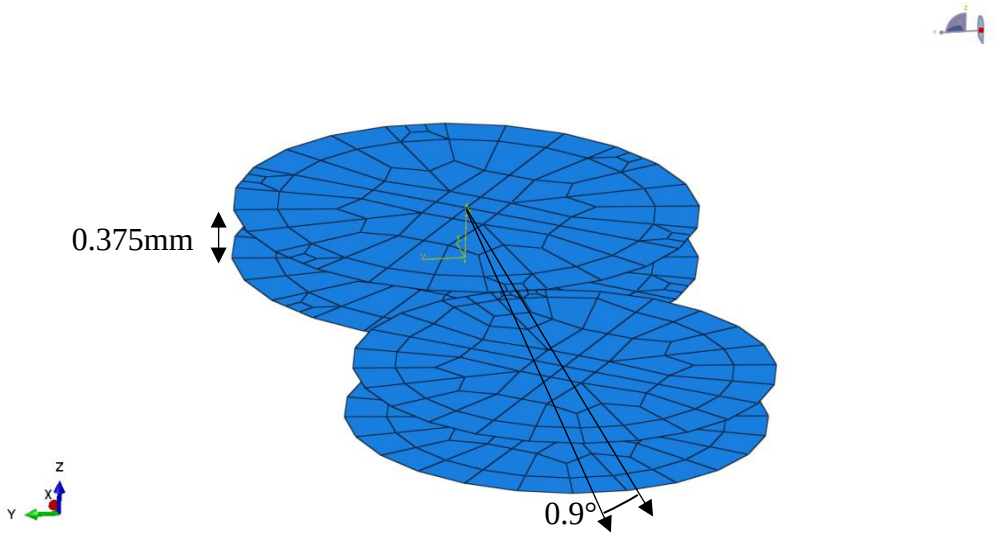

Figure 6.5 Angle of rotation about an axis through the centre of the core wire.

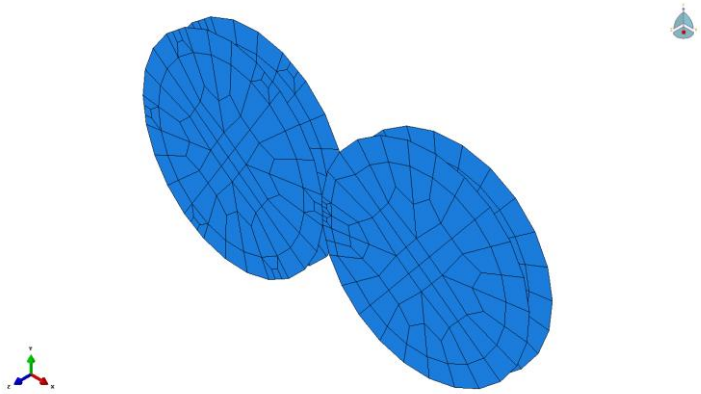

Figure 6.6 Geometry created in ABAQUS 6.10 for export to Hypermesh 9.0.

When imported into Hypermesh 9.0, the two layers of partition lines created a framework for the upper and lower edges of the elements, shown in Figure 6.7. Vertices between partition lines provided locations for nodes. Bottom-up meshing was undertaken using the 'solid mesh' function in the '3D elements' module. Elements were created one at a time by defining the edges with corresponding partition lines.

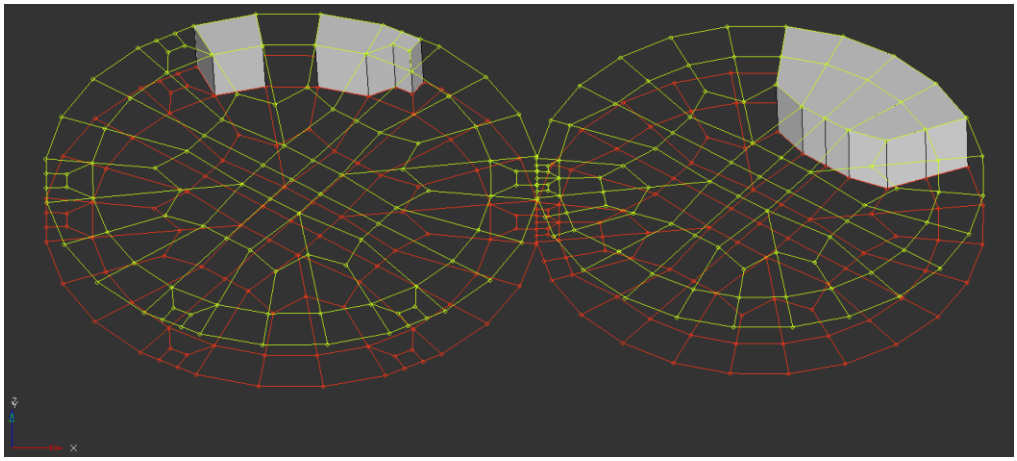

Figure 6.7 Individual generation of elements between sketched lines.

In this way one element deep 'slices' of the wires were created, which were repeatedly copied and stacked upon one another to generate a wire. An example of a 'slice' is shown in Figure 6.8. Copied and translated slices were rotated into position above neighbouring elements to maintain the degree of rotation inherent throughout the helical outer wires or the axial twist for the central wire.

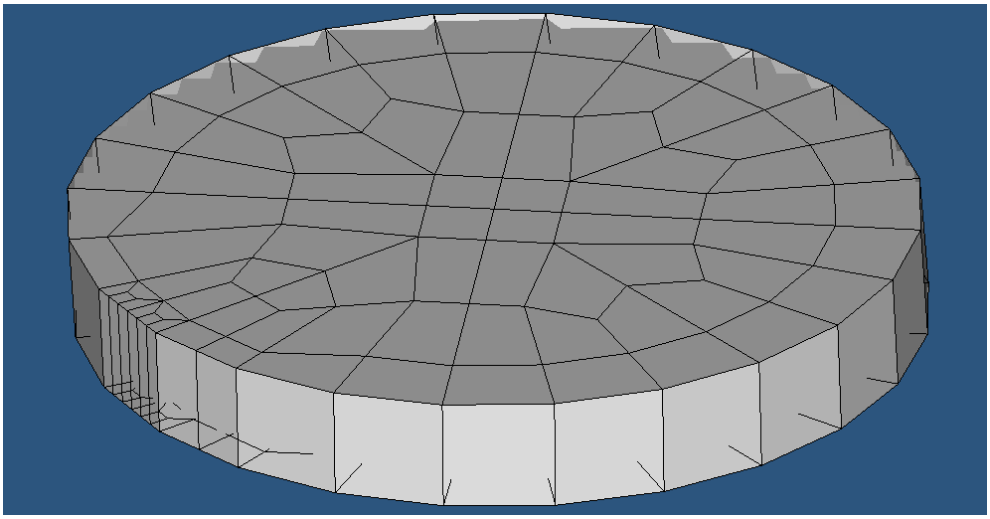

Figure 6.8 One element deep ‘slice’ of a helical outer wire.

400 such slices were copied, translated and rotated to create a complete wire, shown in Figure 6.9 and Figure 6.10. Since each slice was given a rotation of 0.9°, the whole structure possessed a full rotation of 360° upon its central axis and thus represented one full lay length. Once completed, all the elements in a wire were selected and shared nodes between individual elements were merged using the ‘equivalence’ function in the Tools module. The completed wires were then imported into ABAQUS 6.10 and assembled into strands.

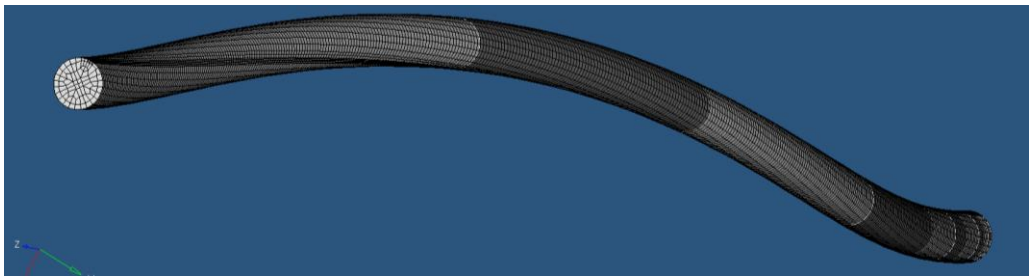

Figure 6.9 Completed helical strand.

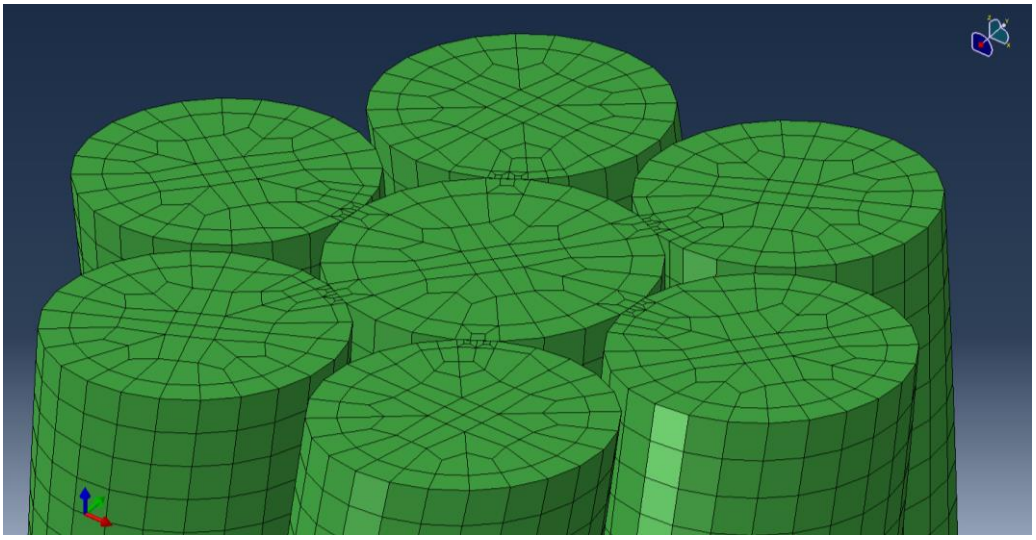

Figure 6.10 Higher mesh density at the region of contact between wires.

6.3 Modelling of tensile tests

Tensile tests were composed of three steps; 'Initial', 'Twist' and 'Displacement'. Kinematic constraints coupled nodes at either end of the strand to reference points away from these surfaces, as shown in Figure 6.11. Boundary conditions were then applied to those reference points for ease of application of rotation displacements to the solid brick elements. All steps were of the 'Static, General' type with the unsymmetric solver.

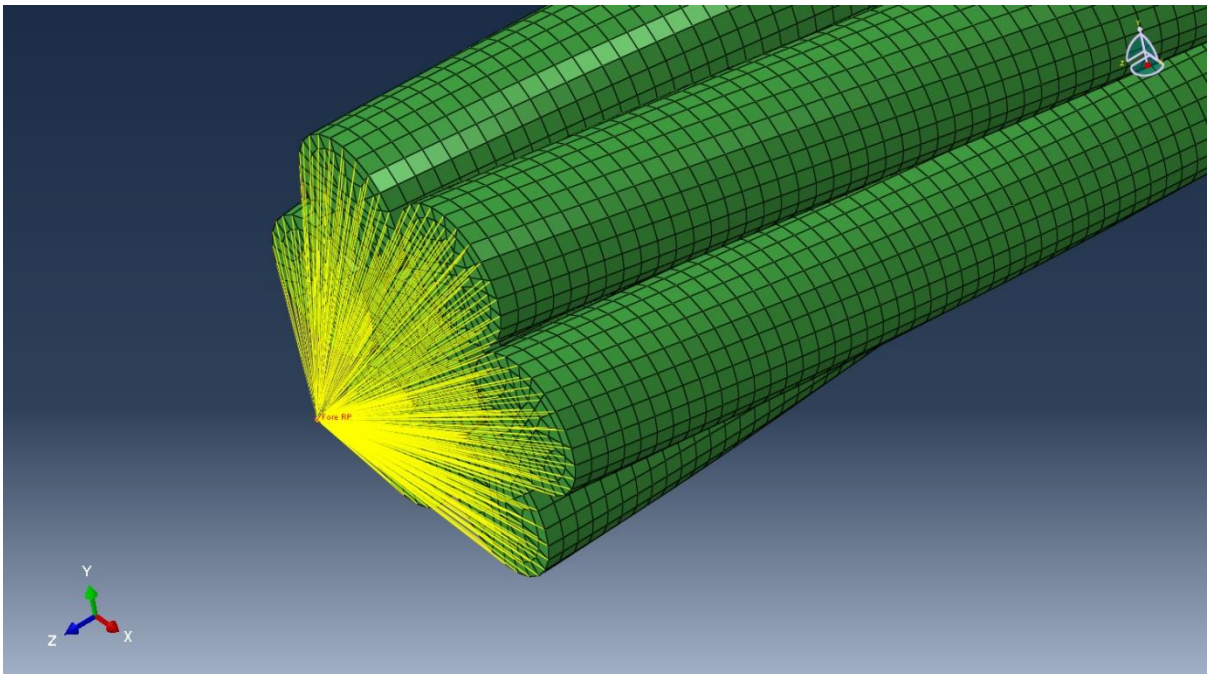

Figure 6.11 Kinematic constraints coupled nodes on the faces of strand cross-sections to reference points.

The following boundary conditions were applied in each step:

- *Initial*
  - The nodes on the base of the strand were fixed such that displacement degrees of freedom for those elements were not permitted, given by the condition: U1 = U2 = U3 = 0.
- *Twist*
  - Rotation around the axis of displacement was applied to the forward-facing nodes, such that UR1 ≠ 0.
- *Displacement*
  - An anti-symmetric boundary condition was also applied to the nodes at the displaced end of the strand such that degrees of freedom transverse to the direction of extension were constrained. This was found to be necessary in order to prevent unravelling of the strand. This was specified by: U1 = U2 = 0.
  - A boundary condition was applied to the forward nodes of the strand, specified by U1 ≠ 0. Displacement was ramped linearly throughout this step.

Surface-to-surface contact properties were defined between the central wire and outer helical wires along the faceted surfaces, shown in Figure 6.12. This offered the advantage of only involving those elements known to participate in contact behaviour, which considerably

reduced the computational cost associated with contact. The "Hard" Contact interaction property available in ABAQUS CAE was applied with default constraint enforcement. Following the work of Jiang and Sun [7, 10], an isotropic penalty friction coefficient of 0.115 was applied to all surface-to-surface contact interactions. This value represents lubricated contact between outer and central wires, which is representative of contact conditions present in both the steel and hybrid strands produced in §4.5 for tensile testing, results for which were presented in §5.6.

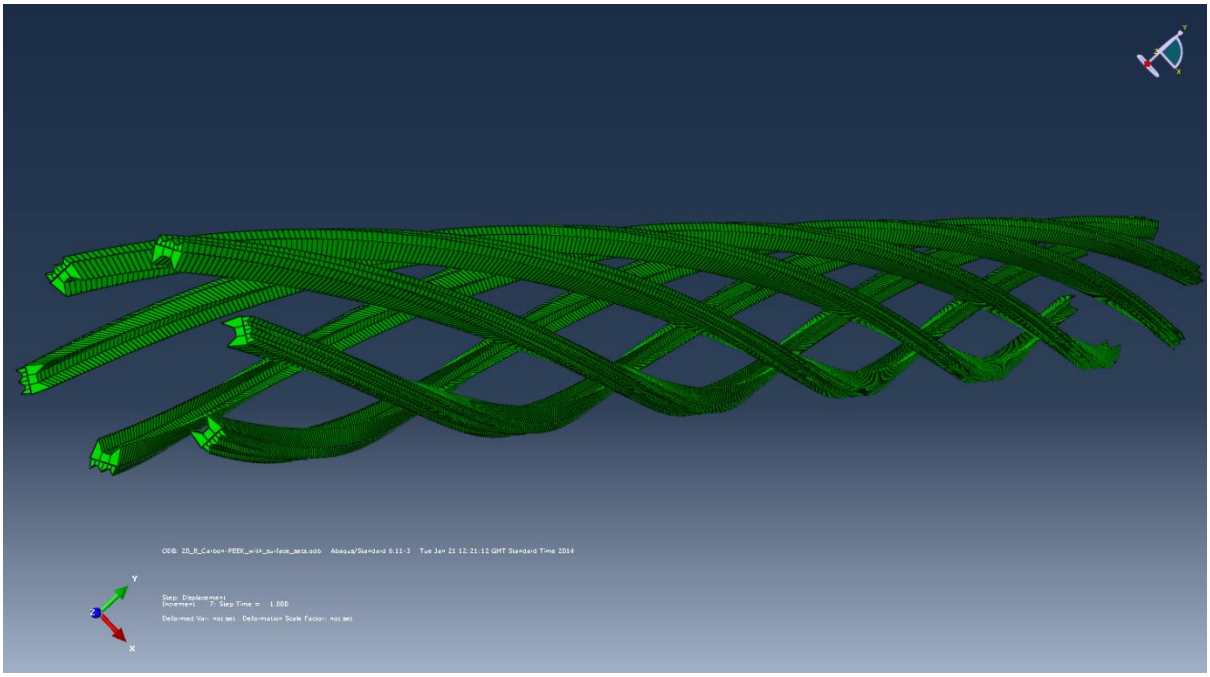

Figure 6.12 Surface-to-surface contact properties were defined between elements in contact between the central and outer wires.

6.3.1 Material properties

Steel wires were represented by material properties collected from experimental data [11]. These material definitions represented steel central wires and the steel outer wires present in all models. Hybrid strands were modelled with the central wire as FRP and outer wires as steel. Data for the properties of these materials were gathered from experiments and manufacturer datasheets and are presented in Table 6.1. Material properties were taken from the following references:

- 'High strength steel' taken from Walton and Yeung [6]
- 'Carbon fibre/PEEK' and 'Glass fibre/PEEK as CETEX TC1200 PEEK resin reinforced with AS-4 carbon fibres and S2 glass fibres, respectively [12]
- 'Carbon fibre/nylon' and 'Glass fibre/nylon' as CETEX TC910 nylon 6 resin reinforced with carbon fibres and glass fibres, respectively [13]
- '6 tows sized carbon/nylon 12', '3 tows unsized carbon/nylon 12' and '9 tows commingled carbon/nylon 12' are taken from mechanical properties report for pultruded rods in §5.5 with Poisson ratios estimated due to a lack of experimental data
- 'PEEK' as KetaSpire KT-820FP [14]
- 'Nylon 12' as Duraform PA Plastic [15]
- 'Carbon fibre/vinyl ester' from experimental data provided by Bridon

Table 6.1 Elastic properties for the core wire, *estimated value.

Material	Tensile modulus (GPa)	Tensile strength (MPa)	Poisson ratio
High tension steel	200	1820	0.26
Carbon fibre/PEEK	178	2280	0.329
Carbon fibre/nylon	100	1900	0.3
Carbon fibre/vinyl ester	146	2100	0.3*
Glass fibre/PEEK	52	1520	0.29
Glass fibre/nylon	30	900	0.3
6 tows sized carbon/nylon 12	54.9	507.2	0.3*
3 tows unsized carbon/nylon 12	51.0	572.7	0.3*
9 tows commingled carbon/nylon 12	54.8	1068.8	0.3*
PEEK	3.65	96.5	0.4
Nylon 12	1.59	43	0.39

6.4 Effect of winding angle on stiffness

The 'Twist' step before axial displacement applied a correcting winding to the strands to account for compressive stresses that arise at the points of contact between individual wires. By introducing an artifice to the model it was necessary to 'calibrate' the degree of winding. In order to find the decrease in stiffness that resulted from the longer helical path made by the outer wires with respect to the straight central wire, a series of models were run with different winding angles. This phenomenon is described in Figure 6.13.

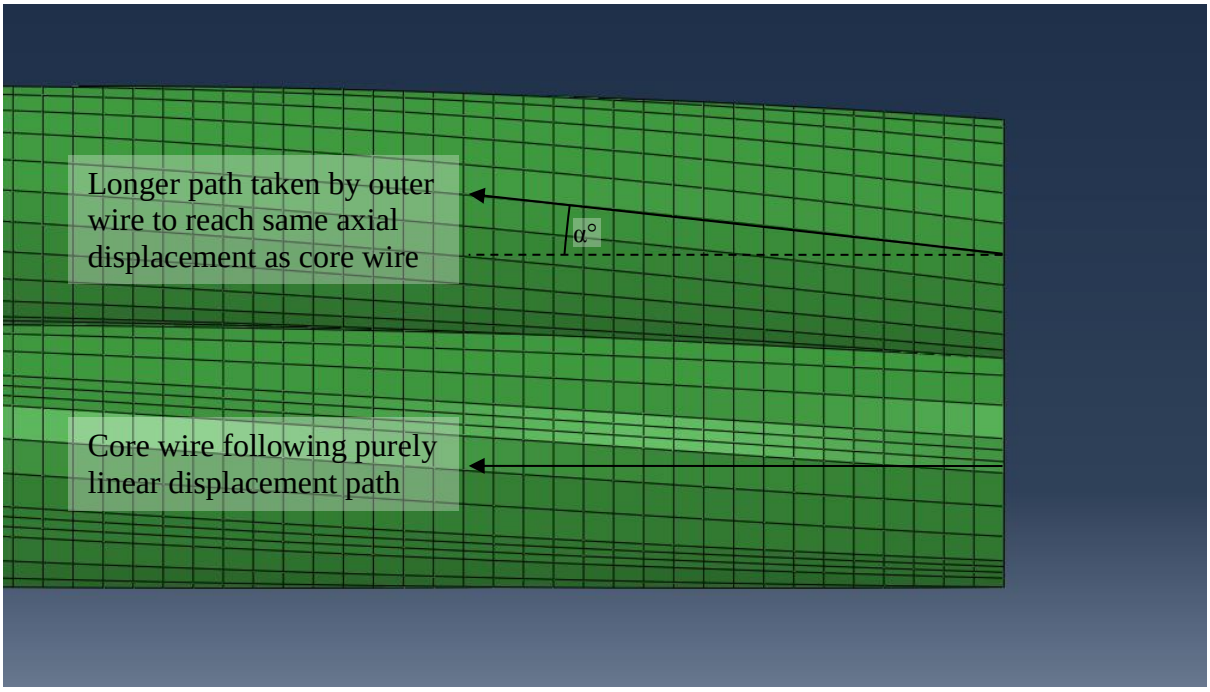

Figure 6.13 Relative difference in extension of the central and outer wires.

These models represented steel strands and as such the central and outer wires were given steel material properties. In all respects each iteration of models in the parametric study were the same, except that the winding angle was varied in increments of 0.05radian. Therefore,

models with the following winding angles were analysed: 0radian (representing no winding at all) 0.05radian, 0.10radian, 0.15radian, 0.20radian, 0.25radian. These values were individually input into the rotation boundary condition for the Twist step, as described in §6.3.

As the rotation that occurred during the Twist step was a purely linear elastic phenomenon, there was a strongly positive linear correlation trend of Young's modulus with the angle of winding, as found in Figure 6.14. A mean stiffness of 167.9GPa was recorded for physical tensile tests of steel strands reported in Figure 5.29 in §5.5.1. This almost matched the stiffness of 170.5GPa for the model of a steel strand with a winding radius of 0.15radian. Therefore, the Twist boundary condition for all further models hybrid strand models was set to 0.15radian to calibrate the winding of the simulated strands with experimental results.

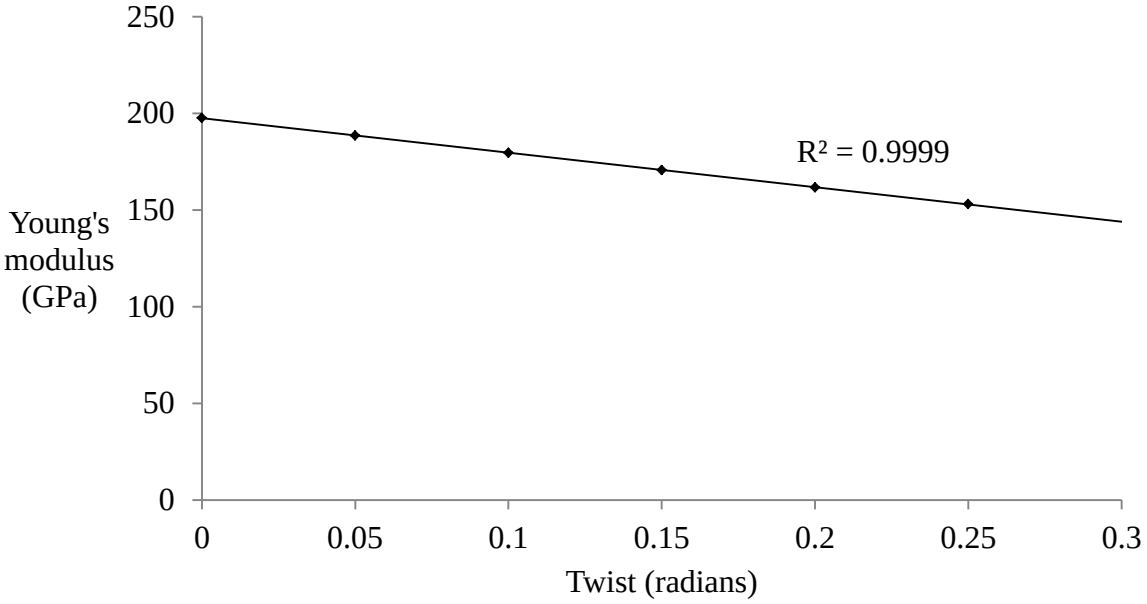

Figure 6.14 Young's modulus of steel strands with variation in Twist angle.

6.5 Modelling of hybrid strands

As shown in Figure 6.15, the stress-strain curves of hybrid strands showed three distinctive regions. All stress-strain curves began at a non-zero intercept, which was due to pre-stressing of the strand in the first winding step. The compressive pre-stressing induced by winding was released at the start of the displacement step and the strand entered a linear elastic region before any plasticity occurred. A higher number of field output requests were made for the elastic region to give better accuracy of calculations of Young's modulus. This came at the cost of higher computational resources, which ultimately placed a practical limit on the number of outputs that could be requested. The models ended in perfect plasticity and often failed to continue a short time after the yield strength was surpassed due to limits on computational resources.

The behaviour of the curve after reaching perfect plasticity was influenced by the mode of failure of the strand. When plasticity was reached at both ends of the strand, the gradient of the curve declined, an example of which is shown in Figure 6.16 for a steel strand. Where plasticity occurred only at one end of the strand, perfect plasticity resulted in a plateau

beyond the yield strength, for instance for a hybrid strand with a Carbon fibre/nylon 12 central rod shown in Figure 6.17. Plasticity localised at the ends of the strand was an artifice of the boundary conditions placed on either side of the model. This is similar to the effect of stress concentration that has been predicted in the finite element modelling of tensile tests of FRP coupons [16].

Hybrid strands with rods representing the carbon fibre/thermoplastic pultrusions manufactured for this project and glass fibre reinforced plastic cores performed approximately equivalently. The highest tensile strength was found for steel strands and hybrid strands containing carbon fibre reinforced PEEK, nylon and vinyl ester. Strands containing unreinforced plastic central wires recorded the least stress at failure.

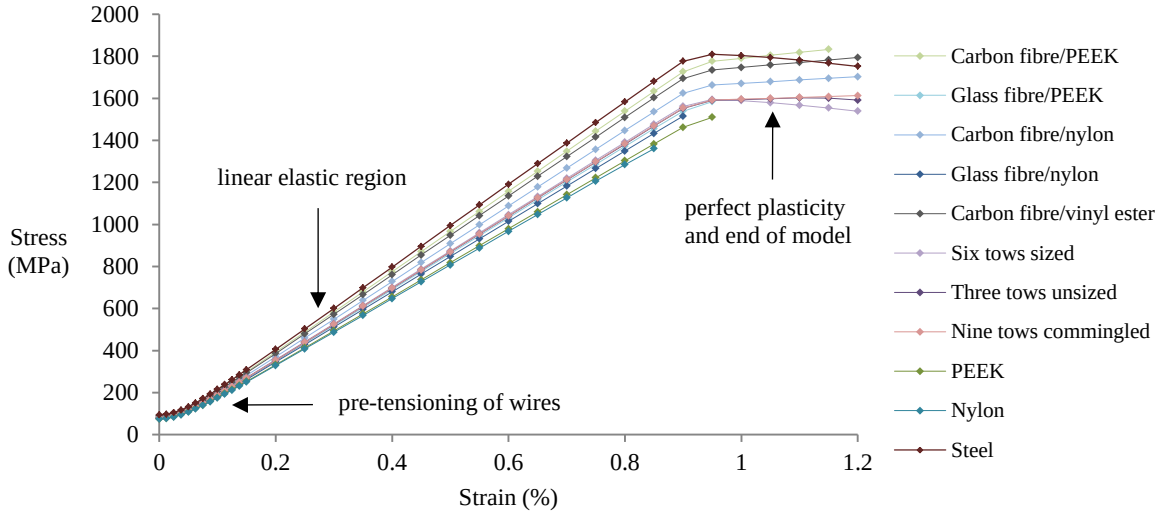

Figure 6.15 Stress-strain curves of steel and hybrid strand models in tension.

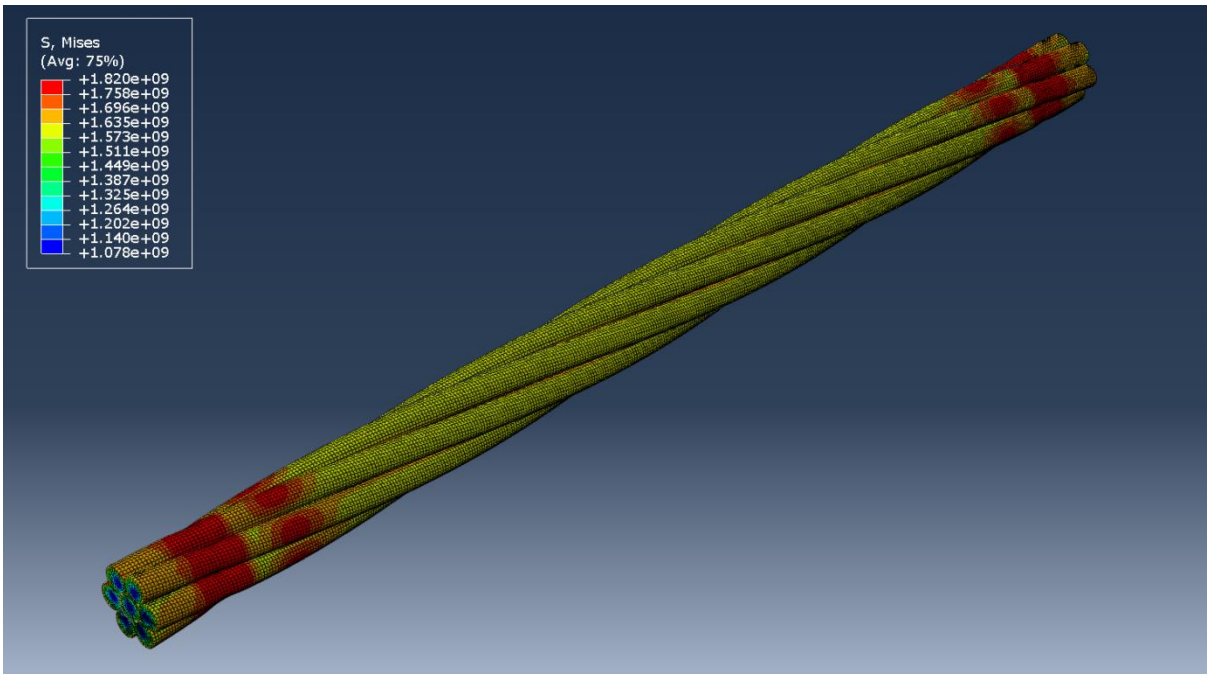

Figure 6.16 Plasticity of model with High strength steel central wire at a strain of 1.5%.

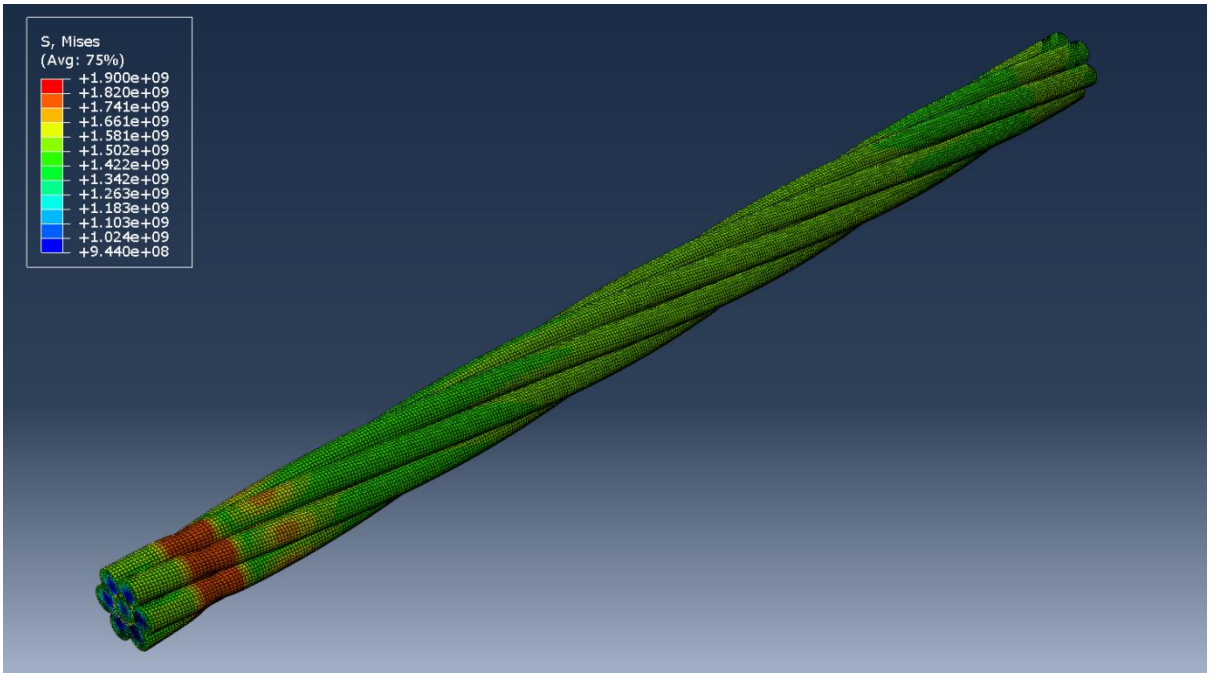

Figure 6.17 Plasticity of model with Carbon fibre/nylon 12 central rod at a strain of 2%.

6.5.1 Mechanical properties of central and outer wires

Figure 6.18 shows the stress-strain behaviour of the central wire isolated from the rest of the strand. There was a wide variation in the performance of strands with different core materials, with unreinforced nylon and PEEK bearing an almost insignificant contribution load, while the greatest was afforded by carbon fibre reinforced plastics and steel wires. By contrast, there was a barely observable variation in the stress-strain curves showing the isolated behaviour of the steel outer wires as the material of the central wire was changed, as can be seen in Figure 6.19. This implies that there was little interaction between the central and outer wires.

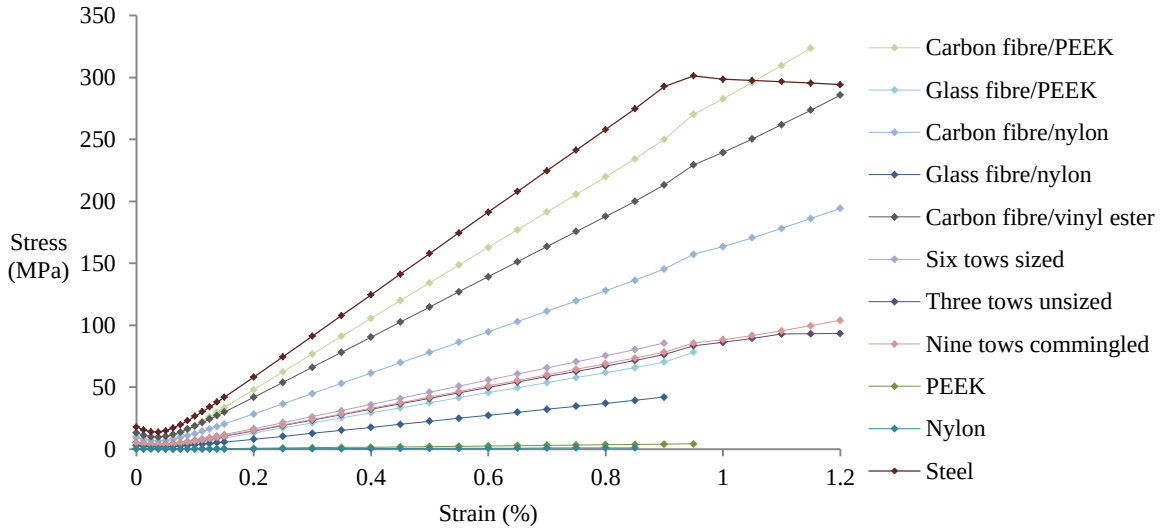

Figure 6.18 Stress-strain curves of the isolated central wire.

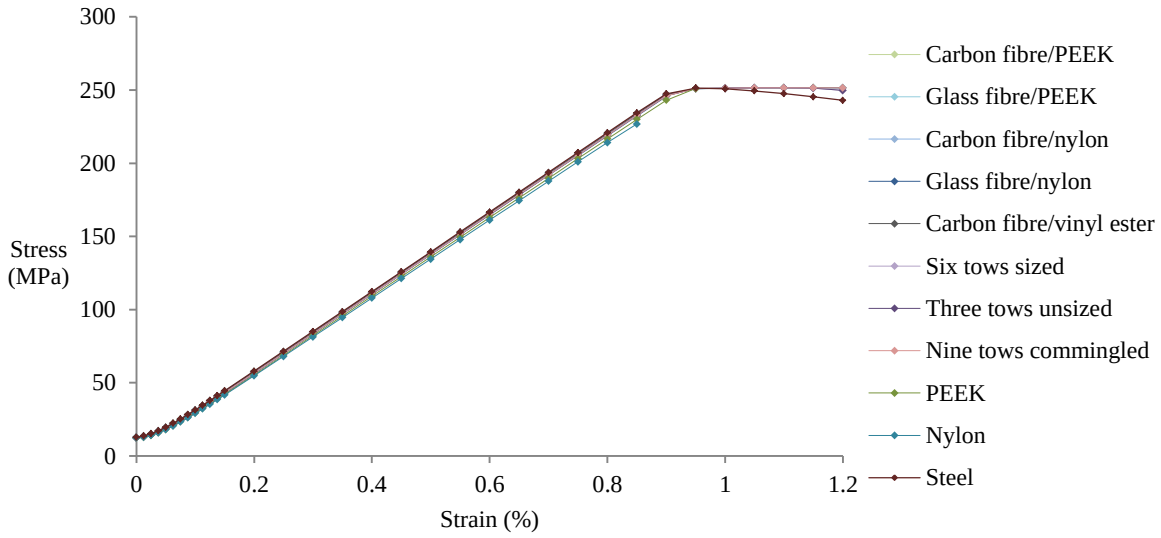

Figure 6.19 Stress-strain curves of one isolated outer wire.

6.5.2 Mechanical properties of hybrid strands

The tensile strength and stiffness of hybrid strands are directly related to the core material, which can be seen in Figure 6.20 and Figure 6.21. The Young's modulus and tensile strength were predicted for conventional steel strands, with respective values of 170.5GPa and 1809MPa. By contrast, the lowest properties were found for the hybrid strand a core of with unreinforced nylon, with Young's modulus of 138.5GPa and tensile strength of 1360.6MPa. Fibre reinforcement of the plastics clearly made a significant contribution to the tensile strength and stiffness of the strands, though the tensile strength of the hybrid strand with a core of unreinforced PEEK was significantly higher than that of unreinforced nylon.

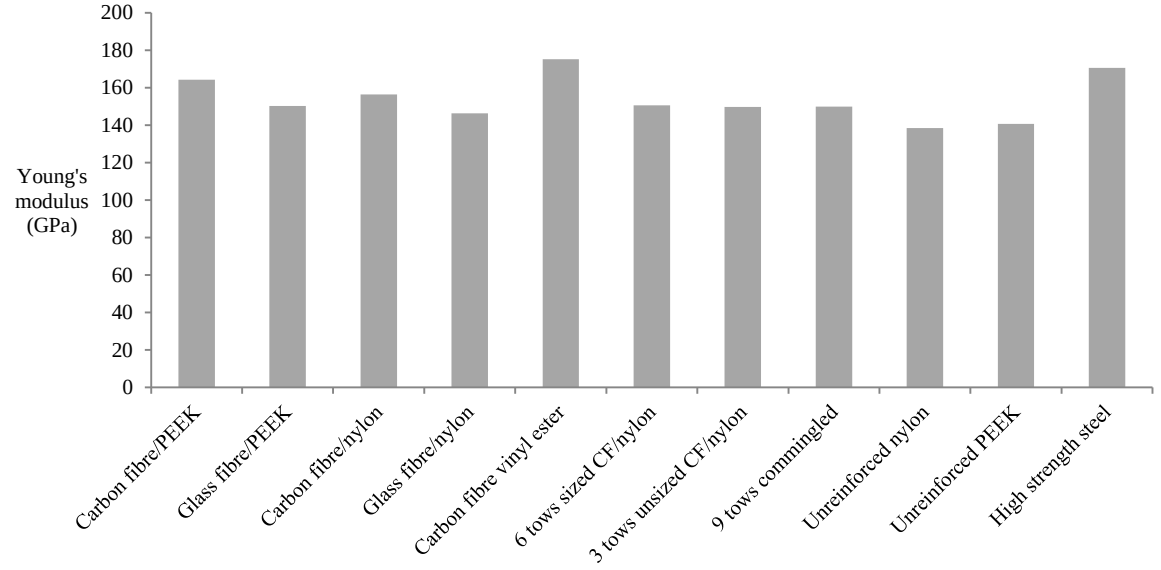

Figure 6.20 Stiffness of hybrid strand models.

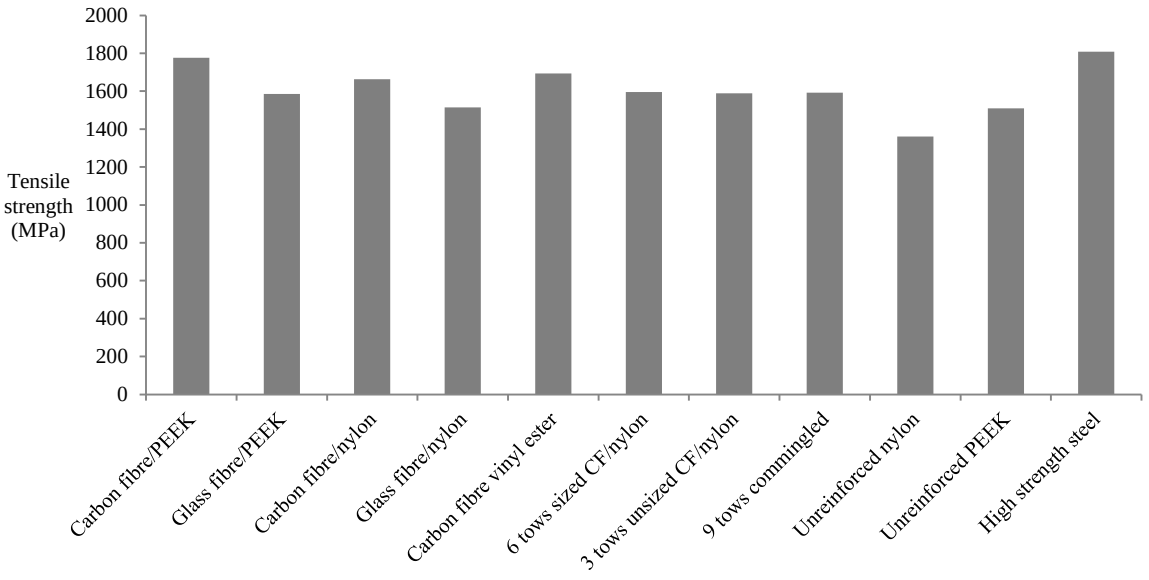

Figure 6.21 Tensile strength of hybrid strand models.

In their study of hybrid ropes with UHMWPE strands, Amils et al. used the parameter of tenacity, or 'breaking load per linear mass', to describe the weight-balanced performance of their hybrid ropes [17]. Tenacity was calculated for each strand by dividing the peak load of the strand by the sum of linear densities for each wire.

$$\text{Tenacity} = \frac{\text{Peak load}}{6(\text{Linear density}_{\text{outer wire}}) + \text{Linear density}_{\text{central wire}}} \quad \text{(eq. 7.4)}$$

As the steel outer wires were the majority contributors to the mass of the strand, this limited the maximum practical weight saving that could be made by replacing the steel central wires with FRP rods. As demonstrated in Figure 6.22, there was little overall change in the linear density of strands with different FRP rod cores. The greatest and least weight savings with respect to a strand with a steel central wire were 14.5% and 12.3%, achieved by replacement of steel wires with unreinforced nylon and glass fibre reinforced PEEK rods, respectively.

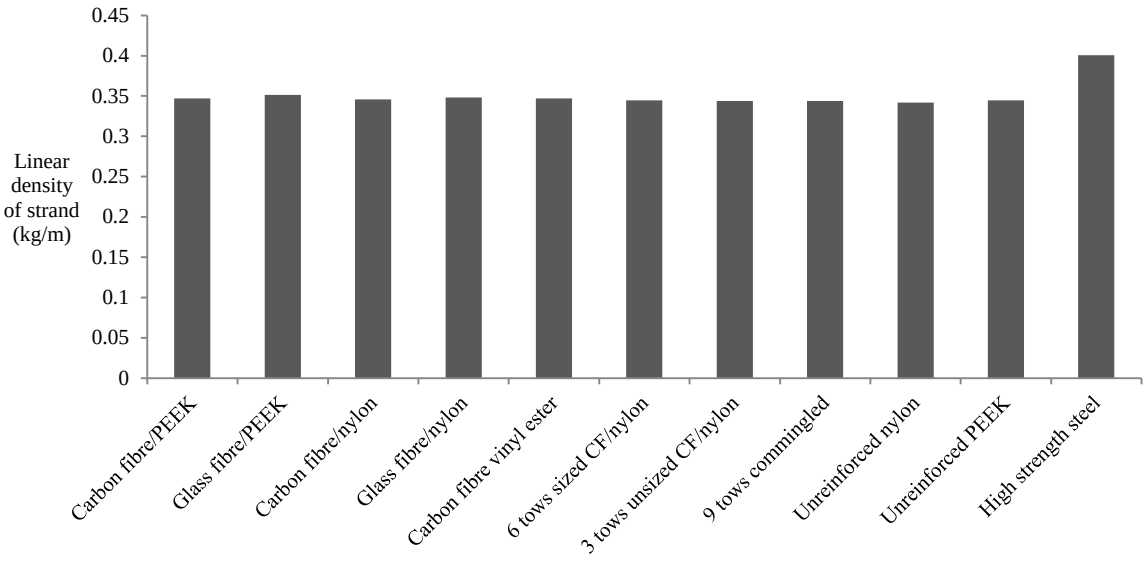

Figure 6.22 Linear density of hybrid strands.

As can be seen in Figure 6.23, only replacement of steel wires with carbon fibre reinforced plastics resulted in hybrid strands with higher tenacity than steel strands. Glass fibres have a relatively high density and thus their hybrid strands could not match the tenacity of a steel strand. Although the unreinforced nylon and PEEK plastics were the lightest, this could not offset their relatively low tensile strength, thus giving the lowest tenacity hybrid strands. Of the hybrid strands with carbon fibre reinforced plastic rods, those with pultruded carbon fibre/thermoplastic rods possessed only marginally higher tenacity than steel strands. The most significant increase in tenacity was found for FRPs from Carbon fibre/PEEK, Carbon fibre/nylon and Carbon fibre/vinyl ester.

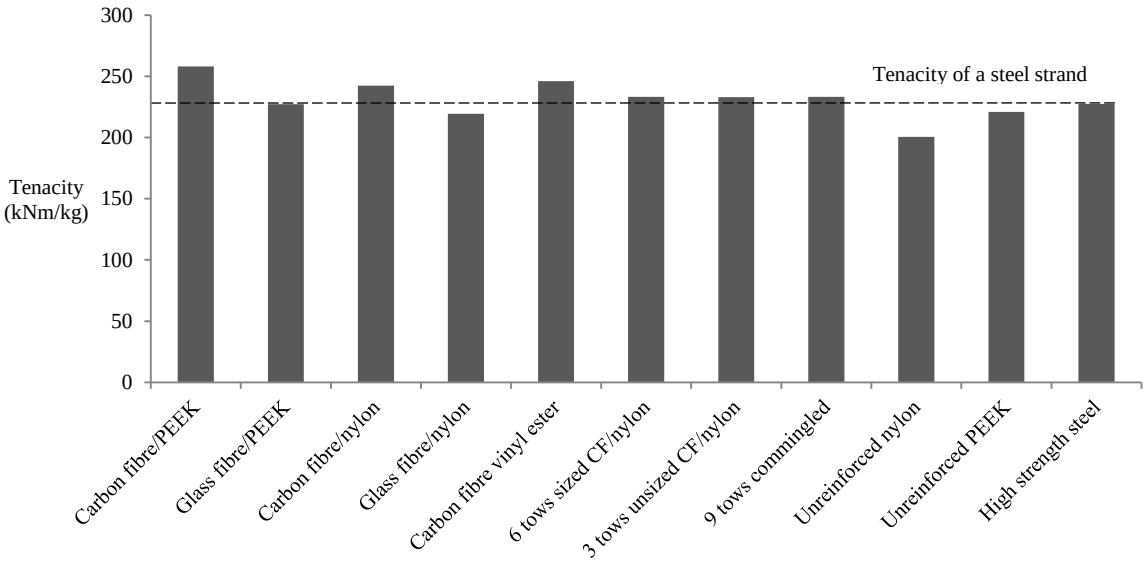

Figure 6.23 Tenacity of hybrid strand models.

6.5.3 Comparison of modelling and experimental results

Allowing for spread in the experimental data, there is strong agreement between mean experimental and predicted Young's modulus, shown in Figure 6.24. This is encouraging since it is an indication that the models were not unduly biased by phenomena such as shear-locking of elements or the over-constraining of boundary conditions that may lead to overestimation of stiffness [18].

However, although tensile strength was also in close agreement between the datasets, it was underestimated by approximately 7% for hybrid strands with carbon fibre/vinyl ester rods and 8.5% for steel strands, as found in Figure 6.25. Since these data were used for the calculation of tenacity, the tenacity for these models was underestimated by approximately 6% for hybrid strands with carbon fibre/vinyl ester rods and 9.5% for steel strands, while remaining in good agreement for the hybrid strands with carbon fibre/thermoplastic pultruded rods, as shown in Figure 6.26.

The consequence of this underestimation was that the model incorrectly predicted that all the hybrid strands with carbon fibre reinforced plastic central wires would exceed steel strands in tenacity, whereas this was not the case. However, the model did accurately predict that the Youngs modulus and tensile strength of hybrid strands with rods from 6 tows of carbon fibre/nylon and 9 tows of commingled tows would be similar. Thus the model was able to capture the modest load sharing with the outer steel wires that was discussed in §7.6; namely that there appears to be a threshold Young's modulus and tensile strength for the central rood above which strand hybridisation becomes effective. While not a complete validation, this gives some measure of optimism for the predictions made by the model for those materials that were not physically tested.

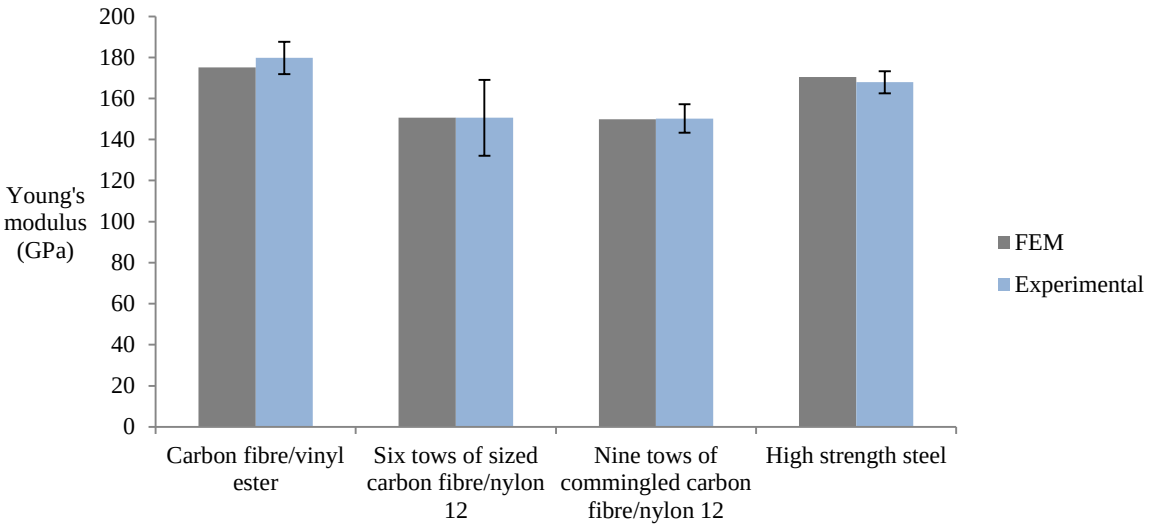

Figure 6.24 Comparison of the Young's modulus of hybrid and steel strands as determined by finite element modelling and tension experiments.

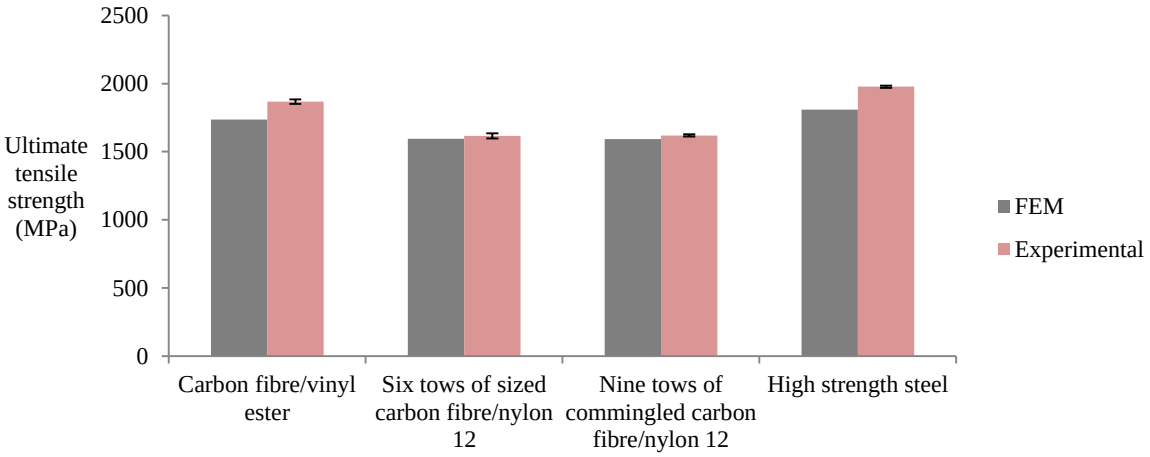

Figure 6.25 Comparison of the ultimate tensile strength of hybrid and steel strands as determined by finite element modelling and tension experiments.

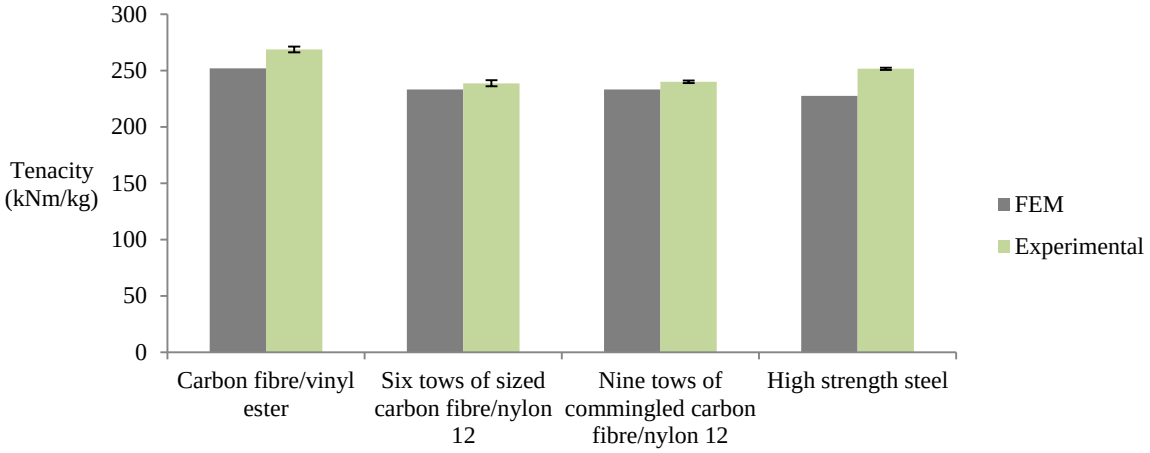

Figure 6.26 Comparison of the tenacity of hybrid and steel strands as determined by finite element modelling and tension experiments.

6.6 Limitations of the model

While it has been shown that the finite element model developed in this section was capable of predicting the Young's modulus and tensile strength of a hybrid strand, it was nonetheless limited in its capabilities. For instance, the model only represented a tensile test and gave no indication of out of plane properties such as bending, nor contact with external geometries that would be encountered if the strand were to run over a sheave or capstan. As it was run entirely using the Implicit solver of ABAQUS 6.10, it was wholly time independent. Therefore the models did not contain information for high speed events such as impact, long term behaviour such as cyclic loading or heating through frictional contact. Nor did the model predict behaviour after initial plasticity; there were no subroutines concerning element deletion or changes in the material model. Furthermore, the model only used isotropic material data so excluded the anisotropic behaviour of composite materials.

However, the greatest single limitation was arguably the build of the model. Each wire was represented by faceted surfaces that gave rise to discrete geometries, which were placed into

contact at the beginning of the model to ensure that surfaces did not interpenetrate. This was a necessary precaution to avoid complications with contact between helical structures but more recent software releases have improved contact algorithms that may be capable of reaching a converged solution with such curved geometries. While the techniques employed by this model did produce a converged solution without interpenetration of elements, they came at the price of invalidating the contact information generated at the touching surfaces. Because the facets were entirely unrepresentative of realistic areas of contact, the stresses that arose through contact were fictitious. Since the model gave no real indication of surface pressures it could not predict behaviour relating to friction or crushing between wires. An example of the visualised contact pressures is shown in Figure 6.27.

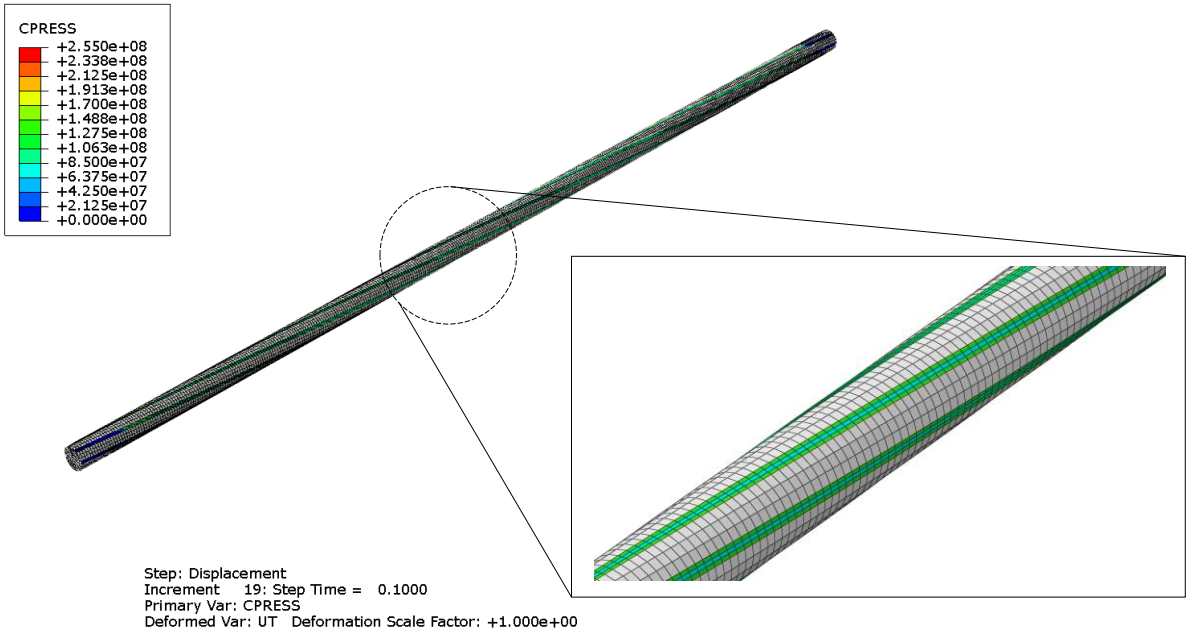

Figure 6.27 Contact pressures along faceted edges of the central wire in the model of a steel strand. This frame was taken at a strain of 0.5%. Contact pressure stated in the legend is given in units of Pa.

6.7 Concluding summary

A seven wire strand was modelled using the finite element method with ABAQUS 6.10. To build the model, cross-sectional geometries of the wires were exported to Hypermesh 9.0 and elements were individually defined in slices. These were then stacked and rotated to give helices with faceted edges, which were exported back to ABAQUS 6.10 and assembled together as a single strand. Boundary conditions representing the experimental procedure for tensile testing described in §4.5.1 were placed upon the ends of the strand, which included a twisting step before the strand was displaced axially. Displacement and load data were outputted from the nodes at either end of the strand during the displacement step to calculate stress-strain behaviour of the strand as it was pulled until its tensile strength was reached.

For modelling of hybrid strands, a high strength steel material model was consistently used for the outer wires and the core material was varied between different FRPs and unreinforced plastics. The strands underwent three distinct phases of deformation; relaxation of pre-stressing of the wires from the twisting step, a linear elastic period and then yielding that continued with perfect plastic behaviour. The Young's modulus and tensile strength of

strands was found to be highest in steel strands and hybrid strands with FRP core rods. Tenacity – a measure of breaking load divided by unit mass that is commonly applied to ropes – was compared for the different hybrid strands. Since the densities of FRPs are much lower than steel, the tenacity of hybrid strands was found to be higher than their absolute breaking strength suggested. Thus the models predicted that hybrid strands with the CFRPs explored in this investigation would surpass the tenacity of a purely steel strand.

A comparison was made between finite element models and the experimental results collected in §5.6 for steel and hybrid strands, including carbon fibre/vinyl ester and pultruded carbon fibre/nylon 12 rods, for the purpose of validation. This indicated general agreement between the model and experimental results, although the models underestimated the tensile strength of the steel and carbon fibre/vinyl ester hybrid strands by 7% and 8.5%, respectively. This translated to an underestimation of tenacity, which showed that the models had incorrectly predicted that hybrid strands with central rods from the in-house pultruded carbon fibre/nylon rods would exceed the tenacity of steel strands. However, the model was able to correctly identify the hybrid strands with carbon fibre/vinyl ester rods as having superior tenacity.

As shown by experimental validation, the models were able to demonstrate the effect of hybridisation on Young's modulus and tensile strength. This represents a new application of finite element modelling techniques to the simulation of ropes, which has thus far been limited to strands with steel wires. Modelling extended the focus of the project to materials outside of the scope of experimental characterisation. By comparing predictions of hybrid strands with a range of polymeric materials for the core rod, simulation validated the finding of the materials selection process and supported the hypothesis of CFRPs as a suitable reinforcement for hybrid ropes. While hybrid strands with the carbon fibre/nylon 12 pultruded rods were unable to match the tenacity of steel strands, they represent a lower limit of the Young's modulus and tensile strength required for an increase in tenacity. This suggests a specification for the strength and stiffness for future candidate materials in hybrid strands.

6.8 References

1. Bechtold, M. and A. Jeays. Calculation of modulus and torque of a 6x19 IWRC rope with a finite element model using beam elements. in Simulating rope applications. 2013. Oxford, OIPEEC
2. Jiang, W.-G., M.K. Warby, and J.L. Henshall, Statically indeterminate contacts in axially loaded wire strand. European Journal of Mechanics - A/Solids, 2008. 27(1), p. 69-78
3. Stanova, E., G. Fedorko, M. Fabian, and S. Kmet, Computer modelling of wire strands and ropes part II: Finite element-based applications. Advances in Engineering Software, 2011. 42(6), p. 322-331
4. Benndorf, H., Beiträge zur theorie der drahtseile. Zeitschr. d. öster-reichischen Ingenieur-u Architektenvereins, 1904. 56(30), p. 433-437
5. Feyrer, K., Wire Ropes: Tension, Endurance, Reliability. Illustrated ed. 2007, Berlin, Springer
6. Singala, K.J., A.A. Mungray, and A.K. Mungray, Degradation Behavior of Polypropylene–Organically Modified Clay Nanocomposites. Industrial & Engineering Chemistry Research, 2012. 51(32), p. 10557-10564

7. Pircheraghi, G., H. Nazockdast, and M.M. Salehi, Interfacial effects and microstructure development in the PP/PP-g-MA/ diamine-modified nanoclay nanocomposite. Micro & Nano Letters, IET, 2011. 6(8), p. 628-632
8. Erdönmez, C. and C.E. İmrak, Modeling and numerical analysis of the wire strand. Journal of Naval Science and Engineering, 2009. 5(1), p. 30-38
9. Erdönmez, C. and C.E. İmrak, Modeling Techniques of Nested Helical Structure Based Geometry for Numerical Analysis. Strojniski Vestnik-Journal of Mechanical Engineering, 2011. 57(4), p. 283-292
10. Soleimani, N., S.M. Khalili, R.E. Farsani, and Z.H. Nasab, Mechanical properties of nanoclay reinforced polypropylene composites at cryogenic temperature. Journal of Reinforced Plastics and Composites, 2012. 31(14), p. 967-976
11. Walton, J.M., Yeung, Y. C. T. Flexible tension members from composite materials. in International Offshore Mechanics and Arctic Engineering Symposium. 1987. American Society of Mechanical Engineers
12. TenCate. CETEX TC1200 PEEK Resin System. 22/11/2012: http://smartsite.tencate.com/TenCate/Aerospace_composites/documents/TCAC%20USA%20docs/TCAC%20USA%20Datasheets/DataSheet/TC1200_DS_Web.pdf
13. TenCate. CETEX TC910 nylon 6 Resin System. 21/09/2014: http://www.tencate.com/emea/Images/CETEX-TC910_DS_081213_Web28-25292.pdf
14. SolvayPlastics. KetaSpire KT-820FP. 21/09/2014: http://catalog.ides.com/datasheet.aspx?I=42041&FMT=PDF&E=111720
15. 3DSystems. Duraform PA Plastic. 21/09/2014: http://www.3dsystems.com/sites/www.3dsystems.com/files/DS_DuraForm_PA_US.pdf
16. De Baere, I., W. Van Paepegem, and J. Degrieck, On the design of end tabs for quasi-static and fatigue testing of fibre-reinforced composites. Polymer Composites, 2009. 30(4), p. 381-390
17. Amils, X., Durmus, B., Smeets, P., Boesten, J., Weis, J. Characteristics of steel hybrid ropes with UHMWPE fibre core and their applications. in Simulating rope applications. 2013. Oxford, OIPEEC
18. Liu, G.R. and S.S. Quek, 3 - Fundamentals for finite element method, in Finite Element Method, G.R. Liu and S.S. Quek, Editors. 2003, Butterworth-Heinemann Oxford. p. 35-66

7 Discussion

A discussion of the origin of the results in §5 is provided in this section. This section makes use of the abbreviations for rod types outlined in Table 5.1 in §5.

7.1 Optical microscopy

7.1.1 Morphology

Micrographs presented in §5.1, such as Figure 5.1 and Figure 5.7, show the presence of sized and unsized carbon fibre tows coiled within the cross-sections, with clearly separated fibre reinforced and unreinforced polymer regions. This suggests that the tows retained their shapes under the pressure of entering the die entrance. The visibility of individual tows suggests that the powder coating acted as a thick barrier that prevented them from intermingling with one another. This may indicate a trade-off between the quantity of the deposited powder and the even distribution of tows within a cross-section. Unsized tows appeared to form thicker and less sinuous shapes than sized tows, as seen in Figure 5.9, suggesting that the absence of the sizing allowed tows to respond with greater flexibility to pressure within the die. It might also suggest that unsized tows were less inhibited in their dispersion by thick coatings of intervening powder. Irregularity in the perimeter of the cross-sections also suggests that the powder did not completely fill the die cavity, which otherwise would have been circular. This may have been due to insufficient pressure at the die entrance to overcome the viscosity of the polymer and force out air from gaps in the powder. 9C featured some of the most severe outer edge distortions, as seen in Figure 5.13. As these rods were also manufactured with a higher powder deposition, it is clear that overloading with powder was a blunt means of filling out the cross-section and that it resulted in surface distortion.

These features contrast with those of EC, which has an even distribution of fibres. The cross-sections shown in Figure 5.15 have nearly perfectly circular perimeters and are largely free from voids. The pultrusion process for carbon fibre/thermoplastic rods clearly needs further optimisation in order to reach a similar level of cross-sectional regularity.

7.1.2 Fibre volume fraction and void content

As noted in §5.2, fibre volume fraction was not directly proportional to the number of filaments in the rods because the quantity of polymer also increased with the number of tows. High performance composites are expected to have fibre volume fractions in the region of 60% [1], which is almost 20% higher than the fibre volume fractions that were recorded in Figure 5.17. The large areas of unreinforced matrix discovered by optical microscopy are therefore unutilised as they could have contributed to higher strength and stiffness if they had been reinforced. As described in §3.3, an upper limit to the fibre volume fraction achievable in the pultrusion process was limited by the overloading of loose carbon fibres at the entrance of the heated die. In order to achieve higher volume fractions, the twin issues of fibre blockage of the die entrance and adequate filling of the die cavity need to be resolved.

Measurement of void content in rods produced from sized and unsized fibres was made imprecise by wide variation in the distribution of voids throughout individual rods. This meant that no statistically significant trends in void content can be deduced between rods

made from different numbers of tows. However, trends can be observed between material types; a lower void content was recorded for 9C than rods from sized or unsized fibres. This provides greater evidence that the commingled rods were better consolidated, although not as well as EC, which had a void content of 1.5%. Since voids are known to detrimentally compromise the strength of composites, as stated in §1.5.1, the void content of EC sets a target for future manufacturing. There is considerable room for improvement and the comparably low void content of 9C is a source of optimism for further progress.

7.1.3 Consequences for mechanical properties

A mixture of fibre reinforced and unreinforced regions within the cross-section represents a major departure from established practice for FRP technology. Although an unreinforced matrix is capable of transferring stress, it will do so unevenly and with a variation in load sharing between reinforced areas. Such nonlinearity in the stress-strain response of pultruded materials to applied load has been attributed to defects such as cracks and voids [2]. The reinforced areas themselves showed considerable variation in their content of large voids, which appeared as the darkest grey areas in the cross-sections. The prevalence of these flaws may explain the deviation from the expected linearity of tensile and flexural strength and stiffness with fibre volume fraction, as is discussed in §7.3 and §7.5.

As found by Weidmer and Manolesos, the flexural strength of a pultrusion can be expected to be reduced by defects in the internal structure [3]. Defects may therefore have contributed to the comparably high statistical variation observed in flexural strength, in which maximal stress is localised to a smaller region of a test specimen, as described in §4.7.1. Thus the particular microstructure, be it reinforced, unreinforced or defective, that finds itself in the concave or convex bend of the flexural test may have a dominant role in influencing observed properties.

7.2 Rod diameters

Variation in cross-sectional area is an important factor for quality control and is typically viewed as a strong indicator of article consistency [4]. Irregularity in the diameter of rods might represent inconsistencies in matrix consolidation or tangling of fibre discontinuities.

7.2.1 Variation in rod diameters

As shown by the results presented in Figure 5.19 in §5.3 , the standard deviation was greatest for rods from 9C at 0.12mm and otherwise not greater than 0.07mm for any other rod type. If a normal distribution were to be assumed, this would suggest that more than two thirds of samples have a dimensional tolerance better than ±0.1mm, or approximately 3% of the mean rod diameter.

9C stood out with a higher variance, quite likely due to the surface area of the commingled tows. In the case of rods pultruded from sized and unsized fibres, the total available surface area for powder spraying is higher than for commingled tows since powder can be deposited on both the top and bottom surfaces of a flattened tow. In each tow there are thousands of carbon filaments upon which powder particles can settle. Minor variations in the size of powder particles, powder flow rate, air pressure and filament distribution might be expected to even out better over a larger number of powder collection sites [5].

By contrast, the commingled tows acquired for this project were not intended for powder spray and their circular geometry presented a minimal surface area for powder deposition. This was evident in the need to modify the standard manufacturing conditions to allow for a greater powder flow rate, as described in §3.2.7. This resulted in powder being deposited in a flurry rather than in a fine coating by electrostatic attraction. Not only were the deposition sites restricted by the much smaller available surface area on the tows but the intermingled nylon filaments also served as an insulating material, which might have repelled incoming powder particles. Since there were only nine tows with a minimally exposed area of carbon fibres, variations in powder deposition were likely to have been higher than in the flattened sized and unsized tows, resulting in a somewhat higher dimensional variance. This may have also contributed to a greater number of defects along the length of the rod, as described in §3.2.6.

By contrast, the standard deviation in the mean diameter of the carbon fibre/epoxy rods was 0.01mm. This is almost an order of magnitude lower than the carbon fibre/thermoplastic pultruded rods, which may represent a target for future optimisation.

7.3 Flexural tests

As observed in Figure 5.21 in §5.4, a positive correlation was found between flexural stiffness and fibre volume fraction of rods produced from sized and unsized fibres. However, as shown by Figure 5.22, a correlation between flexural strength and fibre volume fraction was only observed for rods from unsized fibres. Although it was predicted in §4.7.1 that flexural strength and stiffness would be directly proportional to fibre volume fraction in a manner described by the rule of mixtures, only the flexural stiffness of unsized fibres followed such a trend. This suggests that additional factors influenced flexural properties, further evidence for which can be found in Figure 5.21 and Figure 5.22. These show that the flexural stiffness of 9C was similar to that of rods from sized and unsized fibres but the flexural strength of 9C was higher, while the flexural strength and stiffness of EC was higher than all of the carbon fibre/thermoplastic rods.

7.3.1 Influence of fibre sizing on flexural properties

As noted in §1.5.1, a proportional and linear correlation between flexural strength and fibre volume fraction, or general agreement with the rule of mixtures, is dependent on the assumption of complete bonding between filaments. This might have been a reasonable assumption for the impregnation of unsized fibres, which were hypothesised in §4.7.2 to show a greater disposition to interpenetration by the polymer matrix. However, it may not have been an accurate representation of the case for sized fibres, which were expected to be more tightly bundled. The adhesive sizing on the fibres that acts to hold together the tows may have also discouraged the interpenetration of molten polymer to join together fibres, as described in §3.1.1. Above a certain fibre loading, apparently occurring above 4 tows, the density of regions that could not be easily penetrated by the polymer may have become increasingly detrimental to consolidation of fibre-rich areas. Rather than reinforcing the composite, these poorly consolidated areas may have promoted inadequate load sharing between fibres. As discussed in §7.1.3, flexural strength is influenced by the presence of microstructural defects. The negative effect of sizing in preventing consolidation of the thermoplastic matrix may therefore explain the absence of a correlation between the flexural strength of rods with sized fibres and fibre volume fraction.

7.3.2 Flexural strength of rods from commingled tows

Rods from commingled tows recorded a similar flexural stiffness to rods produced from sized and unsized fibres and a higher flexural strength. Since the tensile strength and stiffness of stretch-broken carbon fibres were predicted in §4.7.1 to be lower than those of longitudinal fibres, the flexural strength and stiffness of 9C might have been expected to have been lower than those from sized or unsized fibres. However, as discussed in §7.1.2, consolidation of the fibres and polymer in 9C was better than that of other carbon fibre/thermoplastic rods. As discussed in §7.1.3, microstructural defects such as voids promote stress concentrations that reduce flexural strength, which may explain why 9C had comparably higher flexural strength than other carbon fibre/thermoplastic rods but not higher flexural stiffness.

The highest flexural strength and stiffness was recorded for EC. While these rods recorded a higher fibre volume fraction, they were also better consolidated with the lowest void content, as shown in Figure 5.18 in §5.2. Similarly to 9C, the difference in flexural strength of EC in comparison to rods from sized and unsized fibres is much greater than the difference in flexural stiffness. These trends suggest that void content and degree of consolidation were highly influential factors in determining the flexural strength of the rods.

7.4 Relationship of flexural properties and rod diameters with line speed

As shown in §5.3, correlations were not observed between the diameter, flexural strength or stiffness of rods and line speed. This is contrary to the findings of several studies in which optimal mechanical properties transpired within specific ranges of line speeds. For instance, Nunes found that a maximal balance between the strength and stiffness of pultrusions manufactured from powder sprayed towpregs occurred within a range of line speeds between 100cm/min and 120cm/min [6]. Chen and Ma also found that optimal line speed depended on the temperature of the die. They concluded that lower line speeds were conducive to better consolidation, provided that the temperature and residence time of a given section of the rod within the die were not high enough to cause degradation of the polymer [7].

The range of line speeds available to those studies was far above that available to this project, which was limited to line speeds between 3cm/min and 9cm/min. This limitation arose from the power of the motor, which required a high gear ratio in order to sustain a large enough torque to pull the tows through the die. This study was therefore unable to discern an underlying relationship between mechanical properties and line speed due to constraints in the scope of its methodology.

7.5 Tensile tests

7.5.1 Young's modulus and tensile strength

A positive correlation was found between Young's modulus and tensile strength and fibre volume fraction for rods produced from sized and unsized fibres, as seen in Figure 5.25 in §5.5.1. This is in contrast with the trends for flexural properties, which were only observed for rods from unsized fibres. The discussion in §7.3.1 concluded that poor consolidation had a dominant influence on flexural strength and was most likely responsible for the absence of a correlation between the flexural strength of rods produced from sized fibres with fibre volume fraction.

As noted in §4.7.1, stress is concentrated into a smaller region of a body in flexion than in tension, which as discussed in §7.3.1 may contribute to greater variability in flexural strength. In addition, microstructural defects such as voids should affect matrix-dependent properties such as bending more than fibre-dependent properties such as tension [8]. These factors suggest that flexural strength and stiffness may be more heavily influenced by poor consolidation than Young's modulus and tensile strength. This is in agreement with observed deterioration of flexural strength and stiffness of pultrusions due to high void content [9].

Nonetheless, tensile strength was affected by voids and poor consolidation of fibres and resin. As was observed with flexural strength and stiffness, 9C was shown to have similar Young's modulus and higher tensile strength than other carbon fibre/thermoplastic rods, while the highest tensile strength was recorded for EC. Tensile strength was therefore related to void content, as shown in Figure 5.17 in §5.2, as well as the degree to which rods were well consolidated, as demonstrated in the micrographs in §5.1.

7.5.2 Strain-to-break and strain energy

The strain-to-break of rods produced from sized and unsized carbon fibres appeared to be inversely proportional to fibre volume fraction and therefore to Young's modulus and tensile strength. A greater number of tows may have reduced extensibility by increasing the number of poorly consolidated fibre-rich regions that would have contributed to crack propagation and tensile failure.

Strain-to-break was similar for 9C and EC, suggesting that good consolidation contributed to better extensibility in both materials. Thus, the hypothesis in §4.7.1 was accurate but imprecise; it was presumed that commingled tows would give rise to better extensibility because of their stretch-broken fibres, whereas their extensibility appears to have been more closely related to their better consolidation. Were it not so, EC (that did not have stretch-broken fibres) would not also have recorded such a high strain-to-break.

It was also hypothesised that 9C would attain greater strain energy on account of their superior flexibility and the more numerous degrees of freedom afforded by their stretch-broken fibres. This was also found to be true but the strain energy of EC surpassed 9C in this capacity. As seen by a comparison of Figure B. 28 and Figure B. 27 in Appendix B, which respectively show stress-strain curves for EC and 9C, the dominant contributor to strain energy was higher stiffness. This occurred by virtue of attaining higher stress values; in the absence of multiple damage events before ultimate failure this gave rise to a larger area under the curve. The relationship between damage events and strain energy is well established in damage models of pultruded rods, such as that developed by Kilic and Haj-Ali [10, 11].

Strain energy is also a quantifier of the difference between the lowest stress at which damage events occurred and ultimate tensile strength. In tension, well-consolidated FRPs are expected to experience a period of continuously linear-elastic behaviour followed by an abrupt catastrophic failure. As a result, stress-strain curves have a triangular area, as shown in Figure 1.6 in §1.4.1. Damage events give rise to a saw-tooth pattern and every fracture reduces the area under the curve, thereby resulting in lower strain energy, as calculated using the methodology in §4.4.2. Examples of this can be seen in stress-strain curves for rods produced from sized and unsized fibres, for instance for 6S and 4U in Figure B. 23 and Figure B. 26, respectively. These curves feature a greater number of damage events than those of EC in Figure B. 28, further demonstrating poorer consolidation in the carbon

fibre/thermoplastic pultruded rods. Thus strain energy was found to be inversely proportional to void content and the degree to which the matrix was well consolidated.

7.6 Hybrid strand tensile tests

The inferior Young's modulus and tensile strength of 6S and 9C in comparison with VE were reflected in their lower contribution to the Young's modulus and tensile strength of the hybrid strands, as shown in Figure 5.29 and Figure 5.30 in §5.6. Despite differences in the Young's modulus and tensile strength of 6S and 9C, as shown in Figure 5.25 and Figure 5.26, the measured differences between hybrid strands with these rods were statistically negligible. This may suggest that below a certain threshold of Young's modulus and tensile strength the central rod acts more like a filling agent rather than a reinforcing material and does not fully contribute to stress transfer. However, as the hybrid strands with 6S recorded a much higher strain-to-break, it is possible that the poor consolidation of these rods may have unintentionally enhanced the hybrid strands by permitting a greater strain-to-break before ultimate failure. This is observable in the multiple damage events shown for stress-strain curves of hybrid strands with 6S, as shown in Figure 5.32 and Figure 5.33.

Although Young's modulus and tensile strength noticeably deteriorated by hybridisation with the carbon fibre/thermoplastic rods, the tenacity of the hybrid strands was only lower by approximately 5%. The consolidation and void content of these rods was much poorer than that of VE; consequently the density of these rods was also much lower, at 1.32g/cm^3 for 6S and 1.22g/cm^3 for 9C. Since unreinforced nylon 12 has a density of approximately 1.00g/cm^3, these pultruded rods are likely to fall within a lower bound of the density of a conceivable structural FRP material. This suggests that a material of similarly low density must be stronger than these rods in order to surpass the tenacity of a steel strand and thus be a viable candidate for replacing the central steel wire in a hybrid strand. It also validates a finding of the materials selection study in §1.7.1 of carbon fibre as a suitable reinforcement.

Since there was only a small difference between the tensile strength of steel strands and hybrid strands with VE, the benefit of hybrid strands only became markedly apparent in measurement of tenacity, which took into account the density of the respective core materials. As the FRPs had much lower densities than steel, the tenacity of hybrid strands with VE was superior to that of the steel strands.

This finding demonstrates the applicability of carbon fibre reinforced plastics to enhancing the tenacity of steel wire ropes. Importantly, it was found that replacing the steel central wire with a FRP rod provided an increase to the Young's modulus and did not lower the ultimate tensile strength of the strand to a significant degree. However, the strain-to-break was lowered considerably, implying a restriction on the extensibility of the strand.

The results concur with a previous study by Amil, et al. that demonstrated superior tenacity for a hybrid steel and polymer rope [12]. However, the effect of hybridisation has not previously been investigated on the level of a strand. Since strands are smaller assemblies of carriers, a direct comparison cannot be made with datasets collected for ropes. In addition to establishing the feasibility of replacement of steel wires with FRP cores, the results shown in §5.6 represent a new contribution to the understanding of hybridisation in strands.

7.7 Finite element modelling of a hybrid FRP and steel strand

General agreement was found between experimental results of the tensile strength and stiffness of hybrid strands with the predictions made by finite element modelling. Despite a slight underestimation in the tensile strength of steel strands, the model was still validated with respect to the prediction of superior tenacity for hybrid strands with carbon fibre/vinyl rods. Simulation of tension in hybrid strands with a range of FRP core materials that were outside of the experimental scope of the investigation demonstrated that improved tenacity was only possible by hybridisation with CFRP cores. Taken together, these findings validated the material selection process and support the aims of the investigation, as stated in §1.3.

Despite the limitation of being unable to predict contact stresses, as outlined in §6.6, the model has been shown to provide valuable predictions for tensile strength and stiffness. As described in §1.10, the simulation of tenacity in hybrid strands represents a new contribution to the finite element modelling of ropes, which has previously been limited to steel wires.

7.8 Summary of discussion

This section summarises the discussion of experimental findings that were presented in §5 and finite element modelling predictions that can be found in §6.

7.8.1 Morphology from optical microscopy and rod diameters

- Sized and unsized tows appeared as distinct bodies, indicating that they did not spread out within the volume of the rod under the pressure of the die. The large separation between individual tows also suggests that powder deposition presented a barrier to fibre dispersion. Unsized tows appeared thicker and less sinuous, suggesting better intermingling of fibres with the polymer matrix than for sized tows.
- Fibre volume fraction was not directly proportional to fibre loading because powder deposition also increased with the number of filaments. Blocking of the die entrance and inadequate filling of the die cavity due to poor consolidation posed an upper limit to the achievable fibre volume fraction.
- Lower void content was found for rods with commingled tows rather than sized or unsized fibres. This validates the assumption that intermingling of reinforcing and matrix fibres would give better consolidation of the rods. The lowest void content of 1.5% was observed for the carbon fibre/epoxy rods, which represents a target for future optimisation.
- Micrographs revealed large regions of unreinforced polymer as well as fibre-rich regions in carbon fibre/thermoplastic pultrusions. In addition to the appearance of large voids, this indicates poor consolidation of the matrix.
- Irregularity of the surface of the rods and variation in rod diameters indicated that the matrix did not adequately fill out the die cavity. Commingled rods showed particularly high variance in rod diameter, which was caused by relatively low surface area of the circular tows. By comparison, sized and unsized tows were flattened and were more tolerant of variations in powder deposition.
- Correlation of cross-sectional features with feedstock types and manufacturing processes has highlighted the relative importance of manufacturing technologies. In particular, the higher void content and suboptimal distribution of fibres and polymer within the cross-sections of rods pultruded with dry fibres can be related to challenges encountered during the manufacturing process. This has informed the value of the experience gained during

article productivity. While the optimisation of powder impregnation techniques is well reported, as described in §2.4, the importance of fibre spreading appears to have been underrepresented in publications.

7.8.2 Flexural properties of rods

- The flexural strength of rods with sized fibres did not correlate with fibre volume fraction, whereas it did for unsized fibres. The adhesive sizing on the tows may have reduced interpenetration of polymer with the sized fibres, leading to poorly consolidated fibre-rich regions within the rod. A greater number of tows may therefore have increased the density of fibre-rich regions, which would have resulted in microstructural defects such as voids.
- Despite the hypothesis that stretch-broken fibres would give rise to lower strength and stiffness, rods produced with commingled tows possessed higher flexural strength than those with sized or unsized fibres. This matches previous evidence from micrographs of better consolidation for rods with commingled tows. Since rods are subjected to greater localised stresses in flexion than tension, void content and the degree to which the matrix was well consolidated were found to be factors that highly influenced flexural strength. These findings agree with previous studies that have correlated lower flexural strength with microstructural defects.
- The range of line speeds available to the pultruder was too low for there to be an observable variation in flexural strength and stiffness with line speed.

7.8.3 Tensile properties of rods

- Novel end tabs permitted even load sharing across the circular surface of the rods during tensile testing of rods and prevented slipping of the coupons.
- In contrast to flexural results, a positive correlation was found between Young's modulus and tensile strength of carbon fibre/thermoplastic rods with fibre volume fraction. This suggests that poor consolidation was less influential on measured tensile properties.
- The tensile strength of rods produced from commingled tows was greater than those produced from sized and unsized fibres, while Young's modulus was similar. This is further confirmation that stress concentration in poorly consolidated regions contributed to lower flexural strength of rods produced from sized fibres.
- Strain-to-break was similar for carbon fibre/epoxy rods and those produced from commingled tows. It was lower in rods produced from sized and unsized fibres. Additionally, strain-to-break was inversely proportional to fibre volume fraction in rods produced from sized and unsized fibres, suggesting that extensibility was lower for higher densities of microstructural defects such as voids. This demonstrated that the expected flexibility afforded by stretch-broken carbon fibres had less influence on extensibility than void content and consolidation of the polymer matrix.
- Strain energy provided a means of quantifying the effect of the numerous damage events that occurred in tensile tests of rods produced from sized and unsized fibres before ultimate failure. These events arose from poor consolidation of the polymer matrix and appeared as sudden drops in stress which served to lower the area under stress-strain curves. Consequently strain energy was considerably higher in rods produced from commingled tows and carbon fibre/epoxy rods.

7.8.4 Tensile properties and tenacity of hybrid strands

- A novel methodology was developed for the preparation and tensile testing of hybrid strands. A technique for the internal adhesion of wires within the gripped length of the strands was successful in preventing slip during the test.
- Replacement of the central steel wire with carbon fibre/thermoplastic pultrusions in hybrid strands was not shown to increase the Young's modulus or tensile strength. However, hybrid strands with carbon fibre/vinyl ester rods had higher Young's modulus and slightly lower tensile strength than steel strands but both these properties were higher than for other hybrid strands. This suggests that below a certain threshold of strength and stiffness the FRP rod acts more like a filling material rather a reinforcing material.
- Despite having a lower tensile strength, the tenacity of hybrid strands with carbon fibre/thermoplastic rods was only slightly lower than steel strands, on account of relatively low density. This suggests that the in-house pultruded rods represent a lower bound of strength and density for a material to be a viable replacement for steel in a hybrid strand.
- The tenacity of hybrid strands with carbon fibre/vinyl ester rods exceeded that of steel strands. This finding validates the materials selection process in identifying carbon fibre as a suitable and thereby validates the central project aim of improving the strength-to-weight ratio of steel strands by hybridisation with CFRPs. These findings represent a novel dataset for the tensile strength and stiffness of hybrid steel and FRP strands.

7.8.5 Finite element modelling of hybrid strands

- Finite element modelling successfully predicted higher tenacity for hybrid strands with carbon fibre/vinyl rods with respect to steel strands.
- Simulation of hybrid strands with a range of polymeric materials outside of the experimental scope of the project validated the material selection process by highlighting the unique increase in tenacity achievable with CFRPs.
- Simulation of ropes has thus far been limited to steel wires. This study therefore represents a novel contribution to the understanding of finite element modelling of hybrid strands.

7.9 References

1. Mazumdar, S.K., Manufacturing Techniques, in Composites Manufacturing, S.K. Mazumdar, Editor. 2001, CRC Press
2. Kilic, H. and R. Haj-Ali, Elastic-degrading analysis of pultruded composite structures. Composite Structures, 2003. 60(1), p. 43-55
3. Wiedmer, S. and M. Manolesos, An Experimental Study of the Pultrusion of Carbon Fiber-Polyamide 12 Yarn. Journal of Thermoplastic Composite Materials, 2006. 19(1), p. 97-112
4. Starr, T.F., Pultrusion for engineers. 2000, Cambridge, Woodhead Publishing
5. Zaniboni, C., Oligomere technologies for cost-effective processing of high performance composites lightweight structures, in Department of Mechanical and Process Engineering. 2010, Swiss Federal Institute of Technology Zurich: Zurich. p. 186
6. Guo, Z. and B. Hagström, Preparation of polypropylene/nanoclay composite fibers. Polymer Engineering & Science, 2013. 53(10), p. 2035-2044

7. Chen, C.-H. and C.-C.M. Ma, Pultruded fibre reinforced polyurethane composites II. Effect of processing parameters on mechanical and thermal properties. Composites Science and Technology, 1992. 45(4), p. 345-352
8. Zhu, H., B. Wu, D. Li, D. Zhang, and Y. Chen, Influence of Voids on the Tensile Performance of Carbon/epoxy Fabric Laminates. Journal of Materials Science & Technology, 2011. 27(1), p. 69-73
9. Haj-Ali, R. and H. Kilic, Nonlinear constitutive models for pultruded FRP composites. Mechanics of Materials, 2003. 35(8), p. 791-801
10. Haj-Ali, R. and H. Kilic, Nonlinear behavior of pultruded FRP composites. Composites Part B: Engineering, 2002. 33(3), p. 173-191
11. Kilic, H. and R. Haj-Ali, Progressive damage and nonlinear analysis of pultruded composite structures. Composites Part B: Engineering, 2003. 34(3), p. 235-250
12. Amils, X., Durmus, B., Smeets, P., Boesten, J., Weis, J. Characteristics of steel hybrid ropes with UHMWPE fibre core and their applications. in Simulating rope applications. 2013. Oxford, OIPEEC

8 Conclusions and suggestions for future work

The concept of hybridisation of steel wires with fibre reinforced plastics has been realised as a means of increasing the strength-to-weight ratio a steel wire strand. A pultrusion line was designed, constructed and developed in order to manufacture carbon fibre/thermoplastic rods suitable for replacing central steel wires. The process of manufacturing optimisation revealed the importance of overcoming technological challenges that are underrepresented in publications, such as the role played by fibre spreading. Hybrid strands were produced by replacing central steel wires with pultruded rods and were tested with a novel methodology that included internal joining of the gripped ends of the strands to prevent slipping. Results showed that the tenacity of hybrid strands with carbon fibre/vinyl central rods exceeded that of steel strands. This finding validated the central hypothesis of the project and demonstrated the feasibility of replacing central steel wires with non-metallic rods. Tensile strength and stiffness were compared with predictions made from finite element models of hybrid strands with a range of core materials. Of the material types simulated, only the tenacity hybrid strands with CFRP rods was higher than that of steel strands, which validated the material selection.

8.1 Concluding remarks on pultrusion

Design and construction of the pultruder was done without the aid of industrial consultation, leading to independent verification of some of the challenges facing practical manufacture:

- The importance of fibre spreading in increasing the available surface area of tows for powder impregnation was underrepresented in journal publications. For this project, a pragmatic rather than sophisticated design using a single pinch roller was found to be the most effective.
- Electrostatic spray needed a high degree of optimisation to be effective. Unfortunately the particular powder spray model used in the project was unable to finely control fibre volume fraction. An advantage of this technology is the wide range of thermoplastic blends and formulations that can be processed but this was found to be outside of the project scope.
- The heating strategy was driven by cost saving measures as more appropriate equipment, such as band heaters that precisely fit the outside of a split die, were prohibitively expensive. Use of heating strips was time consuming but highly cost effective.
- The importance of optimising pre-heating was only discovered after many trials, which illustrated the difficulty of identifying the origin of a problem when many processes were simultaneously under development. Before the temperature of pre-heating was fully optimised, fibre seizing at the die entrance was assumed to be purely dependent on fibre discontinuities rather than softening of the powder.
- Due to a lack of available space in which techniques for cooling the rods could be developed, this process remained the least understood part of the pultruder. Water cooling from a water pipe was found to be adequate in quenching the rods so that they could be pulled by the traction puller but did not allow control of the rate of cooling.
- Caterpillar treads were successful in evenly distributing the compressive loads applied by the traction puller across the rods; there no evidence of crushing of the pultruded rods was encountered.

Some of the challenges in using the pultruder were specific to the format of the materials:

- Recycling of powder was time consuming and future improvements might include automation of this process. Although handling of the powder was onerous, it was not as hazardous as molten resin and did not present safety challenges during its use. In this regard it was well suited to use in a laboratory environment.
- The machine was only partly automated and had to be continually checked for die blockages and snarling of fibres. Manual extraction of excess resin depended on operator skill. Although this became adequate through practice, it was not possible to correct the underlying causes within the scope of the project.
- Commingled tows needed the deposition of additional powder to fill the die cavity. The cross-sectional distribution of fibres and matrix would have been more uniform had the filaments been divided into a larger number of flattened tows.
- Fibre sizing was an important factor in determining matrix impregnation of the tows. In the case of tows with sizing, it was shown to inhibit the degree to which the fibres were well consolidated by the matrix but unsized tows were more susceptible to fibre misalignment and tangling at the die entrance. Optimisation of fibre treatment was outside of the scope of the project.

8.2 Pultruded rod characterisation

Characterisation of pultruded rods revealed that poor article quality arose from inadequate consolidation of the polymer matrix. The prevalence of microstructural defects such as voids and fibre-rich regions was especially high in rods produced from sized fibres. Fibre dispersion and matrix consolidation appeared to be more uniform in rods produced from commingled tows, which consequently recorded lower void content.

- Optical micrographs revealed large areas of unreinforced polymer matrix and poorly consolidated fibre-rich regions of carbon fibre/thermoplastic pultruded rods. Tows were least well dispersed in rods produced from sized fibres, while the best consolidation was observed for those with commingled tows, which also featured lower void content. Fibre volume fraction was not directly proportional to the number of filaments since the deposition of the powder increased with the number of tows, resulting in larger rod diameters for rods with a higher number of filaments. The consolidation of the matrix, fibre volume fraction and void content were superior for a control group of commercially sourced carbon fibre/epoxy rods.
- No correlation was found between flexural strength and fibre volume fraction for the least well consolidated rods produced from sized fibres. These rods were negatively affected by microstructural defects, which appeared to increase in density in rods with a larger number of filaments. Flexural strength was higher for the better consolidated rods with commingled tows, despite the lower predicted strength rods with stretch-broken fibres. This suggests that flexural strength was heavily influenced by poor matrix consolidation and microstructural defects such as voids.
- The tensile strength of rods with commingled tows was greater than that of rods with sized and unsized, while Young's modulus was comparable, suggesting that poor consolidation nonetheless reduced tensile strength. However, a stronger correlation was observed between Young's modulus and tensile strength with fibre volume fraction than for flexural strength and stiffness for all pultruded rods. This suggests that the fibre-dominated tensile strength of the rods was less negatively affected by poor consolidation of the matrix than flexural strength.
- Strain-to-break was similar for carbon fibre/epoxy rods and those produced from commingled tows and was lower in rods produced from sized and unsized fibres. This

demonstrated that the expected flexibility afforded by stretch-broken carbon fibres had less influence on extensibility than void content and consolidation of the polymer matrix.

- Rods produced from sized and unsized fibres experienced progressive damage events before reaching ultimate tensile strength. These damage events are related to stress concentration and inadequate load sharing between poorly consolidated regions within the polymer matrix. Consequently, strain energy was higher in rods produced from commingled tows and the control group of carbon fibre/epoxy rods.

8.3 Hybrid strand experiments and finite element modelling

Hybrid strands were prepared with a novel technique in which the central steel wires were replaced with FRP rods and internally terminated with an epoxy adhesive. A comparison between tensile tests conducted on these hybrid strands with steel strands revealed higher Young's modulus and tenacity among the best performing hybrid strands.

- The Young's modulus and tensile strength of steel strands were higher than those of hybrid strands with carbon fibre/thermoplastic rods. Due to the low density of the FRP rods, the tenacity of these hybrid strands was only marginally lower than the steel strands. These rods therefore represent a lower bound of material properties necessary for the viable replacement for steel in a hybrid strand.
- The Young's modulus and tenacity of hybrid strands with carbon fibre/vinyl ester rods exceeded that of steel strands. This finding demonstrates that the strength-to-weight ratio of steel strands can be improved by replacing the central wire with a CFRP rod. This validates the hypothesis that the tenacity of steel strands can be increased by hybridisation with CFRP core rods. It also constitutes new understanding in the role played by non-metallic carriers in the cross-section of a strand.

Finite element models representing the steel and hybrid strands tested in this investigation were meshed in Hypermesh 9.0 and analysed using ABAQUS 6.10. Numerical analyses predicted improvements in the tenacity of hybrid strands with high performance CFRPs such as carbon fibre/PEEK, whereas glass fibre reinforced and unreinforced plastics are unable to contribute to higher tensile strength and stiffness.

- In order to overcome interpenetration of solid elements, a strand geometry with faceted contact between wires was created in ABAQUS 6.10 and exported to Hypermesh 9.0 for meshing. Boundary conditions and kinematic constraints were applied to the model representing those encountered in the experimental method for tensile testing of strands. The model included individual steps for simulating the pre-stressing experienced by winding of the strand and simulation of the tensile test.
- Analysis indicated that models experienced three distinct phases of deformation; relaxation of pre-stressing of the wires from the winding step, a linear elastic period and then tensile failure. Young's modulus and tensile strength were found to be highest in steel strands and hybrid strands with carbon fibre/PEEK rods.
- A comparison of simulated and experimental results showed a slight overestimation of tensile strength. This led to an incorrect prediction that hybrid strands with the in-house pultruded carbon fibre/nylon 12 rods would have similar tenacity to that of steel strands. However, the model accurately predicted that the Young's modulus and tenacity of hybrid strands with carbon fibre/vinyl ester rods would exceed those of steel hybrid strands. In addition, the model predicted that the Young's modulus and tensile strength of hybrid strands with glass fibre reinforced and unreinforced plastic rods would be lower than those of steel strands.

- This investigation validated the materials selection study, which identified the suitability of carbon fibre reinforced plastics over other core materials. It also expands understanding of finite element modelling for rope applications, which were previously limited to steel strands without FRP central rods.

8.4 Future work

Operation of the pultrusion line was not a streamlined process and was developed largely by trial and error. Many of the technical issues were therefore related to scalability and already have industrial solutions. However, the specifications for a flexible pilot line intended for research and development differ from those of an industrial manufacturing process. The custom building of equipment presented infrastructural challenges that might have been overcome by the wholesale purchase of a functioning pultrusion line, were the project scope to allow it. Nonetheless, the solutions found in developing processes for the laboratory scale pultruder are of particular relevance to the modularity and flexibility required for manufacturing research. This would prove valuable experience for future research and development of pultrusion facilities, especially in highlighting manufacturing challenges that are not well emphasised in commonly accessible publications.

- Apparatus for effective fibre spreading requires a larger space than was available for this project. Since commingled tows were circular and therefore less adequate for powder deposition than the flattened sized and unsized tows, further investigation into optimal formats of carbon fibre tows may improve fibre distribution in rods.
- Although electrostatic spraying of powder was found to be a suitable means of impregnating reinforcing fibres, the equipment used in this project was not designed for this application. A powder spray gun with finer control of air flow and rate of deposition would have permitted greater control of fibre volume fraction. An unused feature of this technology was the large variety of thermoplastics and powder blends that can be processed. Future work could include a study into the comparative opportunities of processing with different polymer matrices and a comparison of the mechanical properties of different carbon fibre reinforced thermoplastics.
- Though cost effective, heating strips needed to be mounted onto the heating die for each operation of the pultruder. A redesigned die block would benefit from customised cartridge heaters mounted into the body of the die halves for greater operational efficiency. In addition, reduced variability in temperature fluctuation would have been possible with more advanced temperature controllers that permit adjustment of PID variables.
- More space would have permitted the development of a more sophisticated method of cooling and would have allowed control of the crystallinity of the thermoplastic matrix. As determined in §3.2.2, the percentage crystallinity of the polymer matrix in rods processed at standard manufacturing conditions was approximately 23.9%, compared with 43.4% for the unprocessed powder. This was shown to result in the stiffness of the polymer matrix being approximately half of that of the unprocessed powder. Thermoplastic crystallinity has been shown to affect matrix-dominated properties such as impact resistance. However, the performance of hybrid strands was evaluated by measurement of Young's modulus and tensile strength, which are fibre-dominated properties. From a rule of mixtures estimation it can be seen that the contributions to FRP tensile strength and stiffness made by the matrix are minimal and therefore would not have strongly influenced the results of tensile tests performed on the hybrid strands. In their service environment, hybrid strands are likely to be involved in loading conditions where polymer crystallinity will influence matrix-dominated properties such as fatigue,

particularly at elevated temperatures. A study on the effect of the cooling rate on polymer crystallinity and therefore on the performance of hybrid strands in service should be conducted as part of future work.

- A more powerful motor would have enabled the pultruder to run at higher rates of article productivity. As no correlation was observed between flexural strength and stiffness with line speed, higher rates of production would have also permitted study of the optimal line speed and greater understanding of the interdependence of manufacturing conditions.

Due to limitations in the scope of the project, strands were only characterised through tensile testing. This single loading condition is not representative of the flexion, torsion and cyclic loading that a hybrid strand would endure during its period of service. Future work should characterise hybrid strands in an expanded range of loading criteria as product development would include testing the performance of hybrid strands in real working environments.

- An improved testing methodology for the tensile testing of rods would include more accurate measurement of strain, for instance with an extensometer or digital image correlation.
- The tensile strength and stiffness of FRPs are fibre-dominated properties. Ropes undergo considerable bending and twisting during operation that introduces shear and compression stresses that were not tested. It is currently unknown how stress is shared between the FRP core and outer wires in a hybrid strand subjected to these loading conditions. This may be especially pertinent to the handling and storing long strands.
- Since tensile testing was performed at a single rate of strain at room temperature, the influence of the viscoelastic properties of the polymer matrix, such as the glass transition temperature, was not studied. Ropes are subjected to high strain rates in impact conditions. Under such circumstances the stiffness and ductility of the polymer matrix would be altered, which would affect the contribution made by the FRP rod to load sharing. As the rods were only tested at room temperature, the degree to which tensile strength and stiffness are retained at the elevated temperatures commonly experienced in working ropes has yet to be explored.
- While there is a body of research that has focussed on the long-term fatigue behaviour of CFRPs and high strength steel, it is unknown how progressive changes to the characteristics of these materials would affect each other in a hybrid strand. Since these materials would be working together, a reduction in the stiffness of one material would concentrate stress in another. A parametric study could therefore be conducted by fatigue testing of hybrid strands under different conditions of load and duration.
- Understanding of good practices for the lubrication of steel wires and the temperatures experienced in steel wire ropes may not directly translate to best practice in hybrid strands. Determination of the abrasion experienced by FRP rods against outer steel wires within strands was outside of the scope of this project, as was long term creep testing of the thermoplastic matrix. This should be undertaken as future work.
- The ultimate purpose of hybrid strands is for use in multi-strand ropes. As additional layers of strands are added around the core of the rope, the outermost strands take an increasingly long helical winding path around the central axis of rotation. It was found that the extensibility of hybrid strands with CFRP rods is lower than that of steel strands. Use of hybrid strands in the outer layers of a multi-strand rope may not be appropriate because of the additional helical extension under load, which could result in tensile failure of outer strands. This may limit the use of hybrid strands to the centre of a multi-strand rope.

The scope of the project limited finite element modelling to the simulation of tensile testing of hybrid strands. Future work should focus on expanding the capabilities of the model to increase its relevance to rope technology.

- At the time of writing it is now possible to resolve contact between helical wires without the need for faceted surfaces. This would allow the model to more accurately represent contact between wires. Since it is exceptionally challenging to determine the contact stresses occurring between wires in a multi-stranded rope, modelling could provide a valuable insight into these mechanisms.
- The material model used in this project was limited to Young's modulus, tensile strength and Poisson ratio. Since composite materials are anisotropic, a more complete characterisation of the engineering constants of the simulated materials would improve the accuracy of the model. Anisotropic material properties serve to complicate the prediction of damage in FRPs, which is non-trivial and requires the use of semi-empirical failure criteria. A more complete knowledge of the strength of FRP rods would permit the use of the 3D Hashin damage criterion, for which subroutines have been written in ABAQUS. In addition, the characterisation of the thermal properties of FRPs would allow the performance of the strand to be evaluated at elevated temperatures.
- A more complete description of material properties would enable the simulation of hybrid strands with different constructions. Experimental tests representing the service conditions of ropes are expensive and modelling can help reduce the cost of research by simulating these environments. This is particularly true for parametric studies of rope construction, which involve many interrelated properties such as the lay angle and the total number of wires. Since optimal parameters are unknown for hybrid strands, finite element modelling could help to reduce the number of necessary physical tests.

Appendix A: Pultruder standard operating procedure

The pultruder was scratch built to provide thermoplastic reinforced rods for a project looking at weight reduction of ropes by replacement of steel wires. It used an electrostatic powder spray to deposit a polymer matrix onto conductive fibre tows. This created an *in situ* towpreg, which was partially consolidated in a pre-heater before being fully consolidated in a split die. The rod was cooled as it emerged from the die and could be cut into desired lengths.

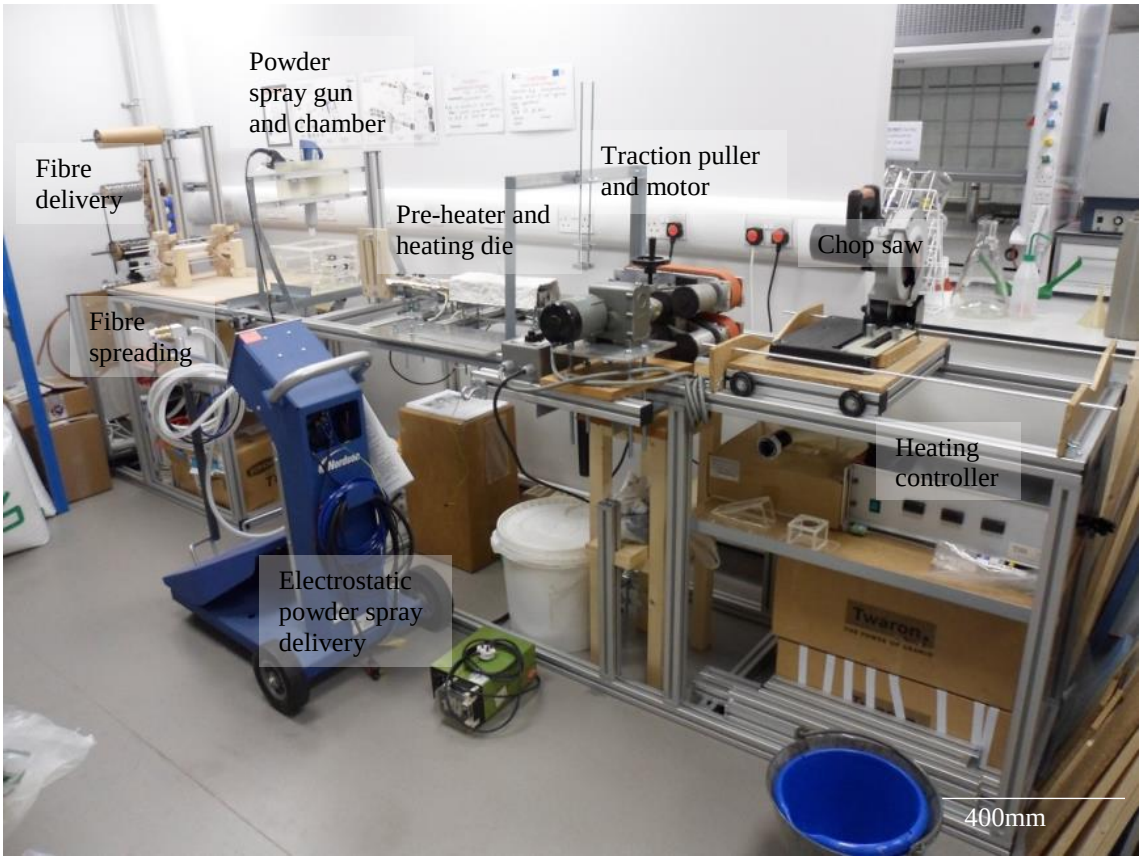

Figure A.1 Overview of pultruder.

The pultruder was a prototype and to some degree was always in a state of development. It was modular with parts could be replaced, upgraded or translated without great difficulty; the whole machine was dismantled, moved and reassembled during the end of the 2013 academic year in less than three days. As there was no manual for the pultruder this document served as a guide for best practice.

- Powder went everywhere
  - This is inevitable and it got in clothes, hair and skin. The utmost consideration was necessary to minimise the spread of powder.
- Wearing of gloves was mandatory
  - Operating the machine involved close proximity to very hot surfaces and actual manipulation of the molten resin. Gloves were absolutely essential, particularly for handling dry or commingled carbon fibres.
- It was imperative to cease operation as soon as it appeared unsafe

    - If tows got caught in the entrance of the die, the motor was unable to pull the fibre tows through the die or the polymer degraded badly, or in the event of any potentially catastrophic error, discretion was the better part of valour.
- Things broke on a continual basis
    - Tape heaters snapped, motor shafts twisted out of shape, vacuum cleaners burned out and fuses broke. The pultruder was built on a shoe string and pretty much everything home-brewed was under specified. However, when things broke they could be easily and cheaply replaced, or improved for longevity.

Laboratory safety always applied

Nothing was held in higher regard than personal safety and any user feeling unsafe in the vicinity of the pultuder was encouraged to either get help immediately or stop using it. Reading of the risk assessment before use was mandatory.

- Thermal gloves were provided for handling the split die. It was heavy but not unmanageably so and steel tongs could be used to move it while it was hot.
- Fingers were kept away from unguarded motor gears and the caterpillar threads.
- Temperature control box was isolated prior to inspection.
- All electronic devices were kept at least one metre away from the powder spray gun when it's was in use. A warning sign and a red strip on the floor displayed the safe distance to warn laboratory users about the risks of bringing electronics close to the machine.
- The chop saw was arguably the most dangerous part of the machine and was easily capable of amputation if misused. A chain at the back of the rail could be hooked onto the saw head to immobilise it.

A step-by-step guide to running the pultruder

Carbon fibres were stored in a plastic box beneath the heating controller. This was kept locked to prevent contamination with powder. The box contained both sized Grafil TR30S 12k carbon fibres and unsized Toray 700S 24k carbon fibres. 11 bobbins of commingled stretch-broken carbon and nylon 12 filaments were kept in another box beneath the powder spreading line. Each commingled tow contained 6k carbon filaments.

The pultruder used to have a complicated system of pulleys and ropes connecting fibre bobbins to the rack but it proved unnecessary. The bobbins were slotted over the steel bars and then the tows were run along the first and second pinch rollers.

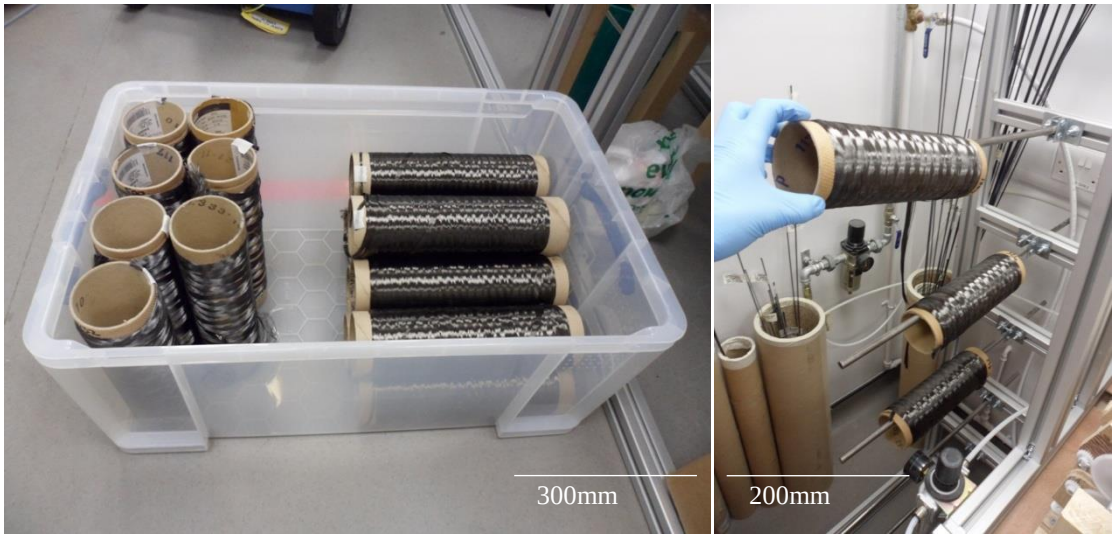

Figure A.2 Fibre bobbins and rack.

Tows were then spaced out as much as possible using the aluminium comb. This ensured that a greater surface area was exposed beneath the spray gun. The tows were also spread out under the second pinch roller, which acted as the sole means of controlling fibre separation. The first pinch roller and the empty space in between the two sets of rollers were thus decommissioned.

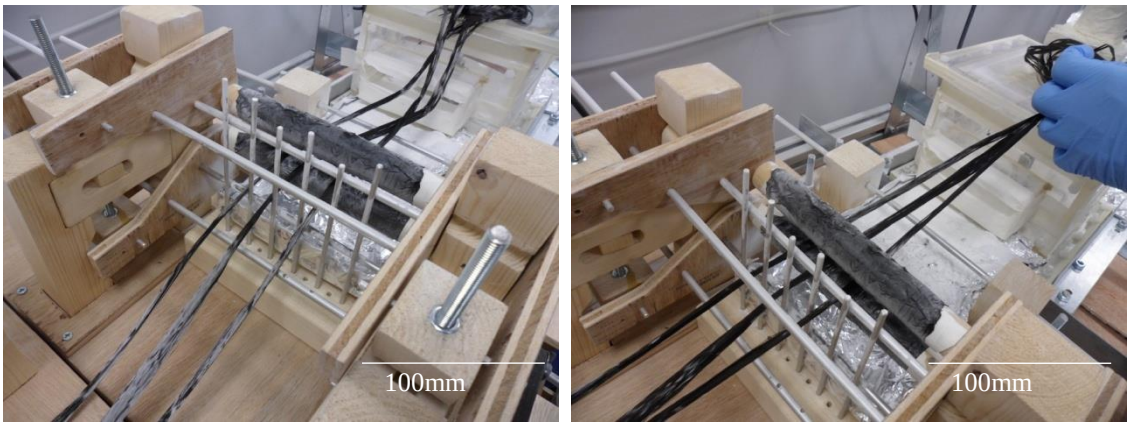

Figure A. 3 Pulling tows through speaders.

The bundle of tows was pushed into the opening of the powder chamber. A couple of aluminium tools were then used for loading the fibres; these were stored on hooks beneath the traction motor. The one that looked like a candy cane was inserted through the powder chamber and used to hoist the tows over the copper bridge and out the other side. The bridge acted as the earth strip for the carbon fibres and was gently abraded before operation to remove the copper oxide layer for better conduction. At this stage a pipe cleaner and the crevice tool on a vacuum cleaner were used to remove excess powder from the bridge before starting.

Once the tows were passed through the powder chamber, the ends were tied to the second tool, which had a loop rather than a hook at its end. This made it considerably easier to pull the tows through the barrel of the pre-heater.

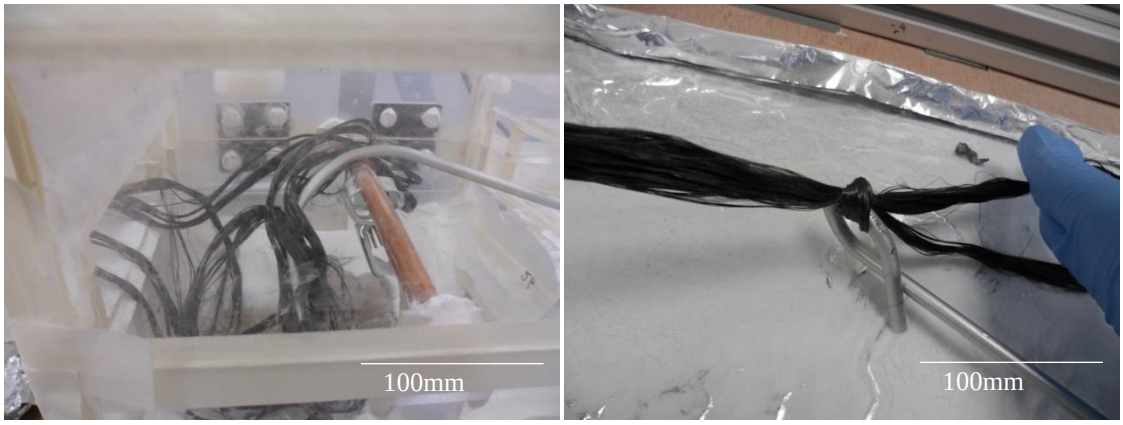

Figure A.4 Pulling tows through powder chamber.

The tows were pulled along the pultruder until the chop saw and were untied from the aluminium loop.

Figure A.5 Pulling tows through pre-heater and traction puller.

The secondary pinch roller was then closed until finger tight. Borrowing an old trick from the rope industry, the tows were tightened by twisting them into a thread. The bottom half of the split die was laid onto the supporting cradle while the tows were twisted together.

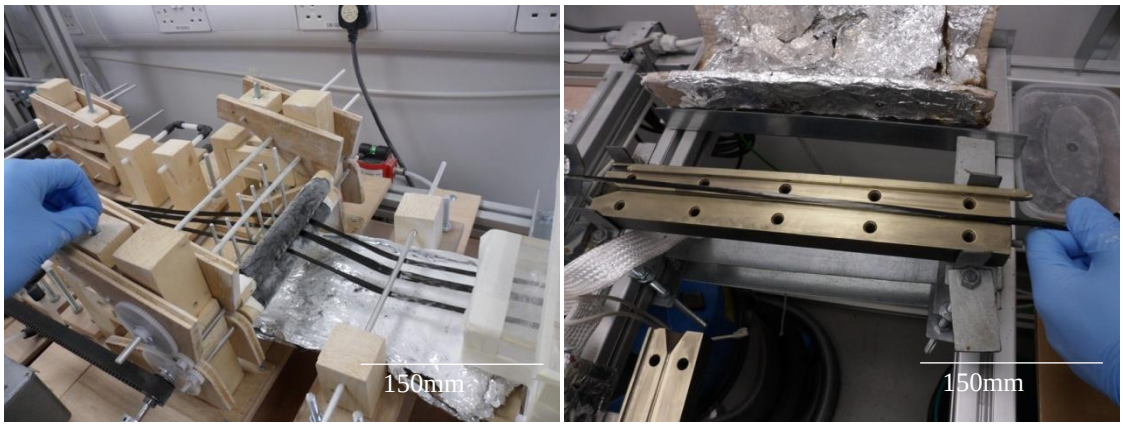

Figure A.6 Twisting tows in open die.

While pulling on the twisted tows with one hand, the top half of the split die was lowered with the other, which then began tapping the top of the die with the soft hammer. Pulling of the tows continued while the hammer gradually pushed the halves of the die together so that the walls of the die would not catch on loose fibres. Thus each type of carbon fibre feedstock was dragged in this manner while the die was gently closed. Once it was clamped shut, bolts were screwed into the holes through the top of the die.

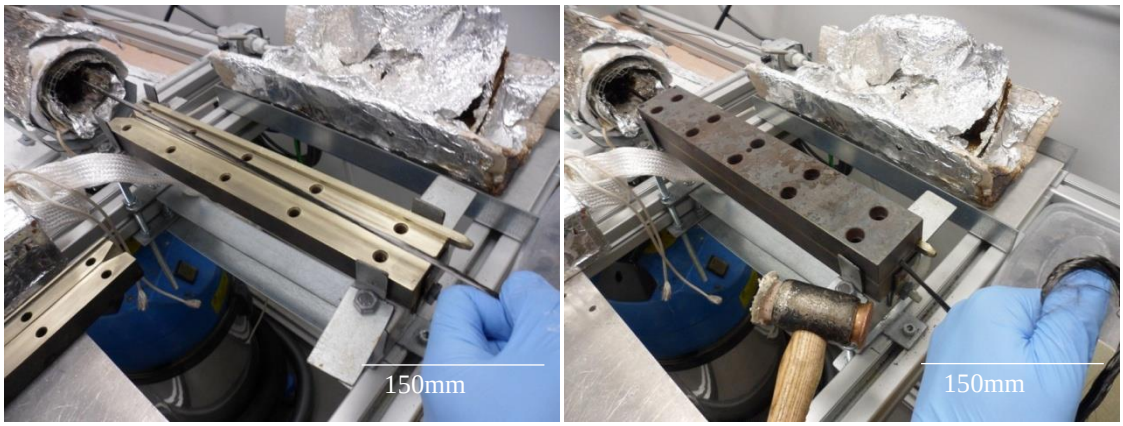

Figure A.7 Closing die with twisted tows.

The heating tape was wrapped into a bundle and passed over and under the heating die. This was possibly the least elegant stage in preparing the pultruder. Commercial pultruders use cartridge or hinged elements that were too expensive for this project. Consequently tape heaters were awkward to use broke over time from frequent handling and scraping against the edges of the die. The cable was uncoiled slightly as towards the end and the bundle was fed towards the plug, which was located behind the pre-heater. The plug for the pre-heater was located below the frame, while the plug for the heating die was above it. A space was left at the centre of the coils for the hole drilled into the top of the split die; this is where the thermocouple was inserted into the die block.

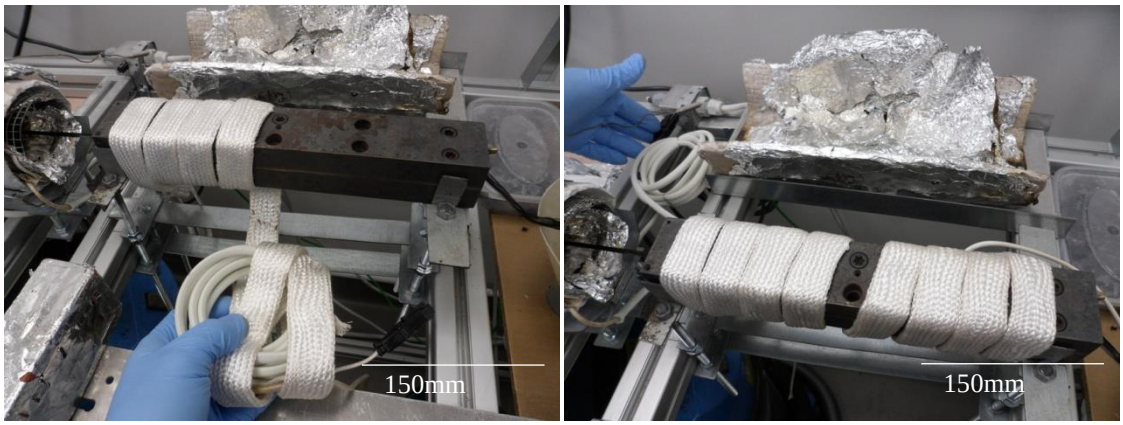

Figure A.8 Wrapping die with heating strip.

The tape was wrapped with a sheet of foil for better insulation and temperature stability. A foil wrapped brick was also placed beneath the die to offer greater insulation and better protection for the coils of the tape heater. A fire cement cover was placed over the coils with a hole for inserting the thermocouple into the die. It was imperative that the thermocouple

was well located before heating, otherwise the monitor would only monitor only the air temperature above the die.

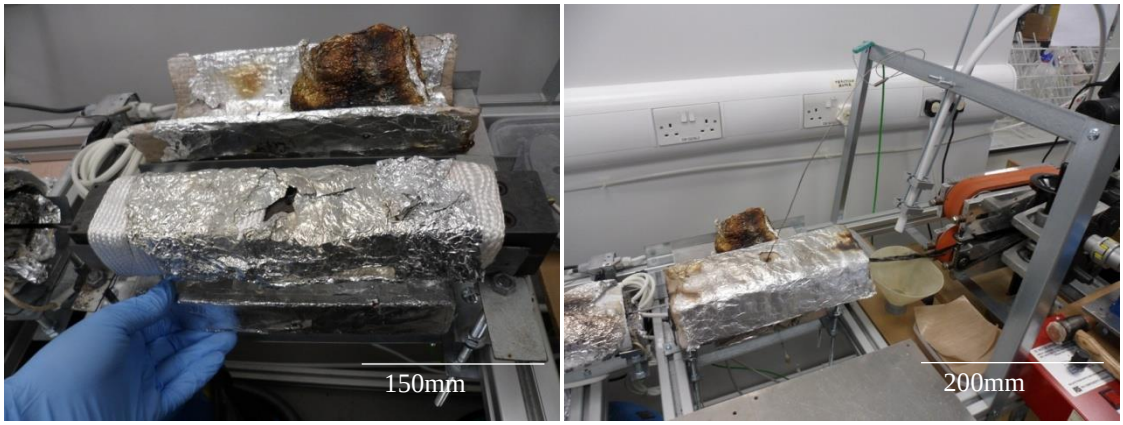

Figure A.9 Insulating die with heating strip.

The water supply was then switched on at the tap behind the fibre delivery racks. Compressed air was provided from a central regulator near the water pipe. Several inline filters were located after the valve. The first was a coarse 40µm filter filled with silica beads and the second was a heavy duty filter that stripped almost all of the particulates, oil and water from the air. The first was intended as an emergency trap in case an emulsion of oil and water spilled down the line.

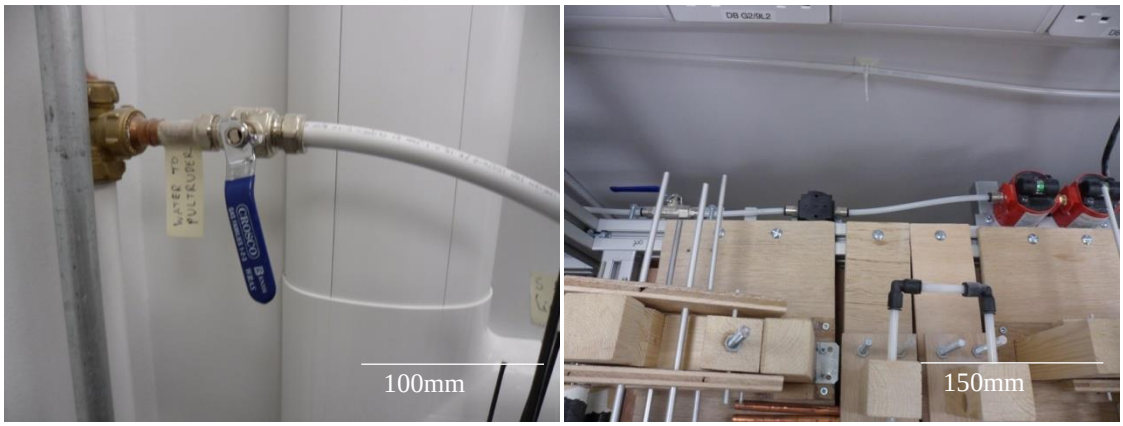

Figure A.10 Water tap and compressed air line.

A third filter-regulator was used to control the air pressure. After the regulator an air stream branched towards the powder spray and the redundant pneumatic spreader assembly, which had its own regulator and valve.

The tows were loaded onto the traction puller and the caterpillar treads were brought together using a handle at the top of the device. The speed of the motor was measured with a stopwatch and intervals drawn onto the upper tread. The motor had units between 1 and 10, which did not correspond to linear steps in the speed of the treads. For example, motor units 2, 3 and 4 corresponded to line speeds of 3.3cm/min, 6.7cm/min and 8.6cm/min, respectively. The line speed was measured and recorded for each operation.

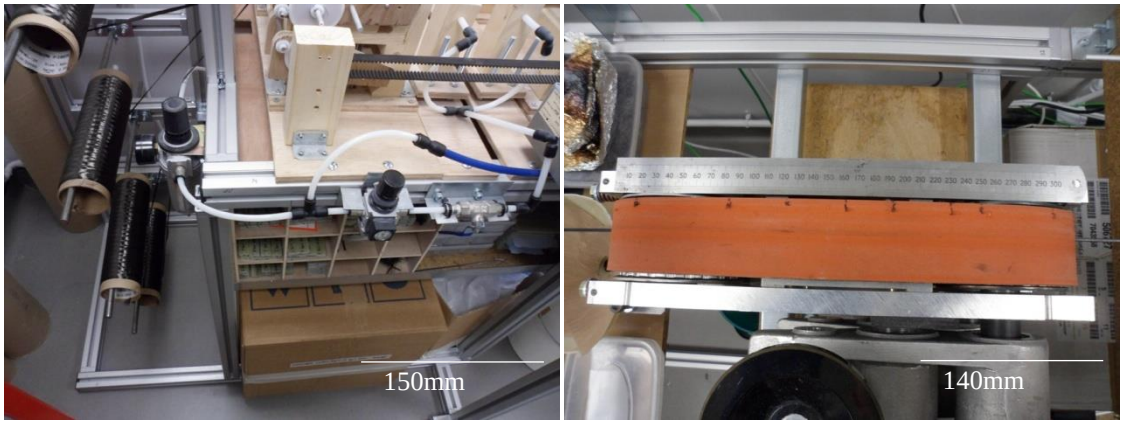

Figure A.11 Regulators and measurement of traction speed.

The temperature controller was then switched on. The power cables and thermocouples for the pre-heater and heating die both were attached at the back of the temperature controller. Since there were no independent switches for these heaters the plugs had to be disconnected in order to isolate them.

The controller was found to vary by about ±10°C and the mean temperature displayed on the controller was 10°C lower than the set point values. Input values were therefore calibrated accordingly with a thermocouple inserted into the die channel. For standard manufacturing conditions for carbon fibre/nylon 12 rods, an input value of 290°C gave a mean value of 280°C. The first channel was not used, the second referred to the heating die temperature and the third referred to the pre-heater.

Figure A.12 Temperature control.

The electrostatic powder spray was then switched on at the control console. Since the spray had a manually operated gun, it had to be fixed into place using a window lock that kept the depressed throughout operation. The platform of the spray unit vibrated during operation to fluidise the powder. For standard operating conditions, the air flow and atomising pressures were set to 1.5bar and 0.29bar, respectively and a voltage of 40kV and current of 15µA were used. A summary of operating parameters can be found in §3.2.5.

Figure A.13 Manual control of electrostatic spray gun.

Ventilation was provided by a vacuum cleaner by way of a hopper underneath the powder chamber. The vacuum cleaner provided a region of low pressure beneath the tows, which drew the powder into the hopper, where it settled to the bottom. It was surprisingly efficient at collecting powder as very little powder escaped the hopper and collected in the vacuum cleaner. The vacuum pressure was adjusted by throttling the fixture on the coupling leading from the hopper to the vacuum cleaner. Ventilation was always activated before the powder spray.

Excessive resin at the die entrance was taken as a sign that there was not a deficiency of polymer, which would have implied that the fibres were insufficiently impregnated. However, this came at the price of having to manually extract the polymer, since it would eventually seize the entrance of the die if it is not frequently removed. The procedure concerning extraction of resin has been covered extensively in §3.2.3.

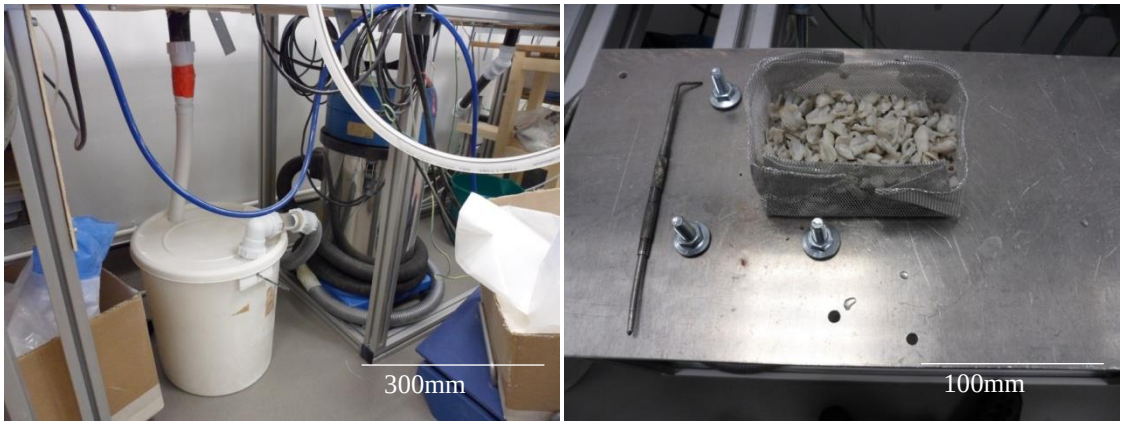

Figure A.14 Vacuum ventilation and removed polymer.

At the end of an operation, tows were cut just before the heating die and at the exit of the powder chamber. The remaining tows were allowed to continue running through the die and the water stream. Cutting the tows slackened the tension in the fibres so any tows still running through the die would not have the same degree of alignment as the already finished rod. This section of the rods was therefore discarded.

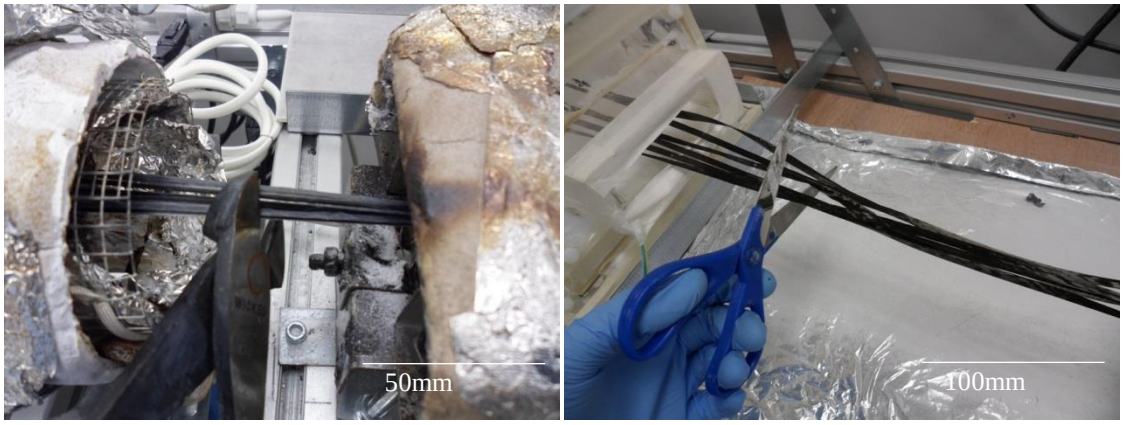

Figure A.15 Terminating feed of tows to heated die.

The pre-heater was then unplugged and allowed to cool.

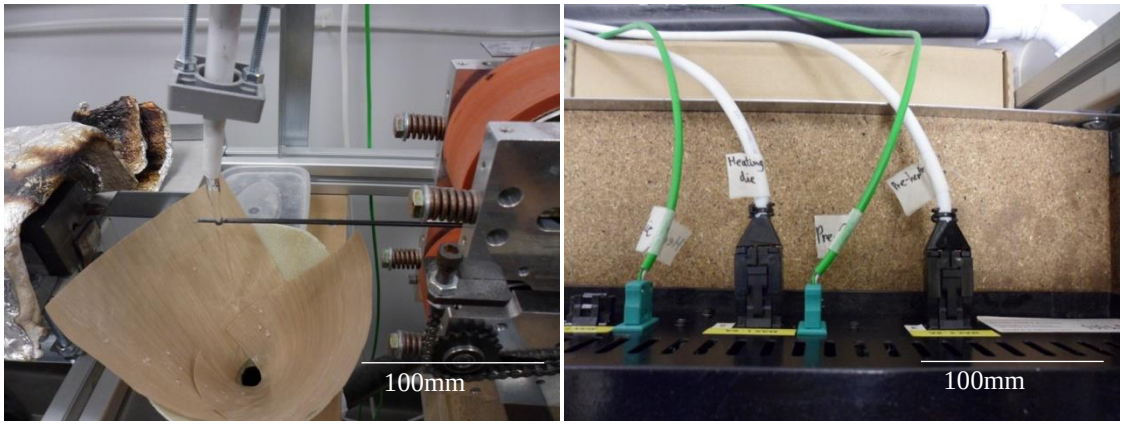

Figure A.16 Shut down of temperature control.

Traces of powder and loose discontinuous carbon fibres were inevitably left inside the die, which rendered it unusable until the die had been annealed to burn off the resin. This was done by ramping the temperature of the die to 450°C. The die was baked it overnight when the laboratory had been vacated to avoid inhalation of noxious fumes. By the following morning the air filtration in the laboratory had safely extracted the fumes.

Figure A.17 Annealing of heated die.

The next day the power cable to the die was unplugged and the cement cover removed with protective gloves. The heating tape was safe to touch with gloves after an hour, whereupon it was uncoiled from around the die.

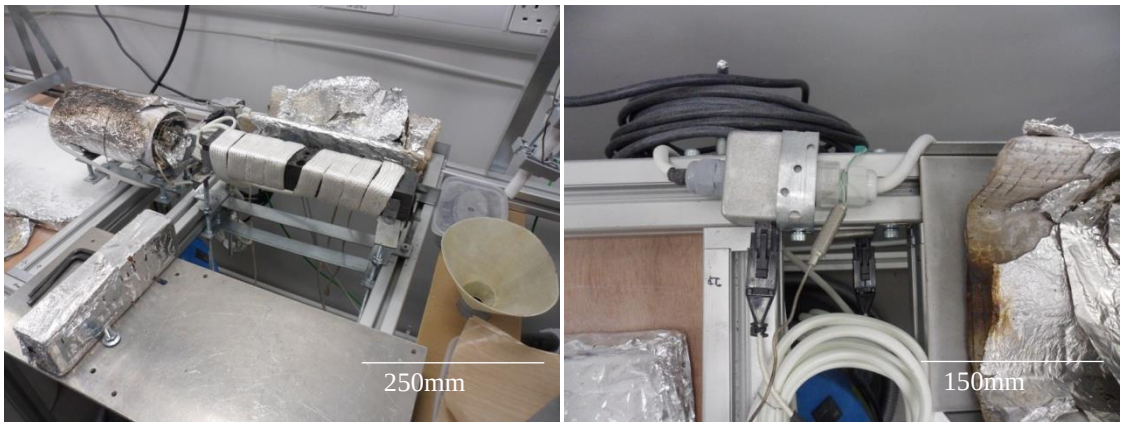

Figure A.18 Cool down of heated die after annealing.

Once the heating tape had been removed, the die was picked up with steel tongs and deposited on the aluminium panel in front of the cradle. Once it had cooled down the bolts were unscrewed and the die was opened by gently tapping with a soft hammer.

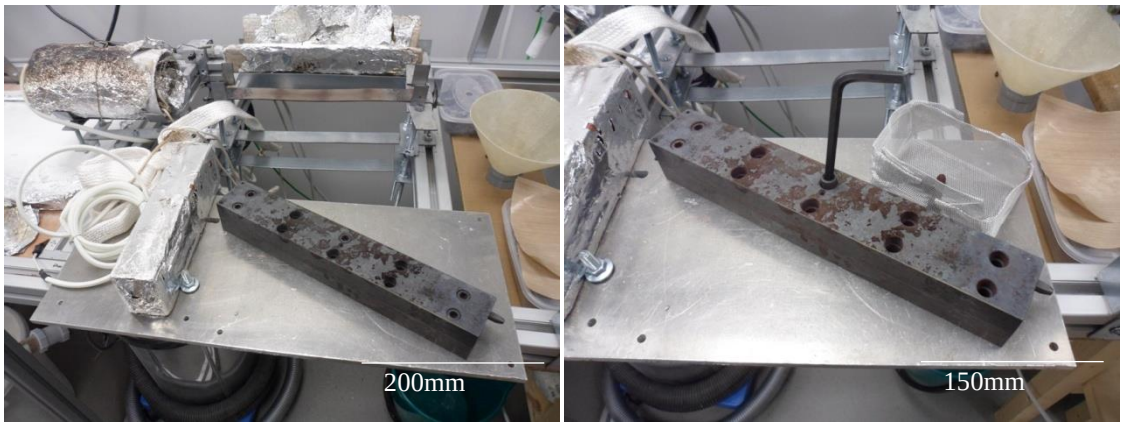

Figure A.19 Opening of die for cleaning.

The die halves were then thoroughly polished with brass wire and washed with acetone.

The hopper could not be allowed to fill to capacity during operation as it would block the ventilation and the powder spray would blow powder into the laboratory. The hopper was therefore emptied after each operation and the powder recycled for the next use. The hopper and supply bag were taken outside, where dust clouds would not pose a health risk to laboratory users.

Figure A.20 Scrubbing die with acetone and filtering nylon 12.

The powder was gently panned into a mesh sieve until the hopper is empty. The sieve caught any discontinuous carbon fibres or impurities that had been sucked into the hopper and ensured that the powder did not agglomerate. The powder was thus repeatedly recycled until it ran out and a fresh supply of nylon 12 was obtained from the Centre for Advanced Additive Manufacturing.

Figure A.21 Sieving recycled powder for re-use.

Appendix B: Stress-strain curves

For the sake of brevity, stress-strain curves from individual reinforcement types and manufacturing conditions have been presented in the on the same graph. Each curve therefore represents one individual test within the series of ten tests that were performed in flexure and tension for each reinforcement type and manufacturing condition.

B.1 Flexural tests

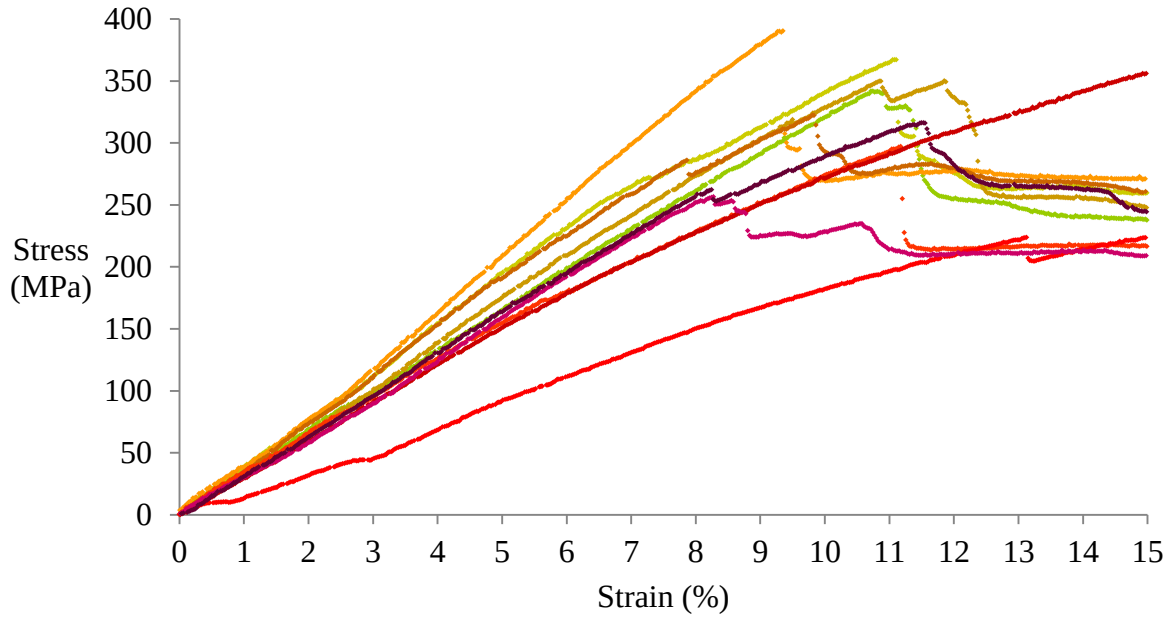

Figure B. 1 Flexural tests for rods manufactured from 4 tows of sized carbon fibres at a line speed of 3.3cm/min.

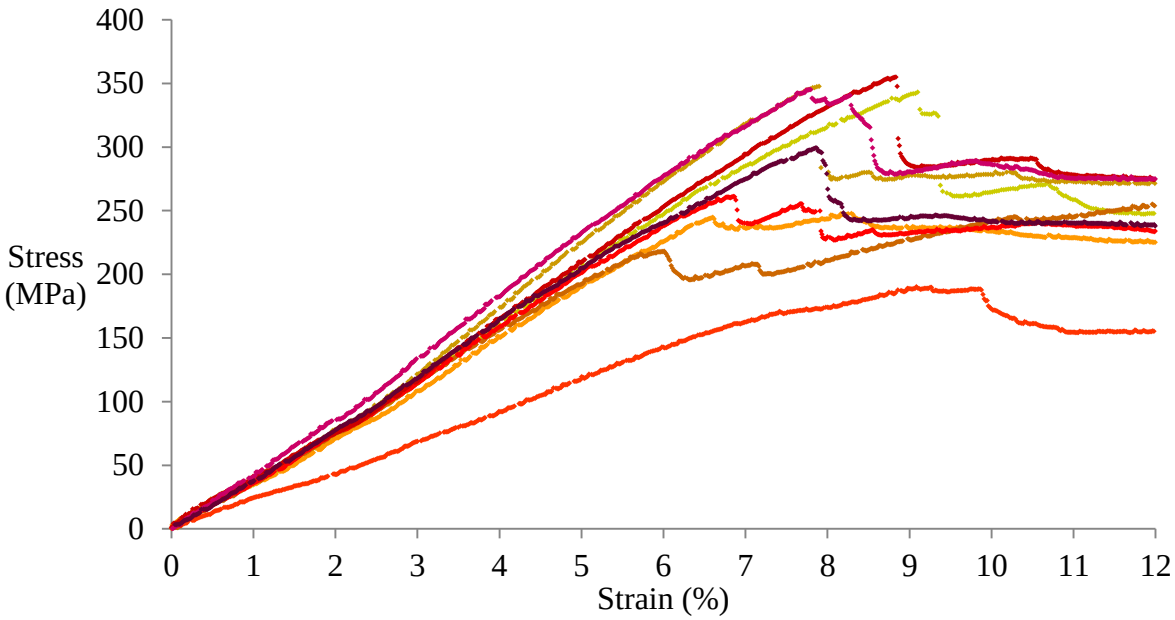

Figure B. 2 Flexural tests for rods manufactured from 4 tows of sized carbon fibres at a line speed of 4.7cm/min.

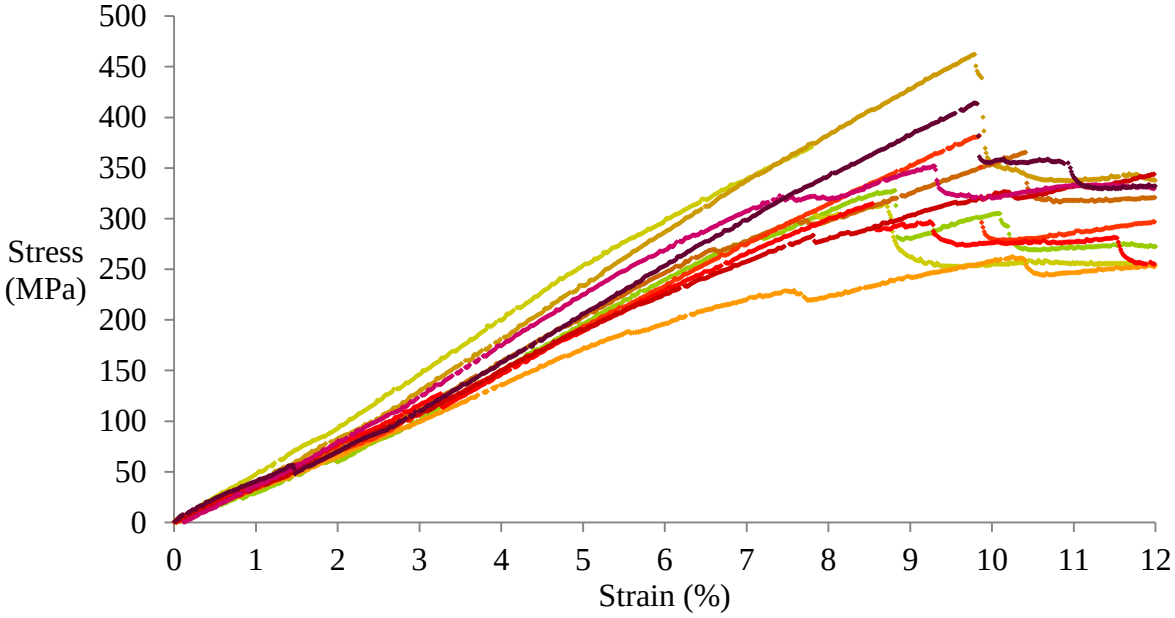

Figure B. 3 Flexural tests for rods manufactured from 4 tows of sized carbon fibres at a line speed of 6.4cm/min.

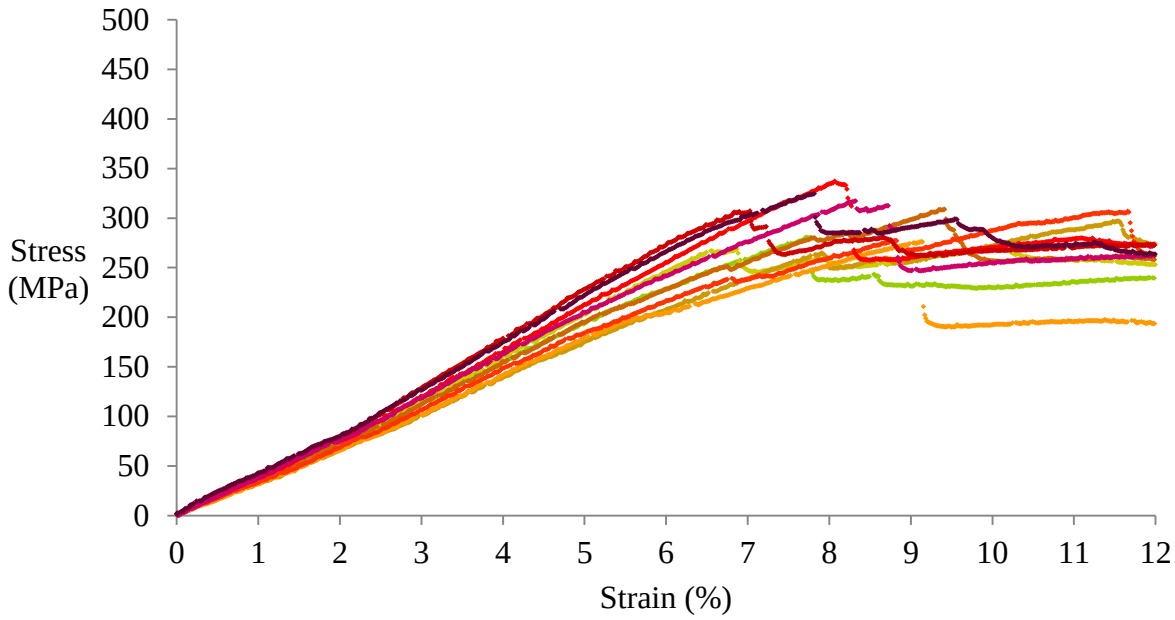

Figure B. 4 Flexural tests for rods manufactured from 4 tows of sized carbon fibres at a line speed of 7.4cm/min.

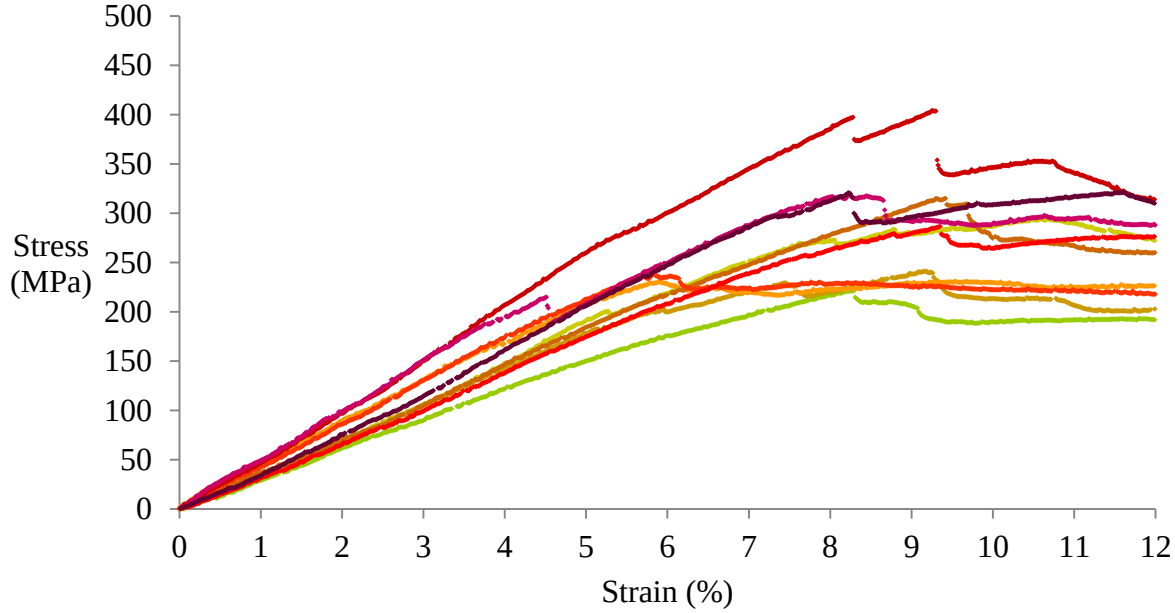

Figure B. 5 Flexural tests for rods manufactured from 4 tows of sized carbon fibres at a line speed of 9.0cm/min.

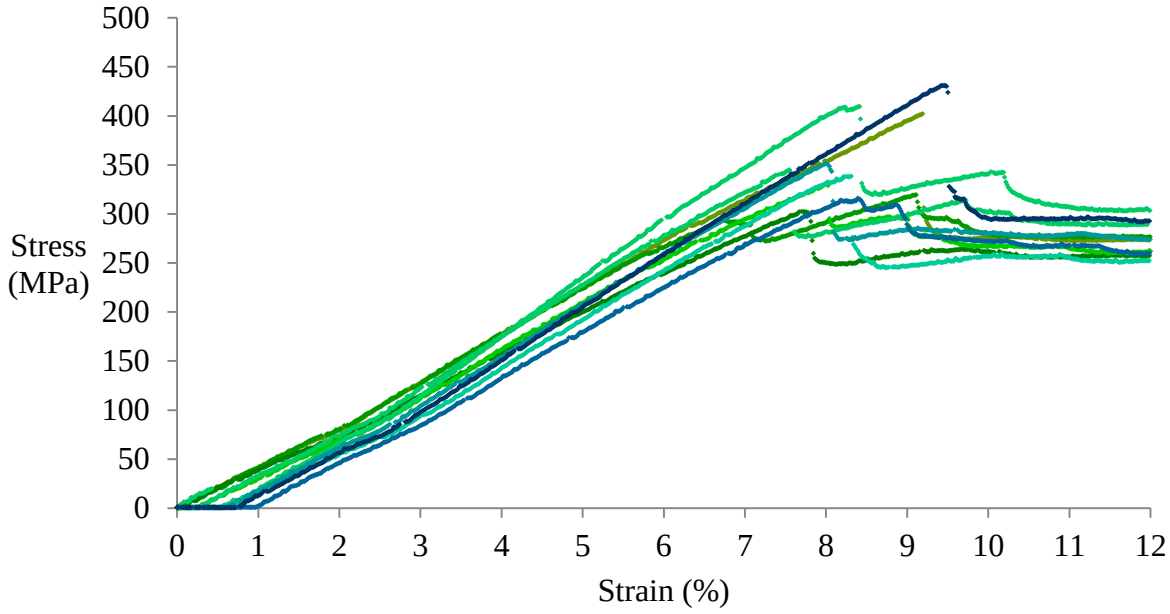

Figure B. 6 Flexural tests for rods manufactured from 5 tows of sized carbon fibres at a line speed of 3.6cm/min.

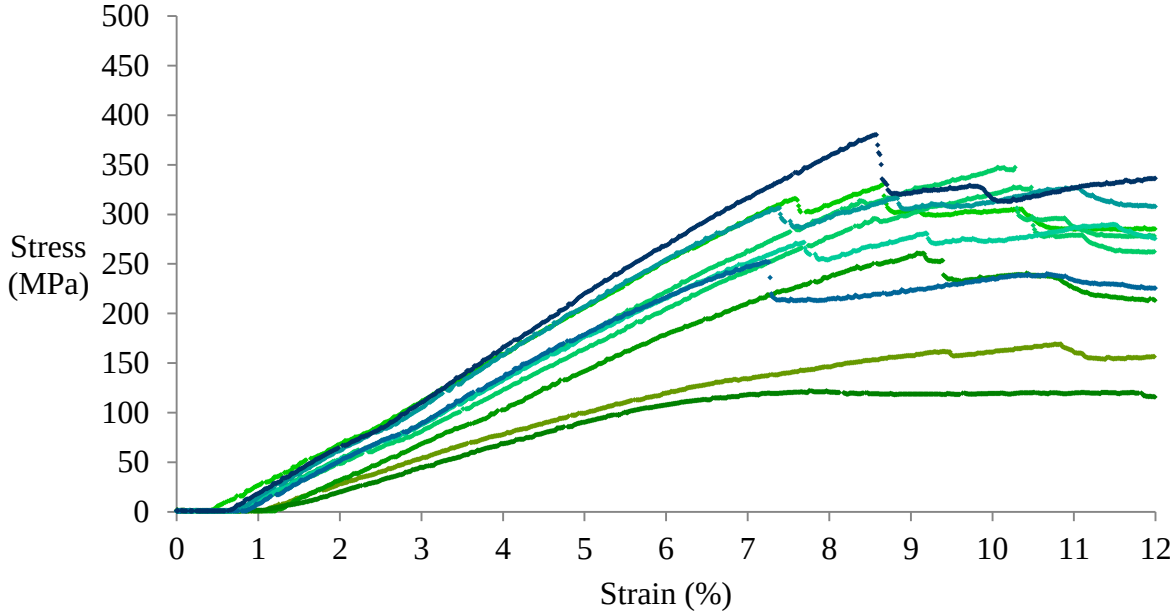

Figure B. 7 Flexural tests for rods manufactured from 5 tows of sized carbon fibres at a line speed of 5.0cm/min.

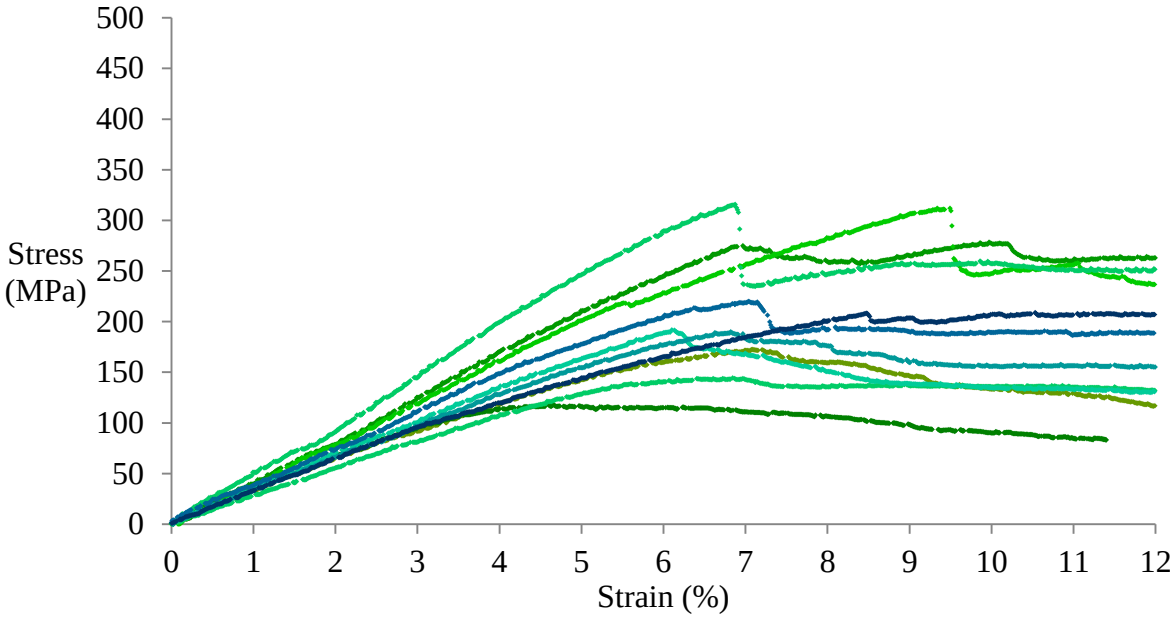

Figure B. 8 Flexural tests for rods manufactured from 5 tows of sized carbon fibres at a line speed of 6.5cm/min.

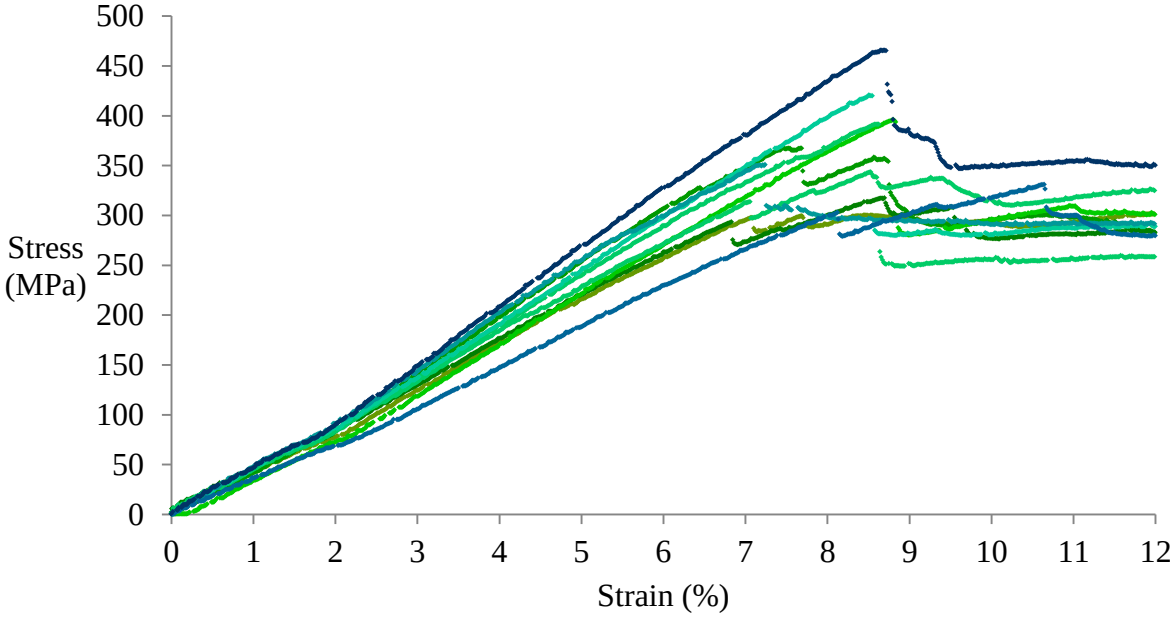

Figure B. 9 Flexural tests for rods manufactured from 5 tows of sized carbon fibres at a line speed of 6.9cm/min.

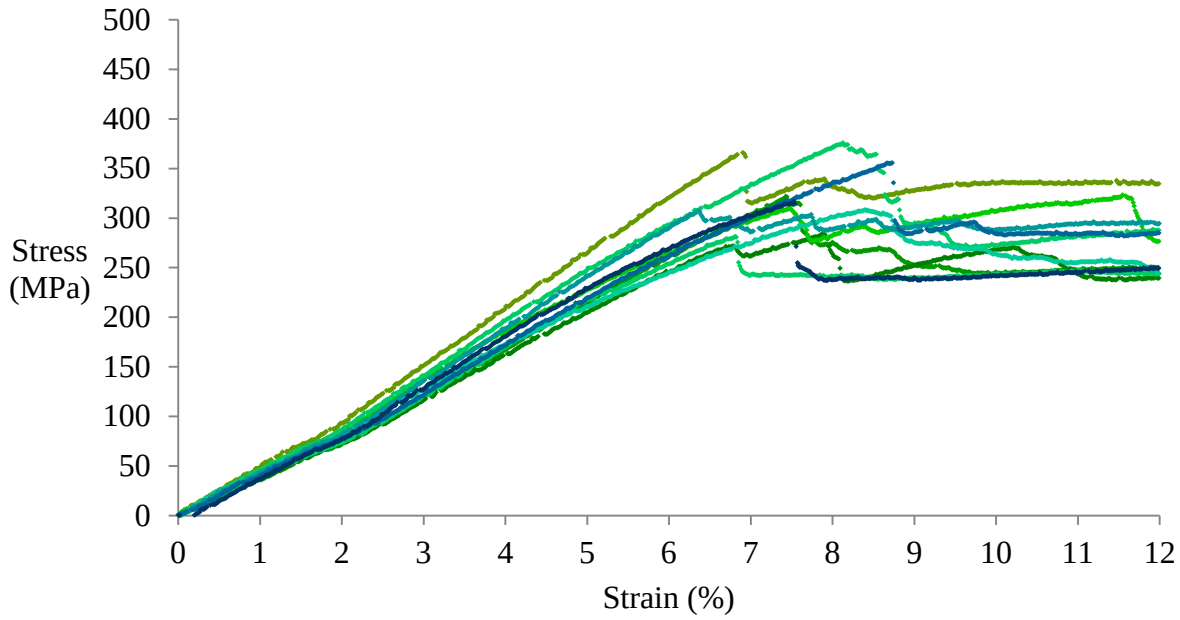

Figure B. 10 Flexural tests for rods manufactured from 5 tows of sized carbon fibres at a line speed of 8.3cm/min.

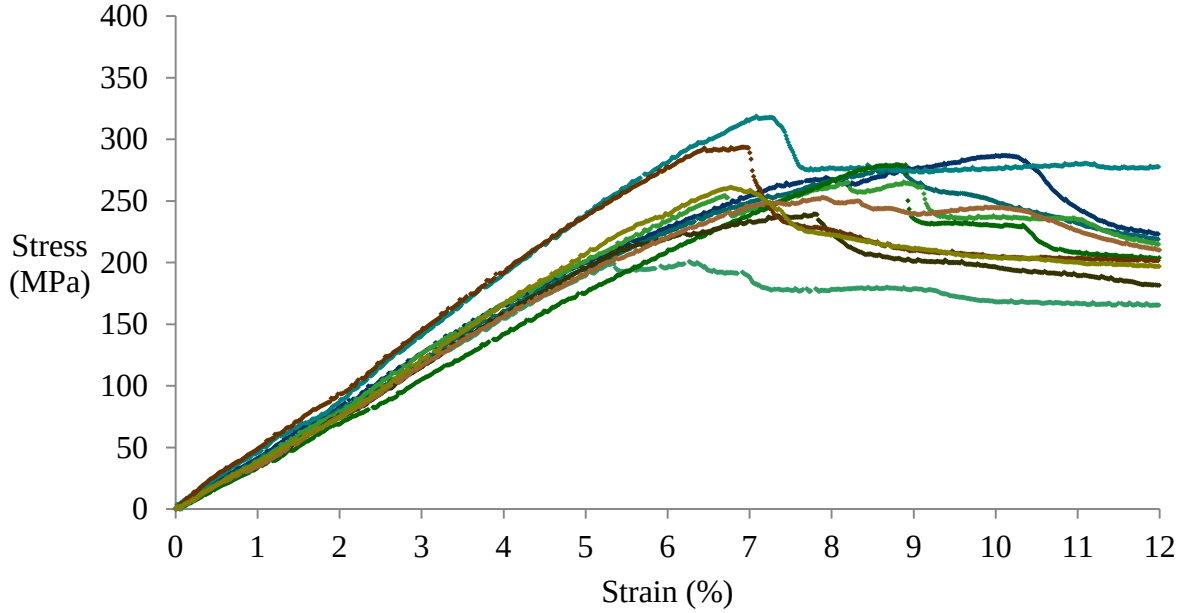

Figure B. 11 Flexural tests for rods manufactured from 6 tows of sized carbon fibres at a line speed of 3.3cm/min.

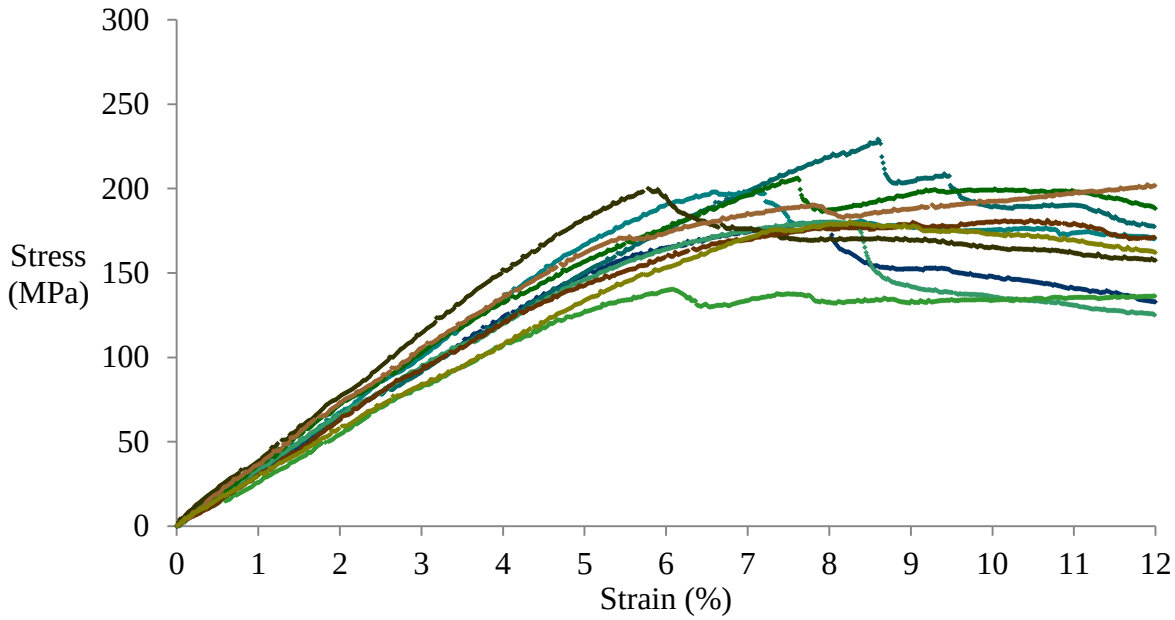

Figure B. 12 Flexural tests for rods manufactured from 6 tows of sized carbon fibres at a line speed of 4.4cm/min.

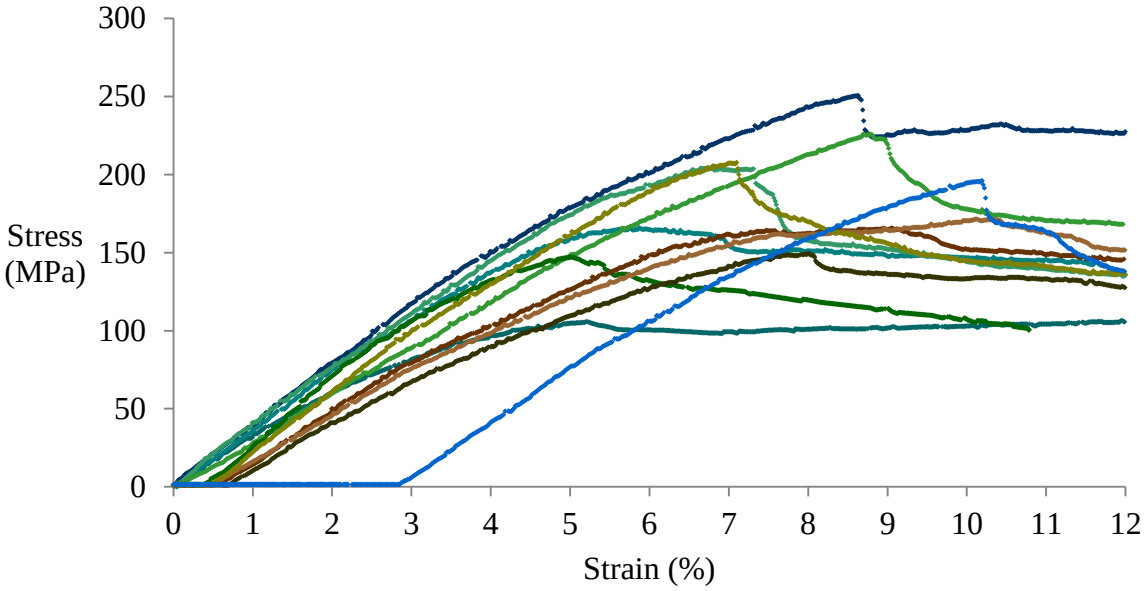

Figure B. 13 Flexural tests for rods manufactured from 6 tows of sized carbon fibres at a line speed of 6.9cm/min.

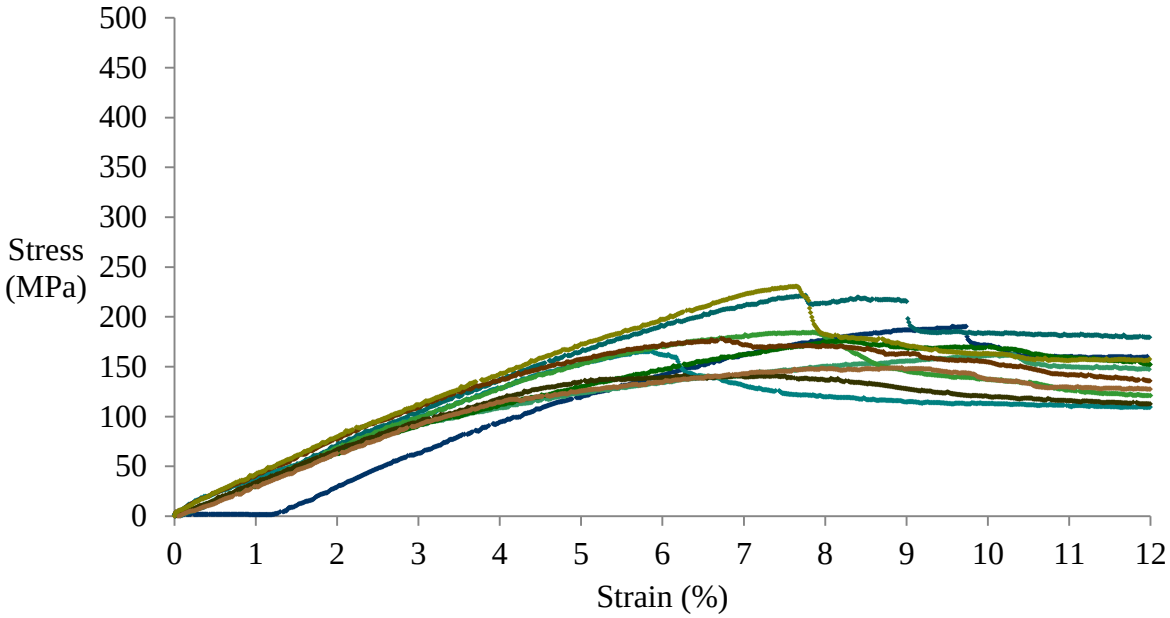

Figure B. 14 Flexural tests for rods manufactured from 6 tows of sized carbon fibres at a line speed of 7.9cm/min.

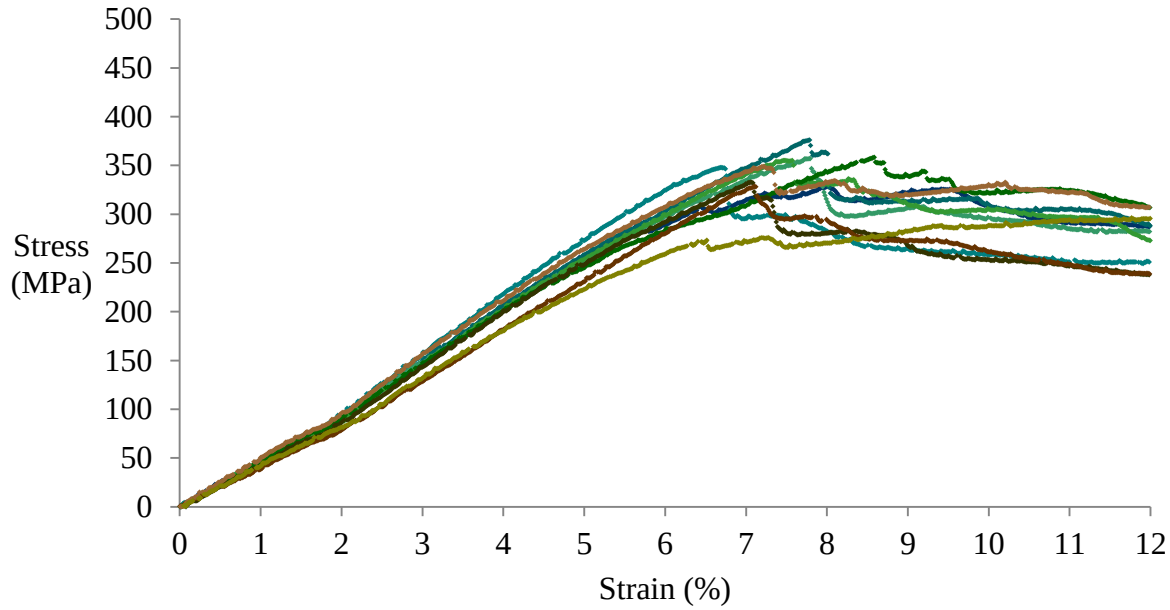

Figure B. 15 Flexural tests for rods manufactured from 6 tows of sized carbon fibres at a line speed of 8.5cm/min.

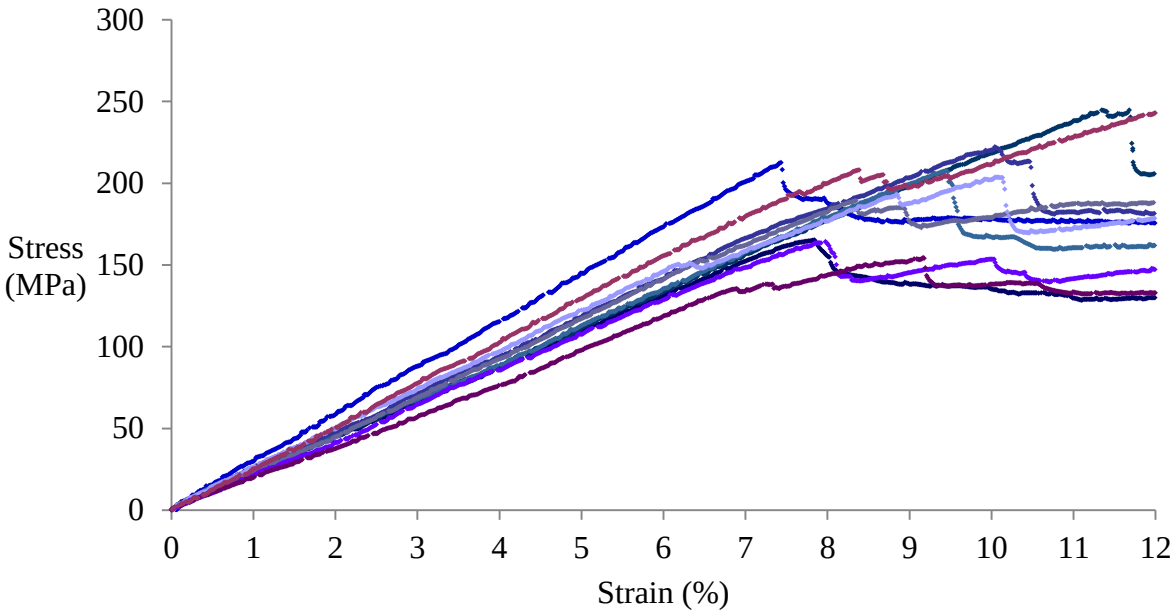

Figure B. 16 Flexural tests for rods manufactured from 2 tows of unsized carbon fibres at a line speed of 3.3cm/min.

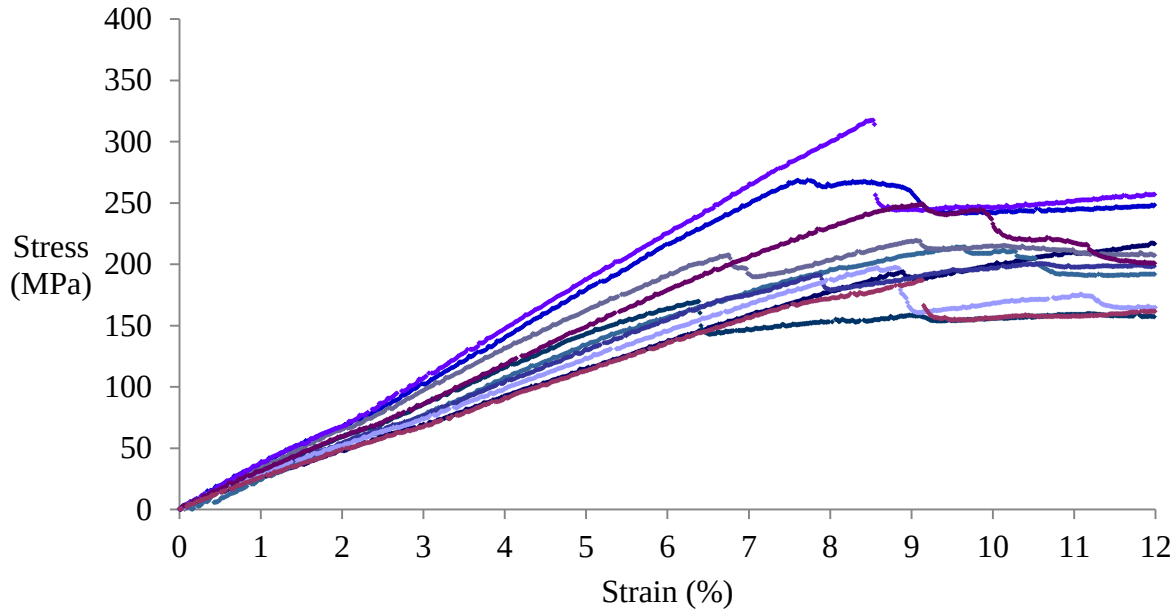

Figure B. 17 Flexural tests for rods manufactured from 3 tows of unsized carbon fibres at a line speed of 3.1cm/min.

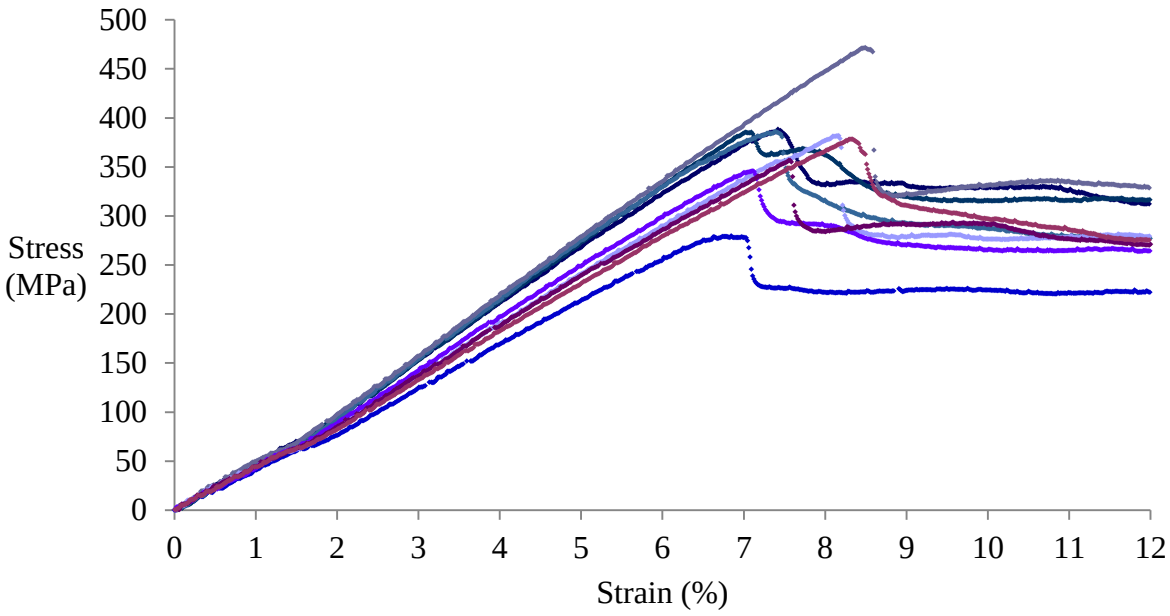

Figure B. 18 Flexural tests for rods manufactured from 4 tows of unsized carbon fibres at a line speed of 3.1cm/min.

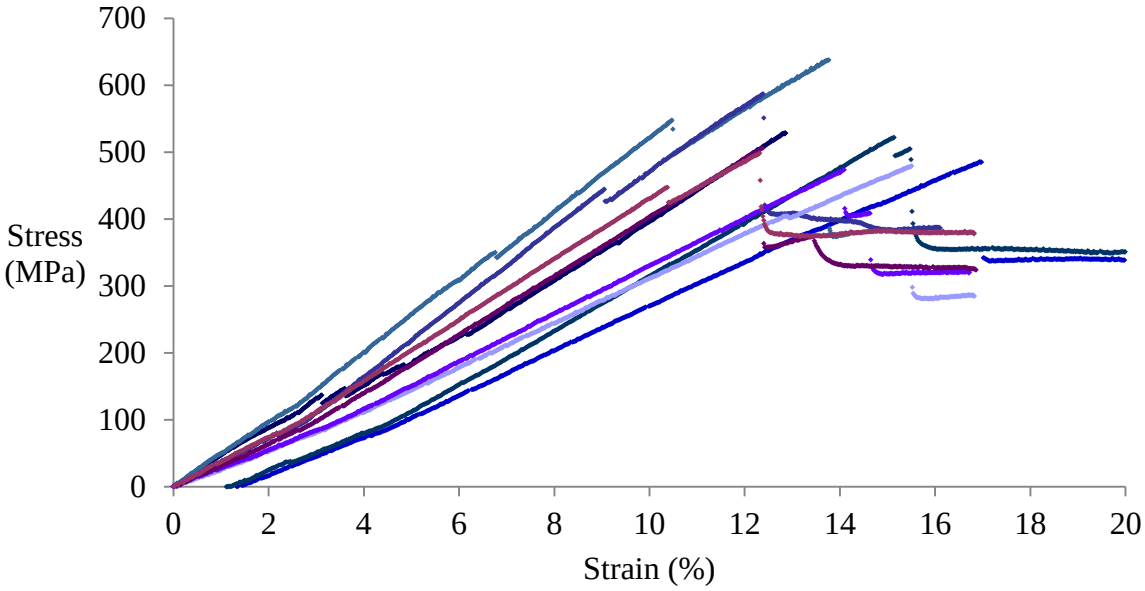

Figure B. 19 Flexural tests for rods manufactured from 9 tows of commingled tows at a line speed of 3.5cm/min.

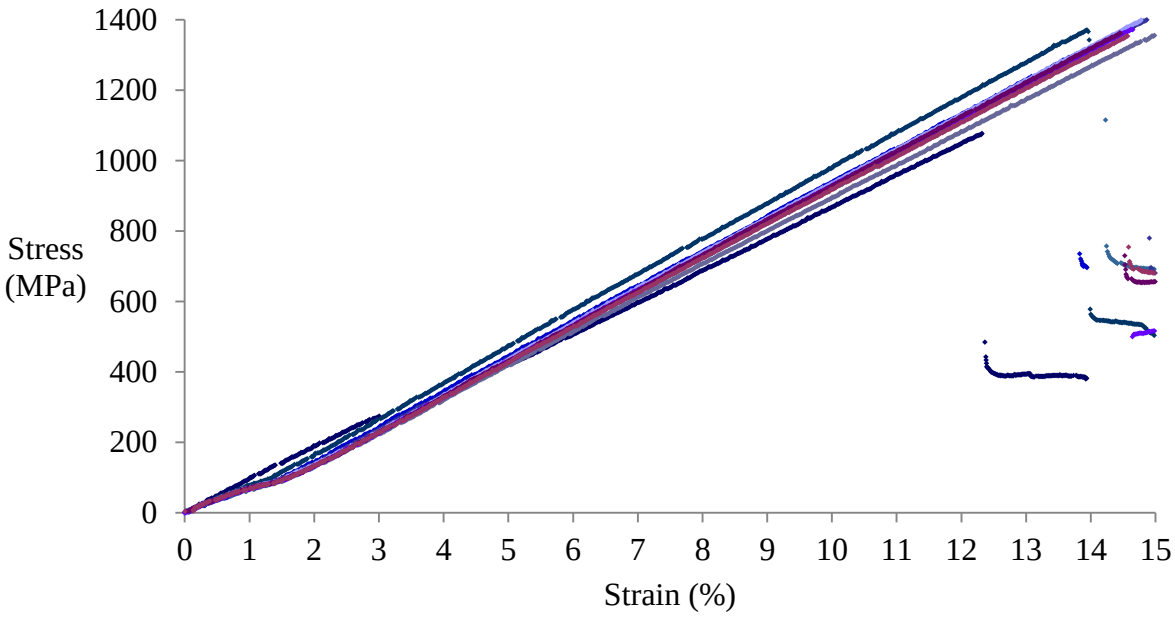

Figure B. 20 Flexural tests for carbon fibre/epoxy rods sourced from Easy Composites.

B.2 Tensile tests

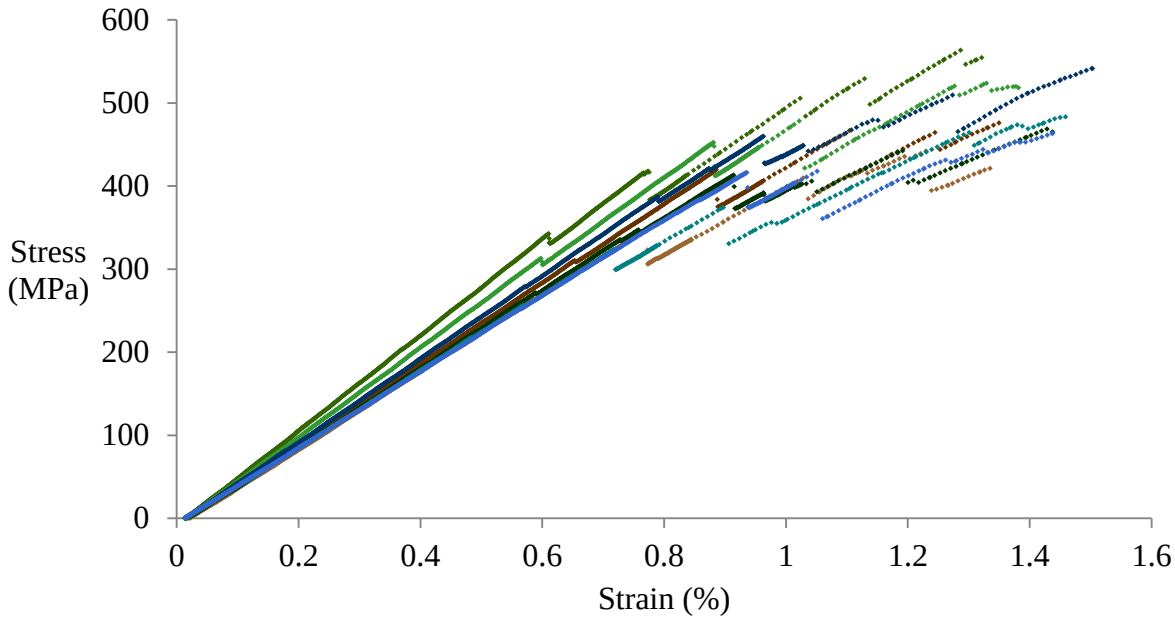

Figure B. 21 Tensile tests for rods manufactured from 4 tows of sized carbon fibres at standard conditions, including a line speed of 3.3cm/min.

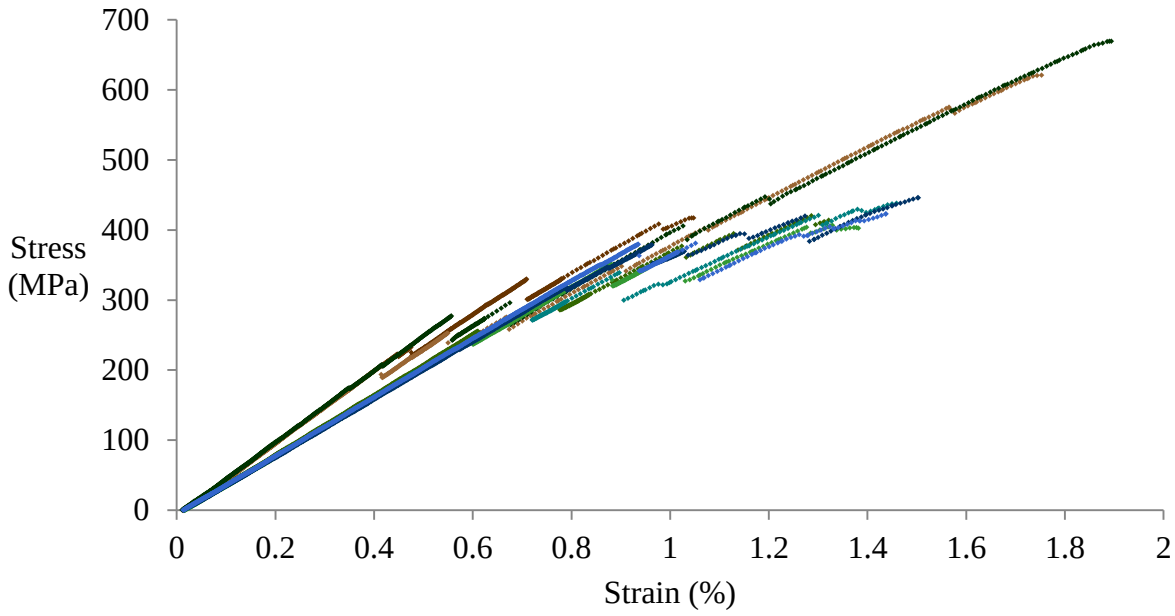

Figure B. 22 Tensile tests for rods manufactured from 5 tows of sized carbon fibres at standard conditions, including a line speed of 3.6cm/min.

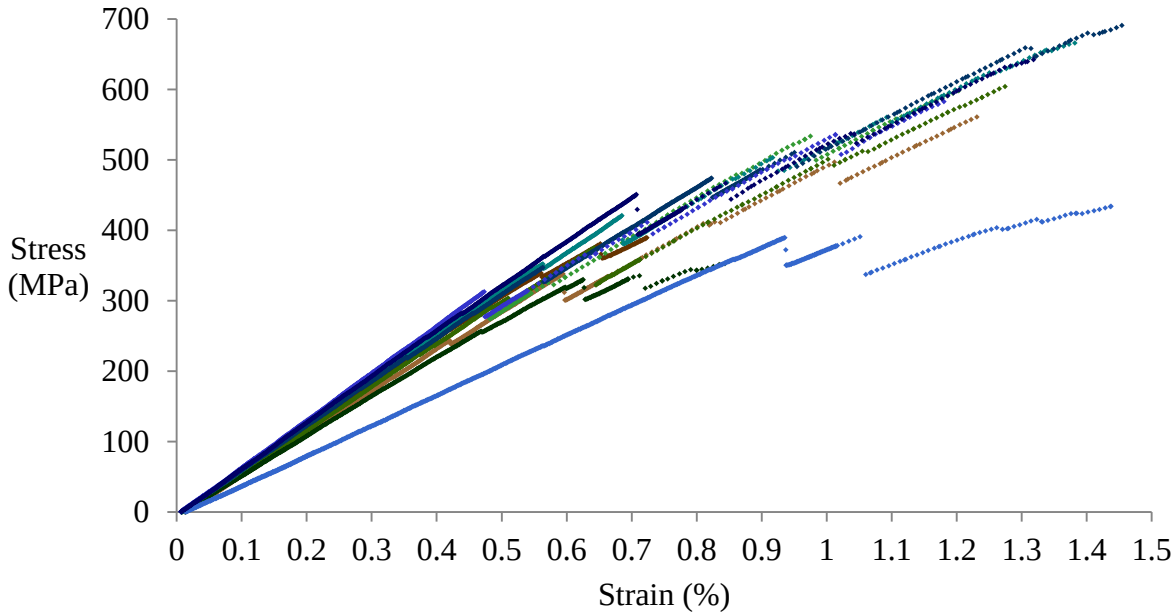

Figure B. 23 Tensile tests for rods manufactured from 6 tows of sized carbon fibres at standard conditions, including a line speed of 3.3cm/min.

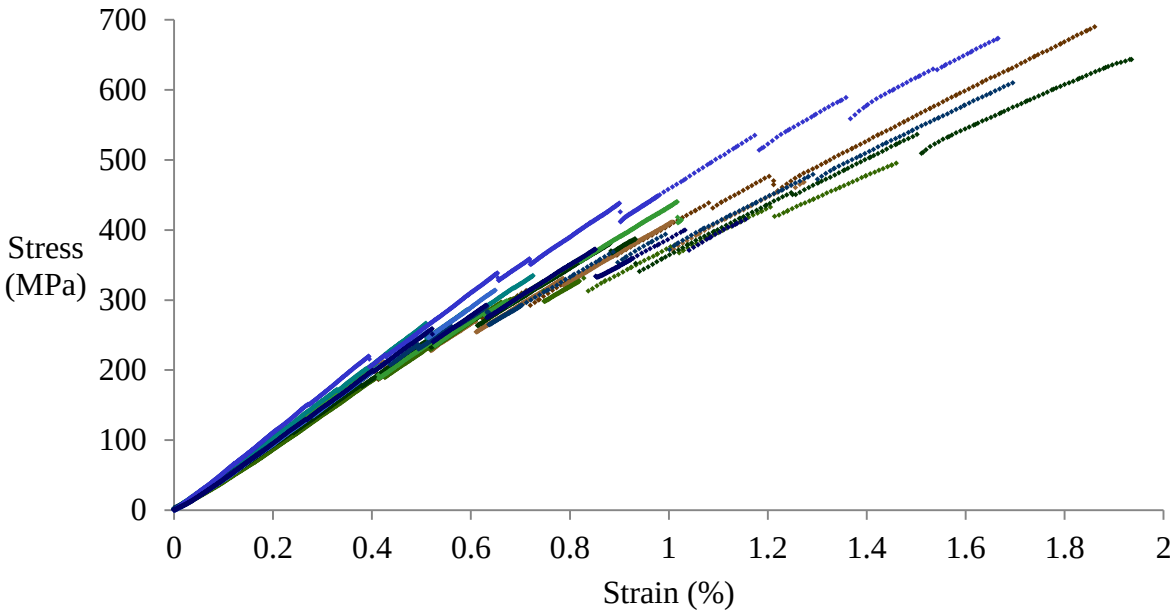

Figure B. 24 Tensile tests for rods manufactured from 2 tows of unsized carbon fibres at standard conditions, including a line speed of 3.3cm/min.

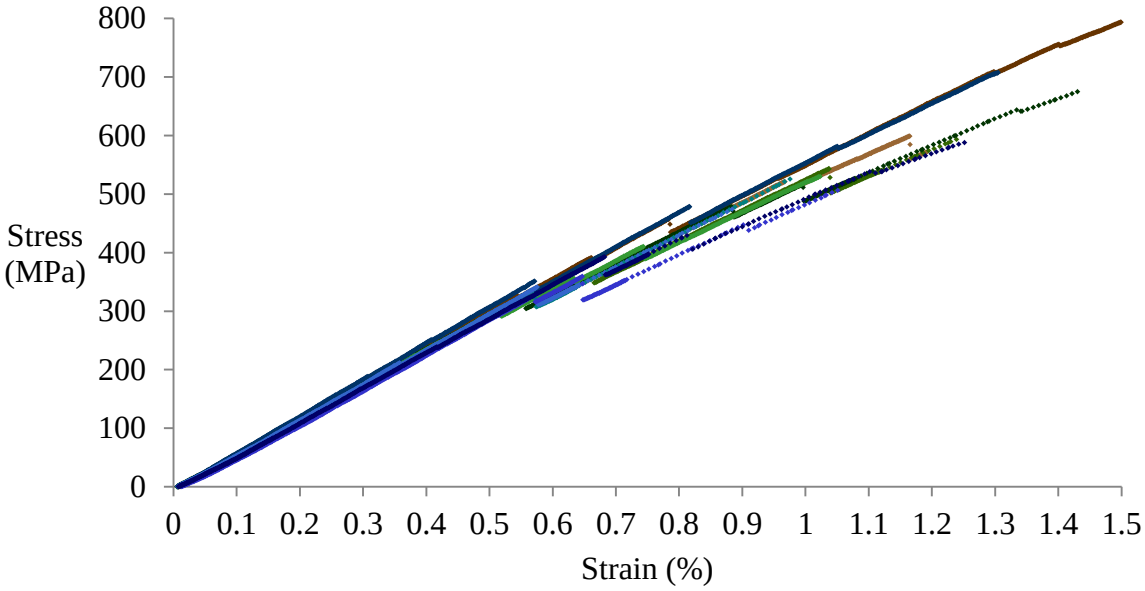

Figure B. 25 Tensile tests for rods manufactured from 3 tows of unsized carbon fibres at standard conditions, including a line speed of 3.2cm/min.

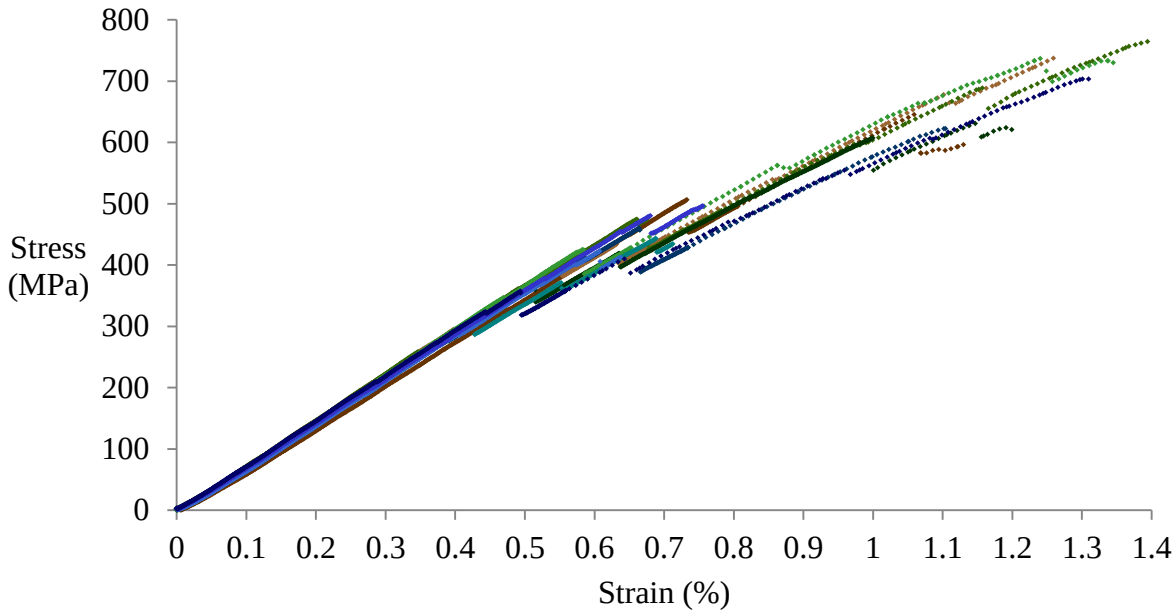

Figure B. 26 Tensile tests for rods manufactured from 4 tows of unsized carbon fibres at standard conditions, including a line speed of 3.1cm/min.

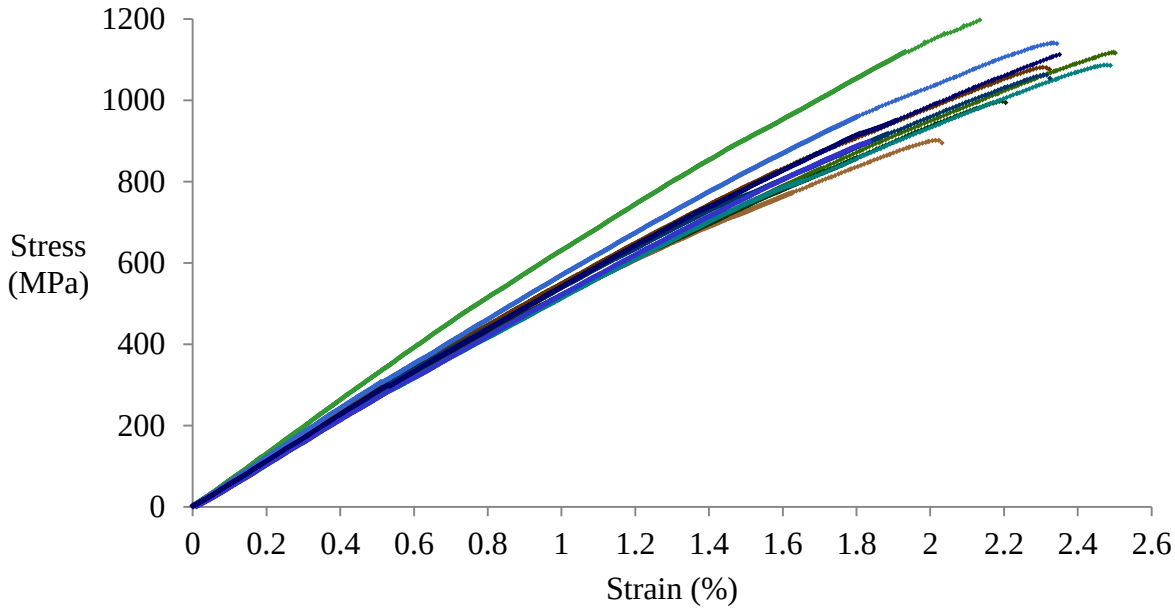

Figure B. 27 Tensile tests for rods manufactured from 9 tows of commingled tows at standard conditions, including a line speed of 3.3cm/min.

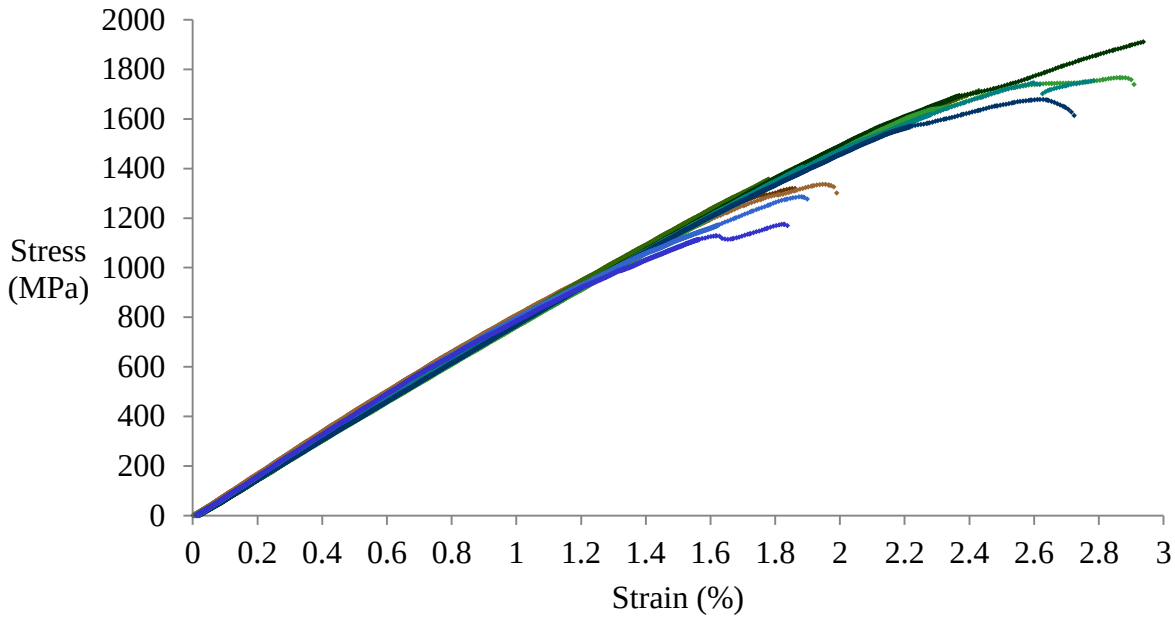

Figure B. 28 Tensile tests of carbon fibre/epoxy rods sourced from Easy Composites.

Appendix C: Hybrid strand test data

Due to software issues it was not possible to export data from the tensile machine used at the Bridon Technology Centre for the testing of strands. Scans of hard copy print-outs of test reports delivered by the machine's software have therefore been attached to this appendix. Included are six tests of fully steel strands, five tests of hybrid strands with 6 tows of sized carbon fibre/nylon 12 rods, four tests of hybrid strands with 9 tows of commingled carbon fibre/nylon 12 rods and five tests of hybrid strands with carbon fibre/vinyl ester rods.

C1. Fully steel strands

Properties	Results
Proof Force at 0.1%	88.8kN
Force at Extension 1.0%	85.1kN
Max Force	101.0kN
Modulus of Elasticity	170.7kN/mm2
Total Elongation at Max Force	6.53%

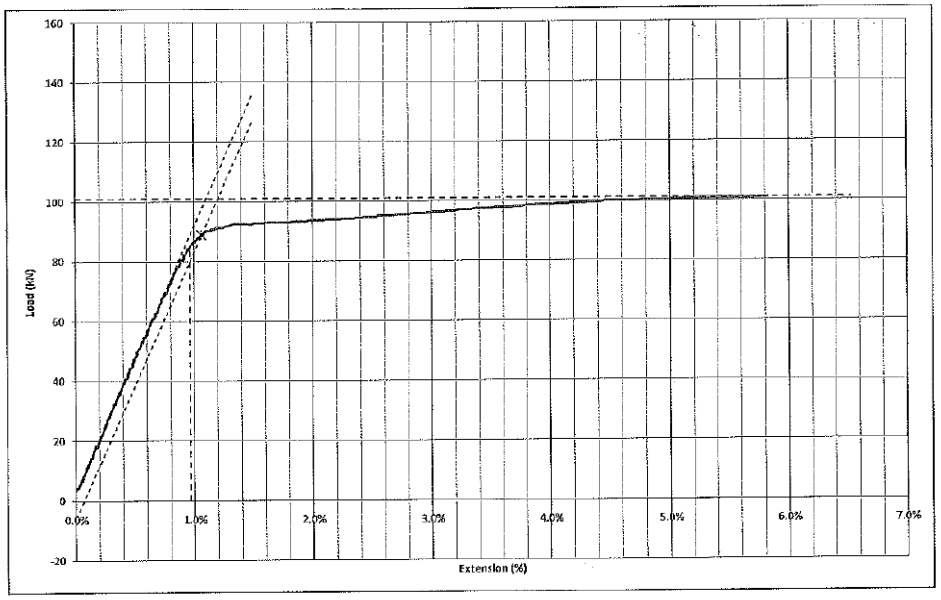

Figure C. 1 Fully steel strand test 1.

Properties	Results
Proof Force at 0.1%	88.8kN
Force at Extension 1.0%	86.0kN
Max Force	100.7kN
Modulus of Elasticity	171.8kN/mm2
Total Elongation at Max Force	6.11%

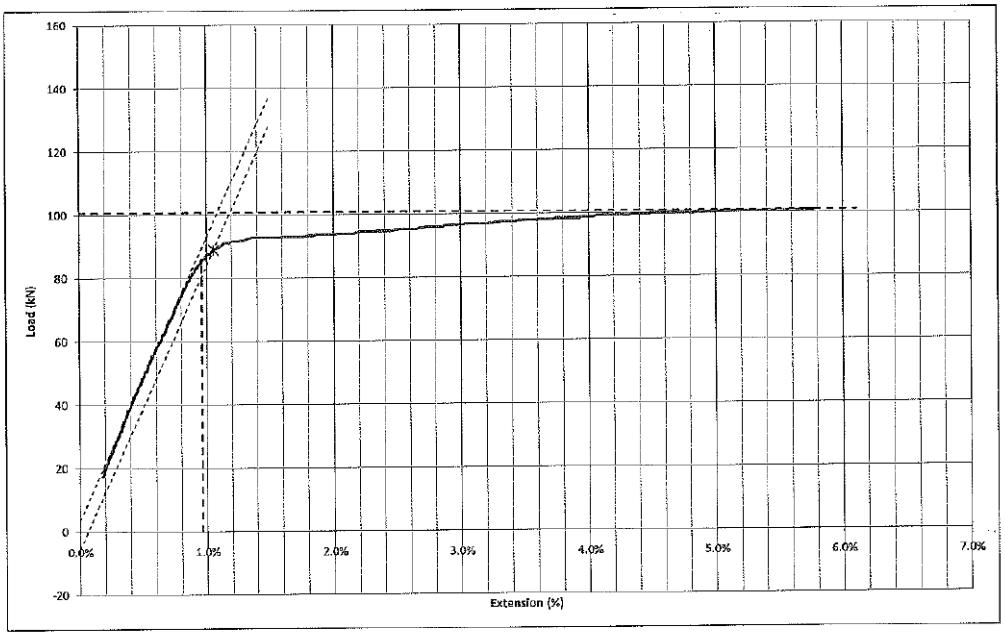

Figure C. 2 Fully steel strand test 2.

Properties	Results
Proof Force at 0.1%	85.4kN
Force at Extension 1.0%	84.5kN
Max Force	100.1kN
Modulus of Elasticity	168.5kN/mm2
Total Elongation at Max Force	6.67%

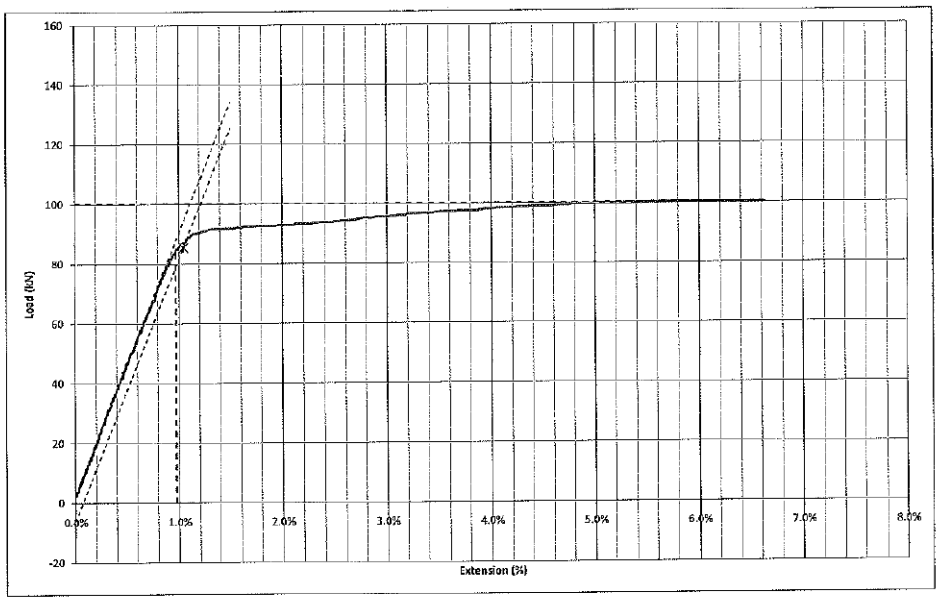

Figure C. 3 Fully steel strand test 3.

Properties	Results
Proof Force at 0.1%	89.6kN
Force at Extension 1.0%	84.8kN
Max Force	100.7kN
Modulus of Elasticity	164.8kN/mm2
Total Elongation at Max Force	5.95%

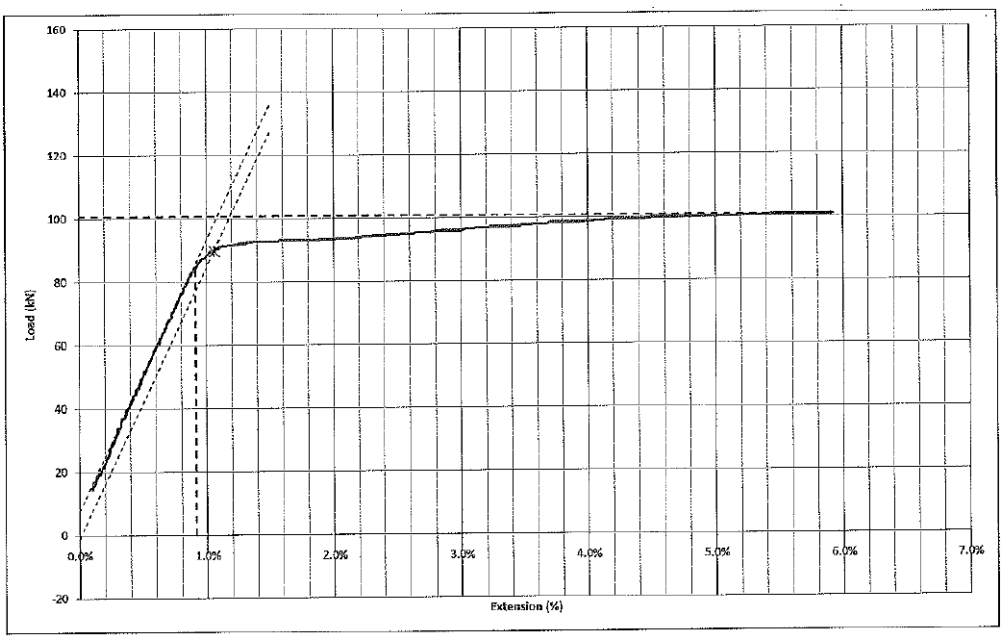

Figure C. 4 Fully steel strand test 4.

Properties	Results
Proof Force at 0.1%	89.6kN
Force at Extension 1.0%	82.3kN
Max Force	100.7kN
Modulus of Elasticity	158.7kN/mm2
Total Elongation at Max Force	6.70%

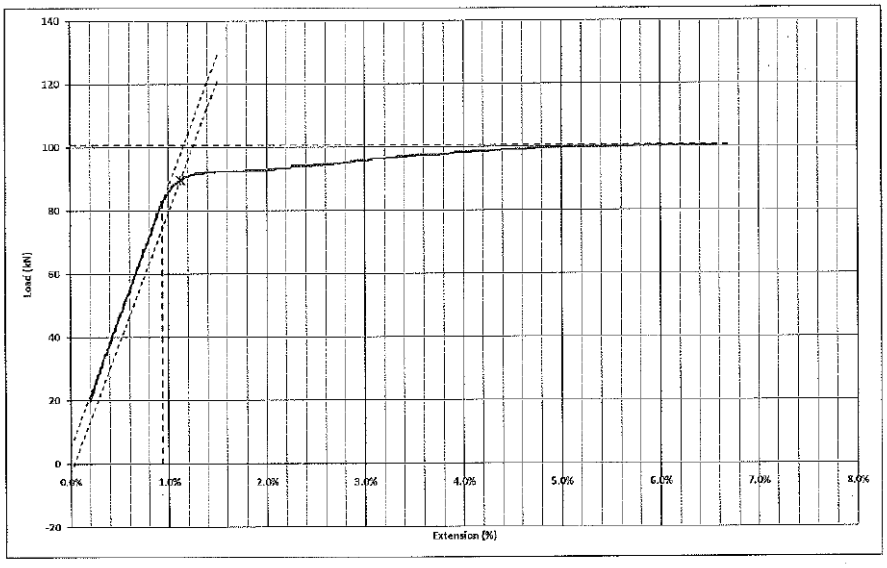

Figure C. 5 Fully steel strand test 5.

Properties	Results
Proof Force at 0.1%	86.3kN
Force at Extension 1.0%	87.1kN
Max Force	101.3kN
Modulus of Elasticity	172.9kN/mm2
Total Elongation at Max Force	7.19%

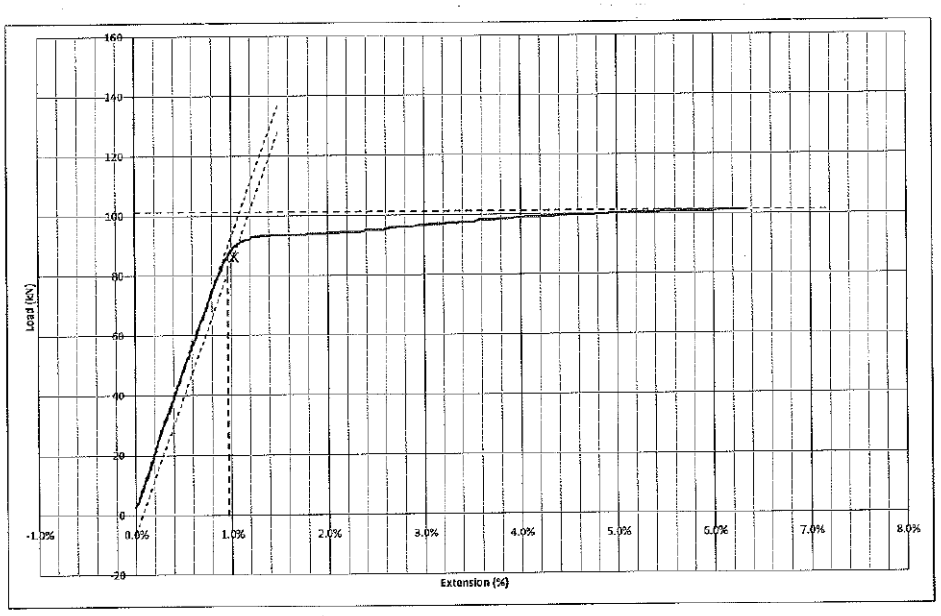

Figure C. 6 Fully steel strand test 6.

C2. 6 tows sized carbon fibre/nylon 12 hybrid strands

Strand Ref. No.	E_{mod} kN/mm²	Proof Force at 0.1% kN	Force at Extension 1% kN	Max. Force kN	Total Elongation at Max. Force %
PW6	158	75.72	76.57	82.82	4.46

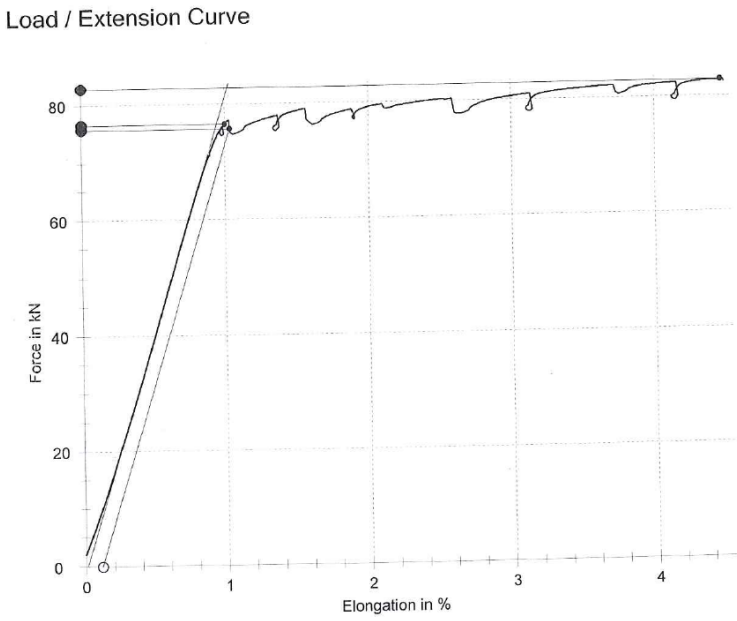

Figure C. 7 6 tows carbon fibre/nylon 12 hybrid strand test 1.

Strand Ref. No.	E_{mod} kN/mm²	Proof Force at 0.1% kN	Force at Extension 1% kN	Max. Force kN	Total Elongation at Max. Force %
PW7	118	76.87	54.53	83.58	3.90

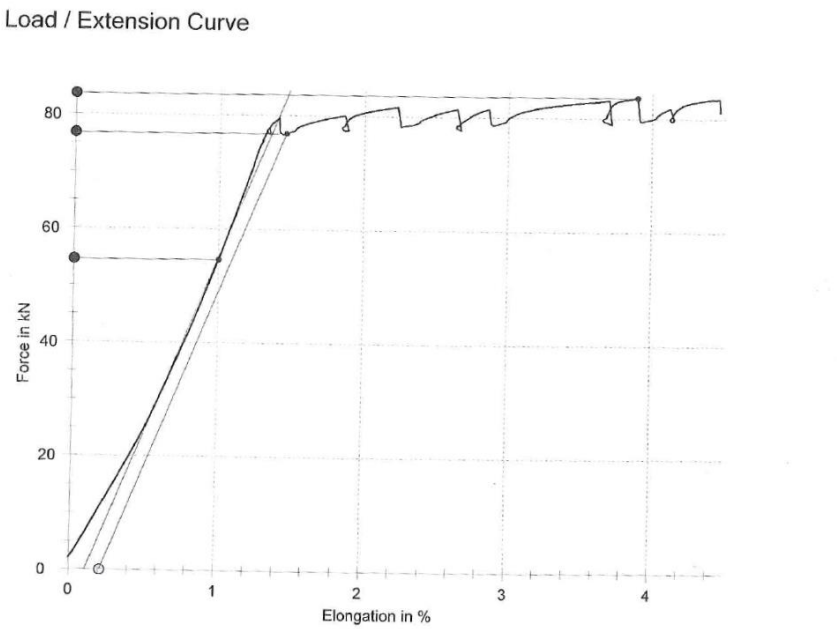

Figure C. 8 6 tows carbon fibre/nylon 12 hybrid strand test 2.

Strand Ref. No.	E_{mod} kN/mm²	Proof Force at 0.1% kN	Force at Extension 1% kN	Max. Force kN	Total Elongation at Max. Force %
PW8	156	73.61	74.20	81.07	2.37

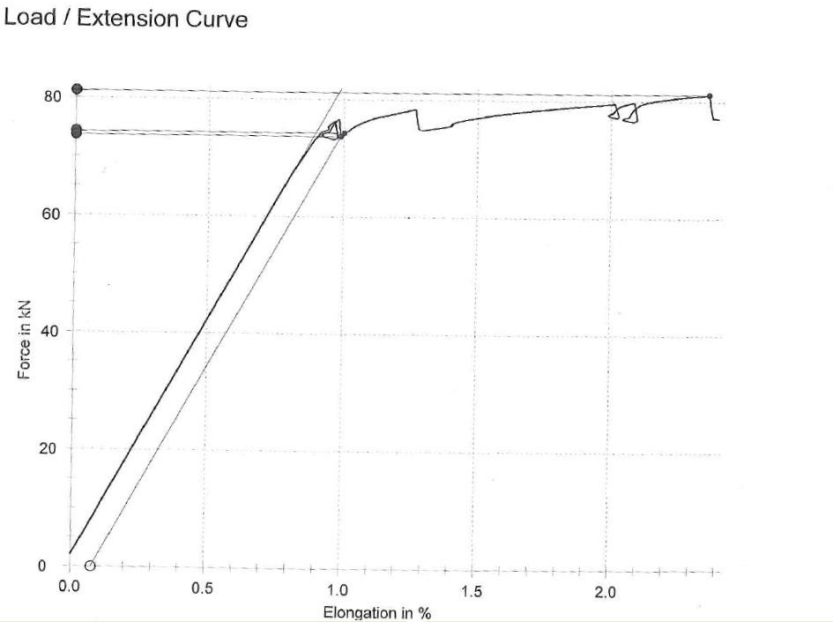

Figure C. 9 6 tows carbon fibre/nylon 12 hybrid strand test 3.

Strand Ref. No.	E_{mod} kN/mm²	Proof Force at 0.1% kN	Force at Extension 1% kN	Max. Force kN	Total Elongation at Max. Force %
PW9	157	75.19	73.64	82.19	3.85

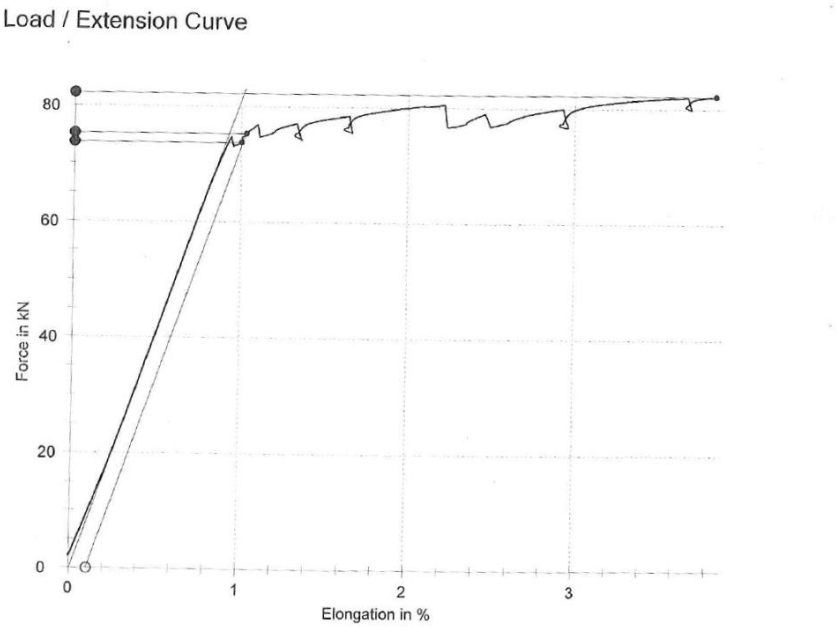

Figure C. 10 6 tows carbon fibre/nylon 12 hybrid strand test 4.

Strand Ref. No.	E_{mod} kN/mm²	Proof Force at 0.1% kN	Force at Extension 1% kN	Max. Force kN	Total Elongation at Max. Force %
PW10	164	76.42	76.65	82.09	2.79

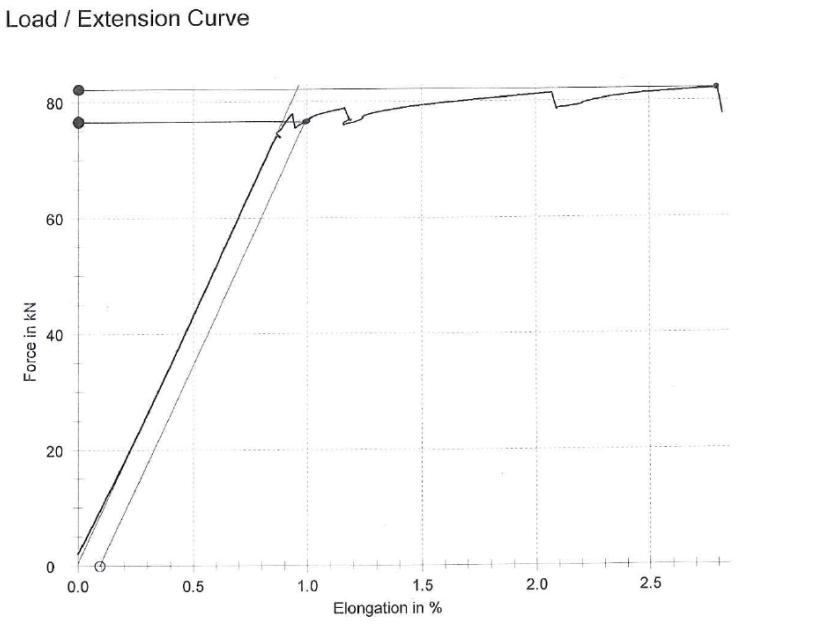

Figure C. 11 6 tows carbon fibre/nylon 12 hybrid strand test 5.

C3. 9 tows commingled carbon fibre/nylon 12 hybrid strands

Strand Ref. No.	E_{mod} kN/mm²	Proof Force at 0.1% kN	Force at Extension 1% kN	Max. Force kN	Total Elongation at Max. Force %
PW13	147	79.58	72.83	82.75	1.46

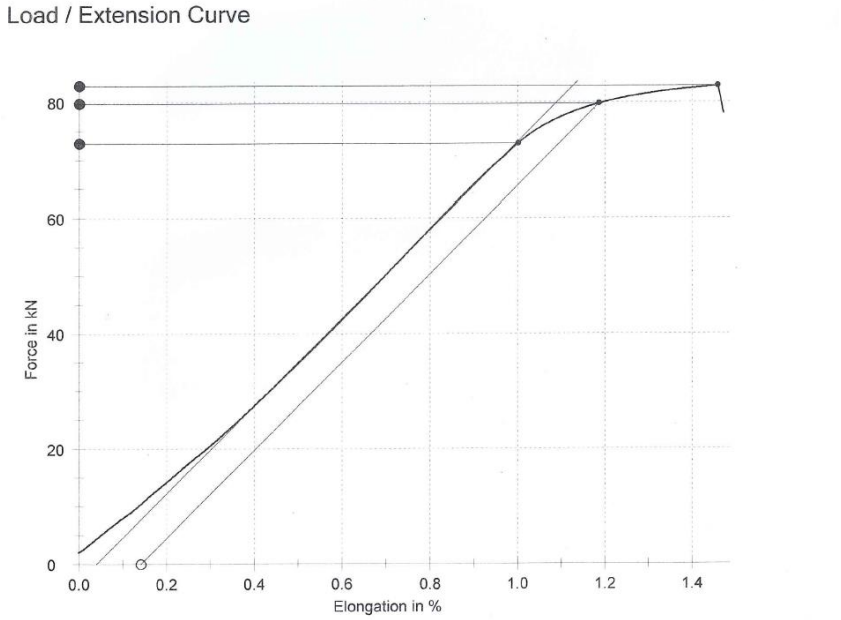

Figure C. 12 9 tows commingled carbon fibre/nylon 12 hybrid strand test 1.

Strand Ref. No.	E_{mod} kN/mm²	Proof Force at 0.1% kN	Force at Extension 1% kN	Max. Force kN	Total Elongation at Max. Force %
PW14	142	78.01	72.22	82.03	1.44

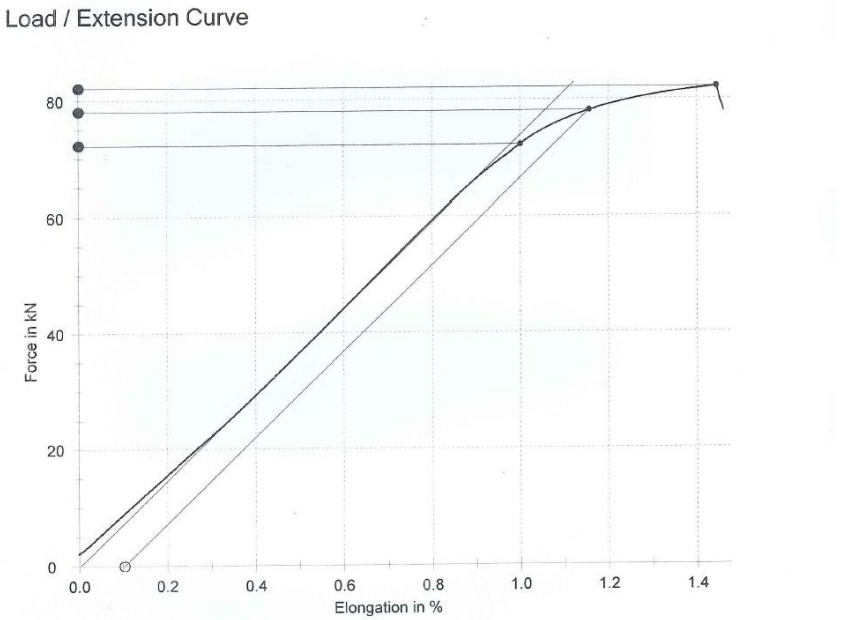

Figure C. 13 9 tows commingled carbon fibre/nylon 12 hybrid strand test 2.

Strand Ref. No.	E_{mod} kN/mm²	Proof Force at 0.1% kN	Force at Extension 1% kN	Max. Force kN	Total Elongation at Max. Force %
PW15	156	78.02	76.82	82.39	1.37

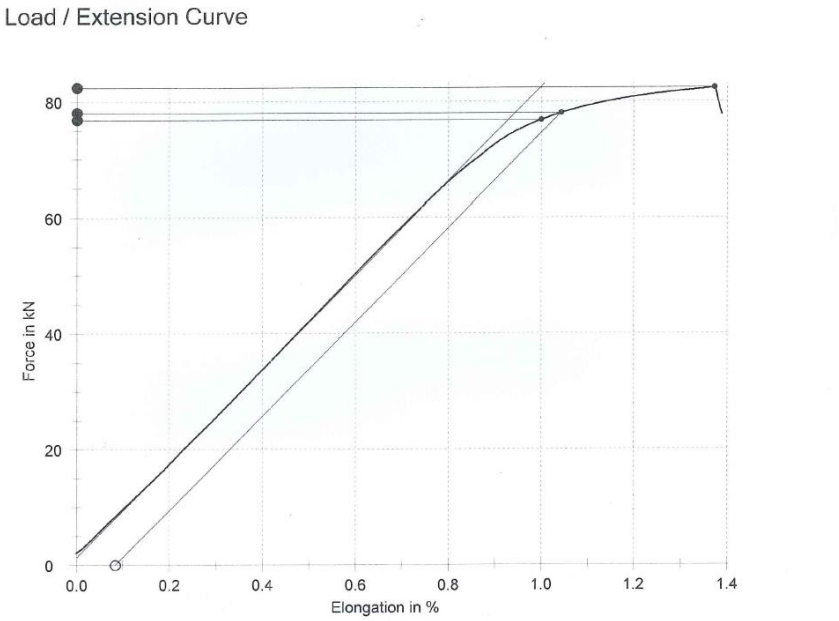

Figure C. 14 9 tows commingled carbon fibre/nylon 12 hybrid strand test 3.

Strand Ref. No.	E_{mod} kN/mm²	Proof Force at 0.1% kN	Force at Extension 1% kN	Max. Force kN	Total Elongation at Max. Force %
PW16	156	77.81	76.78	82.92	1.42

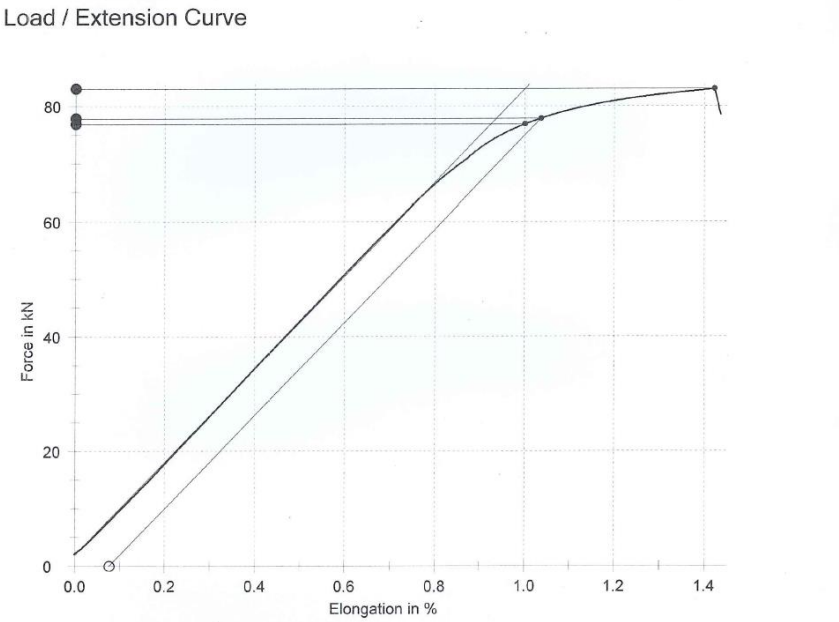

Figure C. 15 9 tows commingled carbon fibre/nylon 12 hybrid strand test 4.

C4. Carbon fibre/vinyl ester hybrid strands

Strand Ref. No.	E_{mod} kN/mm²	Proof Force at 0.1% kN	Force at Extension 1% kN	Max. Force kN	Total Elongation at Max. Force %
PW1	185	84.64	85.73	94.88	1.54

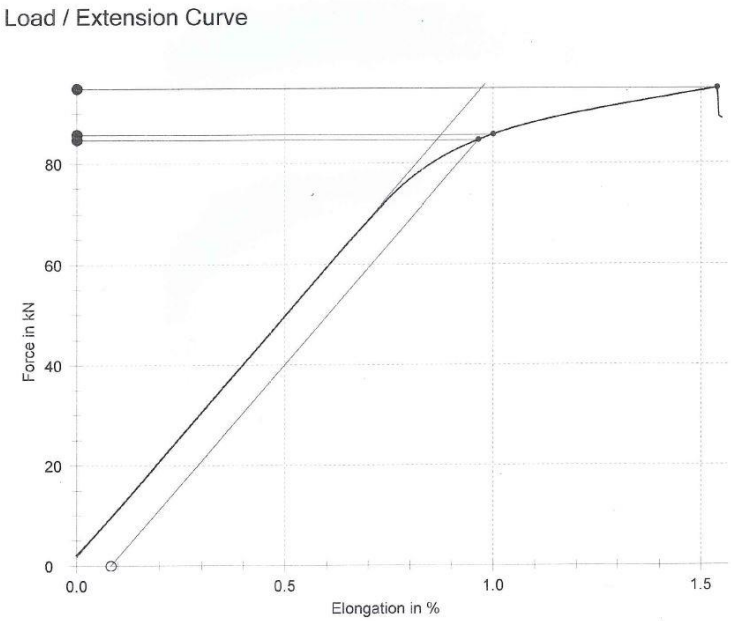

Figure C. 16 Carbon fibre/vinyl ester hybrid strand test 1.

Strand Ref. No.	E_{mod} kN/mm²	Proof Force at 0.1% kN	Force at Extension 1% kN	Max. Force kN	Total Elongation at Max. Force %
PW3	184	86.39	86.75	94.77	1.52

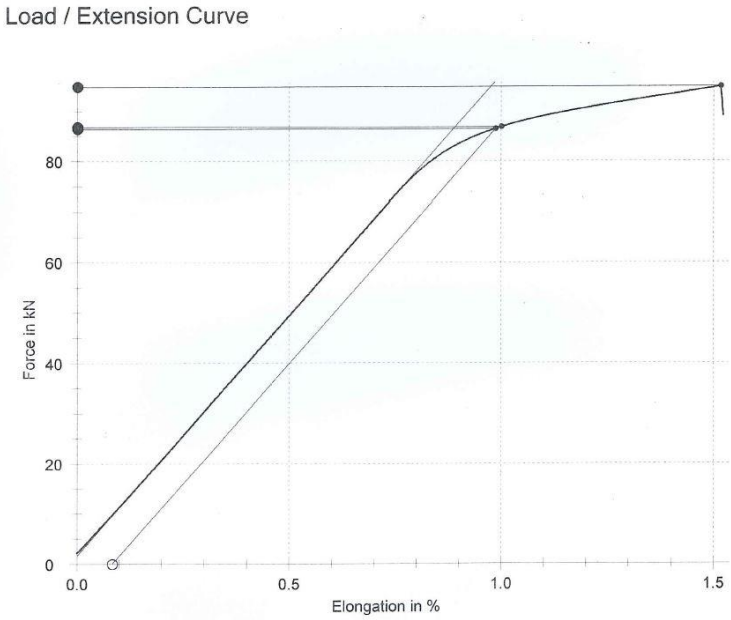

Figure C. 17 Carbon fibre/vinyl ester hybrid strand test 2.

Strand Ref. No.	E_{mod} kN/mm²	Proof Force at 0.1% kN	Force at Extension 1% kN	Max. Force kN	Total Elongation at Max. Force %
PW4	169	85.94	81.68	94.27	1.64

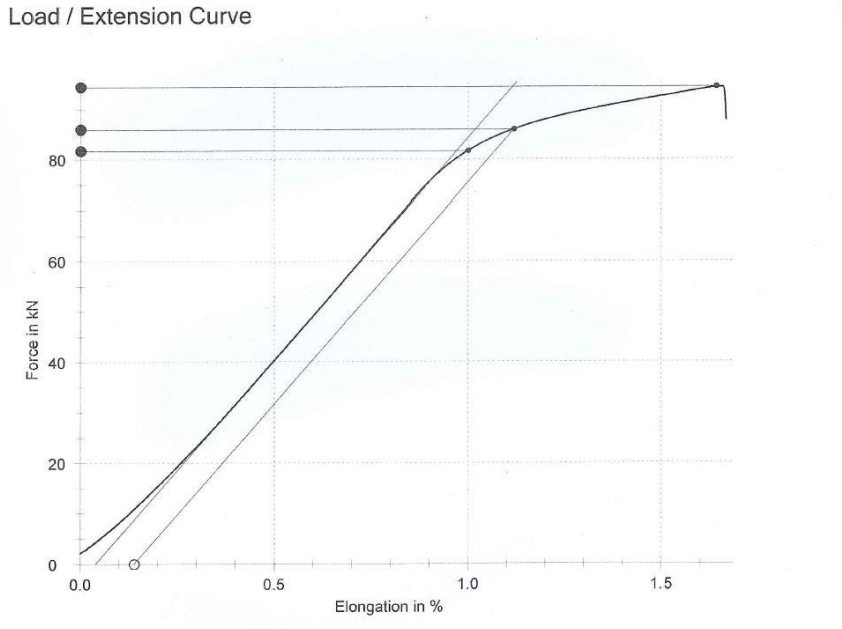

Figure C. 18 Carbon fibre/vinyl ester hybrid strand test 3.

Strand Ref. No.	E_{mod} kN/mm²	Proof Force at 0.1% kN	Force at Extension 1% kN	Max. Force kN	Total Elongation at Max. Force %
PW5	187	90.35	89.66	95.53	1.39

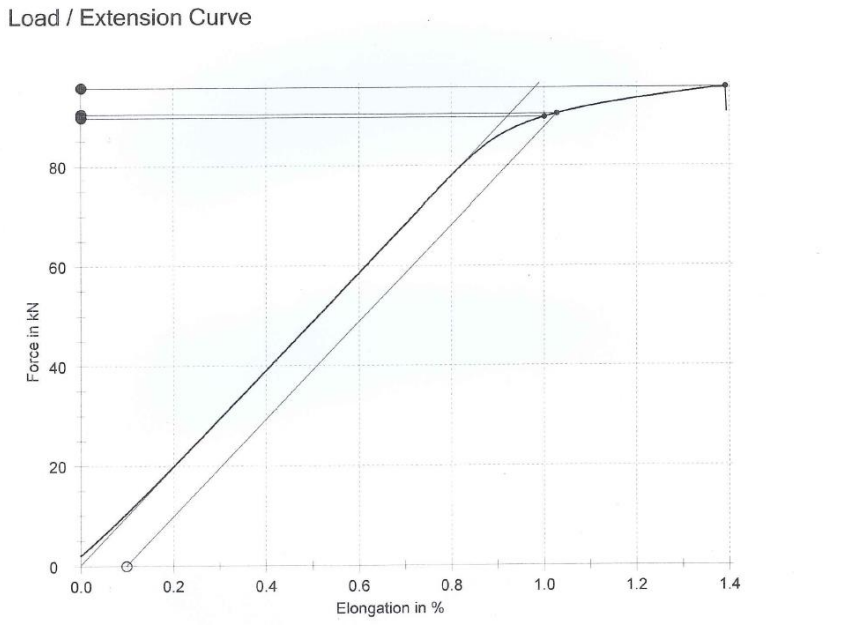

Figure C. 19 Carbon fibre/vinyl ester hybrid strand test 4.

Strand Ref. No.	E_{mod} kN/mm²	Proof Force at 0.1% kN	Force at Extension 1% kN	Max. Force kN	Total Elongation at Max. Force %
PW12	174	86.28	85.33	96.49	1.73

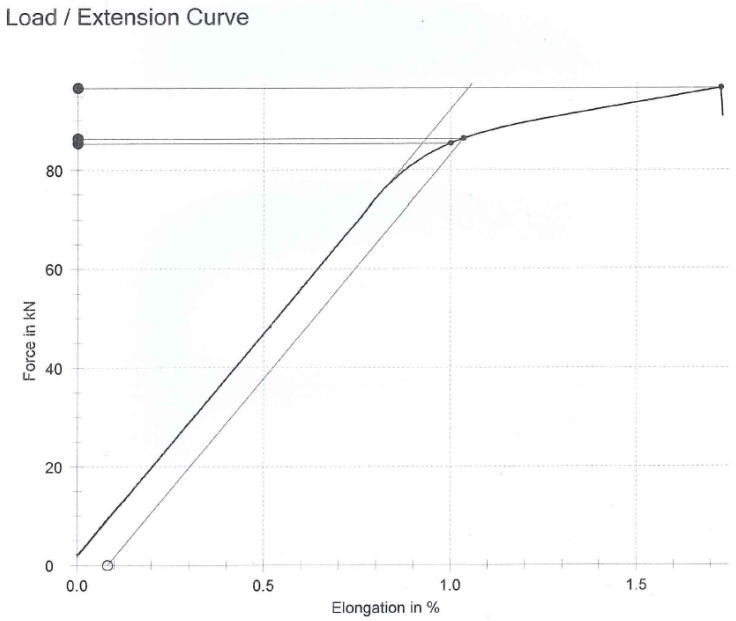

Figure C. 20 Carbon fibre/vinyl ester hybrid strand test 5.

Appendix D: Equipment costs and suppliers for the pultruder

A list of the equipment purchased for construction of the pultruder, as described in §2 is given in Table D. 1. This includes suppliers and the quantity cost for each item.

Table D. 1 List of equipment purchased for construction of the pultruder.

Function or process	Equipment	Supplier	Cost (ex. VAT)
Frame and generic building materials	45mm x 45mm extruded aluminium profile	KJN Aluminium Profiles	£8.49/metre
	45mm x 45mm T-connectors	KJN Aluminium Profiles	£4.10/unit
	12mm chipboard	Wickes	£17.55/sq metre
	12mm plywood	Wickes	£14.85/sq metre
	Interior varnish	Wickes	£15.99/litre
	Wood glue	Wickes	£17.16/litre
	Araldite 2015 epoxy adhesive paste	RS Components	£36.00/200ml
	6mm threaded rod	Wickes	£2.80/metre
	6mm anodised aluminium rod	Wickes	£4.63/metre
	8mm nylon tube	RS Components	£1.25/metre
	8mm pneumatic connectors: stud, elbow, tee	Airlines	2.06/unit, £3.52/unit, £4.43/unit
	8mm pneumatic ball valve	Airlines	£5.28/unit
	35.5mm steel angle	Wickes	£7.72/metre
	35.5mm steel flat bar	Wickes	£4.49/metre
Fibre delivery	½” silver steel rod	Cromwell Industrial Tools	£13.28/metre
	Brass eyelets	Profabrics	£0.32/unit
Fibre spreading	Wooden handles	Fine-tools	£3.17/unit
	2mm acrylic sheet	Wickes	£25.12/sq metre
	Edwards Speedivac 2 vacuum pump	Edwards	£88.00 (second hand purchase)
	Planed timber	Wickes	£2.88/metre
	10mm copper microbore tube	Wickes	£2.10/metre
	Parvalux geared DC shunt motor	RS Components	£231.20/unit
	Parvalux potentiometer controller	RS Components	£253.25/unit
Powder spraying	Encore LT Manual Powder System	Nordson	£2760.00/unit
	6mm acrylic sheet	RS Components	£220.30/sq metre
	M6 nylon screws	RS Components	£11.72/100 units
	M6 nylon nuts	RS Components	£3.82/100 units
	M6 nylon hinge	RS Components	£5.47/2 units
	Dyson DC22 Allergy vacuum	Dyson	£85.00 (second

	cleaner		hand purchase)
	Flexible connector	Wickes	£5.79/unit
	30 litre bucket	H&O Plastics	£12.80/unit
	Regulator and gauge	Airlines	£33.62/unit
	General duty filter	A. B. Tools	£18.95/unit
	Eliminizer combo dust, water and oil filter	Airlines	£341.00/unit
	Silica gel desiccant	RS Components	£32.04/50 units
Pre-heater	FGR-060 Electric tape heater	Omega	£19.50/unit
	1/32 DIN i-Series Thermal controller	Omega	£137.00/unit
	SSRDIN660DC40 Solid state relay	Omega	£38.00/unit
	Ready mixed fire cement	Wickes	£3.49/kg
	Diecast aluminium enclosure	RS Components	£3.41/unit
	Type K miniature plug and socket	RS Components	£4.30/unit
	Inconel sheath Type K thermocouple	RS Components	£15.28/unit
	Galvanised mesh panel	Wickes	£7.39/sq metre
Consolidation heating die	Chrome-plated split steel die	Robert van Doren	£2200.00/unit
	STH102-060 Electric tape heater	Omega	£47.00/unit
	1/32 DIN i-Series Thermal controller	Omega	£137.00/unit
	SSRDIN660DC40 Solid state relay	Omega	£38.00/unit
	Ready mixed fire cement	Wickes	£3.49/kg
	Diecast aluminium enclosure	RS Components	£3.41/unit
	Type K miniature plug and socket	RS Components	£4.30/unit
	Inconel sheath Type K thermocouple	RS Components	£15.28/unit
	Galvanised mesh panel	Wickes	£7.39/sq metre
	Clay airbrick	Wickes	£2.49/unit
Cooling	40mm waste pipe	Wickes	£0.84/metre
	40mm universal compression connector	Wickes	£4.09/unit
Traction pulling	Traction caterpillar puller	Versa Machinery	£3000.00/unit
	Parvalux geared DC shunt motor	RS Components	£231.20/unit
	Parvalux potentiometer controller	RS Components	£253.25/unit
Chop saw	Evolution Rage 3 185mm chop saw	Screw Fix	£109.99/unit
	185mm diamond wheel	Toolstop	£24.90/unit
	Wheels for sliding track	KJN Aluminium Profiles	£11.48/unit